Modeling uncertainty in burn severity using the Composite Burn Index and remotely sensed data

Colton Wells Miller

A dissertation

submitted in partial fulfillment of the

requirements for the degree of

Doctor of Philosophy

University of Washington

2022

Reading Committee:

Ernesto Alvarado, Co-Chair

L. Monika Moskal, Co-Chair

Van R. Kane

Program Authorized to Offer Degree:

College of the Environment

University of Washington

University of Washington

Abstract

Modeling uncertainty in burn severity using the Composite Burn Index and remotely sensed data

Colton Wells Miller

Chairs of the Supervisory Committee:

Ernesto Alvarado

L. Monika Moskal

School of Environmental and Forest Sciences

Methods to link ground-based measurements of burn severity with remotely sensed data vary, and there is no consensus on the best approach. The objectives of this dissertation were to: 1) summarize methodological pathways used to model continuous estimates of burn severity (based on the Composite Burn Index) using remotely sensed data, 2) dive into the fundamental theory regarding spatial alignment and temporal synchrony of field observations and remotely sensed data, and 3) perform an in-depth case study of key methodological decisions using the King Fire to assess tradeoffs in accuracy and sensitivity of the resulting outcomes. A literature review provided the basis for identifying a "decision menu" of analytical choices and a set of rationale for future studies to consider when constructing a workflow. I concluded that considerable challenges arise when comparing results across studies that used different methods due to uncertainty at each step in the analyses and lack of comprehensive comparative studies.

Regarding spatial alignment, I introduced a framework of pixel and plot homogeneity assumptions that is useful for conceptualizing how study design and inherent geometric inaccuracies in data may influence model results. I suggested approaches for future studies to consider when matching field plot size and pixel grain and investigating the effect of this characteristic. Concerning temporal synchrony, I found that a close match between the timing of field observations and remotely sensed data acquisition, while conceptually important, did not, in most cases, reduce model performance. Finally, the sensitivity analysis includes robust assessment of key methodological decisions. I found that overall, while the accuracy and sensitivity of individual choices vary, no single decision drives model outcomes. However, I highlighted pathologies that can arise during model selection and suggest that studies generate criteria for assessing model quality in terms of the specific ecological objectives rather than uncritically picking a model based on performance metrics alone. The results suggest that little additional information can be extracted from Landsat optical bands based on the broad suite of known methods and, instead, focus may turn to ensuring alignment of methodologies with desired ecological applications.

TABLE OF CONTENTS

LIST OF FIGURES

SUPPLEMENTARY FIGURES

LIST OF TABLES

SUPPLEMENTARY TABLES

ACKNOWLEDGEMENTS

I would like to thank my entire committee, Ernesto Alvarado, Monika Moskal, Van Kane, Brian Harvey, and Megan Dethier for their relentless patience, untiring support, and treasured mentorship throughout my graduate program. Additional backing and encouragement came from Ann Briggs via the Professor David G. Briggs Endowed Fellowship in Forest Management as well as Port Blakley. Susan O'Neill with the USFS AirFire team and Morris Johnson with the Fire and Environmental Research Applications team at the Pacific Wildland Fire Sciences Laboratory also contributed to my work through funding of research and fieldwork. Bob McGaughey and Hans Anderson with the USFS Vegetation Monitoring and Remote Sensing Team answered uncountable questions about forestry and lidar. Patti Loesche helped with writing advice and editing when I needed it most. Cody Desautel and the Colville Indian Reservation helped maintain my interest in tribal forestry and making sure my work could be applicable "on-the-ground". Harry Podschwit was more than helpful in providing statistical insight and coding help. Gina Cova and Caden Chamberlain both contributed data and insights to the King Fire case study. An internship Washington State Department of Natural Resources provided me with the time to gain a remote pilot's license to fly unoccupied aerial vehicles and collect remotely sensed data across some of Washington's natural heritage and recreation areas. Not least of all, countless colleagues and friends helped me stay on track and see the light at the end of the tunnel. While not able to name them all, I would like to send gratitude to: Laurel James, Spus Wilder, David L. Peterson, Tom DeLuca, Keala Hagmann, Gary Morishima, Caitlin Littlefield, Derek Churchill, Michelle Trudeau, Amanda Davis, Greg Ettl, Tom Hinkley, Tony Rho, Ryan Haugo, Jon Bakker, and Sándor Tóth. His employer during the last phase of his degree, Vibrant Planet, exhibited gracious tolerance waiting for him to finish.

DEDICATION

This dissertation is dedicated to my family who have provided unwavering support throughout the process: my parents Jim and Margaret, my partner Emmi, and my sister Marissa.

CHAPTER 1. INTRODUCTION

Wildland fire is an inherent part of the Earth system, a planet covered with carbon-rich vegetation, seasonally dry climates, atmospheric oxygen, and widespread lightning and volcanic ignitions (Bowman *et al.* 2009). While modern culture often views fire as a natural hazard with only negative implications, fires have occurred on Earth for over 400 million years and human societies have coexisted with fire since their emergence (Doerr and Santín 2016). Fire is a major ecological disturbance agent that modifies forest landscapes (De Santis and Chuvieco 2009), and many species coevolved with and developed adaptations to it (He *et al.* 2016). Currently, it is estimated that about 350 million ha of land is affected by fire annually (Giglio *et al.* 2013).

Wildland fires not only can burn large areas, but they also burn in different ways across large landscapes (Turner 2010), causing spatial and temporal variation in fire effects (Morgan et al. 2001; de Groot 2006; Jia et al. 2006; Allen and Sorbel 2008). The ecological effects of fire and changes in ecosystems due to fire called 'burn severity' (Lentile et al. 2006). Quantifying heterogeneous burn severity patterns within fire perimeters is challenging because of the extent of burned landscapes and cost of field observations. Complicating these challenges are myriad approaches and no standardized methodology for quantifying burn patterns.

There is no one-size-fits-all approach to evaluating burn severity (Keeley 2009). This lack of a universal definition complicates post-fire assessments, as no one metric can represent 'true' severity (Cocke *et al.* 2005). Instead, the choice of assessment is determined by management, ecological purposes, and field sampling designs (Ryan and Noste 1985). Thus, the number of ways to measure burn severity are virtually unlimited; however, useful measures must be

accurate and precise enough to distinguish ecologically significant severity levels that lead to different successional pathways (Murphy *et al.* 2008).

The Composite Burn Index (CBI, Key and Benson 1999) and related protocols (e.g., Geometrically structured CBI; De Santis and Chuvieco 2009) have emerged as common field measures that provide a link to remotely sensed data for mapping burn severity over large landscapes. However, CBI has been criticized for a number of reasons as a useful and robust index, and studies linking field-based observations of CBI to remotely sensed data have not produced a consensus approach in analytical methods. As a result, there remains considerable uncertainty in the ability to compare results across different fires, vegetation types, and landscapes. This dissertation investigates the analytical decisions that are made when modeling burn severity with CBI plots and remotely sensed data and provides an empirical case study applying those results to the King Fire in the Sierra Nevada ecoregion of California.

Measures of ecosystem change from fire have many applications and assessment methods. Burn severity estimates inform immediate post-fire recovery projects, future fuel treatments, and long-term ecosystem analysis (Miller and Thode 2007). In the immediate post-fire environment, common priorities are to preserve the soil and maintain the vegetation community (Fernandez-García *et al.* 2018). A second key function of severity assessments is to understand how fire effects vary with ecosystem composition and structure. Linking pre-fire conditions with potential post-fire outcomes helps managers to design better fuel treatments, such as thinning and prescribed fires (e.g., Churchill et al., 2013). Severity estimates can also help to predict long-term consequences to a post-fire ecosystem (Macdonald 2007), such as changes to forest succession (Johnstone and Chapin 2006). Managers need predictive models of wildland fire

effects on vegetation communities, wildlife populations, and hydrologic function (Sorbel and Allen 2005), and ongoing records of fire effects allow ecologists to assess effects of climate change over time.

Burn severity estimates can be used to generate predictive models of wildland fire effects on vegetation communities and wildlife populations and are particularly useful for assessing the effects of climate change over time (Sorbel and Allen 2005). Furthermore, the relationship between burn mosaics and tree mortality can inform management seeking to reduce mortality in large, old trees in fire-adapted ecosystems by implementing pre-fire forest treatments (Churchill *et al.* 2013). Linking the initial (pre-fire) conditions of the ecosystem with the immediate and potential future outcomes informs the planning and design of restoration treatments – such as thinning or prescribed fires – intended to mitigate, reduce, or alter how fire behaves on the landscape. Such information is useful to predict the effects of future on vegetation community trajectories (Murphy *et al.* 2008) and facilitate the identification of areas likely to burn or experience uncharacteristic effects when they burn.

The CBI was designed to complement remotely sensed data to overcome challenges in mapping burn severity across large landscapes and provide comparable metrics across fires over time. CBI is a continuous measure of burn severity that encompasses five vegetation strata: substrates; herbs, low shrubs, and trees <1 m; tall shrubs and trees 1-5 m; intermediate trees 5-20 m; and big trees >20 m. It incorporates up to 23 different ecosystem attributes. Observations made by visual estimates are aggregated to a single unitless score ranging from 0 (unburned) to 3 (severely burned). The CBI was designed to evaluate severity in combination with remote sensing imagery, in particular using optical imagery derived from the Landsat family of sensors(Key and

Benson 1999). The sampling protocol provides a standardized way to optimize and match ground-based methods to the constraints of remote sensing (Key and Benson 1999). CBI included ground effects aimed to collectively provide a signal at a scale detectable by the moderate-resolution spatial grain observed by Landsat (Cansler and McKenzie 2012).

CBI is an important metric for evaluating burn severity for several reasons. (1) Its rapid protocol allows quick deployment and assessment over large landscapes. (2) It generally shows robust relationships with spectral fire severity indices, providing strong support for their use in estimating fire effects across landscapes (Parks *et al.* 2019). The index has gained widespread use, especially because generally strong correlations with the delta Normalized Burn Ratio (dNBR) (Key and Benson 2006) demonstrate the sensitivity of dNBR to post-fire effects (Eidenshink *et al.* 2007a). (3) For general assessments of burn severity, the CBI may be considered more complete than other classification systems based on single indicators of burn severity (Sikkink 2015); it integrates multiple metrics across vegetation strata and soil, which can be used together (as site burn severity) to provide an overall idea of damage caused by fire. (4) Such a comprehensive measure of burn severity is desirable if only to generate maps that facilitate broad-scale rehabilitation prioritization (Karau *et al.* 2014). (5) Individual components may also be considered separately, depending on what is considered key for post-fire management (Key and Benson 2006; Zhu *et al.* 2006; Keeley 2009).

Several challenges exist with capturing quality field observations of ecosystem change due to fire using the CBI and similar modified approaches. First, in many cases there are not pre-fire observations for comparison, and the extent of change must be inferred against an hypothesized initial condition (Lentile *et al.* 2006). Furthermore, the visual observations may be prone to

observer bias where estimated changes differ based on the personnel collecting data or site conditions (e.g., distance to unburned areas that can serve as proxy sites for comparison) (Morgan *et al.* 2014; McCarley *et al.* 2017). Another common critique is that measurements are aggregated across vertical strata to a comprehensive, unitless severity score where the individual factors driving estimates of change are obscured (Morgan *et al.* 2014). While some authors suggest focusing on continuous variables that measure the actual fire effect (e.g. tree mortality, fuel consumption, soil water repellency) that avoid the aggregation inherent in a composite measure such as CBI (Morgan *et al.* 2014). That said, the CBI has emerged as a standard for assessing burn severity in the two decades since it's development and continues to be used for both research and management purposes.

The original CBI protocol has been adapted to many environments (Quintano *et al.* 2015) and its relationship with remotely sensed data improved. One major modification was the Geometrically Structured CBI (GeoCBI) (De Santis and Chuvieco 2009), which attempts to account for differences in fractional cover (FCOV) of each stratum or changes in leaf area index (LAI) for intermediate and tall tree strata. These describe the influence of vegetation cover on reflectance of different strata within a given plot (De Santis and Chuvieco 2009). Other composite severity indices are modified by using weights for each stratum (WCBI; e.g. Cansler and McKenzie, 2012) and streamlining assessments for rapid surveys (e.g. Burn Severity Index (BSI); Loboda et al., 2013).

In general, a combination of remotely sensed data and field-based observations are needed for a full evaluation of fire effects due to factors that are temporally sensitive as well as phenomena that are difficult to measure with spectral information alone (French *et al.* 2008). Common

effects of fire include consumption of vegetation, destruction of leaf chlorophyll, exposed soil, charred stems, and altered moisture (Epting *et al.* 2005). These ecological impacts lead to spectral, thermal, and structural changes on the land surface, which can be captured by remote sensors (Epting *et al.* 2005; Mallinis *et al.* 2018). Optical, thermal, and radar data are mainly based on changes in spectral or thermal properties of land surface before and after a fire (Lentile *et al.* 2006). Because the effects of fire vary across spectral regions, different remote sensors show tradeoffs in capturing meaningful changes in post-fire landscapes, and their usefulness depends on the spectral regions captured. For example, multispectral sensors have advantages over sensors based only visible light, because they capture a broader range of fire effects, have negligible atmospheric scattering, and better penetrate thin clouds and smoke (Avery and Berlin 1992).

The sheer scale of wildland fires and resulting spatial and temporal variation pose a challenge for accurately estimating fire effects on the ground (Chen *et al.* 2011). There can be difficulties with access and logistics as well as the costs involved in accessing remote burn sites on the ground (Morgan *et al.* 2014). Thus, field plots may suffer from poor spatial representation (De Santis and Chuvieco 2007) and may require large numbers of plots to represent the range of conditions in a large, heterogeneous burned areas (Morgan *et al.* 2014).

Remote sensing provides a powerful tool to understand patterns of burn severity across large landscape, owing to its ability to provide a synoptic view of large landscapes from spaceborne or airborne sensors (Lentile *et al.* 2006), which enables the quantification of burn severity over a wide variety of temporal and spatial scales (Schepers *et al.* 2014). Remote sensing also allows observation of post-fire effects areas that are remote or inaccessible (Key and Benson 2006;

Lentile *et al.* 2006; Murphy *et al.* 2008) and facilitates the capture of landscape spatial patterns over vast areas (Lentile *et al.* 2006; Wulder *et al.* 2009; Soverel *et al.* 2010).

While a valuable tool, several limitations of remotely sensed data affect their ability to capture landscape change due to fire. These include (1) the availability of adequate post-fire imagery and its timing relative to field campaigns, (2) the spatial synchrony between field plots and remotely sensed data, and (3) the inability of passive sensors to discriminate change across the vertical forest strata. The timing of remotely sensed data acquisition may be limited by image quality and availability. Second, to adequately capture fire effects, the sensor's spatial resolution must correspond to the patch size of the burn (White *et al.* 1996). If the spatial grain of the remotely sensed and observed ecological phenomena are mismatched, then fire effects may be aggregated either too broadly or finely. Third, remotely sensed data also often cannot distinguish between vertical strata (i.e. whether severity ratings come from overstory, soils, or understory) and integrate all parts of the forest, such as those on the ground and in the tree canopy (White *et al.* 1996). This can cause higher correlations with measures of canopy-layer fire severity than ground-layer fire severity (Hoy *et al.* 2008). Additionally, it may result in a failure to detect multiple effects of a fire (Cocke *et al.* 2005).

Overall, the Landsat Earth-observing program in particular has been widely used, likely due to its near-global coverage of multispectral data at 30-m spatial resolution since 1982 (Eidenshink *et al.* 2007a). Landsat data provide continuous spatially and temporally consistent information basis across the U.S., allowing for multitemporal comparison of pre- and post-fire conditions to evaluate patterns of fire-caused change. The relatively high spatial and spectral resolution are adequate to respond to within-stand changes, and scenes are large enough that a fire can often be

encompassed by one image (Epting *et al.* 2005). Furthermore, the Monitoring Trends in Burn Severity (MTBS) program maps wildfires greater than 400 ha in western US and over 100 ha in the eastern US, using NBR and dNBR derived from Landsat imagery (Eidenshink *et al.* 2007b). Therefore, Landsat data is familiar and widely interpretable by both researchers and managers in fire ecology.

Maps are a common tool for quantifying the spatial distribution of fire effects and often a main product of post-fire assessments. Post-fire mitigation and rehabilitation treatments are immensely costly due to the large spatial extents of fires and complex terrain they can impact (Miller and Yool 2002), and maps provide the geospatial information needed to efficiently target recovery activities (Lachowski *et al.* 1997; Sunar and Özkan 2001; Miller and Yool 2002). They also provide baseline information that can be used for management, monitoring, modeling, research (Sorbel and Allen 2005). The spatial element allows deeper understanding of interactions between fire and vegetation (Meng and Meentemeyer 2011) by allowing investigation of landscape patterns and scales of disturbance processes (Turner *et al.* 1994; Chuvieco 1999; Hudak *et al.* 2007). Furthermore, maps may help identify areas where fire had beneficial ecosystem consequences by allowing comparisons to historical burn severity distributions (Pratt *et al.* 2006).

Burn severity maps can use continuous (numerical data that can be measured in infinitely small units) or classified (grouped into categories). In nature, the biophysical symptoms of burn severity vary in a continuous manner (Jain *et al.* 2004; Lentile *et al.* 2006). For example, post-fire landscapes may exhibit a continuum of living trees, ranging from only a few snags among living trees up to 100% mortality (Kennedy and Fontaine 2009). However, managers and post-

fire rehabilitation often rely on classified images that identify areas according to low, moderate, and high severity impacts (Holden and Evans 2010).

Classified maps result in information loss relative to continuous maps, but they do facilitate: 1) visual interpretation of images, 2) comparisons of multiple fires or fires from multiple regions, 3) analysis of the spatial context and spatial pattern of severity, 4) spatially explicit predictions of the impacts of the fire (i.e. soil erosion, water quality, succession, and carbon emissions), and 5) targeted management responses to those impacts (Cansler and McKenzie 2012). Additionally, classified maps can be easier to interpret and allow for the calculation of summary statistics, e.g. 25% of fire classified as high severity (Holden and Evans 2010). Even so, there are several limitations to the classification process. It raises questions about how many classes should be considered, with the tradeoff of fewer classes increasing consistency at expense of map utility (Cocke *et al.* 2005). Also, the process of applying thresholds can bin data into somewhat arbitrary groups, which risks misclassification, discards ecological information (Lentile *et al.* 2006) and can lead to aggregation errors such as Modifiable Aerial Unit Problem (Openshaw 1981; Jelinski and Wu 1996). Finally, classification often results in broad categories that are ambiguous with respect to what the categories mean in terms of quantitative fire effects (Miller and Quayle 2015).

Continuous burn severity maps provide the flexibility to customize maps for different classes through variable thresholding depending on the model used and the user's needs (Boucher *et al.* 2017). Broadly speaking, CBI thresholds are subjective and may differ from study to study depending on the objectives of the analysis (Miller and Thode 2007; Miller *et al.* 2009). The most useful maps are created for a given application, with threshold values chosen according to

the relevant ecology of the application in question (Hall *et al.* 2008). For example, one could identify CBI values associated with specific ecological effects (e.g. delayed regeneration of wind dispersed seeds) and use them to set threshold values of spectral indices (Cansler and McKenzie 2012). Compared to continuous data, classified CBI categories result in a loss information. Classified maps are useful to interpret and identify patterns across multiple burns and targeted management responses (Cansler and McKenzie 2012). However, they require determination of an arbitrary number of categories (Cocke *et al.* 2005) that may be overly broad and ambiguous in terms of quantitative fire effects (Miller and Quayle 2015).

This dissertation focuses on the modeling of CBI and related composite severity measures in continuous form. In part this decision resulted from not retreading prior work by Cansler and McKenzie (2012) in reviewing CBI classification accuracy and the lack of a comprehensive review of continuous methods. Overall, this dissertation focuses on remote sensing of post-fire landscapes using the CBI and related measures as continuous variables to link to remotely sensed data.

Chapter 2 provides a systematic review of empirical studies that linked remotely sensed data to continuous measures of ground-based severity using the Composite Burn Index and related measures. The purpose of this chapter is to review the state of the literature, including where and when studies have been conducted, what types of fires were investigated, and the myriad methods used to sample, process, and analyze data. Chapter 3 takes a deep dive into the spatial and temporal alignment of field observations and remotely sensed data used by the studies found during the Chapter 2 review process. The purpose of this chapter is to establish a conceptual model relating the spatial grain of remotely sensed data to field plot sizes, taking into

consideration the different methods for extracting a pixel value that overlays field plots. Additionally, it demonstrates the existing biases regarding the timing of field campaigns relative to fire ignition and shows that, based on the existing literature, maintaining strict temporal alignment between field observations and remotely sensed data does not necessarily improve model results. Chapter 4 uses the King Fire as a case study to examine the sensitivity of model results between CBI and remotely sensed data to a suite of analytical decisions introduced in Chapter 2 and whether relationships between field observations and remotely sensed data are robust to uncertainties in model form. Chapter 5 provides a conclusion to this work by summarizing key takeaways and potential next directions based on this work.

1.1 References

Allen JL, Sorbel B (2008) 'Assessing the differenced Normalized Burn Ratio's ability to map burn severity in the boreal forest and tundra ecosystems of Alaska's national parks' *International Journal of Wildland Fire* **17**, 463–475.

Avery TE, Berlin GL (1992) 'Fundamentals of Remote Sensing and Airphoto Interpretation. 5th' *Prentice Hall, London*.

Boucher J, Beaudoin A, Hébert C, Guindon L, Bauce É, Hebert C, Guindon L, Bauce E (2017) 'Assessing the potential of the differenced Normalized Burn Ratio (dNBR) for estimating burn severity in eastern Canadian boreal forests.' *International Journal of Wildland Fire* **26**, 32–45. doi:10.1071/WF15122

Bowman DMJS, Balch JK, Artaxo P, Bond WJ, Carlson JM, Cochrane MA, D'Antonio CM, DeFries RS, Doyle JC, Harrison SP (2009) 'Fire in the Earth system' *science* **324**, 481–484.

Cansler CA, McKenzie D (2012) ‘How robust are burn severity indices when applied in a new region? Evaluation of alternate field-based and remote-sensing methods’ *Remote sensing* **4**, 456–483.

Chen XX, Vogelmann JE, Rollins M, Ohlen D, Key CH, Yang LM, Huang CQ, Shi H (2011) ‘Detecting post-fire burn severity and vegetation recovery using multitemporal remote sensing spectral indices and field-collected composite burn index data in a ponderosa pine forest.’ *International Journal of Remote Sensing* **32**, 7905–7927. doi:10.1080/01431161.2010.524678

Churchill DJ, Larson AJ, Dahlgreen MC, Franklin JF, Hessburg PF, Lutz JA (2013) ‘Restoring forest resilience: From reference spatial patterns to silvicultural prescriptions and monitoring’ *Forest Ecology and Management* **291**, 442–457. doi:10.1016/j.foreco.2012.11.007

Chuvieco E (1999) ‘Measuring changes in landscape pattern from satellite images: short-term effects of fire on spatial diversity’ *International Journal of Remote Sensing* **20**, 2331–2346.

Cocke AE, Fulé PZ, Crouse JE (2005) ‘Comparison of burn severity assessments using Differenced Normalized Burn Ratio and ground data’ *International Journal of Wildland Fire* **14**, 189–198.

Doerr SH, Santín C (2016) ‘Global trends in wildfire and its impacts: perceptions versus realities in a changing world’ *Philosophical Transactions of the Royal Society B: Biological Sciences* **371**, 20150345.

Eidenshink J, Schwind B, Brewer K, Zhu ZL, Quayle B, Howard S (2007a) ‘A project for monitoring trends in burn severity’ *Fire Ecology Special Issue* **3**, 2–21.

Eidenshink J, Schwind B, Brewer K, Zhu Z, Quayle B, Howard S (2007b) ‘A project for monitoring trends in burn severity. Fire Ecology 3 (1): 3-21’ *Fire Ecology Special Issue Vol* **3**, 4.

Epting J, Verbyla D, Sorbel B (2005) ‘Evaluation of remotely sensed indices for assessing burn severity in interior Alaska using Landsat TM and ETM+’ *Remote Sensing of Environment* **96**, 328–339.

Fernandez-García V, Quintano C, Taboada A, Marcos E, Calvo L, Fernandez-Manso A (2018) ‘Remote Sensing Applied to the Study of Fire Regime Attributes and Their Influence on Post-Fire Greenness Recovery in Pine Ecosystems’ *Remote Sensing* **10**, 733. doi:http://dx.doi.org/10.3390/rs10050733

French NHF, Kasischke ES, Hall RJ, Murphy KA, Verbyla DL, Hoy EE, Allen JL (2008) ‘Using Landsat data to assess fire and burn severity in the North American boreal forest region: an overview and summary of results’ *International Journal of Wildland Fire* **17**, 443–462.

Giglio L, Randerson JT, Van Der Werf GR (2013) ‘Analysis of daily, monthly, and annual burned area using the fourth-generation global fire emissions database (GFED4)’ *Journal of Geophysical Research: Biogeosciences* **118**, 317–328. doi:10.1002/jgrg.20042

de Groot WJ (2006) ‘Modeling Canadian wildland fire carbon emissions with the Boreal Fire Effects (BORFIRE) model’ *Forest Ecology and Management* S224.

Hall RJ, Freeburn JT, De Groot WJ, Pritchard JM, Lynham TJ, Landry R (2008) 'Remote sensing of burn severity: experience from western Canada boreal fires' *International Journal of Wildland Fire* **17**, 476–489.

He T, Belcher CM, Lamont BB, Lim SL (2016) 'A 350-million-year legacy of fire adaptation among conifers' *Journal of Ecology*. doi:10.1111/1365-2745.12513

Holden ZA, Evans JS (2010) 'Using fuzzy C-means and local autocorrelation to cluster satellite-inferred burn severity classes.' *International Journal of Wildland Fire* **19**, 853–860. doi:10.1071/WF08126

Hoy EE, French NHF, Turetsky MR, Trigg SN, Kasischke ES (2008) 'Evaluating the potential of Landsat TM/ETM+ imagery for assessing fire severity in Alaskan black spruce forests' *International Journal of Wildland Fire* **17**, 500–514.

Hudak AT, Morgan P, Bobbitt MJ, Lentile LB (2007) 'Characterizing stand-replacing harvest and fire disturbance patches in a forested landscape: A case study from Cooney Ridge, Montana'

Jain TB, Graham RT, Pilliod DS (2004) 'Tongue-tied: confused meanings for common fire terminology can lead to fuels mismanagement' *Wildfire July/August: 22-26* 22–26.

Jelinski DE, Wu J (1996) 'The modifiable areal unit problem and implications for landscape ecology' *Landscape ecology* **11**, 129–140.

Jia GJ, Burke IC, Goetz AFH, Kaufmann MR, Kindel BC (2006) 'Assessing spatial patterns of forest fuel using AVIRIS data' *Remote Sensing of Environment* **102**, 318–327.

Johnstone JF, Chapin FS (2006) ‘Effects of soil burn severity on post-fire tree recruitment in boreal forest’ *Ecosystems* **9**, 14–31.

Karau EC, Sikkink PG, Keane RE, Dillon GK (2014) ‘Integrating Satellite Imagery with Simulation Modeling to Improve Burn Severity Mapping’ *Environmental Management* **54**, 98–111. doi:http://dx.doi.org/10.1007/s00267-014-0279-x

Keeley JE (2009) ‘Fire intensity, fire severity and burn severity: a brief review and suggested usage’ *International Journal of Wildland Fire* **18**, 116–126. doi:10.1071/WF07049

Kennedy PL, Fontaine JB (2009) ‘Synthesis of knowledge on the effects of fire and fire surrogates on wildlife in US dry forests’

Key CH, Benson NC (1999) Measuring and remote sensing of burn severity. In ‘Proc. Jt. fire Sci. Conf. Work.’, 284. (University of Idaho and International Association of Wildland Fire Moscow, ID)

Key CH, Benson NC (2006) ‘Landscape assessment (LA)’ *FIREMON: Fire effects monitoring and inventory system Gen Tech Rep RMRS-GTR-164-CD, Fort Collins, CO: US Department of Agriculture, Forest Service, Rocky Mountain Research Station*.

Lachowski H, Hardwick P, Griffith R, Warbington R, Parsons A (1997) ‘Faster, better data: For burned watersheds needing emergency rehab’ *Journal of Forestry*. doi:10.1093/jof/95.6.4

Lentile LB, Holden ZA, Smith AMSS, Falkowski MJ, Hudak AT, Morgan P, Lewis SA, Gessler PE, Benson NC (2006) ‘Remote sensing techniques to assess active fire characteristics and post-fire effects’ *International Journal of Wildland Fire* **15**, 319–345.

doi:10.1071/WF05097

Loboda T V, French NHF, Hight-Harf C, Jenkins L, Miller ME (2013) 'Mapping fire extent and burn severity in Alaskan tussock tundra: An analysis of the spectral response of tundra vegetation to wildland fire' *Remote Sensing of Environment* **134**, 194–209.

Macdonald SE (2007) 'Effects of partial post-fire salvage harvesting on vegetation communities in the boreal mixedwood forest region of northeastern Alberta, Canada' *Forest Ecology and Management* **239**, 21–31.

Mallinis G, Mitsopoulos I, Chrysafi I (2018) 'Evaluating and comparing Sentinel 2A and Landsat-8 Operational Land Imager (OLI) spectral indices for estimating fire severity in a Mediterranean pine ecosystem of Greece' *Giscience & Remote Sensing* **55**, 1–18. doi:10.1080/15481603.2017.1354803

McCarley TR, Kolden CA, Valliant NM, Hudak AT, Smith AMS, Kreitler J (2017) 'Landscape-scale quantification of fire-induced change in canopy cover following mountain pine beetle outbreak and timber harvest' *Forest Ecology and Management* **391**, 164–175. doi:10.1016/j.foreco.2017.02.015

Meng Q, Meentemeyer RK (2011) 'Modeling of multi-strata forest fire severity using Landsat TM Data' *International Journal of Applied Earth Observation and Geoinformation* **13**, 120–126.

Miller JD, Knapp EE, Key CH, Skinner CN, Isbell CJ, Creasy RM, Sherlock JW (2009) 'Calibration and validation of the relative differenced Normalized Burn Ratio (RdNBR) to

three measures of fire severity in the Sierra Nevada and Klamath Mountains, California, USA' *Remote Sensing of Environment* **113**, 645–656.

Miller JD, Quayle B (2015) 'Calibration and validation of immediate post-fire satellite-derived data to three severity metrics.' *Fire Ecology* **11**, 12–30. Available at http://fireecologyjournal.org/docs/Journal/pdf/Volume11/Issue02/012.pdf

Miller JD, Thode AE (2007) 'Quantifying burn severity in a heterogeneous landscape with a relative version of the delta Normalized Burn Ratio (dNBR)' *Remote Sensing of Environment* **109**, 66–80.

Miller JD, Yool SR (2002) 'Mapping forest post-fire canopy consumption in several overstory types using multi-temporal Landsat TM and ETM data' *Remote Sensing of Environment* **82**, 481–496.

Morgan P, Hardy CC, Swetnam TW, Rollins MG, Long DG (2001) 'Mapping fire regimes across time and space: understanding coarse and fine-scale fire patterns' *International Journal of Wildland Fire* **10**, 329–342.

Morgan P, Keane RE, Dillon GK, Jain TB, Hudak AT, Karau EC, Sikkink PG, Holden ZA, Strand EK (2014) 'Challenges of assessing fire and burn severity using field measures, remote sensing and modelling' *International Journal of Wildland Fire* **23**, 1045–1060. doi:10.1071/WF13058

Murphy KA, Reynolds JH, Koltun JM (2008) 'Evaluating the ability of the differenced Normalized Burn Ratio (dNBR) to predict ecologically significant burn severity in Alaskan

boreal forests' *International Journal of Wildland Fire* **17**, 490–499.

Openshaw S (1981) 'The modifiable areal unit problem' *Quantitative geography: A British view* 60–69.

Parks SA, Holsinger LM, Koontz MJ, Collins L, Whitman E, Parisien M-A, Loehman RA, Barnes JL, Bourdon J-F, Boucher J, Boucher Y, Caprio AC, Collingwood A, Hall RJ, Park J, Saperstein LB, Smetanka C, Smith RJ, Soverel N (2019) 'Giving Ecological Meaning to Satellite-Derived Fire Severity Metrics across North American Forests' *Remote Sensing* **11**, 1735. doi:10.3390/rs11141735

Pratt S, Holsinger L, Keane RE (2006) 'Using simulation modeling to assess historical reference conditions for vegetation and fire regimes for the LANDFIRE prototype project' *The LANDFIRE prototype project: nationally consistent and locally relevant geospatial data for wildland fire management* 277–314.

Quintano C, Fernandez-Manso A, Calvo L, Marcos E, Valbuena L, Fernández-Manso A, Calvo L, Marcos E, Valbuena L (2015) 'Land surface temperature as potential indicator of burn severity in forest Mediterranean ecosystems.' *International Journal of Applied Earth Observation and Geoinformation* **36**, 1–12. doi:10.1016/j.jag.2014.10.015

Ryan KC, Noste N V (1985) 'Evaluating prescribed fires' *Lotan, James E; Kilgore, Bruce M; Fischer, William C* 15–18.

De Santis A, Chuvieco E (2007) 'Burn severity estimation from remotely sensed data: Performance of simulation versus empirical models' *Remote Sensing of Environment* **108**,

422–435.

De Santis A, Chuvieco E (2009) ‘GeoCBI: a modified version of the Composite Burn Index for the initial assessment of the short-term burn severity from remotely sensed data.’ *Remote Sensing of Environment* **113**, 554–562. doi:10.1016/j.rse.2008.10.011

Schepers L, Haest B, Veraverbeke S, Spanhove T, Borre J Vanden, Goossens R (2014) ‘Burned Area Detection and Burn Severity Assessment of a Heathland Fire in Belgium Using Airborne Imaging Spectroscopy (APEX)’ *Remote Sensing* **6**, 1803–1826. doi:http://dx.doi.org/10.3390/rs6031803

Sikkink PG (2015) Comparison of six fire severity classification methods using Montana and Washington wildland fires. In ‘Keane, Robert E.; Jolly, Matt; Parsons, Russell; Riley, Karin. Proc. large Wildl. fires Conf. May 19-23, 2014; Missoula, MT. Proc. RMRS-P-73. Fort Collins, CO US Dep. Agric. For. Serv. Rocky Mt. Res. ’, 213–226

Sorbel B, Allen J (2005) ‘Space-based burn severity mapping in Alaska’s National Parks’ *Alaska Park Science* **4**, 4–11.

Soverel NO, Perrakis DDB, Coops NC (2010) ‘Estimating burn severity from Landsat dNBR and RdNBR indices across western Canada’ *Remote Sensing of Environment* **114**, 1896–1909.

Sunar F, Özkan C (2001) ‘Forest fire analysis with remote sensing data’ *International Journal of Remote Sensing* **22**, 2265–2277. doi:10.1080/01431160118510

Turner MG (2010) ‘Disturbance and landscape dynamics in a changing world’ *Ecology*.

doi:10.1890/10-0097.1

Turner MG, Hargrove WW, Gardner RH, Romme WH (1994) ‘Effects of fire on landscape heterogeneity in Yellowstone National Park, Wyoming’ *Journal of Vegetation Science* **5**, 731–742.

White JD, Ryan KC, Key CC, Running SW (1996) ‘Remote sensing of forest fire severity and vegetation recovery’ *International Journal of Wildland Fire* **6**, 125–136.

Wulder MA, White JC, Alvarez F, Han T, Rogan J, Hawkes B (2009) ‘Characterizing boreal forest wildfire with multi-temporal Landsat and LIDAR data’ *Remote Sensing of Environment* **113**, 1540–1555.

Zhu Z, Key C, Ohlen D, Benson N (2006) ‘Evaluate sensitivities of burn severity mapping algorithms for different ecosystems and fire histories in the United States. Final report JFSP 01-1-4-12’ *October* **12**, 35.

CHAPTER 2. DIFFERENT APPROACHES MAKE COMPARING STUDIES OF BURN SEVERITY CHALLENGING: A REVIEW OF METHODS USED TO LINK REMOTELY SENSED DATA WITH THE COMPOSITE BURN INDEX

2.0 ABSTRACT

Field observations of the Composite Burn Index (CBI) are commonly linked to remotely sensed data to understand spatial and temporal patterns of burn severity. However, to date a comprehensive understanding of the tradeoffs between different methods used to model CBI with remotely sensed data is lacking. To fully understand the current state of the science, provide a blueprint towards conducting broad-scale meta-analyses, and identify key decision points and potential rationale, we conducted a review of studies that linked remotely sensed data to continuous estimates of burn severity measured with the CBI and related methods. We provided a roadmap of the wide array of different routes that have been taken and examine potential rationales used to justifying them. We found that different methods used across studies introduces variations that makes it difficult to compare outcomes. Additionally, the existing suite of comparative studies focus on one or few of many possible sources of uncertainty. Thus, compounding error and propagation throughout the many decisions made during analysis is not well understood. Finally, we highlighted key gaps in existing research and provide suggestions for future work, including a broad set of methodological information and key rationales for decision-making that could facilitate future reviews.

2.1 INTRODUCTION

Estimates of burn severity (the ecological effects of fire, or fire-caused change, Lentile *et al.* 2006) inform immediate post-fire recovery projects, future fuel treatments, and long-term ecosystem analysis (Miller and Thode 2007). In the immediate post-fire environment, common priorities are to preserve the soil and maintain the vegetation community (Fernandez-García *et al.* 2018). A second key function of severity assessments is to understand how fire effects vary with ecosystem composition and structure. Linking pre-fire conditions with potential post-fire outcomes helps managers to design better fuel treatments, such as thinning and prescribed fires (*e.g.*, Churchill *et al.* 2013, 2022; Larson *et al.* 2022). Severity estimates can also help to predict long-term consequences to a post-fire ecosystem (Macdonald 2007), such as changes to forest succession (Johnstone and Chapin 2006). Managers need predictive models of wildland fire effects on vegetation communities, wildlife populations, and hydrologic function (Sorbel and Allen 2005), and ongoing records of fire effects allow ecologists to assess effects of climate change over time.

Commonly measured fire effects on the ground include consumption of vegetation, destruction of leaf chlorophyll, exposed soil, charred stems, and altered moisture (Epting *et al.* 2005). These ecological impacts lead to spectral, thermal, and structural changes on the land surface, which can be captured by remote sensors (Epting *et al.* 2005; Mallinis *et al.* 2018). Combinations of these post-fire soil and vegetation conditions, including those with multiple ecosystem attributes, are used to assess severity (**Table 2.1**). Methods may be quantitative or qualitative; all incorporate a choice of fire-related variables that depend on management and ecological objectives as well as sampling scale (Key and Benson 2006). Post-fire site characteristics are

typically considered relative to the pre-disturbance environment (*e.g.*, Miller and Thode, 2007), so severity is also a subjective measurement that can change with the time of observation and information available (Lentile *et al.* 2006).

Table 2.1 Ecosystem attributes used to evaluate burn severity.

Table adapted from De Santis and Chuvieco (2009).

Ecosystem component	**Ecosystem attributes assessed**	**Studies**
Soil	Char and ash cover	Smith et al. (2005)
	Soil and ash color	Neary et al. (2004)
	Consumption and charring of organic soil profiles	Charron and Grene (2002); Johnstone and Chapin (2006); Robichaud et al. (2007)
	Volatilization or transformation of soil components to soluble mineral forms	Turner et al. (1994); Wang et al. (2002); Wells and Campbell (1979)
Vegetation	Percentage of tree mortality	Chappell and Agee (1996)
	Decrease in plant cover	Jain and Graham (2004); Rogan and Yool (2001)
	Canopy consumption and tree mortality	Choung et al. (2004); Dillon et al. (2011); Greene et al. (2004); Isaev et al. (2002); Miyanishi and Jonson ; Odion and Hanson (2006)
	Degree of canopy consumption and mortality	Doerr et al. (2006); Kokaly et al.(2007); Kushla and Ripple (1998); Patterson and Yool (1998); Rogan and Franklin (2001); Ryan and Noste (1985)
	Char height	Knapp and Keeley (2006)
	Proportion of bole circumference scorched/charred	
	Deep Charring	Harvey et al. (2014); Talucci and Krawchuk (2019)

	Proportion of fine branches remaining on the canopy	Moreno and Oechel (1989)
Composite	Combination of factors such as consumption of organic horizon, degree of standing trees, and degree of canopy consumption and mortality	Key and Benson (2002); Michalek et al. (2000); Ryan and Noste (1985); van Wagtendonk et al. (2004)
	Composite Burn Index (CBI) or Geometrically Structured Composite Burn Index (GeoCBI)	De Santis and Chuvieco (2009); Key and Benson (1999)

However, the size and variability of wildland fires pose several challenges for characterizing fire effects on the ground (Chen, Vogelmann, *et al.* 2011). First, accessing remote locations where fires have occurred requires resource-intensive and logistically challenging fieldwork (Morgan *et al.* 2014). Second, the heterogeneity in burn severity across burned landscape requires many plots to represent the range of conditions in burned areas (Morgan *et al.* 2014). Finally, many burned areas are poorly represented spatially from field plots alone, due to the sheer size of burned areas relative to the size and number of field plots that are logistically possible (De Santis and Chuvieco 2007).

Remote sensing is a powerful tool to understand spatial patterns across burned landscapes, providing a synoptic view from space- or airborne sensors, (Lentile *et al.* 2006; Wulder *et al.* 2009; Soverel *et al.* 2010) and allowing observation of post-fire effects inaccessible from the ground (Key and Benson 2006; Lentile *et al.* 2006; Murphy *et al.* 2008). That said, while remotely sensed data provide extensive spatial and temporal coverage that field observations lack (Schepers *et al.* 2014), they must be linked to 'ground-truth' field data (Morgan *et al.* 2014). The

choice of field data depends on the goals of the study; there is no one-size-fits-all approach to evaluating severity (Keeley 2009). The range of potential research questions and applications of these assessments requires different approaches determined by a combination of management, ecological goals, and field sampling designs (Ryan and Noste 1985).

The Composite Burn Index (CBI) (Key and Benson 2006) integrates multiple metrics across vegetation strata and soil, which, used together (as a measure of site burn severity), provide an overall scope of fire damage (**Figure 2.1**). Finally, individual components of the index may also be considered separately, depending on post-fire management needs (Key and Benson 2006; Zhu *et al.* 2006; Keeley 2009). CBI has been adapted in many ways, including general modifications such as the geometrically structured CBI (GeoCBI, De Santis and Chuvieco 2009) and site-specific modifications such as adding or omitting specific attributes.

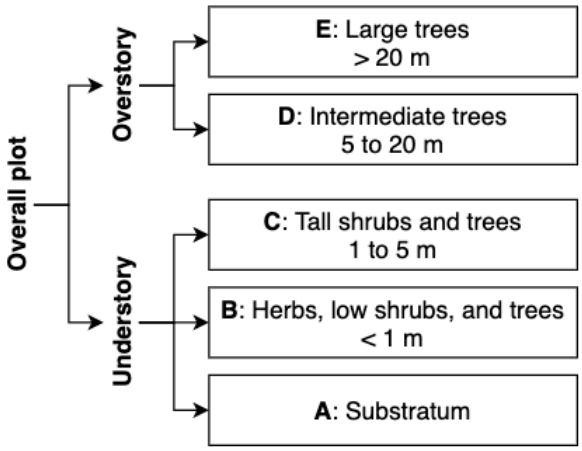

Figure 2.1 Hierarchical structure of the Composite Burn Index (CBI).

CBI has emerged as a popular measure of field-based severity in remote sensing for several reasons. First, the rapid protocol allows quick deployment and assessment over large landscapes (Parks *et al.* 2019). Second, CBI has generally robust relationships with field measures (Saberi *et*

al. 2022) and satellite spectral fire severity indices (French *et al.* 2008), providing strong support for the its use to estimate fire effects across landscapes (Parks *et al.* 2019). Third, for general assessments of severity, the CBI may be more complete than other classification systems based on single indicators of burn severity (Sikkink 2015).

In addition to the CBI, several alternative composite severity measures have been published in the fire ecology literature. The Geometrically Structured CBI (GeoCBI) accounts for differences in fractional cover of each stratum and changes in leaf area index (LAI) for the intermediate and tall tree strata (De Santis and Chuvieco 2009). Fractional cover and LAI describe the influence of vegetation cover on reflectance of different strata within a given plot and from a remote sensing point of view, the spectral response of a plot is strongly related to the vegetation coverage per stratum (De Santis and Chuvieco 2009). In addition to GeoCBI, other modified versions the CBI have been used, including a Weighted CBI (WCBI) (*e.g.*, Cansler and McKenzie, 2012) and a Burn Severity Index (BSI) (Loboda *et al.* 2013). The WCBI generally uses the original CBI protocol for sampling severity across strata, however it weights scores by the fraction of cover for each stratum. While the method is like the GeoCBI in that regard, specific weights are study dependent. The BSI was introduced by Loboda et al. (2013) as a less rigorous approach that mimics CBI plots but saves time in the field.

Many field measures of severity were designed to scale across broad landscapes using remotely sensed data, based on the underlying ecological causes that drive changes in spectral reflectance between pre- and post-fire landscapes (**Table S2.1**). The ecosystem attributes characterized by the CBI and related composite severity measures span the range of change expected to be captured by remotely sensed data. Overall, studies that use remotely sensed data to link to

continuous field measures based on composite severity measures follow a similar methodological framework to each other (**Figure 2.2**). However, key decisions are made at each step. Differences in these decisions result in studies that use many unique avenues, and we have limited understanding on how that may affect findings across studies. The range of choices available for analysis at each step may, in totality, be considered a "decision menu" that depends on the research questions and preferred methodological approaches of the study author(s).

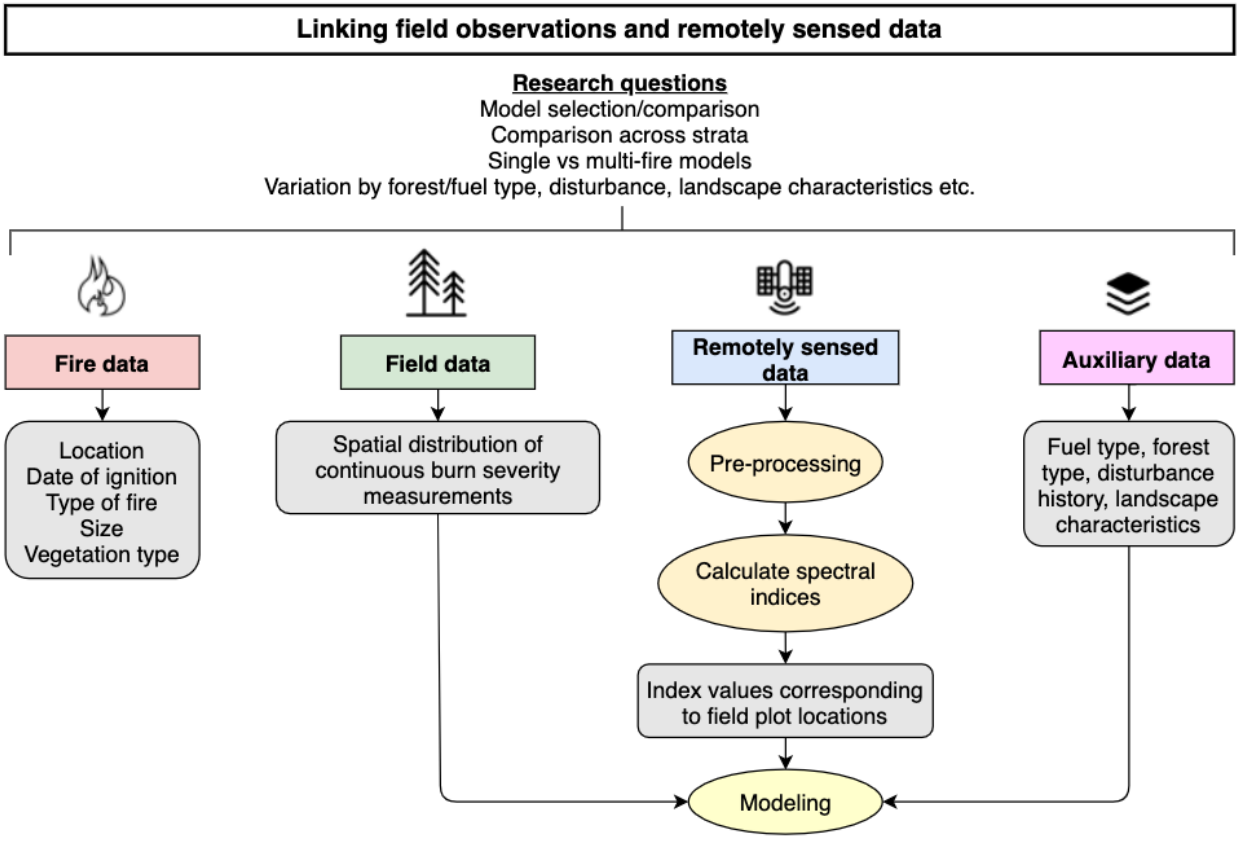

Figure 2.2 Flow diagram showing framework of methods for study design that relate remotely sensed data to continuous measurements of burn severity from the CBI and similar composite severity indices.

To our knowledge, no study has yet summarized the methods and important decision points that link remotely sensed data to CBI as a continuous measure. However, studies such as Stambaugh

et al. (2015) demonstrate the potential for methodological decisions to strongly influence the relationships between remotely sensed data and field observations. For example, R^2 values for the same set of plots ranged from 0.18 to 0.78 depending on whether models used remotely sensed data from initial versus extended assessments, were processed with interpolation or not, and used the delta normalized burn ratio (dNBR) or relativized dNBR (RdNBR). This example highlights the difficulty of comparing model results across studies where methodologies may differ. However, the existing body of literature linking CBI measures to remotely sensed data lacks a comprehensive review of the possible methodological choices that can be made during analysis. This paper seeks to conduct a review of the many choices of the "decision menu" and identify the limitations imposed by the lack of consensus in modeling approaches.

2.1.1 Research questions

The goal of this review was to compare empirical methods used to estimate burn severity measured with CBI both in the field and through remote sensing to understand the impacts of key analytical decisions and research gaps in the existing literature. We did this by exploring:

1. Where and when have studies been conducted?
2. How is burn severity measured in the field?
3. How is burn severity measured from satellites?
4. How are field observations and remotely sensed data modeled together?

Addressing these key questions from our review of 62 studies will improve our understanding of the state of the science regarding sampling of post-fire environments and the ability to map burned landscapes using remotely sensed data. Additionally, the aggregation of research results from the numerous studies that used a variety of analytical methods will provide insights into

whether findings may be generalized across studies or are too study specific to interpret in such a manner.

2.2 METHODS

2.2.1 Review framework

We developed a procedure to guide our process for conducting a systematic literature search, identifying relevant articles, and extracting data for analysis. This review broadly follows the framework developed by Pullin and Stewart (2006) for conducting systematic reviews in conservation and environmental management. While their guidelines for conducting systematic reviews are based on evaluating the effectiveness of management and policy interventions, we used their approach only to develop a search protocol and to identify and review relevant studies to generate a database from papers that used remotely sensed data and continuous measures of burn severity based on the CBI. Therefore, our work does not investigate the efficacy of a specific treatment (*e.g.,* mechanical thinning or prescribed fire) as the systematic review protocol dictates. Our search criteria were based on fire and field measurements and four remote sensing technologies (optical, thermal, radar, and lidar) (**Table 2.2**). For each criterion, a set of keywords was developed for the database queries (Section 2.2).

Table 2.2 Search criteria used during review.

Criterion	Keywords
Fire	Wildfire, burn, fire, severity
Field measurements	Composite burn index, CBI, geometrically structured composite burn index, GeoCBI

Optical data	Landsat, satellite, optical, reflectance, spectral, spectral index, normalized burn ratio, relative normalized burn ratio, relative burn ratio, differenced normalized burn ratio, NBR, dNBR, RdNBR, RBR
Thermal data	Thermal, land surface temperature, LST
Radar data	Radar, synthetic aperture radar, SAR, L-band, X-band, C-band, backscatter
Lidar data	Lidar, light detection and ranging, laser, altimetry

2.2.2 Database queries

The CAB Direct (https://www.cabdirect.org), Environmental Science Collection (https://proquest.libguides.com/environmentalsciencecollection), and Web of Science (https://www.webofknowledge.com) databases were systematically searched for original research that investigated the relationships between remotely sensed data and continuous measures of burn severity assessed with the Composite Burn Index (Key and Benson 2006) or Geometrically Structured Composite Burn Index (De Santis and Chuvieco 2009). Search terms were combined through Boolean operators so that each query contained the keywords for fire, field measurements, and one remote sensing technology. We used the resulting expression to search abstracts in each database. After combining the results from all three databases, duplicate entries were removed (**Figure S2.1**). Any studies that we missed would mainly have been studies published in a journal outside of our database queries (CAB Direct, Environmental Science Collection, Web of Science) or not having the keywords in our search.

2.3 Screening and data extraction

Articles were screened to determine whether each entry met the inclusion criteria. Articles were excluded if they (1) did not use CBI/GeoCBI measurements, (2) used simulated CBI/GeoCBI or simulated remotely sensed data, (3) did not analyze CBI/GeoCBI measurements as continuous

variables, or (4) were not in English. We focus on the use of CBI as a continuous variable because it provides a more flexible approach than categorical measures which classify measurements into bins such as low, moderate, and high severity. Continuous data can be adapted to multiple different ecological phenomena. For example, different studies may use various threshold breakpoints for different levels of severity depending on the model used and the user's needs (Boucher *et al.* 2017) or chosen according to the relevant ecological effects (Hall *et al.* 2008; Cansler and McKenzie 2012). However, severity values are frequently classified in order to compare multiple fires, analyze spatial patterns, or communicate with managers regarding prioritization of response (Cansler and McKenzie 2012). Readers may find additional insights into the use of categorical observations of severity in Cansler and McKenzie (2012).

We selected all empirical studies published in peer-reviewed scientific journals through 2019, excluding published literature reviews, dissertations and theses, and government reports. All articles matching the review criteria were retained regardless of the study's location or ecosystem type. Four additional articles were found through searching the literature cited of the papers included in our search. The articles that met our inclusion criteria were reviewed to extract the relevant information which was entered in a rubric format. The data for each paper were captured in individual databases for information at the article level (**Table S2.2**), fire level (**Table S2.3**), and comparison level (**Table S2.4**). We compiled 62 studies based on the structured database queries, identifying five sections to include in this review (**Table 2.3**). A list of studies included in this review and the number field observations to remotely sensed data comparisons extracted for analysis are included in **2.7.1 Supplementary Information**.

Table 2.3 Sections included in review.

Section	Topics
Study information	Year published, journal
Fire data	Location, timing, type, size
Field data	Modifications, types, distribution by severity, timing, location
Remotely sensed data	Sensor, timing, atmospheric corrections, relative radiometric normalization, georeferencing/co-registration, indices used, dNBR offset, index value extraction methods
Linking models	Models used, field data as predictor or response, evaluation metrics, investigation by strata, single- or multi-fire models

2.2.4 Analysis

To locate fires examined by studies included in this review, we used a combination of georeferenced study maps, the published manuscripts, provided coordinates, or ancillary databases (*e.g.*, *Fire Bundles*, n.d., *Fire Perimeters*, 2020; Picotte et al., 2019; Sikkink et al., 2013). Fires were mapped for cases where we could confidently identify the study fire based on name, location, size, number of field plots, or other identifying characteristics. The spatial mapping of fires allowed us to overlay terrestrial ecosystems of the world (Olson and Dinerstein 2002) and identify which ecosystems may be more or less understood. For fire size, information was found either in the study itself or through ancillary databases.

While our focus was on the use of burn severity as a continuous variable, many included studies that used continuous data in their analysis also reported thresholds used for classifying burn severity. In such cases, we recorded the distribution of field plots classified by unburned, low, moderate, or high burn severity. These data were assessed in two ways: (1) by summing the

number of plots per severity category across the studies, and (2) calculating the proportion of plots placed into different burn severity classes. By assessing classified data, we were able to present some results on the variability of the threshold values used to bin continuous observations. Additionally, because many studies did not show a distribution of continuous plot severity scores, we used this subset of studies that provided classified distributions to gain some understand of how plot severity varied across studies.

To assess the timing of field campaigns, we used the date of ignition for the fire and date of field sampling. The smallest temporal grain we could identify for cases was to the nearest month. Results were limited to studies that reported both the timing of fires (or studied fires that where ignition date was available elsewhere) and the timing of field campaigns.

In some cases, we contacted authors to ask for information not provided in published manuscripts such as field plot size and timing, index value extraction methods, etc. All summary statistics and figures – with the exception of the study map – were conducted using the R programming language (Team 2017). Where presented, standard deviations were calculated using the population standard deviation equation (Zar 1999). Due to missing information, some summary statistics and analyses are based only on cases where data were available. The number of studies, fires, or comparisons for each analysis are presented in each relevant table or figure caption or in the figure itself.

2.3 RESULTS

2.3.1 Study information

2.3.1.1 Studies using CBI, interannual trends, and main journals

The systematic search resulted in 62 papers published in 2004-2019. All used field measures of burn severity based on the CBI protocol (CBI, GeoCBI, WCBI, BSI) as a continuous measure to integrate with remotely sensed data. One to nine papers were published each year ($\mu = 4.1$, $\sigma = 2.2$; **Figure S2.2a**), with no significant linear trend over time ($t = 1.422$, $p = 0.179$). The 62 articles were in 17 scientific journals; half (31) were in either *Remote Sensing of Environment* or *International Journal of Wildland Fire* (**Figure S2.2b**).

2.3.2 Fire data

2.3.2.1 Location of fires

For the 62 studies, 352 of 401 fires were uniquely identified and geospatially located (**Figure 2.3a**). Study fires were most commonly located in temperate conifer forests (185 fires). Less commonly studied ecosystems included boreal forests/taiga (51), temperate broadleaf and mixed forests (47), and deserts and xeric shrublands (38), Mediterranean forests, woodlands, and scrubs (19), and tundra (9). One fire was studied in each of the following: flooded grasslands and savannas, temperate grasslands, savannas and shrublands, and tropical and subtropical grasslands, savannas and shrublands. Fires that were sampled were mostly in the Northern Hemisphere, especially in the United States (283) and Canada (22). Fires were also sampled in China (17), Spain (15), Russia (5), Australia (2), Greece (2), and Belgium, Portugal, and Burkina

Faso (1 each). Two fires from Miller et al. (2009) and 36 from Parks et al. (Parks *et al.* 2019) lacked sufficient information to identify the locations of fires. In the United States, fires were mainly in temperate conifer forests, deserts and xeric shrublands in the West.

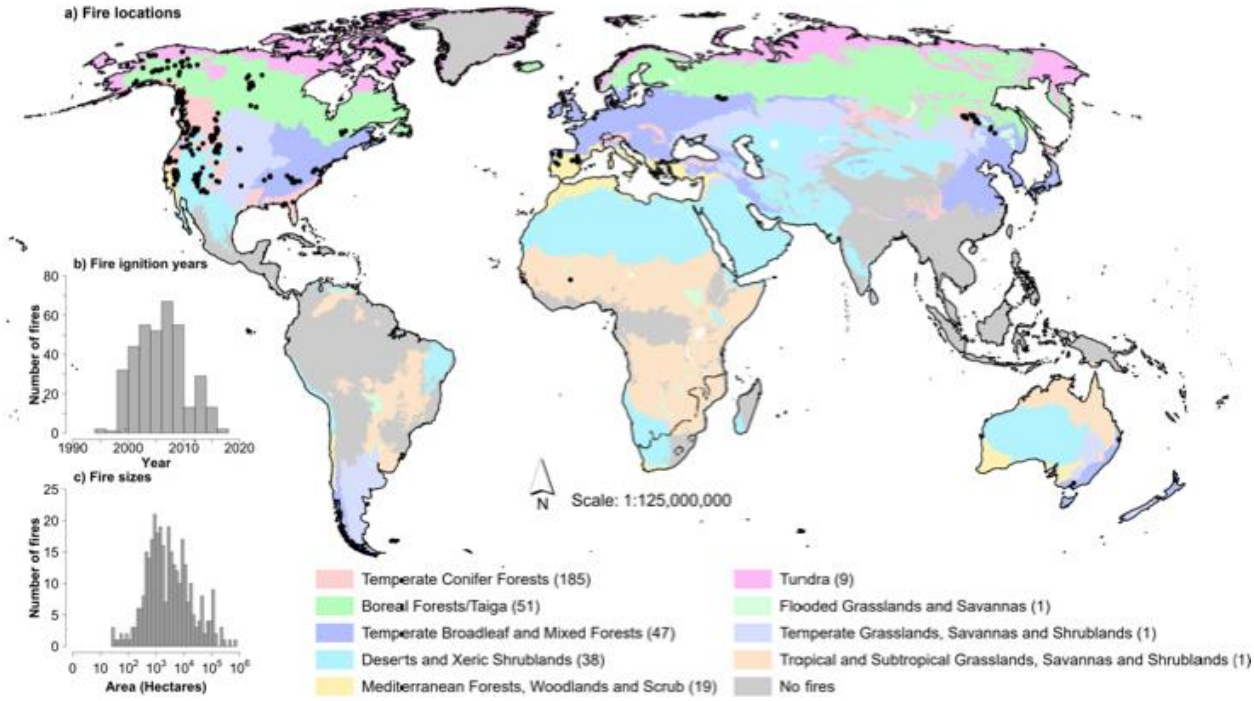

Figure 2.3. (a) Location of fires (black dots) and ecosystem type (N = 352 fires). The number of fires in each ecosystem type are shown in parentheses in the key. (b) Years of fire ignition (N = 401 fires). (c) Fire sizes ($\log_{10}$ hectares) (N = 328 fires). Note: 401 fires were identified in the studies reviewed, but some lacked information on size or location.

2.3.2.2 Number of fires per study

Each study reported 1-263 fires (mean = 9.9 ± 4.9; median per study = 3); 23 investigated a single fire. Of the 62 studies reviewed, only 53 explicitly stated the number of fires in the analysis. The other nine studies either reported multiple or several fires (7), an unknown number (1), or did not specify (1).

2.3.2.3 Timing and type of fires

The earliest identified fire occurred in 1994 and the latest in 2017 (**Figure 2.3b**); 401 unique fires with known ignition dates were identified. Most fires (194 / total) were either explicitly labeled as wildfires or classified as such by MTBS. Others were prescribed fires (74), wildland use fires (28), a combination of prescribed and wildland fires (1). Of the remaining 104 fires, four specified only that they were caused by lightning; the rest (96) did not explicitly identify fire type, but most were likely also wildland fires.

2.3.2.4 Fire sizes

For the 328 fires where information was available, the range of fire sizes was 28-730,855 ha (μ = 18,005, σ = 58,067; **Figure 2.3c**); the majority (65%) were <5,000 ha. The sizes of 74 fires were not explicitly given or found in supplementary searches; sometimes this information was not stated (44), was provided as a sum across several fires (3), or the study reported only the regional burn area and not the specific fire studied (1).

2.3.3 Field data

2.3.3.1 Types of field data used and variation by year

van Wagtendonk et al. (2004) was the first study to use CBI as a continuous measure of burn severity following its introduction at a Joint Fire Science Conference and Workshop by Key and Benson (1999) (**Figure 2.4a**). Studies using the GeoCBI as a continuous variable to link to remotely sensed data were first published in 2009 (De Santis and Chuvieco 2009). While most of the studies reviewed relied on these protocols, four investigated modifications such as weighted

versions (WCBI) (Soverel *et al.* 2010; Cansler and McKenzie 2012; Mallinis *et al.* 2018) or Burn Severity Index (Loboda *et al.* 2013) (**Table 2.4**). The GeoCBI, WCBI, and Burn Severity Index emerged as alternate approaches to field sampling, but CBI remained the most common composite severity measure throughout this review.

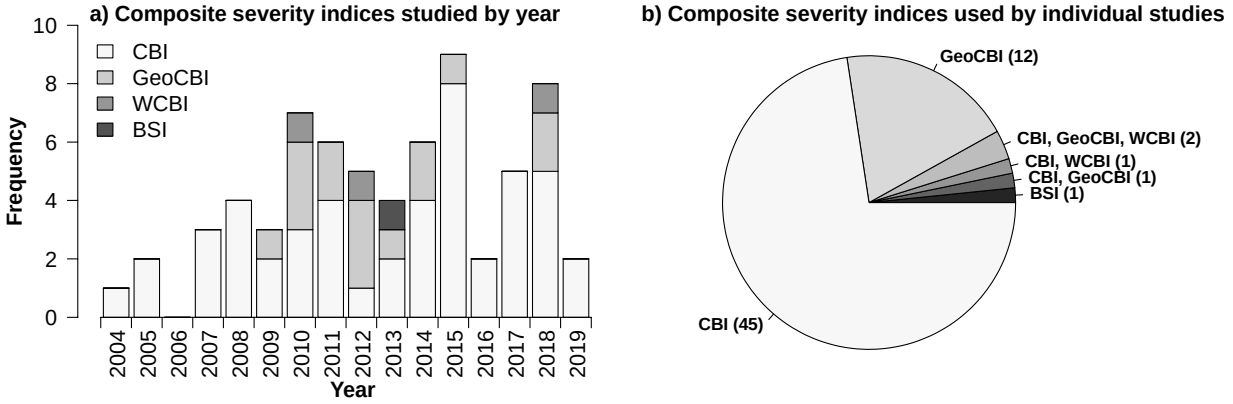

Figure 2.4 (a) Number of reviewed studies that included measurements of Composite Burn Index (CBI), Geometrically Structured CBI (GeoCBI), Weighted CBI (WCBI), or Burn Severity Index (BSI) by year (N = 62). The same study could be in multiple bins if it measured more than one composite severity index. (b) Composite severity indices used by individual studies (N = 62). The number of studies that used each index or combination of indices is in parentheses.

Table 2.4 Types of field data used in studies.

Field measure	Description	Studies
Composite Burn Index (CBI)	Continuous measure of severity using 22 ecosystem attributes averaged across five strata	Key and Benson (2006)
Geometrically Structured CBI (GeoCBI)	Original CBI protocol, but weights by fractional cover of each stratum and incorporates changes in leaf area index (LAI) for intermediate and tall tree strata	De Santis and Chuvieco (2009)

Weighted CBI (WCBI)	Original CBI protocol, but weights scores by fractional cover for each stratum	Cansler and McKenzie (2012)
	Original CBI protocol, but weights each stratum by its estimated percent coverage within plot, with double weight assigned to overstory trees	Soverel et al. (2010)
	Original CBI protocol, but weights each stratum by its estimated percent coverage within plot, with additional 50% weight assigned to overstory trees	Mallinis et al. (2018)
Burn Severity Index (BSI)	Rates field plots according to a 4-point scale (unburned, low, moderate, severe); rates the fractional assessment of burn severity within plots; converts the score for each to a single value by weighting the 4-point scale by the fraction of the plot affected by each severity class	Loboda et al. (2013)

Most (57) studies used a single method (*e.g.*, CBI, GeoCBI, or WCBI) to measure burn severity on the ground; CBI on its own comprised 45 of the 62 papers reviewed in this study, while GeoCBI alone was used in 12 studies (**Figure 2.4b**). Only three papers incorporated multiple methods of measuring severity on the same fire and were compared whether different field methods resulted in better or worse relationships with remotely sensed data (De Santis and Chuvieco 2009; Cansler and McKenzie 2012; Mallinis *et al.* 2018). A fourth study (Soverel *et al.* 2010) collected two types of field data but did not compare their performance in the analysis.

2.3.3.2 Modifications to CBI protocols

The established CBI protocol was sometimes modified for individual study purposes (**Table 2.5**). We identified five ways that the method was adapted, including omitting or adding ecosystem components, modifying the strata height thresholds relative to site-specific vegetation

characteristics, modifying strata weights when calculating overall plot severity, and implementing altered protocols that streamline measurements.

Table 2.5 Modifications of the Composite Burn Index (CBI) protocol.

Modification	Description	Studies
Omitted components	Omit components not present	Allen and Sorbel (2008), Epting et al. (2005), Fernández-García et al. (2018)
	Omit components requiring knowledge of pre-fire environment	
	Omit components relevant to extended assessments	Fernández-García et al. (2018)
Added components	Add components tailored to specific ecosystem	Hoy et al. (2008), Schepers et al. (2014)
Modified height strata	Modify strata height thresholds to match ecosystem structure	Hoy et al. (2008), Stambaugh et al. (2015), Whitman et al. (2018)
Modified strata weights	Used different weights for individual strata when calculating overall plot severity scores	Cansler and McKenzie (2012), Mallinis et al. (2018), Soverel et al. (2010)
Altered protocol	Streamline CBI field sampling, with continuous measures (*e.g.*, %) where possible	Tanase et al. (2015a; b)
	"CBI-like" measurements	Tanase et al. (2015a; b)

2.3.3.3 Inclusion of unburned field plots and

Studies varied in whether they measured unburned plots in addition to burned plots and if they did, varied in how they included them in their analyses. Including unburned plots would extend

the range of the remote sensing measurements to include values for both vegetation that did not burn and vegetation that did burn. Most commonly, the reviewed studies did not specify whether they measured unburned plots in addition to burned plots (24 studies) (**Figure 2.5a**). However, nearly as many studies did include unburned field plots on the sampled fires (21). Additionally, several studies that sampled multiple fires included at least one fire with unburned field plots and one without (3). Two studies collected unburned field plots but excluded them from some analyses; of those, one study excluded the unburned plots altogether, and one excluded them from the continuous severity analysis but not the classification analysis. When unburned field plots were not measured on the ground, some studies incorporated "pseudo-unburned" field plots (5), where areas outside the fire perimeter were assumed to have a CBI (or other burn severity measurement) score of "0" or unburned. Otherwise, unburned field plots were not sampled at all, either on the ground or through remotely sensed data (6).

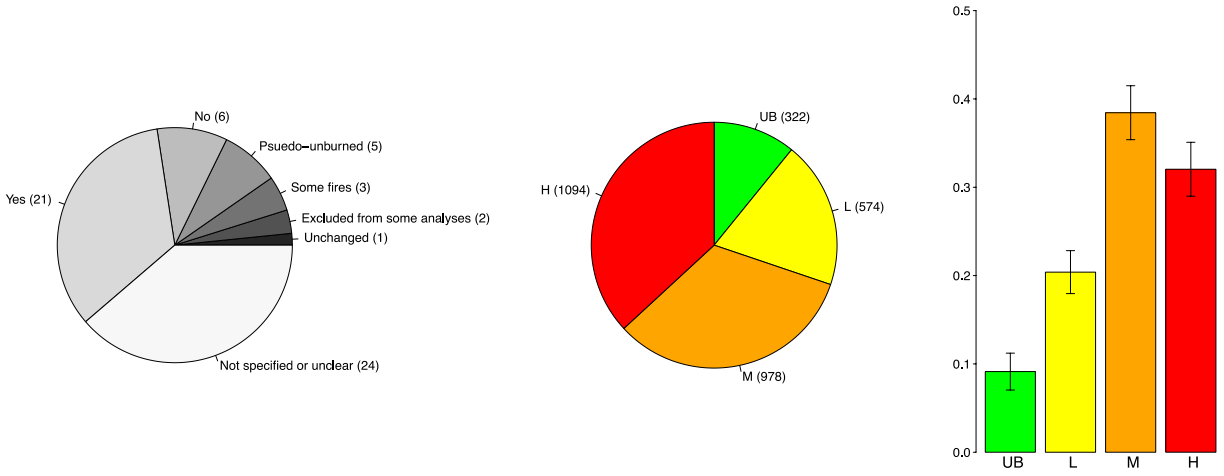

Figure 2.5 (a) Proportions of studies that included unburned plots (N=62 studies). The number of studies (N) of each unburned type are in parentheses. (b) Proportions of field plots by severity class across all fires where information was (N = 21 studies). The number of plots (N) by severity class are in parentheses (N = 2,968 plots). (c) Mean distribution of plots by severity class for each fire; error bars show standard errors of the means (N = 2,968 plots). UB: unburned; L: low; M: moderate; H: high severity.

2.3.3.4 Distribution by severity

The distribution of field plots classified by burn severity (unburned, low, moderate, high) was provided in 21 studies (a combined 2,968 plots). (1) The counts of plots were summed by severity category across studies. In this case, high severity was the most common classification (**Figure 2.5b**); of all field data measured across all studies, there were more high severity plots than any other category. (2) Data were assessed by calculating the proportion of plots placed into different burn severity classes by each study. Here, the highest proportion of plots were in moderate severity areas, followed by high severity, then low severity (**Figure 2.5c**). This means that each study, on average, measured more moderate-severity areas. However, the specific thresholds considered for each severity category varied by study (**Table 2.6**).

Table 2.6 Composite Burn Index (CBI) minimum scores for low-, moderate-, and high-severity classes across studies that provided categorical severity thresholds (N = 17 studies).

CBI ratings range from 0 (unburned/unchanged) to 3 (high severity). See individual study thresholds in **Table S5**.

Statistic	Low	Moderate	High
Average (μ)	0.18	1.23	2.18
Standard deviation (σ)	0.28	0.16	0.13
Minimum	0	1	1.85
Maximum	1.04	1.76	2.25

2.3.3.4 Number of plots per fire and relationship to fire size

For the 357 fires that had recorded plot counts, the average number of plots used per fire was 37.0 (σ = 53.4); 44 fires had no recorded plot counts (**Figure 2.6a**). Both fire size and plot count information were available for 320 fires. The number of plots used per fire increases with fire size, but, as fires get more massive, the plots used increase more slowly (**Figure 2.6b,** log-log slope estimate = 0.2246, $p < 0.001$, $R^2 = 0.10$).

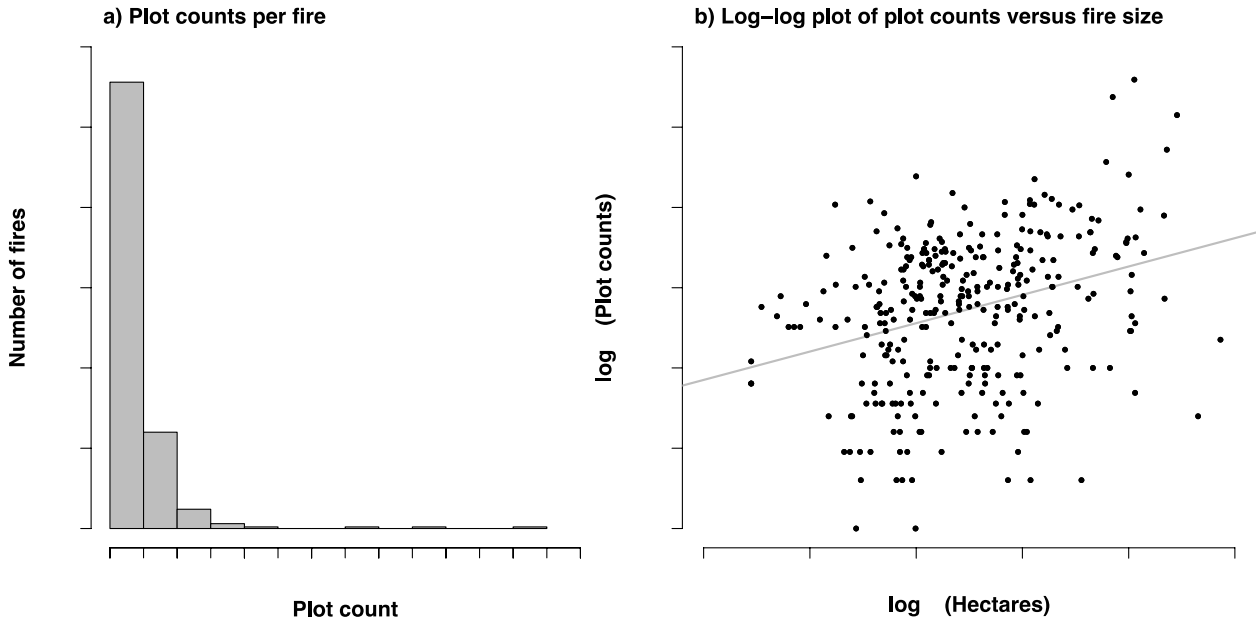

Figure 2.6 (a) Plots counts per fire (N = 357 fires). (b) Log-log plot of number of plots used versus fire size in hectares (N = 320 fires). The grey line shows a linear model fitted through the log-log transformed data.

2.3.3.5 Size and timing of field plots

For the 159 fires where both the date of fire occurrence and timing of field plot measurements were reported, field campaigns occurred 1-40 months after the fire began, with an average delay of 10.5 (σ = 6.0) months (**Figure 2.7a**). Plot size was reported for 137 fires (range = 13-6362 m^2 , average = 1331.0 m^2, σ = 1734.5; **Figure 2.7b**). For these fires, plots were mostly circular (105 fires) and sometimes square (32 fires).

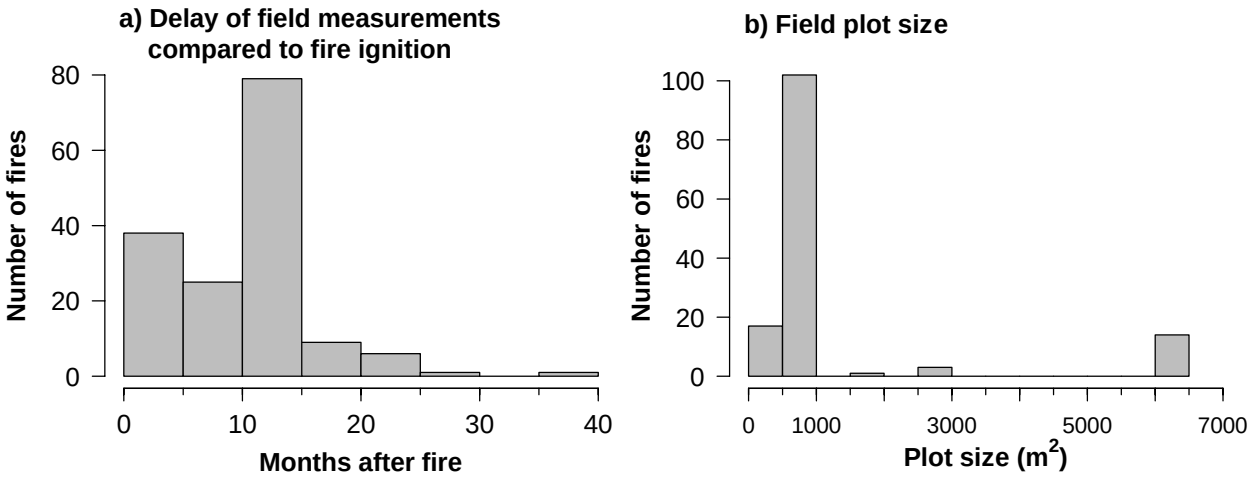

Figure 2.7 (a) Delay of field measurements after fire ignition (N = 159 fires). (b) Field plot size (N = 137 fires).

2.3.3.6 Spatial distribution of field plots

Most studies located field plots using a stratified approach based on homogenous areas identified by dNBR, as suggested in the FIREMON Landscape Assessment protocol (Key and Benson 2006). However, two studies (Schepers *et al.* 2014; Warner *et al.* 2017) located plots in random locations. Schepers et al. (2014) used a split approach, with field measurements in both homogenous and random locations; the randomly located plots were more heterogenous in both burn severity and vegetation type. Warner et al. (2017) used a random approach combined with relatively many samples, which enabled a simpler and more direct estimate of the accuracy of their remotely sensed severity map.

2.3.4 Remotely sensed data

2.3.4.1 Remote sensor technologies

The most used sensors were from the Landsat program (**Table S2.6**). Studies using the Landsat 4-5 (Thematic Mapper, TM) and Landsat 7 (Enhanced Thematic Mapper (ETM+) satellites were the most numerous (60 studies combined), followed by Landsat 8 Operational Land Imager (OLI, 8) and unspecified Landsat sensors (6). Most studies relied on sensors that acquired multispectral imagery with wavelengths encompassing the visible, near infrared, shortwave infrared, and thermal regions of the electromagnetic spectrum (56). Other sensors did not sample at higher wavelengths and thus did not collect shortwave infrared or thermal data. Two studies used Synthetic-aperture radar. Sensors were mounted on platforms ranging from satellites to airplanes to uncrewed aerial vehicles (UAVs).

2.3.4.2 Resolution of remotely sensed data

Because the most used sensors were from the Landsat program, most studies used remotely sensed data with a 30 m spatial resolution. The coarsest spatial resolution (1000 m) was associated with MODIS on NASA Terra and Aquas satellites (Holden *et al.* 2010; Kolden and Rogan 2013; Hultquist *et al.* 2014; Zheng *et al.* 2016), and the finest (0.02 m) was from imagery collected by a consumer-grade RGB camera (Fraser *et al.* 2017).

2.3.4.3 Number of sensors used and inclusion of single or bitemporal data

Most studies used a single sensor (49) or included two sensors (11) (**Figure S2.3a**). Two studies included three or four sensors. For our analysis, all Landsat sensors (TM, ETM+, OLI,) were

combined, so studies using more than one sensor do not reflect those which used different Landsat satellites for pre/post fire imagery. We identified five ways that studies incorporated two or more sensors in their analysis (**Table 2.7**). All studies that used more than one sensor included data from at least one of the Landsat satellites. All but one study that used multiple sensors also collected optical and sometimes also thermal data. The exception was Tanase et al. (2015a) who included both optical and Synthetic aperture radar (SAR) data.

Table 2.7 Five ways that studies incorporated two or more sensors into their analysis.

Ways studies incorporated two or more sensors	**Studies**
Used optical sensors interchangeably with those from the Landsat program	Karau and Keane (2010), De Santis and Chuvieco (2009)
Compared model performance between Landsat and at least one other sensor	Fraser et al. (2017), Garcia-Llamas et al. (2019), Holden et al. (2010), Mallinis et al. (2018),van Wagtendonk et al. (2004), Veraverbeke et al . (Veraverbeke *et al.* 2012), Wu et al. (2015)
Compared model performance between Landsat and at least one other sensor, along with their synergy	Chen et al. (2015), Tanase et al. (2015a)
Down-sampled low-resolution imagery to use in conjunction with Landsat data	Kolden and Rogan (2013)
Incorporated MODIS data as auxiliary information to estimate LST from Landsat imagery	Zheng et al. (2016)

Regarding single and bitemporal remotely sensed data, studies mostly included bitemporal imagery (38) (**Figure S2.3b**). Sixteen studies that included bitemporal data also analyzed relationships using single-date indices. The least common strategy was to include only single-date indices (8); three of these were based on Multiple Endmember Spectral Mixture Analysis.

2.3.4.4 Atmospheric corrections (absolute radiometric corrections)

The studies reviewed used several atmospheric correction methods for optical data; most common were top of atmosphere (or at-sensor reflectance, 23 studies) or surface reflectance derived by various methods (28) (**Figure S2.4**). Eight studies did not specify the level of radiometric correction. Of those, two stated only radiometric corrections were used, and three stated only that atmospheric corrections were used. Of the studies using surface reflectance, the most commonly stated method was Dark Object Subtraction (DOS, 9), followed by the cosine of the solar zenith angle correction (COST, 4) (Chavez 1996). Other studies used unspecified surface reflectance (15) or used different methods depending on which band was assessed (1) One study quantified the effect of using four atmospheric correction methods (Fang and Yang 2014).

2.3.4.5 Relative radiometric normalization

Some bi-temporal datasets used pseudo-invariant features (PIFs) to conduct radiometric normalization or assess its necessity (10 studies). Most commonly, studies that conducted relative radiometric normalization used PIFs to regress the pre-fire values against the post-fire values (4), but normalization of post-fire reflectance to the pre-fire image also occurred (1). The remaining studies that identified PIFs examined them and found that no further relative radiometric normalization was required (5). Except for one case, there was no mention of how PIFs were located; that study that specified that its method used the iteratively re-weighted multivariate alteration detection (IR-MAD) algorithm to select PIFs, which were then used to normalize the target images on a band-wise basis. The other studies that did not identify PIFs stated that no scene-to-scene radiometric normalization was applied (2) or used pre-processed

imagery prepared by the Monitoring Trends in Burn Severity (MTBS), Burned Area Emergency Response (BAER), or Rapid Assessment of Vegetation Condition after Wildfire (RAVG) programs (5). The remaining 43 studies did not evaluate the need for relative radiometric normalization.

2.3.4.6 Georeferencing/co-registration

Georeferencing/co-registration was used in some bitemporal datasets to reduce geometric error between image pairs (**Table 2.8**). Studies usually did not specify any type of georeferencing or co-registration (27 studies). For the studies that explicitly stated that they did use co-registration, the most common method was to co-register data between image pairs (10). For methods used in the remaining studies, see **Table 2.8**.

Table 2.8 Specified methods for georeferencing/co-registration used by studies.

Method	Number of studies
Did not specify use of co-registration	27
Co-registered data between image pairs	10
Co-registering image pairs to a high-resolution orthophoto	3
No co-registration was performed	3
Data misalignment was inspected visually or quantitatively, and co-registration was not needed	3
Use data that is not co-registered (MTBS)	3
Both co-registration between image pairs and co-registration to a high-resolution orthophoto (differed by sensor)	1
Unspecified geometric normalization	1

Most studies that undertook co-registration used ground control points to tie images together (specifying 30, 34, 40, 80, or enough control points to achieve specified RMSE; 5 studies). One study used the Imagine Autosync feature in ERDAS, which matches images using automatically generated tie-points. Studies that reported the accuracy of co-registration (6) did so using either pixel accuracy or RMSE. Pixel accuracy was reported within 0.5 pixels (1) or 1 pixel (1); RMSE was reported using pixel units (4) at levels of 0.014, 0.16, 0.5 or lower, and 0.5. Transformations used included first-order (2), second-order (3), and third-order (1) polynomials. Resampling methods reported were nearest neighbor (2) and bilinear (1).

2.3.4.7 Types of indices

Most indices used in the studies reviewed were based on the optical region of the electromagnetic spectrum, which incorporates portions of the visible, infrared, and shortwave infrared regions (**Figure 2.8a**). Less common were mixed indices, combining spectral regions with thermal indices, followed by thermal- and radar-based indices. Regarding temporal form, indices were mostly single-date or bitemporal using an absolute (pre-post) difference (**Figure 2.8b**). Less common were relativized bitemporal indices (*e.g.*, RdNBR, RBR). Finally, the least temporal used types of indices were bitemporal ratio indices (pre/post) (2 indices: Radar Burn Ratio, image ratioing) and combination bitemporal absolute difference and single-date NBR and NDVI were among the most studied spectral indices. The top three indices were based on NBR: dNBR (50 studies), followed by RdNBR (25), and NBR (19) (**Figure 2.8c**). The next most common indices were dNDVI (18 studies) and NDVI (12). Although 105 indices were related to CBI, most appeared in only one or two studies (76 indices; see **Table S2.7**).

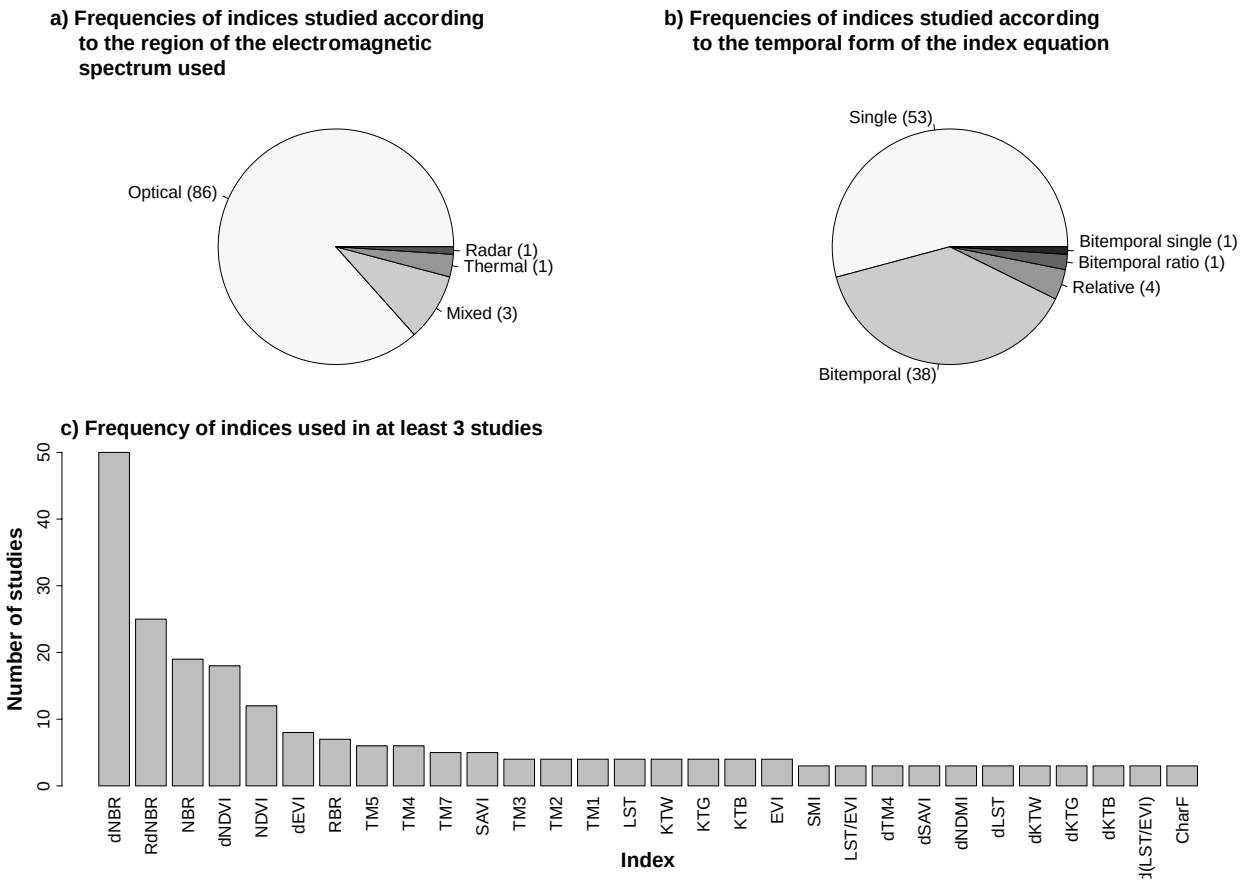

Figure 2.8 (a) Frequencies of indices studied (N = 105 indices) according to the region of the electromagnetic spectrum used. Optical: *visible, near infrared, and shortwave infrared*; Mixed: *combination of optical and thermal*. (b) Frequencies of indices studied (N = 105 indices) according to the temporal form of the index equation. Single: *single-date index*; Bitemp: *bitemporally differenced (pre-post) index*; Relative: *relativized bitemporal index*; Bitemp-ratio: *bitemporal ratio (pre/post) index*; Bitemp-single: *combination of bitemporally differenced and single-date index*. (c) Frequency of indices used in at least 3 studies (76 additional indices were used in only one or two studies; for more detail, including description of index abbreviations, see **Table S2.7**).

2.3.4.8 Number of indices per study and combinations of temporal form

The mean number of indices used in each study was 5.0 (σ = 5.7), with up to 26 indices in a single study (**Figure 2.9a**). Absolute difference pre/post-fire indices were the most common (50 studies), followed by relativized bi-temporal indices (26), single-date post-fire indices (23), and

ratio indices (3). Most commonly, studies included only absolute indices (21, **Figure 2.9b**). Many studies had both absolute and relativized indices (13); absolute, relativized, and single-date indices (10); or just single-date indices (8). Less commonly, studies reported a combination of single and absolute indices (4) or only relativized indices (3). Least used were absolute, single-date, and ratio indices; absolute and ratio indices; or just ratio indices (1 study each).

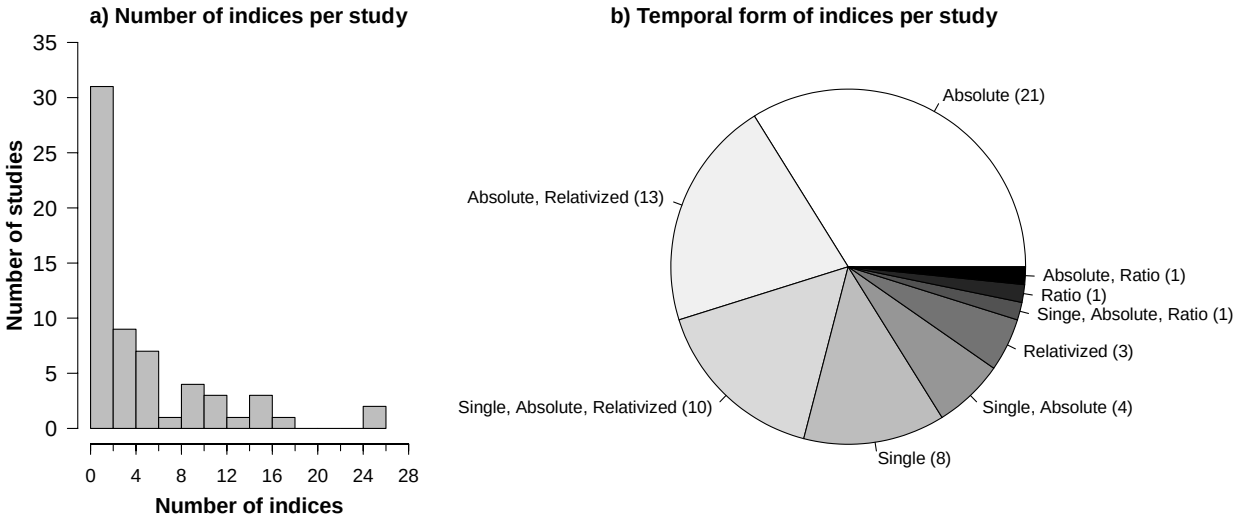

Figure 2.9 (a) Number of indices used per study. (b) Proportions of studies using indices of different temporal form. Number of studies for each method is shown in parentheses.

2.3.4.9 dNBR offset

Most of the studies reviewed (54 of 62) included dNBR as a spectral index. However, the majority of those studies (34) did not include a dNBR offset value (**Figure 2.10**). We found that eight studies did not specify whether an offset value was included or not. Six studies did explicitly state that an offset was included. Additionally, two studies provided analyses both with and without an offset, and two other studies tested whether including an offset value improved the relationship with field data but ultimately excluded it from their analyses. Finally, two studies

used MTBS/BAER data, which includes an offset value for RdNBR indices, but not in the calculation of dNBR.

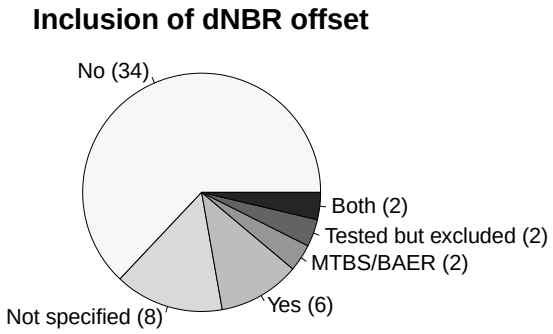

Figure 2.10 Number of studies that included a dNBR offset for those that used dNBR as an index (N = 62 studies). The number of studies for each method is shown in parentheses.

2.3.4.10 Pixel value extraction methods

Many studies (22) did not specify how the value of indices for field plots was determined (**Table 2.9**). The studies that did specify their method most commonly extracted the value of the pixel over plot center (14), used a 3x3 focal mean window centered on the plot (12), or bilinear smoothing (7). For smoothing types used in the remaining 9 studies, see **Table 2.9**.

Only two studies quantitatively compared different smoothing methods; one compared bilinear with no smoothing (Stambaugh *et al.* 2015), and one used four methods for QuickBird imagery in their comparison with ASTER and Landsat data (Holden *et al.* 2010).

Table 2.9 Pixel value extraction methods by citation including parameters and frequency of use in studies (N = 62 studies).

Pixel value extraction method	Description	Parameters	Frequency
None specified	N/A		22
None	Pixel value overlaying plot center		14
Focal mean	Mean is calculated for the pixels encountered in a neighborhood around a cell	3x3	12
		6x6	1
		12x12	1
Bilinear	Mean is calculated for the values of the four nearest pixels to plot center weighted by their distance to the point		7
Mean values of sample points within plot	Mean of pixel values overlaying sample points within plot	5	2
		175	1
		900	1
Area-weighted	Weighted plot averaging; weights assigned based on each pixel's percentage of area within a plot		3
Mean values of pixels within distance of plot	Mean of pixel values for cells falling within specified distance of plot	within 15 m of plot center (weighting center double)	1
		4 pixels closest to plot center	2
Object-based	Mean of pixel values within defined objects		1

2.3.5 Linking models

2.3.5.1 Model(s) used and field data as predictor or response

Fifteen classes of models were used in analyses (**Table 2.10**); the most common was linear regression (36 comparisons), followed by quadratic regression (17), and exponential models (9). For the models used in the remaining 30 comparisons, see **Table 2.10**.

Table 2.10 Models used in analysis and (a) whether field data was a predictor or (b) response variable, (c) analysis was based only on correlation, or (d) not specified (N = 108 comparisons).

Model type	**Model form**	**(a) Predictor**	**(b) Response**	**(c) Correlation**	**(d) Not specified**
Pearson	$\rho_{X,Y} = \frac{cov(X,Y)}{\sigma_X \sigma_Y}$			6	
Spearman	$r_s = \rho_{rgX,rgY}$ where raw scores X_i, Y_i are converted to ranks rgX_i, rgY_i			2	
Linear	$y = a + bx$	29	7		1
Quadratic	$y = ax^2 + bx + c$	16	1		
Cubic	$y = ax^3 + bx^2 + cx + d$	1	1		
Natural	$y = \ln(ax + b)$	2			
logarithm	$y = a\ln(x) + b$	1			
	$y = a * \ln\left(\frac{bx+c}{d}\right)$		1		
Exponential	$y = a + bx^c$	1			
	$y = a + b * exp(bx)$		4		
	$y = ax^b$	1			
	$y = ab^x$	1			
	$y = ae^{bx}$		1		

	$y = 1 - exp(ax)$	1			
Saturated	$y = x(ax + b)^{-1}$	3			
growth	$y = x(a\|x\| + b)^{-1}$	1			
Gompertz	$y = a + (b - a)exp\left[-exp\left[c * exp(1) * (d - x)/\left((b - a) * log(10)\right) + 1\right]\right]$	1			
Sigmoidal	$y = a - b(ln(c/x) - 1)$		1		
Non-linear	Not specified	2	2		
Multiple linear regression	Study-dependent	4	1		
GAM	Study-dependent	1			
Regression tree	Study-dependent	1			
SVR	Study-dependent	2			
RF	Study-dependent	2			
GPR	Study-dependent	1			
Total		75	19	8	1

Field data were much more commonly used as a predictor variable (75 comparisons) than as a response variable (19). This pattern held across almost all general model types. However, for three models, field data was used solely as a response variable: the natural logarithm model, the exponential models, and the sigmoidal model. For cubic and unspecified non-linear models, the same number of comparisons used field data as a predictor variable and a response variable. Eight analyses just reported correlation statistics between the two observation methods.

2.3.5.2 Model performance metrics

Many methods were used assess or quantify the performance of models that related remotely sensed data to field plots (**Table 2.11**). The most common metric was R^2 (46 studies), followed by RMSE (17), R^2_{adj} (14), p (13), and r (13). Most studies used a single evaluation metric (24) or two metrics (27, **Figure S2.5**). Eleven studies assessed three or four metrics.

Table 2.11 Model performance metrics and their frequency of occurrence.

Metric	Description	Frequency
R^2	Coefficient of determination: proportion of the variance in the dependent variable that is predictable from the independent variable(s)	46
RMSE	Root-mean-square error: measure of the differences between values (sample or population values) predicted by a model or an estimator and the values observed	17
R^2_{adj}	Adjusted R^2: accounts for the phenomenon of the R^2 automatically and spuriously increasing when extra explanatory variables are added to the model	14
p	Probability value: probability of obtaining test results at least as extreme as the results actually observed, assuming that the null hypothesis is correct	13
r	Pearson correlation coefficient: linear correlation between two variables *X* and *Y*	13
	Actual versus fitted graph: visualization of actual versus predicted values	9
AIC	Akaike information criterion: estimator of out-of-sample prediction error and thereby relative quality of statistical models for a given set of data	3
r_s	Spearman's rank correlation coefficient: nonparametric measure of rank correlation (statistical dependence between the rankings of two variables)	3
BIC	Bayesian information criterion: criterion for model selection among a finite set of models; the model with the lowest BIC is preferred. It is based, in part, on the likelihood function and it is closely related to the Akaike information criterion (AIC).	1

MAE	Mean absolute error: measure of errors between paired observations expressing the same phenomenon	1
RSE	Residual standard error: standard deviation of its sampling distribution or an estimate of that standard deviation	1

2.3.5.3 Field plot measurements by strata

The CBI rating encompasses five vegetation strata, commonly separated into understory (A-C) and overstory (D-E) components (**Figure 2.1**). Of the 62 studies reviewed, 14 modeled CBI across strata. Three methods investigated whether relationships between field observations and remotely sensed data varied by strata (**Table 2.12**). The most common method separately modeled the understory components (A-C), overstory components (C-D), and overall severity (5 studies). Studies also modeled each individual stratum separately (4), or modeled the soil or substrate component (A) and surface or vegetation components (B-E) as well as the composite or overall severity (3 studies). Only two studies modeled just the overstory components (D-E) and overall severity.

Table 2.12 Different ways of partitioning ecosystem strata for modeling.

Methods for modeling strata	**Studies**
Model each stratum separately	Allen and Sorbel (2008), Chen et al. (Chen *et al.* 2015), Meng and Meentemeyer (2011), Stambaugh et al. (2015)
Combine individual strata to model the understory (substratum; herbs, low shrubs, and trees <1 m; tall shrubs and trees 1-5 m), overstory (intermediate trees	Chen et al. (2011), Hoy et al. (2008), Tanase et al. (2011), Warner et al. (2017),Wu et al. (2015)

5-20 m; tall trees > 20 m), and overall severity separately	
Model only overstory and overall severity	Tanase et al. (2015b; a)
Model the soil (or substrate), surface (or vegetation), and overall or composite measures of severity separately	Fernández-García et al. (2018), Garcia-Llamas et al. (2019), Kolden and Rogan (2009)

2.3.5.3 Single-fire vs multi-fire models

Most studies analyzed single-fire local models (33); in other words, relationships between field plots and remotely sensed data were fire-specific (**Figure S2.6**). Other studies investigated regional models (19), combined field plots across multiple fires, or evaluated both local and regional models (10).

2.4 DISCUSSION

This review highlights the many ways that continuous measures of severity based on the CBI have been linked to remotely sensed data and outlines the range of methods and decisions in the process. Five main topics were investigated: (1) study information, (2) fire data, (3) field data, (4) remotely sensed data, and (5) linking models. Overall, we found wide variability in the methodological decisions and analytical tools used by the included studies. This finding raises the challenge of knowing whether differences between studies results are driven by site-specific ecological and fire differences or were affected by differences in the methodological approaches. Additionally, we found several key research gaps that warrant future investigation. Finally, we encourage future studies to provide explicit description and justification behind their

methodological approaches to make comparisons among findings in separate studies more possible.

2.4.1 Comparative investigations

There is no one consensus for the best way to connect field observations to remotely sensed data, and uncertainties exist at every decision point. First of all, there is no universal, one-size-fits-all approach to evaluating burn severity (Cocke *et al.* 2005; Keeley 2009). While some studies suggest more utility that tree-level measurements that directly assess ecological effects may be preferable to a composite index that aggregates semi-quantitative estimates of change across a plot (Morgan *et al.* 2014; Furniss *et al.* 2020), the choice of assessment should be determined by management, ecological purposes, and field sampling designs (Ryan and Noste 1985). We identified, where available, analyses that compared important decision points in linking field observations of CBI as a continuous variable to remotely sensed data. The numerous analytical decisions and paths that studies applied prevented strong generalizations from being made, especially considering that relatively few studies compared multiple approaches at key decision points in the workflow. Of those that did, many returned mixed results. Consequentially, the choice of how burn severity is measured and modeled influences study outcomes.

One such example relates to the comparison of different composite severity measures (CBI, GeoCBI, and WCBI). Three studies (De Santis and Chuvieco 2009; Cansler and McKenzie 2012; Mallinis *et al.* 2018) compared multiple ground measures of severity and found that no one method seemed to in the greatest correspondence between field- and satellite-based estimates of burn severity across different regions. For both Cansler and McKenzie (2012) and Mallinis et al. (2018), who both included analysis of CBI, GeoCBI, and WCBI, the best performing field

measurement depended on which spectral index (and in the case of Mallinis et al. (2018), which sensor) was used. De Santis and Chuvieco (De Santis and Chuvieco 2009) compared CBI and GeoCBI and found that GeoCBI peformed best for two of the three fires assessed, while CBI performed best on the third. Thus, while metrics of fractional cover, leaf area index, or other weighting approaches did in some cases improve burn severity models, the mixed results failed to provide a convincing answer as to which composite severity measure is best.

Another example of the lack of consensus about how to sample fires relates to the inclusion of unburned and low-severity field plots in the field sample set, which provides an anchor at the low range of CBI for assessing relationships with remotely sensed data. The bias that we identified of field plots tending towards moderate- and high-severity areas likely occurs for two reasons: (1) attempts to overcome the saturation of remotely sensed indices at high severities (van Wagtendonk *et al.* 2004; De Santis *et al.* 2010; Veraverbeke *et al.* 2012; Parks *et al.* 2014) and (2) the importance of these areas to management (Robichaud 2000; Miller and Thode 2007; French *et al.* 2008; Cansler and McKenzie 2012; Fernández-García *et al.* 2018). While we found substantial variation in the thresholds used in classification, it was clear that the underrepresentation of lower range of severities occurred despite that variation. The fact that only one of the two studies that excluded unburned plots from their analysis (Murphy *et al.* 2008) provided a rationale (the unburned sites (CBI = 0) disproportionately influenced the linear fit to produce remaining non-liner residual structure) highlights the need for more comparative analyses in this realm.

These examples highlight the uncertainty that often remains following quantitative assessments of methodological approaches. This is not unique to methods based on composite severity

indices, however, as Furniss et al. (2020) found that estimates of tree-level metrics such as mortality of stems and basal area could vary widely for a single spectral index value. Such uncertainties are unsatisfying and provide reason for caution when applying methodologies developed in one context, for example based on a single fire or ecosystem type, outside the scope of inference. For example, some influential studies (like Cansler and McKenzie's (2012) comparison of multiple pixel value extraction methods) are widely cited by subsequent investigators but without validating their effectiveness in subsequent studies or in new regions. However, such studies may be highly site- and context-specific and it is unclear how broadly applicable their results are. In other cases, attempts to compare different approaches, such as using sensors with varying spatial resolution, are confounded by lurking variables – in this case the spectral resolution of different sensors and the spatial synchrony with field plots (van Wagtendonk *et al.* 2004; Holden and Evans 2010; Tanase *et al.* 2015a; Mallinis *et al.* 2018; Garcia-Llamas *et al.* 2019). While several of these studies found slight improvements were found for sensors with high spatial resolution compared to Landsat imagery (Holden and Evans 2010; Mallinis *et al.* 2018; Garcia-Llamas *et al.* 2019), it is difficult to disentangle their results to isolate the effects of the spatial resolution of the sensors. Finally, there may not yet exist any comparative studies in the current literature assessing the effect of georeferencing remotely sensed data on model results. While 27 of 62 studies conducted or investigating need for georeferencing (or co-registration between image pairs), no studies presented comparative analysis of the impacts on model results.

Realistically, only studies that replicate their methodological approach (*e.g.*, use similar methods of collecting field observations, include unburned field plots, extract pixel values over plot center with the same method, etc.) can be compared across each other. It is not well-quantified what

level of uncertainty arises in comparing results across different studies where methodologies were not consistent. Therefore, more broad-scale comparative studies are needed to understand the transferability of methods across landscapes and methods/technologies.

2.4.2 Compounding uncertainty

Studies have investigated individual slices of the "decision menu" (the many potential analytical approaches to a particular step in the analysis, **Figure 2.2**) but none have looked at how uncertainty compounds across the whole analysis process from beginning to end. Stambaugh et al. (2015) assessed the compounding uncertainty across three decision points: 1) two index value extraction methods (none and bilinear interpolation), 2) two timings of remotely sensed data (initial vs. extended assessment), and 3) two spectral indices (dNBR vs. RdNBR). Their analysis thus followed $2^3 = 8$ different pathways and showed that R^2 for models of overall CBI values ranged from 0.03 to 0.61. This study demonstrates the importance of understanding not just how each slice of the decision menu can affect model results but also how those uncertainties can be compounded through different analytical pathways. Additionally, because many of the comparative studies discussed above provide mixed results when looking at a single decision point, it is unclear how important such choices are at the global scale of analysis. A comprehensive study of the many potential analytical approaches would help understand when differences at different decision points wash out and when they do not, allowing us to understand when we are seeing "true" differences between studies and when those are due to differences in the methods used.

2.4.3 Key gaps

We identified several key research gaps or biases in the studies reviewed. The previous sections addressed the importance of comparative studies targeting key points in the "decision menu" of an analysis. Here, we identify where individual studies are absent or lacking from the literature identified in our review.

The uneven distribution in the types and locations of fires studied has important implications for how widely applicable the results are across different fires and geographies in the future. First, most fires were wildfires, with some prescribed and wildland fire use fires. While this makes sense from a perspective of pre-fire management and post-fire intervention, there is reason to question whether prescribed fires behave in fundamentally different ways than wildfire. For example, Arkle et al. (2010) found that prescribed fires did not mimic the ecological effects that followed wildfire in a riparian ecosystem; both the extent and severity of vegetation burned was substantially lower in the prescribed fire compared to nearby wildfires. How severity models based on remotely sensed data under such conditions might differ remains unclear. Second, there was a heavy geographical bias towards the United States and especially the western United States, as well as a heavy focus on temperate coniferous forests. These results reflect that the western United States has a long history of wildfire research. This focus could be due partly to the region's high spatial variability in fire regimes and biodiversity (Heyerdahl *et al.* 2001; Morgan *et al.* 2001). However, the concentration of fire research in this area may also mean that a major swath of ecosystems elsewhere is unstudied. For example, our focus on CBI excluded studies from Australia, where alternative visual estimation approaches have been used (Hammill and Bradstock 2006; Chafer 2008). Although other regions may have different ways of doing

field estimates of severity not included in this review, the ability to make comparisons between those studies and CBI is limited.

The limited range in the size and timing of field plot collection limits our understanding of how field data at different scales affects model variability and of long-term ecosystem change. First, there was a strong bias towards 30-m diameter plots, raising the question of what spatial scales are missing in current analyses. The CBI was initially designed with 30-m diameter plots to match the spatial grain of imagery collected by the Landsat satellite program (Eidenshink *et al.* 2007) but has since been adapted and related to many different sensors of both higher and lower resolution (**Table S2.6**). It remains unclear how sampling very large field plots may impact relationships with remotely sensed data, especially those of relatively coarse spatial resolution. Second, we found a relative lack of more extended intervals between fire occurrence and field data collection (on the order of 3-10 years post-fire), as well as an absence of studies conducting repeated measurements. While the collection of field data is often limited by site accessibility, high costs, and time constraints (Chuvieco *et al.* 2006; Boucher *et al.* 2017), there are clearly opportunities for studies that sample outside the range of commonly used field plot sizes and timing delays. For example, studies could collect enormous field plots, however such an endeavor might take weeks to months, and environmental factors such as rain or wind could affect measurements (Meng and Meentemeyer 2011).

The 15 model forms used across the studies begs the question of how robust results are to uncertainty in model form. The sheer number of model forms in the studies reviewed shows the diversity of statistical approaches used to link remotely sensed data to field observations. We identified two main considerations in the choice of model form: (1) the behavior of remote

sensor and ecosystem considerations (sensor saturation, nonlinearity at high severities), and (2) model performance (based on evaluation metrics). Although studies such as van Wagtendonk et al. (2004) modeled CBI using a quadratic model, the predicted reduction in CBI at high dNBR values is not an expected behavior of the sensor-ecosystem dynamic (Hall *et al.* 2008). Thus, some studies argued for nonlinear models with saturated growth characteristics (*e.g.*, CBI = dNBR × $(a[\text{dNBR}] + b)^{-1}$; Hall *et al.* 2008), even when this choice is not strictly supported by model evaluation metrics. The motivations for selecting different model forms were seldom described, but many studies clearly tried to find the best descriptor of the observed relationship. In studies that considered the sensor-ecosystem dynamic, predicting a trend that is feasible in the real world overrode the aim for strong performance (Hall *et al.* 2008; Boucher *et al.* 2017). That said, studies rarely compared more than a few models and the robustness of relationships to uncertainty in model form is not well understood.

Finally, the mixed results in the 14 of 62 studies that modeled CBI across strata demonstrated that conceptual models of remote sensed data reported strengths or weaknesses in correlating with specific burn severity measures that would not be expected from theory. Specifically, we identified some studies showed stronger relationships in lower canopy strata – in conflict with excepted theory that passive remotely sensed data are limited by low signal penetration (Chen *et al.* 2015) and disproportionately capture changes in the upper canopy (Kasischke *et al.* 2008). Several studies support the theory that passive sensors are more likely to detect fire effects in the upper part of the vegetation stratum (Patterson and Yool 1998; Hudak *et al.* 2004; De Santis and Chuvieco 2009). Conceptually, the ability to capture change in lower canopy strata is impacted by vegetation density, as burned landscapes may reflect more changes in the overstory strata due to the shielding effect of vegetation or their remains (Soverel *et al.* 2011; Tanase *et al.* 2011).

While relationships between field observations and remotely sensed data were generally strong in the overstory components, large tree stratum, and vegetation components (Chen, Vogelmann, *et al.* 2011; Meng and Meentemeyer 2011; Chen *et al.* 2015; Stambaugh *et al.* 2015; Wu *et al.* 2015; Warner *et al.* 2017), two studies did however find that the understory components outperformed higher canopy strata (Hoy *et al.* 2008; Tanase *et al.* 2011). These exceptions to the conceptual rule-of-thumb that passive remotely sensed data are limited in their ability to detect change in lower canopy strata deserve more scrutiny and better understanding of the conditions under which lower forest strata may be observed.

2.4.4 Importance of providing rationales

Our research highlighted the importance – especially given the lack of consensus on analytical methods – of providing rationales for each decision in the analysis workflow that link back to the research objectives. For example, regarding the two previously stated considerations that drove the choice of model form in the reviewed studies, it would be beneficial for future investigators to more explicitly give the rationale behind their model selection methods and state the conditions under which those models can be appropriately interpreted. Choosing to sacrifice model performance for predictions that correspond to expected behavior of the sensor and ecosystem dynamic may create difficult comparisons across fires or regions, but it also provides considerable benefit in that they reflect the true nature of the system. Both approaches are equally valid given conforming research objectives, however we suggest that studies (1) consider the purpose of their analysis when determining appropriate models to assess and (2) convey whether weaker model performance metrics may result from their decisions.

Similarly, we found that studies did not always state their rationale for using field data as either predictor or response variables depending on their research objectives. In typical regression analysis, a causal relationship is implied between one or more predictors and a response (Bordacconi and Larsen 2014). Cansler and McKenzie (2012) used this logic to argue for CBI as a predictor variable, because burn severity changes reflectance, not the other way around. They further stated that CBI has the greatest certainty associated with its meaning and thus should be used to predict the variables with no inherent ecological meaning (*e.g.*, dNBR or RdNBR). Conversely, in some cases CBI (or other ground severity measure) may serve as a response variable with remotely sensed data serving as the predictor variable if the main study goal is to predict severity on the ground (Zhu *et al.* 2006). In these cases, studies taking this approach follow the logic that the known value in a satellite image (*e.g.*, RdNBR) is the predictor variable being used to model the unknown value on the ground (*e.g.*, tree mortality) as the response variable. Both approaches have their benefits and challenges, though readers could benefit from more sturdies explicitly describing when and why field data are considered as predictor versus response variables, as model configuration affects the ability to compare across studies.

The analytical process of modeling of continuous composite severity measures using remotely sensed data can be split into three main phases: collection of field data, collection of remotely sensed data, and modeling. We provide a figure that breaks down the main decisions that can be made at each phase (**Figure 2.11** – **Figure 2.13)**. This blueprint for preparation and analysis should be useful for considering key decisions in study design as well as emphasizing the choices that should be justified when reporting study results (see example rationales in **Table 2.14**).

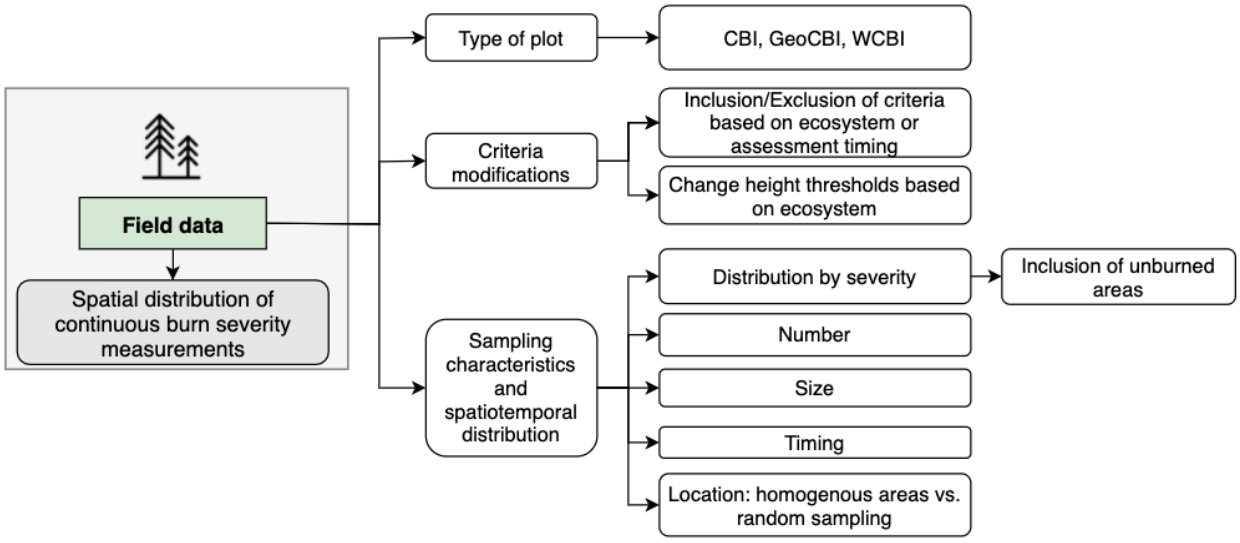

Figure 2.11 Analytical decisions to be made during field data sampling.

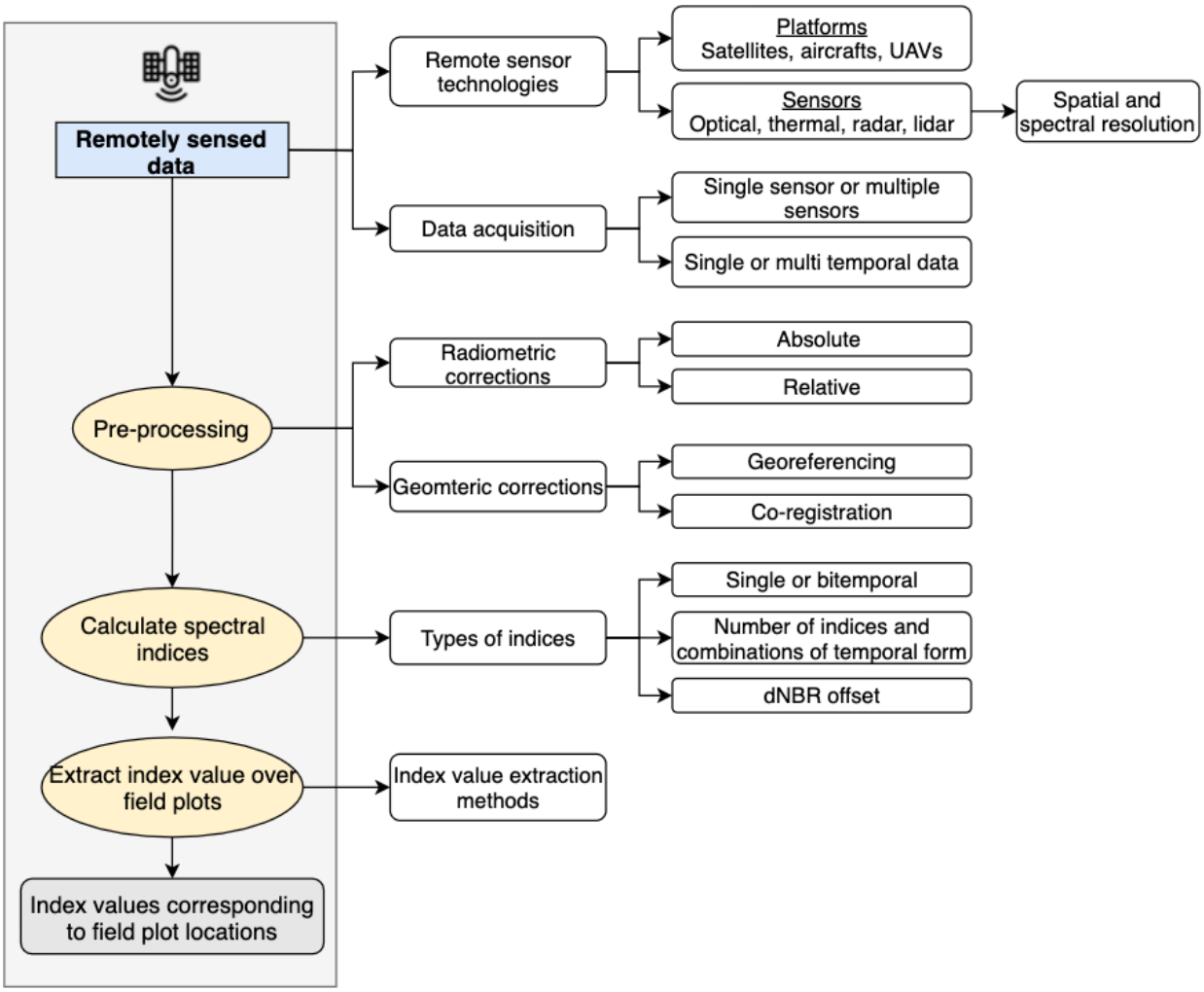

Figure 2.12 Analytical decisions to be made during remotely sensed data acquisition and processing.

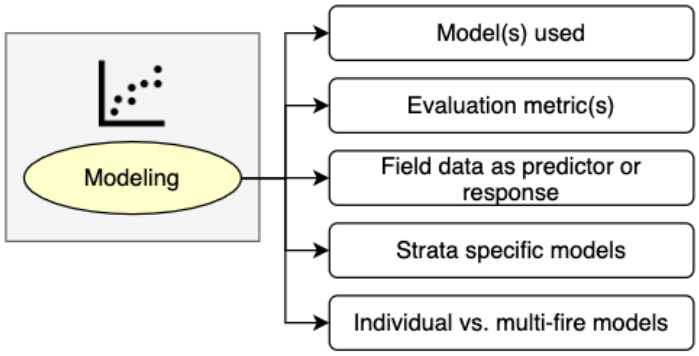

Figure 2.13 Analytical decisions to be made during modeling phase.

2.4.5 Study limitations

One major limitation of this study is that we did not evaluate the specific equations used to calculate each spectral index included in the studies. A few references provide incomplete equations – for example, in the original Miller and Thode (2007) study presenting RdNBR, they do not include multiplying by 1000 explicitly in the equation, nor any modifications needed to deal with 0 in the denominator. Additionally, many studies do not explicitly include the use of offset values in the equation. We captured this information where available but recommend that authors more explicitly state the form of the equations for spectral indices as well as any use of offset values. We did not endeavor to include the correct equations here (**Table S7**); however, we note the issue with past inconsistencies.

Many of the North American studies used overlapping CBI datasets (so the dataset are not really independent – *e.g.*, Cansler and McKenzie (2012) data was used by Karau et al. (2014) as well as Parks et al. (Parks *et al.* 2014, 2018, 2019). We also note that much of the CBI datasets analyzed by the papers in this review are available in a data repository for reanalysis (Picotte *et al.* 2019).

We did not include studies in our review that used direct forest measurements, for example the percentage of tree mortality or char and ash color (see **Table 2.1**). This may have introduced some geographic bias in which studies were excluded since some regions may rely more heavily on severity measurements based on direct, individual metrics. For example Morgan et al. (2014) recommend recording actual fire measurements that have logical and mechanistic connections to the properties a sensor can detect, avoiding the use of composite measures such as CBI that collapse multiple ecosystem attributes into a single index. Several studies have begun to record direct measures of burn severity rather than CBI only (*e.g.*, Whitman *et al.* 2018; Harvey *et al.*

2019; Saberi *et al.* 2022), though detailed field measures of burn severity remain rare compared to the widespread use of CBI.

2.4.6 Recommendations

Given the difficulty of synthesizing results across studies that used varying methodologies, we support efforts such as Picotte et al. (2019) to aggregate and disseminate datasets based on composite severity field observations from investigators. This could provide the necessary information to conduct a meta-analysis of the effects of compounding error across the "decision menu" presented in this review. Additionally, we recommend future studies complete the following:

- Collect and share field data in such a way that the original and modified composite severity measures identified in this review (CBI and GeoCBI/WCBI) could all be calculated, thus facilitating further comparisons among the different field measures. Such a request may require the development of a new CBI field collection form which could be used to collect raw field measurements that could be used to calculate any of these.
- Report full detail of any processing and analysis. For this review, we followed up with authors where information was missing, however we were not able to obtain information requested in every case. For a list of recommended information to report, **Table 2.13.**
- Report the reasoning for methodological choices at each step in the analysis. One of the goals of this review was to identify key analytical decisions and potential reasons why investigators may want to make one decision vs another (**Table 2.14**).

Table 2.13 Key elements suggested to report for each phase of study design and analysis.

Phase	Elements to report
Fire(s)	• Fire name • Fire location, including latitude and longitude or other explicitly identifying information (in the case of multiple fires of the same name and/or year) • Fire date (month/year); at least date of ignition (may also include date of containment, control, and/or out if possible) * • Fire type (*e.g.*, prescribed fire, wildland fire, wildland fire use) • Fire size • Ecosystem/vegetation type, topographic conditions, and other potentially valuable site-specific information
Field plots	• Number of field plots • Type of field plots (*e.g.*, CBI, GeoCBI, WCBI, etc.) • Field plot size • Field plot shape (circular or square) • Field plot timing (month/year) • Field plot distribution (UB, L, M, H), including whether unburned field plots (true plots or pseudo plots) where included
Remotely sensed data	• Pre- and post-fire sensor(s) used • Pre- and post-fire remotely sensed data acquisition timing • Spatial and spectral resolution of remotely sensed data • Atmospheric corrections (*e.g.*, use of top of atmosphere or surface reflectance) • Georeferencing/co-registration • Radiometric normalization Indices used, including whether offset values were included

Modeling	• Pixel value extraction method • Model form, including use of field plots as predictor or response variables • Model performance metric(s) assessed

*Contained: Measure of the line around a fire; Controlled: The fire is not likely to get outside the line; Out: No hot embers, no smoke, no fire

Table 2.14 Key decisions and potential rationales for each phase of study design and analysis.

Phase	Decision	Potential rationales
Field data	Which type of field severity index to capture (CBI, GeoCBI, WCBI, BSI)	Compare multiple field methods
		Provide data for strata % cover so weightings can be calculated
		Use best performing index based on literature
	Modifications to field protocol (inclusion/exclusion of ecosystem attributes, change to height thresholds)	Match sampling methods to specific ecosystem characteristics
		Match timing of remotely sensed data collection
	Distribution by severity, including sampling of unburned areas	Obtain balanced number of observations across fire(s)
		Anchor models at low end of severity/identify thresholds of change that can be attributed to fire and not due to artifacts of mismatched phenology or other
	Number of field plots	Capture variability of burned landscape
		Tradeoff in intensity of sampling effort (sample less) and power of statistical tests (sample more)
	Size of field plots	Match area observed by remotely sensed data

	Shape of field plots	Justifications for circular or square plots not provided by existing literature
	Timing of data collection	Match timing of remotely sensed data (synchronize data collection with availability of remotely sensed data)
		Capture immediate or delayed effects of fire (initial assessment vs. extended assessment)
	Location of field plots (homogeneous areas vs. random sampling)	Mitigate geometric errors in locations of field plots and remotely sensed data (sample in homogeneous areas)
		Investigate relationships at edges (random sampling)
Remotely sensed data	Type of sensor(s) sampled	Compare new technologies to long history of Landsat data
		Identify tradeoffs in passive versus active remote sensors
	Radiometric corrections	Test different algorithms
		Use well-known method or justification of existing literature
	Geometric corrections	Use well-known method or justification of existing literature
	Types of indices (single or bitemporal, number of indices, inclusion of offset)	Single date: avoid challenge of pairing pre- and post-fire images based on phenology and moisture between two collection dates (van Wagtendonk *et al.* 2004; Parks *et al.* 2018); less expensive, less time consuming, reduce inherent error found in bitemporal approaches (Koutsias *et al.* 1999)
		Bitemporal: avoid difficulties in mapping spectrally similar areas, such as water, shadow, or dark soil and recent burns (Bastarrika *et al.* 2011; Veraverbeke, Lhermitte, *et al.* 2011) or senescent vegetation and older burns (Pereira and Setzer 1993; Pereira 1999); avoid misclassification of non-flammable features (Kolden and Rogan 2009); control for spectral variability unrelated to fire, such as that

		due to image differences in solar illumination, atmosphere, phenology, and spatial registration (Escuin *et al.* 2008; Verbyla *et al.* 2008) or differences in the pre-fire forest condition (Cansler and McKenzie 2012; McCarley, Kolden, Vaillant, *et al.* 2017)
		Offset: account for interannual variation in phenology (Miller *et al.* 2009); make comparisons among multiple fires (Miller and Thode 2007; Parks *et al.* 2014)
	Index value extraction	Compare multiple methods; use method based on prior literature
Modeling	Model(s) used	Identify strongest performing model based on evaluation metrics
	Evaluation metric(s)	Match expected behavior of system Focus on overall fit of model Identify presence of extreme values in a dataset, which could happen, for example, if few high severity areas are included in field observations and pick robust evaluation metrics (*e.g.*, MAE over RMSE)
	Field data as predictor or response variable	Predict thresholds that correspond to ecological phenomena of interest (use field data as predictor) Map ecologically relevant response (use field data as response)
	Strata specific models	Investigate behavior of remotely sensed data in different forest strata Predict ecosystem changes in specific strata (*e.g.*, big trees)
	Individual vs. multi-fire models	Focus on site-specific results Identify generality of models across large landscapes or regions

2.5 Conclusion

This review of studies linking remotely sensed data to continuous measures of burn severity measured with the Composite Burn Index highlights: 1) the wide range in analytical approaches and lack of consensus in methodological decisions; 2) the scarcity of comparative studies at any one point in the "decision menu" and absence of a comprehensive beginning-to-end quantitative analysis of compounding uncertainty throughout the analysis framework; and 3) key gaps in research relating to the distribution in the types and locations of fires studied, limited range in the size and timing of field plot collection, and modeling of CBI across strata.

The results of this review provided a framework for future studies linking remotely sensed to continuous measures of severity by summarizing the key analytical decisions and the distribution of studies using such techniques. We avoided concluding which methods or decisions perform best and instead focused on the importance of understanding the wide varieties of ways this type of research has been done and its potential impacts on our understanding of the state of the science. We found that much uncertainty remains in light of a lack of comparative analysis and biases in the study designs. In the absence of a consensus approach to modeling severity using remotely sensed data, we suggested future research explicitly state their rationales for each analytical decision and how it relates to their specific research questions.

2.6 References

Allen JL, Sorbel B (2008) 'Assessing the differenced Normalized Burn Ratio's ability to map burn severity in the boreal forest and tundra ecosystems of Alaska's national parks' *International Journal of Wildland Fire* **17**, 463–475.

Arkle RS, Pilliod DS (2010) ‘Prescribed fires as ecological surrogates for wildfires: a stream and riparian perspective’ *Forest Ecology and Management* **259**, 893–903.

Bastarrika A, Chuvieco E, Martín MP (2011) ‘Mapping burned areas from Landsat TM/ETM+ data with a two-phase algorithm: Balancing omission and commission errors’ *Remote Sensing of Environment* **115**, 1003–1012.

Bordacconi MJ, Larsen MV (2014) ‘Regression to causality: Regression-style presentation influences causal attribution’ *Research & Politics* **1**, 2053168014548092.

Boucher J, Beaudoin A, Hébert C, Guindon L, Bauce É, Hebert C, Guindon L, Bauce E (2017) ‘Assessing the potential of the differenced Normalized Burn Ratio (dNBR) for estimating burn severity in eastern Canadian boreal forests.’ *International Journal of Wildland Fire* **26**, 32–45. doi:10.1071/WF15122

Cahoon Jr DR, Stocks BJ, Levine JS, Cofer III WR, Pierson JM (1994) ‘Satellite analysis of the severe 1987 forest fires in northern China and southeastern Siberia’ *Journal of Geophysical Research: Atmospheres* **99**, 18627–18638.

Cansler CA, McKenzie D (2012) ‘How robust are burn severity indices when applied in a new region? Evaluation of alternate field-based and remote-sensing methods’ *Remote sensing* **4**, 456–483.

Chafer CJ (2008) ‘A comparison of fire severity measures: An Australian example and implications for predicting major areas of soil erosion’ *CATENA* **74**, 235–245. doi:https://doi.org/10.1016/j.catena.2007.12.005

Chang Y, Zhu Z, Feng Y, Li Y, Bu R, Hu Y (2016) 'The spatial variation in forest burn severity in Heilongjiang Province, China' *Natural Hazards* **81**, 981–1001. doi:http://dx.doi.org/10.1007/s11069-015-2116-9

Chappell CB, Agee JK (1996) 'Fire severity and tree seedling establishment in Abies magnifica forests, southern Cascades, Oregon' *Ecological Applications* **6**, 628–640.

Charron I, Greene DF (2002) 'Post-wildfire seedbeds and tree establishment in the southern mixedwood boreal forest' *Canadian Journal of Forest Research* **32**, 1607–1615.

Chavez PS (1996) 'Image-based atmospheric corrections-revisited and improved' *Photogrammetric engineering and remote sensing* **62**, 1025–1035.

Chen G, Hay GJ, Castilla G, St-Onge B, Powers R (2011) 'A multiscale geographic object-based image analysis to estimate lidar-measured forest canopy height using Quickbird imagery' *International Journal of Geographical Information Science* **25**, 877–893.

Chen G, Metz MR, Rizzo DM, Meentemeyer RK (2015) 'Mapping burn severity in a disease-impacted forest landscape using Landsat and MASTER imagery' *International Journal of Applied Earth Observation and Geoinformation* **40**, 91–99. doi:10.1016/j.jag.2015.04.005

Chen XX, Vogelmann JE, Rollins M, Ohlen D, Key CH, Yang LM, Huang CQ, Shi H (2011) 'Detecting post-fire burn severity and vegetation recovery using multitemporal remote sensing spectral indices and field-collected composite burn index data in a ponderosa pine forest.' *International Journal of Remote Sensing* **32**, 7905–7927. doi:10.1080/01431161.2010.524678

Choung Y, Byung-Chun LEE, Jae-Hyoung CHO, Kyu-Song LEE, In-Soo J, Sun-Hee KIM, Sun-Kee H, Hui-Cheul J, Choung H-L (2004) 'Forest responses to the large-scale east coast fires in Korea' *Ecological research* **19**, 43–54.

Churchill DJ, Jeronimo SMA, Hessburg PF, Cansler CA, Povak NA, Kane VR, Lutz JA, Larson AJ (2022) 'Post-fire landscape evaluations in Eastern Washington, USA: Assessing the work of contemporary wildfires' *Forest Ecology and Management* **504**, 119796.

Churchill DJ, Larson AJ, Dahlgreen MC, Franklin JF, Hessburg PF, Lutz JA (2013) 'Restoring forest resilience: From reference spatial patterns to silvicultural prescriptions and monitoring' *Forest Ecology and Management* **291**, 442–457. doi:10.1016/j.foreco.2012.11.007

Chuvieco E, Martin MP, Palacios A (2002) 'Assessment of different spectral indices in the red-near-infrared spectral domain for burned land discrimination' *International Journal of Remote Sensing* **23**, 5103–5110.

Chuvieco E, Riaño D, Danson FM, Martin P (2006) 'Use of a radiative transfer model to simulate the postfire spectral response to burn severity' *Journal of Geophysical Research: Biogeosciences* **111**,.

Cocke AE, Fulé PZ, Crouse JE (2005) 'Comparison of burn severity assessments using Differenced Normalized Burn Ratio and ground data' *International Journal of Wildland Fire* **14**, 189–198.

Datt B (1999) 'A new reflectance index for remote sensing of chlorophyll content in higher

plants: tests using Eucalyptus leaves' *Journal of Plant Physiology* **154**, 30–36.

Dillon GK, Holden ZA, Morgan P, Crimmins MA, Heyerdahl EK, Luce CH (2011) 'Both topography and climate affected forest and woodland burn severity in two regions of the western US, 1984 to 2006' *Ecosphere* **2**, 1–33.

Doerr SH, Shakesby RA, Blake WH, Chafer CJ, Humphreys GS, Wallbrink PJ (2006) 'Effects of differing wildfire severities on soil wettability and implications for hydrological response' *Journal of Hydrology* **319**, 295–311.

Eidenshink J, Schwind B, Brewer K, Zhu ZL, Quayle B, Howard S (2007) 'A project for monitoring trends in burn severity' *Fire Ecology Special Issue* **3**, 2–21.

Epting J, Verbyla D, Sorbel B (2005) 'Evaluation of remotely sensed indices for assessing burn severity in interior Alaska using Landsat TM and ETM+' *Remote Sensing of Environment* **96**, 328–339.

Escuin S, Navarro R, Fernandez P (2008) 'Fire severity assessment by using NBR (Normalized Burn Ratio) and NDVI (Normalized Difference Vegetation Index) derived from LANDSAT TM/ETM images' *International Journal of Remote Sensing* **29**, 1053–1073.

Fang L, Yang J (2014) 'Atmospheric effects on the performance and threshold extrapolation of multi-temporal Landsat derived dNBR for burn severity assessment.' *International Journal of Applied Earth Observation and Geoinformation* **33**, 10–20. doi:10.1016/j.jag.2014.04.017

Fernandez-García V, Quintano C, Taboada A, Marcos E, Calvo L, Fernandez-Manso A (2018)

‘Remote Sensing Applied to the Study of Fire Regime Attributes and Their Influence on Post-Fire Greenness Recovery in Pine Ecosystems’ *Remote Sensing* **10**, 733. doi:http://dx.doi.org/10.3390/rs10050733

Fernández-García V, Santamarta M, Fernández-Manso A, Quintano C, Marcos E, Calvo L (2018) ‘Burn severity metrics in fire-prone pine ecosystems along a climatic gradient using Landsat imagery’ *Remote Sensing of Environment* **206**, 205–217.

Fernández-Manso A, Quintano C, Fernandez-Manso A, Quintano C (2015) ‘Evaluating Landsat ETM+ emissivity-enhanced spectral indices for burn severity discrimination in Mediterranean forest ecosystems.’ *Remote Sensing Letters* **6**, 302–310. doi:10.1080/2150704X.2015.1029093

Fire Bundles. Available at https://www.mtbs.gov/direct-download

(2020) Fire Perimeters. Available at https://frap.fire.ca.gov/mapping/gis-data/

Fraser RH, Sluijs J Vander, Hall RJ (2017) ‘Calibrating Satellite-Based Indices of Burn Severity from UAV-Derived Metrics of a Burned Boreal Forest in NWT, Canada’ *Remote Sensing* **9**, 279. doi:http://dx.doi.org/10.3390/rs9030279

French NHF, Kasischke ES, Hall RJ, Murphy KA, Verbyla DL, Hoy EE, Allen JL (2008) ‘Using Landsat data to assess fire and burn severity in the North American boreal forest region: an overview and summary of results’ *International Journal of Wildland Fire* **17**, 443–462.

Furniss TJ, Kane VR, Larson AJ, Lutz JA (2020) ‘Detecting tree mortality with Landsat-derived spectral indices: Improving ecological accuracy by examining uncertainty’ *Remote Sensing*

of Environment **237**, 111497.

Garcia-Llamas P, Suarez-Seoane S, Manuel Fernandez-Guisuraga J, Fernandez-Garcia V, Fernandez-Manso A, Quintano C, Taboada A, Marcos E, Calvo L (2019) 'Evaluation and comparison of Landsat 8, Sentinel-2 and Deimos-1 remote sensing indices for assessing burn severity in Mediterranean fire-prone ecosystems' *International Journal of Applied Earth Observation and Geoinformation* **80**, 137–144. doi:10.1016/j.jag.2019.04.006

García MJL, Caselles V (1991) 'Mapping burns and natural reforestation using Thematic Mapper data' *Geocarto International* **6**, 31–37.

Gerard F, Plummer S, Wadsworth R, Sanfeliu AF, Iliffe L, Balzter H, Wyatt B (2003) 'Forest fire scar detection in the boreal forest with multitemporal SPOT-VEGETATION data' *IEEE Transactions on Geoscience and Remote Sensing* **41**, 2575–2585.

Gitelson A, Merzlyak MN (1994) 'Spectral reflectance changes associated with autumn senescence of Aesculus hippocastanum L. and Acer platanoides L. leaves. Spectral features and relation to chlorophyll estimation' *Journal of plant physiology* **143**, 286–292.

Gitelson AA, Viña A, Ciganda V, Rundquist DC, Arkebauer TJ (2005) 'Remote estimation of canopy chlorophyll content in crops' *Geophysical Research Letters* **32**,.

Greene DF, Noël J, Bergeron Y, Rousseau M, Gauthier S (2004) 'Recruitment of Picea mariana, Pinus banksiana, and Populus tremuloides across a burn severity gradient following wildfire in the southern boreal forest of Quebec' *Canadian Journal of Forest Research* **34**, 1845–1857.

Hall RJ, Freeburn JT, De Groot WJ, Pritchard JM, Lynham TJ, Landry R (2008) ‘Remote sensing of burn severity: experience from western Canada boreal fires’ *International Journal of Wildland Fire* **17**, 476–489.

Hammill KA, Bradstock RA (2006) ‘Remote sensing of fire severity in the Blue Mountains: influence of vegetation type and inferring fire intensity’ *International Journal of Wildland Fire* **15**, 213–226.

Harvey BJ, Andrus RA, Anderson SC (2019) ‘Incorporating biophysical gradients and uncertainty into burn severity maps in a temperate fire-prone forested region’ *Ecosphere*. doi:10.1002/ecs2.2600

Harvey BJ, Donato DC, Turner MG (2014) ‘Recent mountain pine beetle outbreaks, wildfire severity, and postfire tree regeneration in the US Northern Rockies’ *Proceedings of the National Academy of Sciences* **111**, 15120–15125.

Heyerdahl EK, Brubaker LB, Agee JK (2001) ‘Spatial controls of historical fire regimes: a multiscale example from the interior west, USA’ *Ecology* **82**, 660–678.

Holden ZA, Evans JS (2010) ‘Using fuzzy C-means and local autocorrelation to cluster satellite-inferred burn severity classes.’ *International Journal of Wildland Fire* **19**, 853–860. doi:10.1071/WF08126

Holden ZA, Morgan P, Smith AMS, Vierling L (2010) ‘Beyond Landsat: a comparison of four satellite sensors for detecting burn severity in ponderosa pine forests of the Gila Wilderness, NM, USA.’ *International Journal of Wildland Fire* **19**, 449–458. doi:10.1071/WF07106

Hoy EE, French NHF, Turetsky MR, Trigg SN, Kasischke ES (2008) 'Evaluating the potential of Landsat TM/ETM+ imagery for assessing fire severity in Alaskan black spruce forests' *International Journal of Wildland Fire* **17**, 500–514.

Huang C, Song K, Kim S, Townshend JRG, Davis P, Masek JG, Goward SN (2008) 'Use of a dark object concept and support vector machines to automate forest cover change analysis' *Remote sensing of environment* **112**, 970–985.

Hudak AT, Robichaud P, Evans JS, Clark J, Lannom K, Morgan P, Stone C (2004) 'Field validation of Burned Area Reflectance Classification (BARC) products for post fire assessment'

Huete AR (1988) 'A soil-adjusted vegetation index (SAVI)' *Remote sensing of environment* **25**, 295–309.

Hultquist C, Chen G, Zhao K (2014) 'A comparison of Gaussian process regression, random forests and support vector regression for burn severity assessment in diseased forests' *Remote sensing letters* **5**, 723–732.

Isaev AS, Korovin GN, Bartalev SA, Ershov D V, Janetos A, Kasischke ES, Shugart HH, French NHF, Orlick BE, Murphy TL (2002) 'Using remote sensing to assess Russian forest fire carbon emissions' *Climatic Change* **55**, 235–249.

Jain TB, Graham RT (2004) Is forest structure related to fire severity? Yes, no, maybe: Methods and insights in quantifying the answer. In 'Shepperd, Wayne D.; Eskew, Lane G.[Comps.]. Silvic. Spec. places Proc. Natl. Silvic. Work. Granby, CO. RMRS-P-34. Fort Collins, CO.

USDA For. Serv. Rocky Mt. Res. Stn.', 217–234

Johnstone JF, Chapin FS (2006) 'Effects of soil burn severity on post-fire tree recruitment in boreal forest' *Ecosystems* **9**, 14–31.

Karau EC, Keane RE (2010) 'Burn severity mapping using simulation modelling and satellite imagery super(A)' *International Journal of Wildland Fire* **19**, 710–724. doi:10.1071/WF09018

Karau EC, Sikkink PG, Keane RE, Dillon GK (2014) 'Integrating Satellite Imagery with Simulation Modeling to Improve Burn Severity Mapping' *Environmental Management* **54**, 98–111. doi:http://dx.doi.org/10.1007/s00267-014-0279-x

Kasischke ES, Turetsky MR, Ottmar RD, French NHF, Hoy EE, Kane ES (2008) 'Evaluation of the composite burn index for assessing fire severity in Alaskan black spruce forests' *International Journal of Wildland Fire* **17**, 515–526.

Kaufman YJ, Remer LA (1994) 'Detection of forests using mid-IR reflectance: an application for aerosol studies' *IEEE transactions on geoscience and remote sensing* **32**, 672–683.

Kauth RJ, Thomas GS (1976) The tasselled cap--a graphic description of the spectral-temporal development of agricultural crops as seen by Landsat. In 'LARS Symp.', 159

Keeley JE (2009) 'Fire intensity, fire severity and burn severity: a brief review and suggested usage' *International Journal of Wildland Fire* **18**, 116–126. doi:10.1071/WF07049

Key CH, Benson NC (1999) Measuring and remote sensing of burn severity. In 'Proc. Jt. fire

Sci. Conf. Work.', 284. (University of Idaho and International Association of Wildland Fire Moscow, ID)

Key CH, Benson N (2002) 'Landscape Assessment. Fire effects monitoring and inventory protocol'

Key CH, Benson NC (2006) 'Landscape assessment (LA)' *FIREMON: Fire effects monitoring and inventory system Gen Tech Rep RMRS-GTR-164-CD, Fort Collins, CO: US Department of Agriculture, Forest Service, Rocky Mountain Research Station*.

Knapp EE, Keeley JE (2006) 'Heterogeneity in fire severity within early season and late season prescribed burns in a mixed-conifer forest' *International Journal of Wildland Fire* **15**, 37–45.

Kokaly RF, Rockwell BW, Haire SL, King TV V (2007) 'Characterization of post-fire surface cover, soils, and burn severity at the Cerro Grande Fire, New Mexico, using hyperspectral and multispectral remote sensing' *Remote Sensing of Environment* **106**, 305–325.

Kolden CA, Rogan J (2009) 'Spectral unmixing of MODIS pixels to derive burn severity: an alternative approach to Landsat-derived dNBR.' (Association of American Geographers, 1710 16th St, NW Washington, DC 20009 USA) Available at https://search.proquest.com/docview/745927669?accountid=14784

Kolden CA, Rogan J (2013) 'Mapping wildfire burn severity in the Arctic tundra from downsampled MODIS data' *Arctic, Antarctic, and Alpine Research* **45**, 64–76.

Koutsias N, Karteris M, Chuvico E (2000) 'The use of intensity-hue-saturation transformation of

Landsat-5 Thematic Mapper data for burned land mapping' *Photogrammetric Engineering and Remote Sensing* **66**, 829–840.

Koutsias N, Karteris M, Fernandez-Palacios A, Navarro C, Jurado J, Navarro R, Lobo A (1999) Burnt land mapping at local scale. In 'Remote Sens. large wildfires'. pp. 157–187. (Springer)

Kushla JD, Ripple WJ (1998) 'Assessing wildfire effects with Landsat thematic mapper data' *International Journal of Remote Sensing* **19**, 2493–2507.

Larson AJ, Jeronimo SMA, Hessburg PF, Lutz JA, Povak NA, Cansler CA, Kane VR, Churchill DJ (2022) 'Tamm Review: Ecological principles to guide post-fire forest landscape management in the Inland Pacific and Northern Rocky Mountain regions' *Forest Ecology and Management* **504**, 119680.

Lentile LB, Holden ZA, Smith AMSS, Falkowski MJ, Hudak AT, Morgan P, Lewis SA, Gessler PE, Benson NC (2006) 'Remote sensing techniques to assess active fire characteristics and post-fire effects' *International Journal of Wildland Fire* **15**, 319–345. doi:10.1071/WF05097

Liu HQ, Huete A (1995) 'A feedback based modification of the NDVI to minimize canopy background and atmospheric noise' *IEEE transactions on geoscience and remote sensing* **33**, 457–465.

Loboda T V, French NHF, Hight-Harf C, Jenkins L, Miller ME (2013) 'Mapping fire extent and burn severity in Alaskan tussock tundra: An analysis of the spectral response of tundra

vegetation to wildland fire' *Remote Sensing of Environment* **134**, 194–209.

Macdonald SE (2007) 'Effects of partial post-fire salvage harvesting on vegetation communities in the boreal mixedwood forest region of northeastern Alberta, Canada' *Forest Ecology and Management* **239**, 21–31.

Mallinis G, Mitsopoulos I, Chrysafi I (2018) 'Evaluating and comparing Sentinel 2A and Landsat-8 Operational Land Imager (OLI) spectral indices for estimating fire severity in a Mediterranean pine ecosystem of Greece' *Giscience & Remote Sensing* **55**, 1–18. doi:10.1080/15481603.2017.1354803

Malthus TJ, Andrieu B, Danson FM, Jaggard KW, Steven MD (1993) 'Candidate high spectral resolution infrared indices for crop cover' *Remote Sensing of Environment* **46**, 204–212.

McCarley TR, Kolden CA, Vaillant NM, Hudak AT, Smith AMSS, Wing BM, Kellogg BS, Kreitler J (2017) 'Multi-temporal LiDAR and Landsat quantification of fire-induced changes to forest structure' *Remote sensing of environment* **191**, 419–432. doi:10.1016/j.rse.2016.12.022

McCarley TR, Kolden CA, Valliant NM, Hudak AT, Smith AMS, Kreitler J (2017) 'Landscape-scale quantification of fire-induced change in canopy cover following mountain pine beetle outbreak and timber harvest' *Forest Ecology and Management* **391**, 164–175. doi:10.1016/j.foreco.2017.02.015

Meddens AJH, Kolden CA, Lutz JA (2016) 'Detecting unburned areas within wildfire perimeters using Landsat and ancillary data across the northwestern United States' *Remote Sensing of*

Environment **186**, 275–285.

Meng Q, Meentemeyer RK (2011) 'Modeling of multi-strata forest fire severity using Landsat TM Data' *International Journal of Applied Earth Observation and Geoinformation* **13**, 120–126.

Michalek JL, French NHF, Kasischke ES, Johnson RD, Colwell JE (2000) 'Using Landsat TM data to estimate carbon release from burned biomass in an Alaskan spruce forest complex' *International Journal of Remote Sensing* **21**, 323–338.

Miller JD, Knapp EE, Key CH, Skinner CN, Isbell CJ, Creasy RM, Sherlock JW (2009) 'Calibration and validation of the relative differenced Normalized Burn Ratio (RdNBR) to three measures of fire severity in the Sierra Nevada and Klamath Mountains, California, USA' *Remote Sensing of Environment* **113**, 645–656.

Miller JD, Thode AE (2007) 'Quantifying burn severity in a heterogeneous landscape with a relative version of the delta Normalized Burn Ratio (dNBR)' *Remote Sensing of Environment* **109**, 66–80.

Moreno JM, Oechel WC (1989) 'A simple method for estimating fire intensity after a burn in California chaparral.' *ACTA OECOL(OECOL PLANT)* **10**, 57–68.

Morgan P, Hardy CC, Swetnam TW, Rollins MG, Long DG (2001) 'Mapping fire regimes across time and space: understanding coarse and fine-scale fire patterns' *International Journal of Wildland Fire* **10**, 329–342.

Morgan P, Keane RE, Dillon GK, Jain TB, Hudak AT, Karau EC, Sikkink PG, Holden ZA,

Strand EK (2014) ‘Challenges of assessing fire and burn severity using field measures, remote sensing and modelling’ *International Journal of Wildland Fire* **23**, 1045–1060. doi:10.1071/WF13058

Murphy KA, Reynolds JH, Koltun JM (2008) ‘Evaluating the ability of the differenced Normalized Burn Ratio (dNBR) to predict ecologically significant burn severity in Alaskan boreal forests’ *International Journal of Wildland Fire* **17**, 490–499.

Musyimi Z, Said MY, Zida D, Rosenstock TS, Udelhoven T, Savadogo P, Leeuw J de, Aynekulu E, de Leeuw J, Aynekulu E (2017) ‘Evaluating fire severity in Sudanian ecosystems of Burkina Faso using Landsat 8 satellite images’ *Journal of Arid Environments* **139**, 95–109. doi:10.1016/j.jaridenv.2016.11.005

Neary DG (2004) ‘An overview of fire effects on soils’ *Southwest Hydrology* **3**, 18–19.

Nelson RF (1983) ‘Detecting forest canopy change due to insect activity using Landsat MSS’ *Photogrammetric Engineering and Remote Sensing* **49**, 1303–1314.

Odion DC, Hanson CT (2006) ‘Fire severity in conifer forests of the Sierra Nevada, California’ *Ecosystems* **9**, 1177–1189.

Olson DM, Dinerstein E (2002) ‘The Global 200: Priority ecoregions for global conservation (PDF file)’ *Annals of the Missouri Botanical Garden* **89**, 125–126.

Parker BM, Lewis T, Srivastava SK (2015) ‘Estimation and evaluation of multi-decadal fire severity patterns using Landsat sensors’ *Remote Sensing of Environment* **170**, 340–349. doi:http://dx.doi.org/10.1016/j.rse.2015.09.014

Parks SA, Dillon GK, Miller C (2014) ‘A new metric for quantifying burn severity: the Relativized Burn Ratio’ *Remote Sensing* **6**, 1827–1844.

Parks SA, Holsinger LM, Koontz MJ, Collins L, Whitman E, Parisien M-A, Loehman RA, Barnes JL, Bourdon J-F, Boucher J, Boucher Y, Caprio AC, Collingwood A, Hall RJ, Park J, Saperstein LB, Smetanka C, Smith RJ, Soverel N (2019) ‘Giving Ecological Meaning to Satellite-Derived Fire Severity Metrics across North American Forests’ *Remote Sensing* **11**, 1735. doi:10.3390/rs11141735

Parks SA, Holsinger LM, Voss MA, Loehman RA, Robinson NP (2018) ‘Mean Composite Fire Severity Metrics Computed with Google Earth Engine Offer Improved Accuracy and Expanded Mapping Potential’ *Remote Sensing* **10**, 879. doi:10.3390/rs10060879

Patterson MW, Yool SR (1998) ‘Mapping fire-induced vegetation mortality using Landsat Thematic Mapper data: A comparison of linear transformation techniques’ *Remote Sensing of Environment* **65**, 132–142.

Pereira JMC (1999) ‘A comparative evaluation of NOAA/AVHRR vegetation indexes for burned surface detection and mapping’ *IEEE transactions on geoscience and remote sensing* **37**, 217–226.

Pereira JMC, Sá ACL, Sousa AMO, Silva JMN, Santos TN, Carreiras JMB (1999) Spectral characterisation and discrimination of burnt areas. In ‘Remote Sens. large wildfires’. pp. 123–138. (Springer)

Pereira MC, Setzer AW (1993) ‘Spectral characteristics of fire scars in Landsat-5 TM images of

Amazonia' *Remote Sensing* **14**, 2061–2078.

Picotte J, Arkle RS, Bastian H, Benson N, Cansler A, Caprio T, Dillon G, Key C, Klein RN, Kopper K, Meddens AJH, Ohlen D, Parks SA, Peterson DW, Pilliod D, Prichard S, Robertson K, Sparks A, Thode A (2019) Composite Burn Index (CBI) Data for the Conterminous US, Collected Between 1996 and 2018: U.S. Geological Survey data release. doi:10.5066/P91BH1BZ

Picotte JJ, Robertson KM (2011) 'Validation of remote sensing of burn severity in south-eastern US ecosystems' *International Journal of Wildland Fire* **20**, 453–464. doi:http://dx.doi.org/10.1071/WF10013

Pinty B, Verstraete MM (1992) 'GEMI: a non-linear index to monitor global vegetation from satellites' *Vegetatio* **101**, 15–20.

Pullin AS, Stewart GB (2006) 'Guidelines for systematic review in conservation and environmental management' *Conserv. Biol.* doi:10.1111/j.1523-1739.2006.00485.x

Qi J, Chehbouni A, Huete AR, Kerr YH, Sorooshian S (1994) 'A modified soil adjusted vegetation index' *Remote sensing of environment* **48**, 119–126.

Quintano C, Fernandez-Manso A, Calvo L, Marcos E, Valbuena L, Fernández-Manso A, Calvo L, Marcos E, Valbuena L (2015) 'Land surface temperature as potential indicator of burn severity in forest Mediterranean ecosystems.' *International Journal of Applied Earth Observation and Geoinformation* **36**, 1–12. doi:10.1016/j.jag.2014.10.015

Robichaud PR (2000) 'Evaluating the effectiveness of postfire rehabilitation treatments.' (US

Department of Agriculture, Forest Service, Rocky Mountain Research Station)

Robichaud PR, Lewis SA, Laes DYM, Hudak AT, Kokaly RF, Zamudio JA (2007) 'Postfire soil burn severity mapping with hyperspectral image unmixing' *Remote Sensing of Environment* **108**, 467–480.

Rogan J, Franklin J (2001) 'Mapping wildfire burn severity in southern California forests and shrublands using Enhanced Thematic Mapper imagery' *Geocarto International* **16**, 91–106.

Rogan J, Yool SR (2001) 'Mapping fire-induced vegetation depletion in the Peloncillo Mountains, Arizona and New Mexico' *International Journal of Remote Sensing* **22**, 3101–3121.

Rouse Jr J, Haas RH, Schell JA, Deering DW (1974) 'Monitoring vegetation systems in the Great Plains with ERTS'

Ryan KC, Noste N V (1985) 'Evaluating prescribed fires' *Lotan, James E; Kilgore, Bruce M; Fischer, William C* 15–18.

Saberi SJ, Agne MC, Harvey BJ (2022) 'Do you CBI what I see? The relationship between the Composite Burn Index and quantitative field measures of burn severity varies across gradients of forest structure' *International Journal of Wildland Fire*.

De Santis A, Asner GP, Vaughan PJ, Knapp DE (2010) 'Mapping burn severity and burning efficiency in California using simulation models and Landsat imagery' *Remote Sensing of Environment* **114**, 1535–1545. doi:10.1016/j.rse.2010.02.008

De Santis A, Chuvieco E (2007) ‘Burn severity estimation from remotely sensed data: Performance of simulation versus empirical models’ *Remote Sensing of Environment* **108**, 422–435.

De Santis A, Chuvieco E (2009) ‘GeoCBI: a modified version of the Composite Burn Index for the initial assessment of the short-term burn severity from remotely sensed data.’ *Remote Sensing of Environment* **113**, 554–562. doi:10.1016/j.rse.2008.10.011

Schepers L, Haest B, Veraverbeke S, Spanhove T, Borre J Vanden, Goossens R (2014) ‘Burned Area Detection and Burn Severity Assessment of a Heathland Fire in Belgium Using Airborne Imaging Spectroscopy (APEX)’ *Remote Sensing* **6**, 1803–1826. doi:http://dx.doi.org/10.3390/rs6031803

Sikkink PG (2015) Comparison of six fire severity classification methods using Montana and Washington wildland fires. In ‘Keane, Robert E.; Jolly, Matt; Parsons, Russell; Riley, Karin. Proc. large Wildl. fires Conf. May 19-23, 2014; Missoula, MT. Proc. RMRS-P-73. Fort Collins, CO US Dep. Agric. For. Serv. Rocky Mt. Res. ’, 213–226

Sikkink PG, Dillon GK, Keane RE, Morgan P, Karau EC, Holden ZA, Silverstein RP (2013) ‘Composite Burn Index (CBI) data and field photos collected for the FIRESEV project, western United States’

Smith AMS, Drake NA, Wooster MJ, Hudak AT, Holden ZA, Gibbons CJ (2007) ‘Production of Landsat ETM+ reference imagery of burned areas within Southern African savannahs: comparison of methods and application to MODIS’ *International Journal of Remote Sensing* **28**, 2753–2775.

Smith AMS, Wooster MJ, Drake NA, Dipotso FM, Falkowski MJ, Hudak AT (2005) 'Testing the potential of multi-spectral remote sensing for retrospectively estimating fire severity in African Savannahs' *Remote sensing of environment* **97**, 92–115.

Sorbel B, Allen J (2005) 'Space-based burn severity mapping in Alaska's National Parks' *Alaska Park Science* **4**, 4–11.

Soverel NO, Coops NC, Perrakis DDB, Daniels LD, Gergel SE (2011) 'The transferability of a dNBR-derived model to predict burn severity across 10 wildland fires in western Canada' *International Journal of Wildland Fire* **20**, 518–531.

Soverel NO, Perrakis DDB, Coops NC (2010) 'Estimating burn severity from Landsat dNBR and RdNBR indices across western Canada' *Remote Sensing of Environment* **114**, 1896–1909.

Stambaugh MC, Hammer LD, Godfrey R (2015) 'Performance of Burn-Severity Metrics and Classification in Oak Woodlands and Grasslands' *Remote Sensing* **7**, 10501–10522. doi:http://dx.doi.org/10.3390/rs70810501

Talucci AC, Krawchuk MA (2019) 'Dead forests burning: the influence of beetle outbreaks on fire severity and legacy structure in sub-boreal forests' *Ecosphere* **10**, e02744.

Tanase MA, Kennedy R, Aponte C (2015a) 'Fire severity estimation from space: a comparison of active and passive sensors and their synergy for different forest types' *International Journal of Wildland Fire* **24**, 1062–1075. doi:10.1071/WF15059

Tanase MA, Kennedy R, Aponte C (2015b) 'Radar burn ratio for fire severity estimation at

canopy level: an example for temperate forests.' *Remote Sensing of Environment* **170**, 14–31. doi:10.1016/j.rse.2015.08.025

Tanase M, de la Riva J, Pérez-Cabello F, Riva J de la, Pérez-Cabello F (2011) 'Estimating burn severity at the regional level using optically based indices.' *Canadian Journal of Forest Research* **41**, 863. doi:10.1139/x11-011

Tane Z, Roberts D, Veraverbeke S, Casas A, Ramirez C, Ustin S (2018) 'Evaluating Endmember and Band Selection Techniques for Multiple Endmember Spectral Mixture Analysis using Post-Fire Imaging Spectroscopy' *Remote Sensing* **10**, 389. doi:10.3390/rs10030389

Team RC (2017) 'R Core Team (2017). R: A language and environment for statistical computing' *R Found Stat Comput Vienna, Austria*.

Trigg S, Flasse S (2001) 'An evaluation of different bi-spectral spaces for discriminating burned shrub-savannah' *International Journal of Remote Sensing* **22**, 2641–2647.

Turner MG, Hargrove WW, Gardner RH, Romme WH (1994) 'Effects of fire on landscape heterogeneity in Yellowstone National Park, Wyoming' *Journal of Vegetation Science* **5**, 731–742.

Veraverbeke S, Harris S, Hook S (2011) 'Evaluating spectral indices for burned area discrimination using MODIS/ASTER (MASTER) airborne simulator data' *Remote Sensing of Environment* **115**, 2702–2709.

Veraverbeke S, Hook SJ (2013) 'Evaluating spectral indices and spectral mixture analysis for assessing fire severity, combustion completeness and carbon emissions' *International*

Journal of Wildland Fire **22**, 707–720. doi:http://dx.doi.org/10.1071/WF12168

Veraverbeke S, Hook S, Hulley G (2012) 'An alternative spectral index for rapid fire severity assessments' *Remote Sensing of Environment* **123**, 72–80. doi:10.1016/j.rse.2012.02.025

Veraverbeke S, Lhermitte S, Verstraeten WW, Goossens R (2011) 'Evaluation of pre/post-fire differenced spectral indices for assessing burn severity in a Mediterranean environment with Landsat Thematic Mapper' *International Journal of Remote Sensing* **32**, 3521–3537.

Veraverbeke S, Stavros En, Hook SJ (2014) 'Assessing fire severity using imaging spectroscopy data from the Airborne Visible/Infrared Imaging Spectrometer (AVIRIS) and comparison with multispectral capabilities' *Remote Sensing of Environment* **154**, 153–163. doi:10.1016/j.rse.2014.08.019

Verbyla DL, Kasischke ES, Hoy EE (2008) 'Seasonal and topographic effects on estimating fire severity from Landsat TM/ETM+ data' *International Journal of Wildland Fire* **17**, 527–534.

Vogelmann JE (1990) 'Comparison between two vegetation indices for measuring different types of forest damage in the north-eastern United States' *Remote Sensing* **11**, 2281–2297.

van Wagtendonk JW, Root RR, Key CH, Wagtendonk JW van, Root RR, Key CH (2004) 'Comparison of AVIRIS and Landsat ETM+ detection capabilities for burn severity' *Remote Sensing of Environment* **92**, 397–408. doi:10.1016/j.rse.2003.12.015

Wang GG (2002) 'Fire severity in relation to canopy composition within burned boreal mixedwood stands' *Forest Ecology and Management* **163**, 85–92.

Warner TA, Skowronski NS, Gallagher MR (2017) ‘High spatial resolution burn severity mapping of the New Jersey Pine Barrens with WorldView-3 near-infrared and shortwave infrared imagery’ *International Journal of Remote Sensing* **38**, 598–616. doi:10.1080/01431161.2016.1268739

Wells CG, Campbell RE, DeBano LF, Lewis CE, Fredriksen RL, Franklin EC, Froelich RC, Dunn PH (1979) Effects of fire on soil: a state-of-knowledge. In ‘Gen. Tech. Rep. WO’. (United States Department of Agriculture, Forest Service)

White JD, Ryan KC, Key CC, Running SW (1996) ‘Remote sensing of forest fire severity and vegetation recovery’ *International Journal of Wildland Fire* **6**, 125–136.

Whitman E, Parisien M-AA, Thompson DK, Hall RJ, Skakun RS, Flannigan MD (2018) ‘Variability and drivers of burn severity in the northwestern Canadian boreal forest.’ *Ecosphere* **9**, e02128. doi:10.1002/ecs2.2128

Wu Z, Middleton B, Hetzler R, Vogel J, Dye D (2015) ‘Vegetation burn severity mapping using Landsat-8 and WorldView-2’ *Photogrammetric Engineering & Remote Sensing* **81**, 143–154.

Wulder MA, White JC, Alvarez F, Han T, Rogan J, Hawkes B (2009) ‘Characterizing boreal forest wildfire with multi-temporal Landsat and LIDAR data’ *Remote Sensing of Environment* **113**, 1540–1555.

Xiao X, Boles S, Liu J, Zhuang D, Liu M (2002) ‘Characterization of forest types in Northeastern China, using multi-temporal SPOT-4 VEGETATION sensor data’ *Remote*

Sensing of Environment **82**, 335–348.

Yu X, Guo X, Wu Z (2014) 'Land surface temperature retrieval from Landsat 8 TIRS—Comparison between radiative transfer equation-based method, split window algorithm and single channel method' *Remote sensing* **6**, 9829–9852.

Zar JH (1999) 'Biostatistical analysis.' (Pearson Education India)

Zheng Z, Zeng Y, Li S, Huang W, Zhong Z, YongNian Z, SongNian L, Wei H (2016) 'A new burn severity index based on land surface temperature and enhanced vegetation index' *International Journal of Applied Earth Observation and Geoinformation* **45**, 84–94. doi:10.1016/j.jag.2015.11.002

Zhu Z, Key C, Ohlen D, Benson N (2006) 'Evaluate sensitivities of burn severity mapping algorithms for different ecosystems and fire histories in the United States. Final report JFSP 01-1-4-12' *October* **12**, 35.

2.7.1 SUPPLEMENTARY INFORMATION 1

Table S2.1 Typical post-fire change in spectral regions and their ecological causes.

Spectral region	**Typical change after fire**	**Ecological cause**	**Studies**
Red	Increases	Decrease in chlorophyll absorption	van Wagtendonk et al. (2004)
Near-infrared	Decreases	Consumption or damage of leaves	Epting et al. (2005), Key and Benson (2006), Miller and Thode (2007), van Wagtendonk et al. (2004)
		Reduction in leaf area index	Chuvieco et al. (2006)
Shortwave Infrared	Increases	Reduction of canopy shadow and moisture	Epting et al. (2005), van Wagtendonk et al. (2004), White et al. (1996)
		Canopy combustion, exposed ash and bare soil, charred large logs	Pereira et al. (1999), van Wagtendonk et al. (2004)
		Drying of vegetation and soil, decreased vegetation density, increased exposed substrate, and presence of charred fuels	Key and Benson (2006), Miller and Thode (2007)
Thermal	Increases	Decrease in transpirational cooling and exposure of lower emissivity soil	Cahoon Jr et al. (1994), García and Caselles (1991), Zheng et al. (2016)

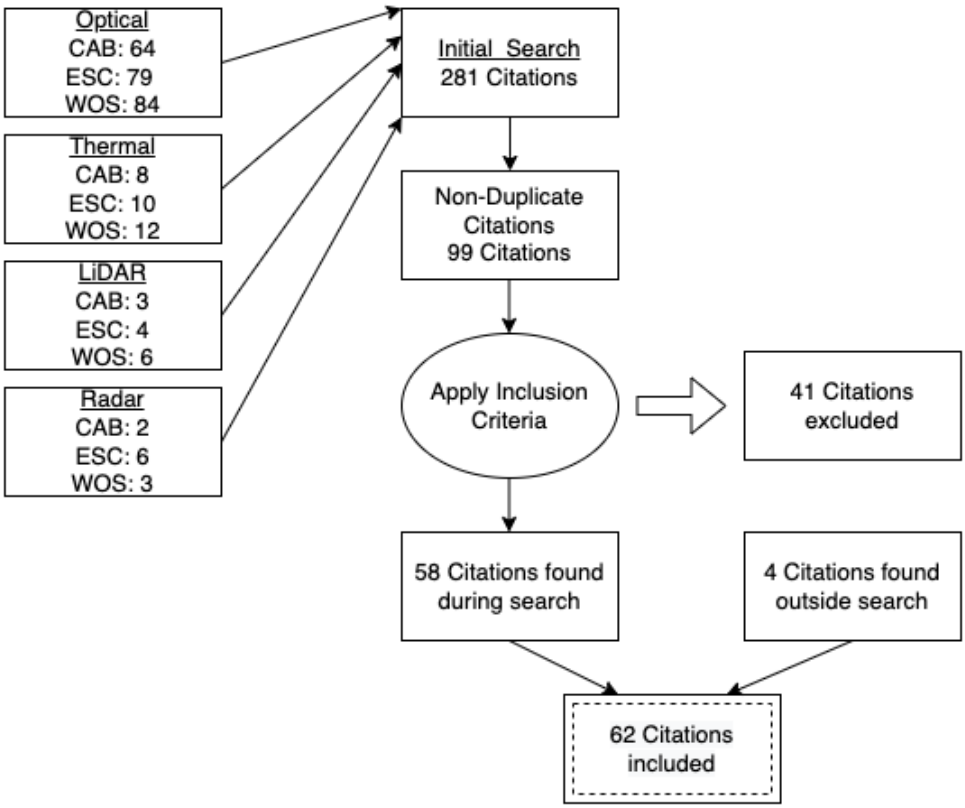

Figure S2.1 Flow chart showing systematic review process to identify 62 citations to include for review. CAB: CAB Direct; ESC: Environmental Science Collection; WOS: Web of Science.

Table S2.2 Article-level information extracted from each included citation.

Field	Description and examples
Author(s)	study main authors
Year	year study published
Journal	journal where study published
Lat/Long	study latitude and longitude if provided
Location name	study location name, *e.g.*, western North America
Ecosystem type	studied ecosystem type, *e.g.*, Boreal forest

Sensor used	type of sensor, *e.g.*, TM, ETM+, OLI
TOA or SR	whether top of atmosphere or surface reflectance imagery was used
Indices used	type of spectral indices used, *e.g.*, dNBR, RdNBR
dNBR offset inclusion	whether study indicates offset was used in calculation of spectral indices (dNBR)
Single or bi-temporal imagery	whether single imagery or bitemporal imagery was used
Radiometric normalization	whether bitemporal imagery was radiometrically normalized before index calculation
Georeferencing/co-registration	
Smoothing	type of smoothing, if any, *e.g.*, 3x3 mean, bilinear
Indices	indices used in analysis, *e.g.*, dNBR, RdNBR
Absolute or relativized spectral indices	whether absolute or relativized indices were used
Field plot distribution (UB, L, M, H)	the distribution of field plots across severity classes, if given
Type of model/regression used	type of model/regression used, *e.g.*, linear, quadratic
CBI predictor or response	whether CBI plots were used as a predictor or response variable in statistical analysis
Metric assessed	statistical metrics assessed, *e.g.*, pearson correlation, R^2, p
Comparison across strata	CBI strata assessed, *e.g.* overall, understory, overstory, both

Table S2.3 Fire-level information extracted from each included citation.

Field	**Description and Examples**
Fire name(s)	name(s) of fire(s)
Fire location(s)	fire location(s)
Fire date(s)	fire date(s) (month, year if available)
Fire type(s)	fire type(s), *e.g.*, prescribed, wildland, wildland fire use
Fire size(s)	size of the fire(s)

Number of field plots	number of field plots used for each fire
Type of field plots	whether CBI, GeoCBI, or WCBI was used
Field plot size	size of the field plots
Field plot shape	circular or square
Field plot timing	timing of field plot collection (month, year if available)
Unburned field plots	whether unburned field plots were collected (yes/no)

Table S2.4 Comparison-level information extracted from each included citation.

Field	**Description and Examples**
Fire name(s)	name(s) of fire(s) studied
Fire location(s)	fire location(s)
Fire date(s)	fire date(s) (month, year if available)
Fire type(s)	fire type(s), *e.g.*, prescribed, wildland, wildland fire use
Fire size(s)	size of the fire(s)
Number of field plots	number of field plots used for each fire
Type of field plots	whether CBI, GeoCBI, or WCBI was used
Field plot size	size of the field plots
Field plot shape	circular or square
Field plot timing	timing of field plot collection (month, year if available)
Pre-fire data	what sensor was used for pre-fire remotely sensed data *e.g.*, TM/ETM+
Pre-fire timing	timing of pre-fire remotely sensed data collection (month, year if available)
Post-fire data	what sensor was used for post-fire remotely sensed data *e.g.*, TM/ETM+
Post-fire timing	timing of post-fire remotely sensed data collection (month, year if available)
Spatial resolution	the spatial resolution of remotely sensed data

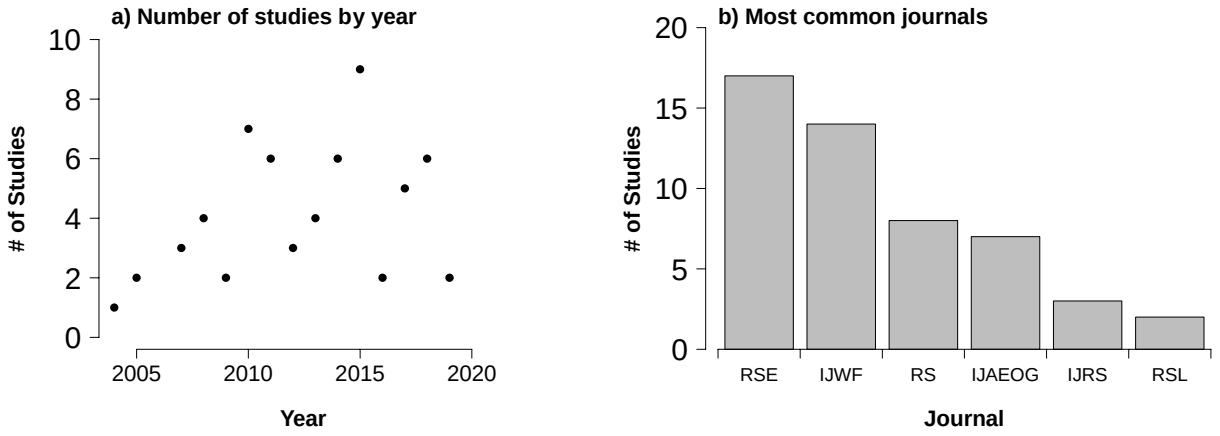

Figure S2.2 (a) Number of studies relating remotely sensed data to CBI as a continuous measure of burn severity by year (N = 62 studies). (b) Most common journals that published at least two studies in this review. RSE: *Remote Sensing of Environment*; IJWF: *International Journal of Wildland Fire*; RS: Remote Sensing; IJAEOG: *International Journal of Applied Earth Observation and Geoinformation*; IJRS: *International Journal of Remote Sensing*; RSL: *Remote Sensing Letters*. Eleven journals published one citation: *Arctic, Antarctic, and Alpine Research*; *Canadian Journal of Forest Research*; *Ecosphere*; *Environmental Management*; *Fire Ecology*; *Forests*; *GIScience and Remote Sensing*; *Journal of Arid Environments*; *Natural Hazards*; *Photogrammetric Engineering and Remote Sensing*; and *Rangeland Ecology and Management*.

Table S2.5 Thresholds for severity classification across studies where values were provided.

Unburned	Low	Moderate	High	Studies
0.0-0.29	0.30-1.75	1.76-2.23	2.24-3.0	Boucher et al. (2017)
0-1.04	1.04-1.16	1.16-1.85	1.85-3.0	Chang et al. (2016)
NA	0.00-0.99	1.00-1.99	2.00-3.00	Chen et al. (2011)
Not given				Epting et al. (2005)
0.00-0.09	0.10-1.24	1.25-2.24	2.25-3.00	Fernandez-Manso and Quintano (2015)
0	0-1	1-2	2-3	Karau and Keane (2010)
0-0.1	0.1-1.24	1.25-2.24	2.25-3.0	Karau et al. (2014)
0-0.1	0.1-1.24	1.25-2.24	2.25-3.0	Miller and Thode (2007)

0-0.1	0.1-1.24	1.25-2.24	2.25-3.0	Musyimi et al. (2017)
0.00-0.09	0.10-1.24	1.25-2.24	2.25-3.00	Parker et al. (2015)
NA	□1.25	1.26-2.25	>2.26	Stambaugh et al. (2015)
0	0.1-1.24	1.25-2.24	2.25-3	Quintano et al. (2015)
0	0< CBI <=1	1<CBI <=2	>2	Tanase et al. (2015a)
0-0.1	0.1-1.24	1.25-2.24	2.25-3.0	Cansler and McKenzie (2012)
0-0.75	0.75-1.25	1.25-1.75; 1.75-2.25	2.25-3	Picotte and Robertson (2011)
<=1.25	<=1.25	1.25<CBI<=2.25	>2.25	Parks et al. (2014)
0	0.1-1.25	1.26-2.25	2.26-3.0	Mallinis et al. (2018)
Unchanged to low 0-1.25	Unchanged to low 0-1.25	1.26-2.25	2.26-3.0	Miller et al. (2009)

Table S2.6 Remote sensing technologies used in the studies reviewed and the number of studies in which they were included. Sensor refers to the specific instrument used to acquire data. Spectral range is the wavelengths of the electromagnetic spectrum that the sensor samples. Wavelengths is the general regions of the electromagnetic spectrum sampled (VIS: *visible*; NIR: *near infrared*; SWIR: *short wave infrared*; TIR: *thermal infrared*; RGB: *red, green,* blue) Number of bands is the number of raster bands captured over the spectral range. Spatial resolution is the pixel size of remotely sensed imagery. Temporal resolution is the revisit period of the sensor over the same location. Citations used is the number of studies that included the specified sensor.

Sensor	**Spectral range (μm)**	**Wavelengths**	**Number of bands**	**Spatial resolution (m)**	**Temporal resolution (days)**	**Studies used**
TM, ETM+	0.45 – 12.5	VIS, NIR, SWIR, TIR	7	30 (120 TIR)	16	60
OLI/TIRS	0.435 – 12.51	VIS, NIR, SWIR, TIR	10	30 (100 TIR)	16	8
Landsat (unspecified)	--	VIS, NIR, SWIR, TIR	--	--	--	5

AVIRIS	0.4 – 2.5	VIS, NIR, SWIR	224	20	--	4
MASTER	0.457 – 12.878	VIS, NIR, SWIR, TIR	50	5 – 50 (altitude dependent)	--	3
MODIS	Bands 1-19 from 0.405 to 2.155; Bands 20-36 from 3.66 to 14.28	VIS, NIR, SWIR, TIR	36	250 (bands 1-2) 500 (bands 3-7) 1000 (bands 8-36)	16	3
ALOS PALSAR	15 – 30 cm	Radio	--	10 and 100	42	2
Sentinel-2	0.4924 – 2.2024	VIS, NIR, SWIR		10, 20, 60 (band dependent)	10 days each for S2A and S2B (5 days combined)	2
APEX	0.38 – 2.5	VIS, NIR, SWIR	Up to 334 (default 114)	22.5 µm (VNIR) 30 µm (SWIR)	--	1
ASTER	0.52 – 11.65	VIS, NIR, SWIR, TIR	14	15 (VNIR) 30 (SWIR) 90 (TIR)	16	1
Deimos-1	0.52 – 0.90	VIS, NIR	3	22	1 – 3	1
QuickBird	0.45 – 0.90	VIS, NIR	4	2.62 m (nadir) to 2.90 m (20° off-nadir)	1 – 3.5	1
SPOT4	0.50 – 1.75	VIS, NIR, SWIR	4	10 (R) 20 (G, NIR, SWIR)	2 – 3	1

SPOT5	0.49 – 1.7	VIS, NIR, SWIR	4	10 (VNIR) 20 (SWIR)	2 – 3	1
WV-2	0.442 – 1.043	VIS, NIR	8	1.8	1.1 – 3.7	1
WV-3	0.40 – 2.365	VIS, NIR, SWIR	16	1.24 (VNIR) 3.70 (SWIR)	1 – 4.5	1
UAV*	RGB	VIS	3	~ 0.02	--	1

* UAV specifications given for imagery captured in study but platform highly adaptable to other sensors

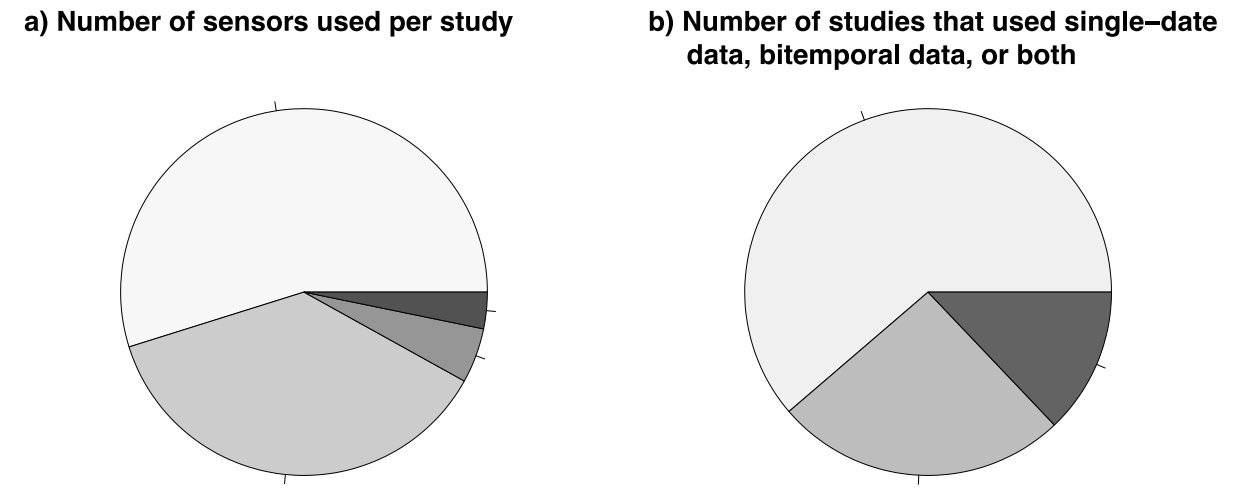

Figure S2.3 (a) Number of sensors used in each study (N = 62 studies). All Landsat sensors (TM, ETM+, OLI) were combined before analysis. (b) Number of studies that used single-date data, bitemporal data, or both (N = 62 studies). The number of studies for each criterion is shown in parentheses.

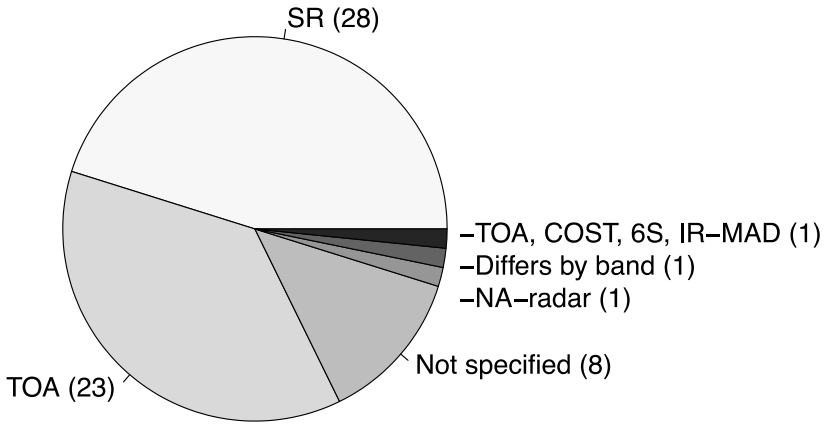

Figure S2.4 Atmospheric correction methods used by studies (N = 62 studies). The number of studies for each method is shown in parentheses. SR: *surface reflectance*; TOA: *top-of-atmosphere*; COST: *cosine of the solar zenith angle correction*; 6S: *second simulation of the satellite signal in the solar*; IR-MAD: *iteratively re-weighted multivariate alteration detection*.

Table S2.7 Indices used in studies with abbreviation, temporal and radiometric type, frequency in studies of this review, and key study reference.

Index	Abbreviation	Temporal	Radiometric	Frequency	Key studies
% black or brown trees	%BlorBr	Single	Spectral	1	Vereverbeke and Hook (2013)
Burned area index	BAI	Single	Spectral	1	Chuvieco et al. (2002)
burned fraction	BF/BurnF	Single	Spectral	2	Veraverbeke et al. (2014)
Char fraction	CF/CHAR	Single	Spectral	3	Veraverbeke et al. (2014)
Char soil index	CSI	Single	Spectral	1	Smith et al. (2007)
Enhanced vegetation index	EVI	Single	Spectral	4	Liu and Huete (1995)
green crown veg	GCV	Single	Spectral	1	Fraser et al. (2017)

Global environmental monitoring index	GEMI	Single	Spectral	1	Pinty et al. (1992)
Neighborhood texture	GEOTEX	Single	Spectral	1	Chen et al. (2011)
Green fraction/Green tree fraction	GF/GV/GTF	Single	Spectral	2	Fraser et al. (2017); Tane et al. (2018)
Hue	H	Single	Spectral	1	Koutsias et al. (2000)
Intensity	I	Single	Spectral	1	Koutsias et al. (2000)
Kauth-Thomas Brightness Transform	KTB	Single	Spectral	4	Kauth and Thomas (1976)
Kauth-Thomas Greenness Transform	KTG	Single	Spectral	4	Kauth and Thomas (1976)
Kauth-Thomas Wetness Transform	KTW	Single	Spectral	4	Kauth and Thomas (1976)
	LST/EVI	Single	Spectral	3	Zheng et al. (2016)
Mid-infrared burn index	MIRBI	Single	Spectral	2	Trigg and Flasse (2001)
modified soil-adjusted vegetation index	MSAVI	Single	Spectral	2	Qi et al. (1994)
modified soil-adjusted vegetation index 2	MSAVI2	Single	Spectral	1	Qi et al. (1994)

Normalized burn ratio	NBR	Single	Spectral	19	García and Lopez (1991)
Normalized difference SWIR index	NDSWIR	Single	Spectral	1	Gerard et al. (2003)
Normalized difference vegetation index	NDVI	Single	Spectral	12	Rouse et al. (1974)
Non-photosynthetic fraction of SMA	NPV	Single	Spectral	1	Tane et al. (2018)
Principle component 1	PC1	Single	Spectral	1	Patterson and Yool (1998)
Principle component 2	PC2	Single	Spectral	2	Patterson and Yool (1998)
Principle component 2	PC3	Single	Spectral	1	Patterson and Yool (1998)
Ratio TM band 4 / TM band 5	Ratio 4/5	Single	Spectral	2	Malthus et al. (1993)
Ratio TM band 7 / TM band 4	Ratio 7/4	Single	Spectral	2	Kushla and Ripple (1998)
Ratio TM band 7 / TM band 5	Ratio 7/5	Single	Spectral	2	Epting et al. (2005)
Saturation	S	Single	Spectral	1	Koutsias et al. (2000)
Soil-adjusted vegetation index	SAVI	Single	Spectral	5	Heuete et al. (1988)
SWIR-MIR index	SMI	Single	Spectral	3	Veraverbeke et al. (2012)

Spectral reflectance of individual bands (MODIS)	SR_MODIS	Single	Spectral	1	--
Spectral reflectance of individual bands 1-50 (MASTER)	SR_MASTER	Single	Spectral	1	--
TM band 1 reflectance	TM1	Single	Spectral	4	--
TM band 2 reflectance	TM2	Single	Spectral	4	--
TM band 3 reflectance	TM3	Single	Spectral	4	--
TM band 4 reflectance	TM4	Single	Spectral	6	--
TM band 5 reflectance	TM5	Single	Spectral	6	--
TM band 6 reflectance	TM6	Single	Spectral	1	--
TM band 7 reflectance	TM7	Single	Spectral	5	--
Internal texture	TXIT	Single	Spectral	1	Hultquist et al. (2014)
Vegetation index 3	VI3	Single	Spectral	1	Kaufman and Remer (1994)
Land surface temperature	LST	Single	Thermal	4	Yu et al. (2014)

LSE-enhanced NBR version 1	ENBRv1	Single	Mixed	1	Veraverbeke et al. (2011)
LSE-enhanced NBR version 2	ENBRv2	Single	Mixed	1	Veraverbeke et al. (2011)
LSE-enhanced NDVI version 1	ENDVIv1	Single	Mixed	1	Fernández-Manso and Quintano (2015)
LSE-enhanced NDVI version 2	ENDVIv2	Single	Mixed	1	Fernández-Manso and Quintano (2015)
Ratio of LST to EVI	LST/EVI	Single	Mixed	3	Zheng e tal. (2016)
Normalized difference vegetaion index - Thermal	NDVIT	Single	Mixed	1	Smith et al. (2007)
NIR-SWIR-Emmissivity version 1	NSEv1	Single	Mixed	2	Veraverbeke et al. (2011)
NIR-SWIR-emissivity version 2	NSEv2	Single	Spectral	1	Veraverbeke et al. (2011)
Soil adjusted vegetation index - Thermal	SAVIT	Single	Mixed	1	Smith et al. (2007)
pixel and object-based canopy loss	CLobject	Bi-temporal	Spectral	1	Wu et al. (2015)
pixel and object-based canopy loss	CLpixel	Bi-temporal	Spectral	1	Wu et al. (2015)

SWIR1 to NIR ratio difference	d7/4	Bi-temporal	Spectral	1	Kushla and Ripple (1998)
SWIR2 to NIR ratio difference	d7/5	Bi-temporal	Spectral	1	Vogelmann (1990)
Difference in scene components char	dCHAR	Bi-temporal	Spectral	1	Kolden and Rogan (2013)
Chlorophyll index red-edge	dCIre1	Bi-temporal	Spectral	1	Gitelson et al. (2005)
differenced enhanced vegetation index	dEVI	Bi-temporal	Spectral	8	Zheng et al. (2016)
green normalized difference vegetation index	dGNDVI	Bi-temporal	Spectral	1	Mallinis et al. (2018)
Change in GV fraction	dGV	Bi-temporal	Spectral	1	Kolden and Rogan (2013)
differenced integrated forest index	dIFI	Bi-temporal	Spectral	1	Huang et al. (2008)
Differenced tassled-cap brightness	dKTB	Bi-temporal	Spectral	2	Meddens et al. (2016); McCarley et al. (2017)
Differenced tassled-cap greenness	dKTG	Bi-temporal	Spectral	2	Meddens et al. (2016); McCarley et al. (2017)

Differenced tassled-cap wetness	dKTW	Bi-temporal	Spectral	2	Meddens et al. (2016); McCarley et al. (2017)
Modified simple ratio red-edge	dMSRre1	Bi-temporal	Spectral	1	Datt (1999)
Modified simple ratio red-edge narrow	dMSRre1n	Bi-temporal	Spectral	1	Datt (1999)
differenced nromalized burn index	dNBR	Bi-temporal	Spectral	50	Key and Benson (2006)
differenced normalized burn ratio narrow	dNBRn	Bi-temporal	Spectral	1	Mallinis et al. (2018)
differenced normalized differenced moisture index	dNDMI	Bi-temporal	Spectral	3	Meddens et al. (2016); McCarley et al. (2017)
Normalized difference SWIR index	dNDSWIR	Bi-temporal	Spectral	1	Gerard et al. (2003)
differenced normalized difference vegetation index	dNDVI	Bi-temporal	Spectral	18	Xiao et al. (2002)
normalized difference	dNDVIre1	Bi-temporal	Spectral	1	Gitelson and Merzlyak (1994)

vegetation index red edge1					
normalized difference vegetation index red edge1 narrow	dNDVIre1n	Bi-temporal	Spectral	1	Gitelson and Merzlyak (1994)
Change in NPV fraction	dNPV	Bi-temporal	Spectral	1	Kolden and Rogan (2013)
differences of pixel to pixel in each band (TM1-7)	dSR	Bi-temporal	Spectral	1	McCarley et al. (2017)
ratios of pixel to pixel in each band	image ratioing	Bi-temporal	Spectral	1	Nelson (1983)
differenced LST	dLST	Bi-temporal	Thermal	3	García-Llamas et al. (2019)
	d(LST/EVI)	Bi-temporal	Mixed	2	Zheng et al. (2016)
Radar Burn Ratio	Radar Burn Ratio (RBR)	Bi-temporal ratio	Radar	2	Tanase et al. (2015b)
Relative burn ratio	RBR	Relativized	Spectral	7	Parks et al. (2014)
Relative differenced normalized burn ratio	RdNBR	Relativized	Spectral	25	Miller and Thode (2007)
Relativized differenced normalized	RdNDMI	Relativized	Spectral	1	Veraverbeke et al. (2011)

differenced moisture index					
Relativized differenced normalized differenced vegetation index	RdNDVI	Relativized	Spectral	1	Veraverbeke et al. (2011)

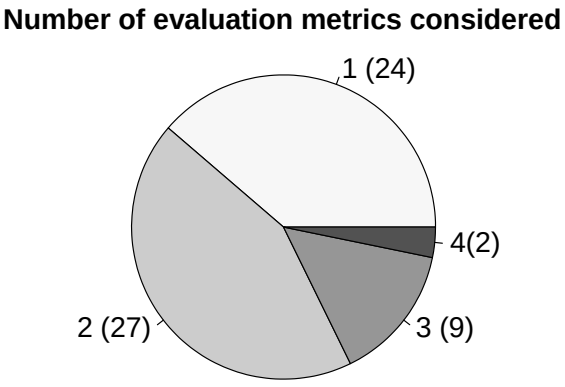

Figure S2.5 Number of evaluation metrics considered by each study (N = 62 studies). The number of studies that used each number of metrics is shown in parentheses.

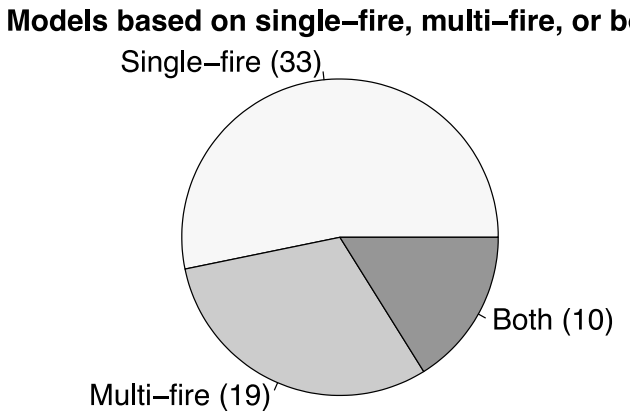

Figure S2.6 Use of models based on a single-fire, multiple fires or combination (N = 62 studies). The number of studies that used each type of model is shown in parentheses.

2.7.1.1 Supplementary References

Allen JL, Sorbel B (2008) 'Assessing the differenced Normalized Burn Ratio's ability to map burn severity in the boreal forest and tundra ecosystems of Alaska's national parks' *International Journal of Wildland Fire* **17**, 463–475.

Arkle RS, Pilliod DS (2010) 'Prescribed fires as ecological surrogates for wildfires: a stream and riparian perspective' *Forest Ecology and Management* **259**, 893–903.

Bastarrika A, Chuvieco E, Martín MP (2011) 'Mapping burned areas from Landsat TM/ETM+ data with a two-phase algorithm: Balancing omission and commission errors' *Remote Sensing of Environment* **115**, 1003–1012.

Bordacconi MJ, Larsen MV (2014) 'Regression to causality: Regression-style presentation influences causal attribution' *Research & Politics* **1**, 2053168014548092.

Boucher J, Beaudoin A, Hébert C, Guindon L, Bauce É, Hebert C, Guindon L, Bauce E (2017) 'Assessing the potential of the differenced Normalized Burn Ratio (dNBR) for estimating burn severity in eastern Canadian boreal forests.' *International Journal of Wildland Fire* **26**, 32–45. doi:10.1071/WF15122

Cahoon Jr DR, Stocks BJ, Levine JS, Cofer III WR, Pierson JM (1994) 'Satellite analysis of the severe 1987 forest fires in northern China and southeastern Siberia' *Journal of Geophysical Research: Atmospheres* **99**, 18627–18638.

Cansler CA, McKenzie D (2012) 'How robust are burn severity indices when applied in a new region? Evaluation of alternate field-based and remote-sensing methods' *Remote sensing* **4**,

456–483.

Chafer CJ (2008) ‘A comparison of fire severity measures: An Australian example and implications for predicting major areas of soil erosion’ *CATENA* **74**, 235–245. doi:https://doi.org/10.1016/j.catena.2007.12.005

Chang Y, Zhu Z, Feng Y, Li Y, Bu R, Hu Y (2016) ‘The spatial variation in forest burn severity in Heilongjiang Province, China’ *Natural Hazards* **81**, 981–1001. doi:http://dx.doi.org/10.1007/s11069-015-2116-9

Chappell CB, Agee JK (1996) ‘Fire severity and tree seedling establishment in Abies magnifica forests, southern Cascades, Oregon’ *Ecological Applications* **6**, 628–640.

Charron I, Greene DF (2002) ‘Post-wildfire seedbeds and tree establishment in the southern mixedwood boreal forest’ *Canadian Journal of Forest Research* **32**, 1607–1615.

Chavez PS (1996) ‘Image-based atmospheric corrections-revisited and improved’ *Photogrammetric engineering and remote sensing* **62**, 1025–1035.

Chen G, Hay GJ, Castilla G, St-Onge B, Powers R (2011) ‘A multiscale geographic object-based image analysis to estimate lidar-measured forest canopy height using Quickbird imagery’ *International Journal of Geographical Information Science* **25**, 877–893.

Chen G, Metz MR, Rizzo DM, Meentemeyer RK (2015) ‘Mapping burn severity in a disease-impacted forest landscape using Landsat and MASTER imagery’ *International Journal of Applied Earth Observation and Geoinformation* **40**, 91–99. doi:10.1016/j.jag.2015.04.005

Chen XX, Vogelmann JE, Rollins M, Ohlen D, Key CH, Yang LM, Huang CQ, Shi H (2011) 'Detecting post-fire burn severity and vegetation recovery using multitemporal remote sensing spectral indices and field-collected composite burn index data in a ponderosa pine forest.' *International Journal of Remote Sensing* **32**, 7905–7927. doi:10.1080/01431161.2010.524678

Choung Y, Byung-Chun LEE, Jae-Hyoung CHO, Kyu-Song LEE, In-Soo J, Sun-Hee KIM, Sun-Kee H, Hui-Cheul J, Choung H-L (2004) 'Forest responses to the large-scale east coast fires in Korea' *Ecological research* **19**, 43–54.

Churchill DJ, Jeronimo SMA, Hessburg PF, Cansler CA, Povak NA, Kane VR, Lutz JA, Larson AJ (2022) 'Post-fire landscape evaluations in Eastern Washington, USA: Assessing the work of contemporary wildfires' *Forest Ecology and Management* **504**, 119796.

Churchill DJ, Larson AJ, Dahlgreen MC, Franklin JF, Hessburg PF, Lutz JA (2013) 'Restoring forest resilience: From reference spatial patterns to silvicultural prescriptions and monitoring' *Forest Ecology and Management* **291**, 442–457. doi:10.1016/j.foreco.2012.11.007

Chuvieco E, Martin MP, Palacios A (2002) 'Assessment of different spectral indices in the red-near-infrared spectral domain for burned land discrimination' *International Journal of Remote Sensing* **23**, 5103–5110.

Chuvieco E, Riaño D, Danson FM, Martin P (2006) 'Use of a radiative transfer model to simulate the postfire spectral response to burn severity' *Journal of Geophysical Research: Biogeosciences* **111**,.

Cocke AE, Fulé PZ, Crouse JE (2005) ‘Comparison of burn severity assessments using Differenced Normalized Burn Ratio and ground data’ *International Journal of Wildland Fire* **14**, 189–198.

Datt B (1999) ‘A new reflectance index for remote sensing of chlorophyll content in higher plants: tests using Eucalyptus leaves’ *Journal of Plant Physiology* **154**, 30–36.

Dillon GK, Holden ZA, Morgan P, Crimmins MA, Heyerdahl EK, Luce CH (2011) ‘Both topography and climate affected forest and woodland burn severity in two regions of the western US, 1984 to 2006’ *Ecosphere* **2**, 1–33.

Doerr SH, Shakesby RA, Blake WH, Chafer CJ, Humphreys GS, Wallbrink PJ (2006) ‘Effects of differing wildfire severities on soil wettability and implications for hydrological response’ *Journal of Hydrology* **319**, 295–311.

Eidenshink J, Schwind B, Brewer K, Zhu ZL, Quayle B, Howard S (2007) ‘A project for monitoring trends in burn severity’ *Fire Ecology Special Issue* **3**, 2–21.

Epting J, Verbyla D, Sorbel B (2005) ‘Evaluation of remotely sensed indices for assessing burn severity in interior Alaska using Landsat TM and ETM+’ *Remote Sensing of Environment* **96**, 328–339.

Escuin S, Navarro R, Fernandez P (2008) ‘Fire severity assessment by using NBR (Normalized Burn Ratio) and NDVI (Normalized Difference Vegetation Index) derived from LANDSAT TM/ETM images’ *International Journal of Remote Sensing* **29**, 1053–1073.

Fang L, Yang J (2014) ‘Atmospheric effects on the performance and threshold extrapolation of

multi-temporal Landsat derived dNBR for burn severity assessment.' *International Journal of Applied Earth Observation and Geoinformation* **33**, 10–20. doi:10.1016/j.jag.2014.04.017

Fernandez-García V, Quintano C, Taboada A, Marcos E, Calvo L, Fernandez-Manso A (2018) 'Remote Sensing Applied to the Study of Fire Regime Attributes and Their Influence on Post-Fire Greenness Recovery in Pine Ecosystems' *Remote Sensing* **10**, 733. doi:http://dx.doi.org/10.3390/rs10050733

Fernández-García V, Santamarta M, Fernández-Manso A, Quintano C, Marcos E, Calvo L (2018) 'Burn severity metrics in fire-prone pine ecosystems along a climatic gradient using Landsat imagery' *Remote Sensing of Environment* **206**, 205–217.

Fernández-Manso A, Quintano C, Fernandez-Manso A, Quintano C (2015) 'Evaluating Landsat ETM+ emissivity-enhanced spectral indices for burn severity discrimination in Mediterranean forest ecosystems.' *Remote Sensing Letters* **6**, 302–310. doi:10.1080/2150704X.2015.1029093

Fire Bundles. Available at https://www.mtbs.gov/direct-download

(2020) Fire Perimeters. Available at https://frap.fire.ca.gov/mapping/gis-data/

Fraser RH, Sluijs J Vander, Hall RJ (2017) 'Calibrating Satellite-Based Indices of Burn Severity from UAV-Derived Metrics of a Burned Boreal Forest in NWT, Canada' *Remote Sensing* **9**, 279. doi:http://dx.doi.org/10.3390/rs9030279

French NHF, Kasischke ES, Hall RJ, Murphy KA, Verbyla DL, Hoy EE, Allen JL (2008) 'Using

Landsat data to assess fire and burn severity in the North American boreal forest region: an overview and summary of results' *International Journal of Wildland Fire* **17**, 443–462.

Furniss TJ, Kane VR, Larson AJ, Lutz JA (2020) 'Detecting tree mortality with Landsat-derived spectral indices: Improving ecological accuracy by examining uncertainty' *Remote Sensing of Environment* **237**, 111497.

Garcia-Llamas P, Suarez-Seoane S, Manuel Fernandez-Guisuraga J, Fernandez-Garcia V, Fernandez-Manso A, Quintano C, Taboada A, Marcos E, Calvo L (2019) 'Evaluation and comparison of Landsat 8, Sentinel-2 and Deimos-1 remote sensing indices for assessing burn severity in Mediterranean fire-prone ecosystems' *International Journal of Applied Earth Observation and Geoinformation* **80**, 137–144. doi:10.1016/j.jag.2019.04.006

García MJL, Caselles V (1991) 'Mapping burns and natural reforestation using Thematic Mapper data' *Geocarto International* **6**, 31–37.

Gerard F, Plummer S, Wadsworth R, Sanfeliu AF, Iliffe L, Balzter H, Wyatt B (2003) 'Forest fire scar detection in the boreal forest with multitemporal SPOT-VEGETATION data' *IEEE Transactions on Geoscience and Remote Sensing* **41**, 2575–2585.

Gitelson A, Merzlyak MN (1994) 'Spectral reflectance changes associated with autumn senescence of Aesculus hippocastanum L. and Acer platanoides L. leaves. Spectral features and relation to chlorophyll estimation' *Journal of plant physiology* **143**, 286–292.

Gitelson AA, Viña A, Ciganda V, Rundquist DC, Arkebauer TJ (2005) 'Remote estimation of canopy chlorophyll content in crops' *Geophysical Research Letters* **32**,.

Greene DF, Noël J, Bergeron Y, Rousseau M, Gauthier S (2004) 'Recruitment of Picea mariana, Pinus banksiana, and Populus tremuloides across a burn severity gradient following wildfire in the southern boreal forest of Quebec' *Canadian Journal of Forest Research* **34**, 1845–1857.

Hall RJ, Freeburn JT, De Groot WJ, Pritchard JM, Lynham TJ, Landry R (2008) 'Remote sensing of burn severity: experience from western Canada boreal fires' *International Journal of Wildland Fire* **17**, 476–489.

Hammill KA, Bradstock RA (2006) 'Remote sensing of fire severity in the Blue Mountains: influence of vegetation type and inferring fire intensity' *International Journal of Wildland Fire* **15**, 213–226.

Harvey BJ, Andrus RA, Anderson SC (2019) 'Incorporating biophysical gradients and uncertainty into burn severity maps in a temperate fire-prone forested region' *Ecosphere*. doi:10.1002/ecs2.2600

Harvey BJ, Donato DC, Turner MG (2014) 'Recent mountain pine beetle outbreaks, wildfire severity, and postfire tree regeneration in the US Northern Rockies' *Proceedings of the National Academy of Sciences* **111**, 15120–15125.

Heyerdahl EK, Brubaker LB, Agee JK (2001) 'Spatial controls of historical fire regimes: a multiscale example from the interior west, USA' *Ecology* **82**, 660–678.

Holden ZA, Evans JS (2010) 'Using fuzzy C-means and local autocorrelation to cluster satellite-inferred burn severity classes.' *International Journal of Wildland Fire* **19**, 853–860.

doi:10.1071/WF08126

Holden ZA, Morgan P, Smith AMS, Vierling L (2010) ‘Beyond Landsat: a comparison of four satellite sensors for detecting burn severity in ponderosa pine forests of the Gila Wilderness, NM, USA.’ *International Journal of Wildland Fire* **19**, 449–458. doi:10.1071/WF07106

Hoy EE, French NHF, Turetsky MR, Trigg SN, Kasischke ES (2008) ‘Evaluating the potential of Landsat TM/ETM+ imagery for assessing fire severity in Alaskan black spruce forests’ *International Journal of Wildland Fire* **17**, 500–514.

Huang C, Song K, Kim S, Townshend JRG, Davis P, Masek JG, Goward SN (2008) ‘Use of a dark object concept and support vector machines to automate forest cover change analysis’ *Remote sensing of environment* **112**, 970–985.

Hudak AT, Robichaud P, Evans JS, Clark J, Lannom K, Morgan P, Stone C (2004) ‘Field validation of Burned Area Reflectance Classification (BARC) products for post fire assessment’

Huete AR (1988) ‘A soil-adjusted vegetation index (SAVI)’ *Remote sensing of environment* **25**, 295–309.

Hultquist C, Chen G, Zhao K (2014) ‘A comparison of Gaussian process regression, random forests and support vector regression for burn severity assessment in diseased forests’ *Remote sensing letters* **5**, 723–732.

Isaev AS, Korovin GN, Bartalev SA, Ershov D V, Janetos A, Kasischke ES, Shugart HH, French NHF, Orlick BE, Murphy TL (2002) ‘Using remote sensing to assess Russian forest fire

carbon emissions' *Climatic Change* **55**, 235–249.

Jain TB, Graham RT (2004) Is forest structure related to fire severity? Yes, no, maybe: Methods and insights in quantifying the answer. In 'Shepperd, Wayne D.; Eskew, Lane G.[Comps.]. Silvic. Spec. places Proc. Natl. Silvic. Work. Granby, CO. RMRS-P-34. Fort Collins, CO. USDA For. Serv. Rocky Mt. Res. Stn.', 217–234

Johnstone JF, Chapin FS (2006) 'Effects of soil burn severity on post-fire tree recruitment in boreal forest' *Ecosystems* **9**, 14–31.

Karau EC, Keane RE (2010) 'Burn severity mapping using simulation modelling and satellite imagery super(A)' *International Journal of Wildland Fire* **19**, 710–724. doi:10.1071/WF09018

Karau EC, Sikkink PG, Keane RE, Dillon GK (2014) 'Integrating Satellite Imagery with Simulation Modeling to Improve Burn Severity Mapping' *Environmental Management* **54**, 98–111. doi:http://dx.doi.org/10.1007/s00267-014-0279-x

Kasischke ES, Turetsky MR, Ottmar RD, French NHF, Hoy EE, Kane ES (2008) 'Evaluation of the composite burn index for assessing fire severity in Alaskan black spruce forests' *International Journal of Wildland Fire* **17**, 515–526.

Kaufman YJ, Remer LA (1994) 'Detection of forests using mid-IR reflectance: an application for aerosol studies' *IEEE transactions on geoscience and remote sensing* **32**, 672–683.

Kauth RJ, Thomas GS (1976) The tasselled cap--a graphic description of the spectral-temporal development of agricultural crops as seen by Landsat. In 'LARS Symp.', 159

Keeley JE (2009) ‘Fire intensity, fire severity and burn severity: a brief review and suggested usage’ *International Journal of Wildland Fire* **18**, 116–126. doi:10.1071/WF07049

Key CH, Benson NC (1999) Measuring and remote sensing of burn severity. In ‘Proc. Jt. fire Sci. Conf. Work.’, 284. (University of Idaho and International Association of Wildland Fire Moscow, ID)

Key CH, Benson N (2002) ‘Landscape Assessment. Fire effects monitoring and inventory protocol’

Key CH, Benson NC (2006) ‘Landscape assessment (LA)’ *FIREMON: Fire effects monitoring and inventory system Gen Tech Rep RMRS-GTR-164-CD, Fort Collins, CO: US Department of Agriculture, Forest Service, Rocky Mountain Research Station*.

Knapp EE, Keeley JE (2006) ‘Heterogeneity in fire severity within early season and late season prescribed burns in a mixed-conifer forest’ *International Journal of Wildland Fire* **15**, 37–45.

Kokaly RF, Rockwell BW, Haire SL, King TV V (2007) ‘Characterization of post-fire surface cover, soils, and burn severity at the Cerro Grande Fire, New Mexico, using hyperspectral and multispectral remote sensing’ *Remote Sensing of Environment* **106**, 305–325.

Kolden CA, Rogan J (2009) ‘Spectral unmixing of MODIS pixels to derive burn severity: an alternative approach to Landsat-derived dNBR.’ (Association of American Geographers, 1710 16th St, NW Washington, DC 20009 USA) Available at https://search.proquest.com/docview/745927669?accountid=14784

Kolden CA, Rogan J (2013) ‘Mapping wildfire burn severity in the Arctic tundra from downsampled MODIS data’ *Arctic, Antarctic, and Alpine Research* **45**, 64–76.

Koutsias N, Karteris M, Chuvico E (2000) ‘The use of intensity-hue-saturation transformation of Landsat-5 Thematic Mapper data for burned land mapping’ *Photogrammetric Engineering and Remote Sensing* **66**, 829–840.

Koutsias N, Karteris M, Fernandez-Palacios A, Navarro C, Jurado J, Navarro R, Lobo A (1999) Burnt land mapping at local scale. In ‘Remote Sens. large wildfires’. pp. 157–187. (Springer)

Kushla JD, Ripple WJ (1998) ‘Assessing wildfire effects with Landsat thematic mapper data’ *International Journal of Remote Sensing* **19**, 2493–2507.

Larson AJ, Jeronimo SMA, Hessburg PF, Lutz JA, Povak NA, Cansler CA, Kane VR, Churchill DJ (2022) ‘Tamm Review: Ecological principles to guide post-fire forest landscape management in the Inland Pacific and Northern Rocky Mountain regions’ *Forest Ecology and Management* **504**, 119680.

Lentile LB, Holden ZA, Smith AMSS, Falkowski MJ, Hudak AT, Morgan P, Lewis SA, Gessler PE, Benson NC (2006) ‘Remote sensing techniques to assess active fire characteristics and post-fire effects’ *International Journal of Wildland Fire* **15**, 319–345. doi:10.1071/WF05097

Liu HQ, Huete A (1995) ‘A feedback based modification of the NDVI to minimize canopy background and atmospheric noise’ *IEEE transactions on geoscience and remote sensing*

33, 457–465.

Loboda T V, French NHF, Hight-Harf C, Jenkins L, Miller ME (2013) 'Mapping fire extent and burn severity in Alaskan tussock tundra: An analysis of the spectral response of tundra vegetation to wildland fire' *Remote Sensing of Environment* **134**, 194–209.

Macdonald SE (2007) 'Effects of partial post-fire salvage harvesting on vegetation communities in the boreal mixedwood forest region of northeastern Alberta, Canada' *Forest Ecology and Management* **239**, 21–31.

Mallinis G, Mitsopoulos I, Chrysafi I (2018) 'Evaluating and comparing Sentinel 2A and Landsat-8 Operational Land Imager (OLI) spectral indices for estimating fire severity in a Mediterranean pine ecosystem of Greece' *Giscience & Remote Sensing* **55**, 1–18. doi:10.1080/15481603.2017.1354803

Malthus TJ, Andrieu B, Danson FM, Jaggard KW, Steven MD (1993) 'Candidate high spectral resolution infrared indices for crop cover' *Remote Sensing of Environment* **46**, 204–212.

McCarley TR, Kolden CA, Vaillant NM, Hudak AT, Smith AMSS, Wing BM, Kellogg BS, Kreitler J (2017) 'Multi-temporal LiDAR and Landsat quantification of fire-induced changes to forest structure' *Remote sensing of environment* **191**, 419–432. doi:10.1016/j.rse.2016.12.022

McCarley TR, Kolden CA, Valliant NM, Hudak AT, Smith AMS, Kreitler J (2017) 'Landscape-scale quantification of fire-induced change in canopy cover following mountain pine beetle outbreak and timber harvest' *Forest Ecology and Management* **391**, 164–175.

doi:10.1016/j.foreco.2017.02.015

Meddens AJH, Kolden CA, Lutz JA (2016) 'Detecting unburned areas within wildfire perimeters using Landsat and ancillary data across the northwestern United States' *Remote Sensing of Environment* **186**, 275–285.

Meng Q, Meentemeyer RK (2011) 'Modeling of multi-strata forest fire severity using Landsat TM Data' *International Journal of Applied Earth Observation and Geoinformation* **13**, 120–126.

Michalek JL, French NHF, Kasischke ES, Johnson RD, Colwell JE (2000) 'Using Landsat TM data to estimate carbon release from burned biomass in an Alaskan spruce forest complex' *International Journal of Remote Sensing* **21**, 323–338.

Miller JD, Knapp EE, Key CH, Skinner CN, Isbell CJ, Creasy RM, Sherlock JW (2009) 'Calibration and validation of the relative differenced Normalized Burn Ratio (RdNBR) to three measures of fire severity in the Sierra Nevada and Klamath Mountains, California, USA' *Remote Sensing of Environment* **113**, 645–656.

Miller JD, Thode AE (2007) 'Quantifying burn severity in a heterogeneous landscape with a relative version of the delta Normalized Burn Ratio (dNBR)' *Remote Sensing of Environment* **109**, 66–80.

Moreno JM, Oechel WC (1989) 'A simple method for estimating fire intensity after a burn in California chaparral.' *ACTA OECOL(OECOL PLANT)* **10**, 57–68.

Morgan P, Hardy CC, Swetnam TW, Rollins MG, Long DG (2001) 'Mapping fire regimes

across time and space: understanding coarse and fine-scale fire patterns' *International Journal of Wildland Fire* **10**, 329–342.

Morgan P, Keane RE, Dillon GK, Jain TB, Hudak AT, Karau EC, Sikkink PG, Holden ZA, Strand EK (2014) 'Challenges of assessing fire and burn severity using field measures, remote sensing and modelling' *International Journal of Wildland Fire* **23**, 1045–1060. doi:10.1071/WF13058

Murphy KA, Reynolds JH, Koltun JM (2008) 'Evaluating the ability of the differenced Normalized Burn Ratio (dNBR) to predict ecologically significant burn severity in Alaskan boreal forests' *International Journal of Wildland Fire* **17**, 490–499.

Musyimi Z, Said MY, Zida D, Rosenstock TS, Udelhoven T, Savadogo P, Leeuw J de, Aynekulu E, de Leeuw J, Aynekulu E (2017) 'Evaluating fire severity in Sudanian ecosystems of Burkina Faso using Landsat 8 satellite images' *Journal of Arid Environments* **139**, 95–109. doi:10.1016/j.jaridenv.2016.11.005

Neary DG (2004) 'An overview of fire effects on soils' *Southwest Hydrology* **3**, 18–19.

Nelson RF (1983) 'Detecting forest canopy change due to insect activity using Landsat MSS' *Photogrammetric Engineering and Remote Sensing* **49**, 1303–1314.

Odion DC, Hanson CT (2006) 'Fire severity in conifer forests of the Sierra Nevada, California' *Ecosystems* **9**, 1177–1189.

Olson DM, Dinerstein E (2002) 'The Global 200: Priority ecoregions for global conservation (PDF file)' *Annals of the Missouri Botanical Garden* **89**, 125–126.

Parker BM, Lewis T, Srivastava SK (2015) ‘Estimation and evaluation of multi-decadal fire severity patterns using Landsat sensors’ *Remote Sensing of Environment* **170**, 340–349. doi:http://dx.doi.org/10.1016/j.rse.2015.09.014

Parks SA, Dillon GK, Miller C (2014) ‘A new metric for quantifying burn severity: the Relativized Burn Ratio’ *Remote Sensing* **6**, 1827–1844.

Parks SA, Holsinger LM, Koontz MJ, Collins L, Whitman E, Parisien M-A, Loehman RA, Barnes JL, Bourdon J-F, Boucher J, Boucher Y, Caprio AC, Collingwood A, Hall RJ, Park J, Saperstein LB, Smetanka C, Smith RJ, Soverel N (2019) ‘Giving Ecological Meaning to Satellite-Derived Fire Severity Metrics across North American Forests’ *Remote Sensing* **11**, 1735. doi:10.3390/rs11141735

Parks SA, Holsinger LM, Voss MA, Loehman RA, Robinson NP (2018) ‘Mean Composite Fire Severity Metrics Computed with Google Earth Engine Offer Improved Accuracy and Expanded Mapping Potential’ *Remote Sensing* **10**, 879. doi:10.3390/rs10060879

Patterson MW, Yool SR (1998) ‘Mapping fire-induced vegetation mortality using Landsat Thematic Mapper data: A comparison of linear transformation techniques’ *Remote Sensing of Environment* **65**, 132–142.

Pereira JMC (1999) ‘A comparative evaluation of NOAA/AVHRR vegetation indexes for burned surface detection and mapping’ *IEEE transactions on geoscience and remote sensing* **37**, 217–226.

Pereira JMC, Sá ACL, Sousa AMO, Silva JMN, Santos TN, Carreiras JMB (1999) Spectral

characterisation and discrimination of burnt areas. In ‘Remote Sens. large wildfires’. pp. 123–138. (Springer)

Pereira MC, Setzer AW (1993) ‘Spectral characteristics of fire scars in Landsat-5 TM images of Amazonia’ *Remote Sensing* **14**, 2061–2078.

Picotte J, Arkle RS, Bastian H, Benson N, Cansler A, Caprio T, Dillon G, Key C, Klein RN, Kopper K, Meddens AJH, Ohlen D, Parks SA, Peterson DW, Pilliod D, Prichard S, Robertson K, Sparks A, Thode A (2019) Composite Burn Index (CBI) Data for the Conterminous US, Collected Between 1996 and 2018: U.S. Geological Survey data release. doi:10.5066/P91BH1BZ

Picotte JJ, Robertson KM (2011) ‘Validation of remote sensing of burn severity in south-eastern US ecosystems’ *International Journal of Wildland Fire* **20**, 453–464. doi:http://dx.doi.org/10.1071/WF10013

Pinty B, Verstraete MM (1992) ‘GEMI: a non-linear index to monitor global vegetation from satellites’ *Vegetatio* **101**, 15–20.

Pullin AS, Stewart GB (2006) ‘Guidelines for systematic review in conservation and environmental management’ *Conserv. Biol.* doi:10.1111/j.1523-1739.2006.00485.x

Qi J, Chehbouni A, Huete AR, Kerr YH, Sorooshian S (1994) ‘A modified soil adjusted vegetation index’ *Remote sensing of environment* **48**, 119–126.

Quintano C, Fernandez-Manso A, Calvo L, Marcos E, Valbuena L, Fernández-Manso A, Calvo L, Marcos E, Valbuena L (2015) ‘Land surface temperature as potential indicator of burn

severity in forest Mediterranean ecosystems.' *International Journal of Applied Earth Observation and Geoinformation* **36**, 1–12. doi:10.1016/j.jag.2014.10.015

Robichaud PR (2000) 'Evaluating the effectiveness of postfire rehabilitation treatments.' (US Department of Agriculture, Forest Service, Rocky Mountain Research Station)

Robichaud PR, Lewis SA, Laes DYM, Hudak AT, Kokaly RF, Zamudio JA (2007) 'Postfire soil burn severity mapping with hyperspectral image unmixing' *Remote Sensing of Environment* **108**, 467–480.

Rogan J, Franklin J (2001) 'Mapping wildfire burn severity in southern California forests and shrublands using Enhanced Thematic Mapper imagery' *Geocarto International* **16**, 91–106.

Rogan J, Yool SR (2001) 'Mapping fire-induced vegetation depletion in the Peloncillo Mountains, Arizona and New Mexico' *International Journal of Remote Sensing* **22**, 3101–3121.

Rouse Jr J, Haas RH, Schell JA, Deering DW (1974) 'Monitoring vegetation systems in the Great Plains with ERTS'

Ryan KC, Noste N V (1985) 'Evaluating prescribed fires' *Lotan, James E; Kilgore, Bruce M; Fischer, William C* 15–18.

Saberi SJ, Agne MC, Harvey BJ (2022) 'Do you CBI what I see? The relationship between the Composite Burn Index and quantitative field measures of burn severity varies across gradients of forest structure' *International Journal of Wildland Fire*.

De Santis A, Asner GP, Vaughan PJ, Knapp DE (2010) ‘Mapping burn severity and burning efficiency in California using simulation models and Landsat imagery’ *Remote Sensing of Environment* **114**, 1535–1545. doi:10.1016/j.rse.2010.02.008

De Santis A, Chuvieco E (2007) ‘Burn severity estimation from remotely sensed data: Performance of simulation versus empirical models’ *Remote Sensing of Environment* **108**, 422–435.

De Santis A, Chuvieco E (2009) ‘GeoCBI: a modified version of the Composite Burn Index for the initial assessment of the short-term burn severity from remotely sensed data.’ *Remote Sensing of Environment* **113**, 554–562. doi:10.1016/j.rse.2008.10.011

Schepers L, Haest B, Veraverbeke S, Spanhove T, Borre J Vanden, Goossens R (2014) ‘Burned Area Detection and Burn Severity Assessment of a Heathland Fire in Belgium Using Airborne Imaging Spectroscopy (APEX)’ *Remote Sensing* **6**, 1803–1826. doi:http://dx.doi.org/10.3390/rs6031803

Sikkink PG (2015) Comparison of six fire severity classification methods using Montana and Washington wildland fires. In ‘Keane, Robert E.; Jolly, Matt; Parsons, Russell; Riley, Karin. Proc. large Wildl. fires Conf. May 19-23, 2014; Missoula, MT. Proc. RMRS-P-73. Fort Collins, CO US Dep. Agric. For. Serv. Rocky Mt. Res. ’, 213–226

Sikkink PG, Dillon GK, Keane RE, Morgan P, Karau EC, Holden ZA, Silverstein RP (2013) ‘Composite Burn Index (CBI) data and field photos collected for the FIRESEV project, western United States’

Smith AMS, Drake NA, Wooster MJ, Hudak AT, Holden ZA, Gibbons CJ (2007) 'Production of Landsat ETM+ reference imagery of burned areas within Southern African savannahs: comparison of methods and application to MODIS' *International Journal of Remote Sensing* **28**, 2753–2775.

Smith AMS, Wooster MJ, Drake NA, Dipotso FM, Falkowski MJ, Hudak AT (2005) 'Testing the potential of multi-spectral remote sensing for retrospectively estimating fire severity in African Savannahs' *Remote sensing of environment* **97**, 92–115.

Sorbel B, Allen J (2005) 'Space-based burn severity mapping in Alaska's National Parks' *Alaska Park Science* **4**, 4–11.

Soverel NO, Coops NC, Perrakis DDB, Daniels LD, Gergel SE (2011) 'The transferability of a dNBR-derived model to predict burn severity across 10 wildland fires in western Canada' *International Journal of Wildland Fire* **20**, 518–531.

Soverel NO, Perrakis DDB, Coops NC (2010) 'Estimating burn severity from Landsat dNBR and RdNBR indices across western Canada' *Remote Sensing of Environment* **114**, 1896–1909.

Stambaugh MC, Hammer LD, Godfrey R (2015) 'Performance of Burn-Severity Metrics and Classification in Oak Woodlands and Grasslands' *Remote Sensing* **7**, 10501–10522. doi:http://dx.doi.org/10.3390/rs70810501

Talucci AC, Krawchuk MA (2019) 'Dead forests burning: the influence of beetle outbreaks on fire severity and legacy structure in sub-boreal forests' *Ecosphere* **10**, e02744.

Tanase MA, Kennedy R, Aponte C (2015a) ‘Fire severity estimation from space: a comparison of active and passive sensors and their synergy for different forest types’ *International Journal of Wildland Fire* **24**, 1062–1075. doi:10.1071/WF15059

Tanase MA, Kennedy R, Aponte C (2015b) ‘Radar burn ratio for fire severity estimation at canopy level: an example for temperate forests.’ *Remote Sensing of Environment* **170**, 14–31. doi:10.1016/j.rse.2015.08.025

Tanase M, de la Riva J, Pérez-Cabello F, Riva J de la, Pérez-Cabello F (2011) ‘Estimating burn severity at the regional level using optically based indices.’ *Canadian Journal of Forest Research* **41**, 863. doi:10.1139/x11-011

Tane Z, Roberts D, Veraverbeke S, Casas A, Ramirez C, Ustin S (2018) ‘Evaluating Endmember and Band Selection Techniques for Multiple Endmember Spectral Mixture Analysis using Post-Fire Imaging Spectroscopy’ *Remote Sensing* **10**, 389. doi:10.3390/rs10030389

Team RC (2017) ‘R Core Team (2017). R: A language and environment for statistical computing’ *R Found Stat Comput Vienna, Austria*.

Trigg S, Flasse S (2001) ‘An evaluation of different bi-spectral spaces for discriminating burned shrub-savannah’ *International Journal of Remote Sensing* **22**, 2641–2647.

Turner MG, Hargrove WW, Gardner RH, Romme WH (1994) ‘Effects of fire on landscape heterogeneity in Yellowstone National Park, Wyoming’ *Journal of Vegetation Science* **5**, 731–742.

Veraverbeke S, Harris S, Hook S (2011) ‘Evaluating spectral indices for burned area

discrimination using MODIS/ASTER (MASTER) airborne simulator data' *Remote Sensing of Environment* **115**, 2702–2709.

Veraverbeke S, Hook SJ (2013) 'Evaluating spectral indices and spectral mixture analysis for assessing fire severity, combustion completeness and carbon emissions' *International Journal of Wildland Fire* **22**, 707–720. doi:http://dx.doi.org/10.1071/WF12168

Veraverbeke S, Hook S, Hulley G (2012) 'An alternative spectral index for rapid fire severity assessments' *Remote Sensing of Environment* **123**, 72–80. doi:10.1016/j.rse.2012.02.025

Veraverbeke S, Lhermitte S, Verstraeten WW, Goossens R (2011) 'Evaluation of pre/post-fire differenced spectral indices for assessing burn severity in a Mediterranean environment with Landsat Thematic Mapper' *International Journal of Remote Sensing* **32**, 3521–3537.

Veraverbeke S, Stavros En, Hook SJ (2014) 'Assessing fire severity using imaging spectroscopy data from the Airborne Visible/Infrared Imaging Spectrometer (AVIRIS) and comparison with multispectral capabilities' *Remote Sensing of Environment* **154**, 153–163. doi:10.1016/j.rse.2014.08.019

Verbyla DL, Kasischke ES, Hoy EE (2008) 'Seasonal and topographic effects on estimating fire severity from Landsat TM/ETM+ data' *International Journal of Wildland Fire* **17**, 527–534.

Vogelmann JE (1990) 'Comparison between two vegetation indices for measuring different types of forest damage in the north-eastern United States' *Remote Sensing* **11**, 2281–2297.

van Wagtendonk JW, Root RR, Key CH, Wagtendonk JW van, Root RR, Key CH (2004)

‘Comparison of AVIRIS and Landsat ETM+ detection capabilities for burn severity’ *Remote Sensing of Environment* **92**, 397–408. doi:10.1016/j.rse.2003.12.015

Wang GG (2002) ‘Fire severity in relation to canopy composition within burned boreal mixedwood stands’ *Forest Ecology and Management* **163**, 85–92.

Warner TA, Skowronski NS, Gallagher MR (2017) ‘High spatial resolution burn severity mapping of the New Jersey Pine Barrens with WorldView-3 near-infrared and shortwave infrared imagery’ *International Journal of Remote Sensing* **38**, 598–616. doi:10.1080/01431161.2016.1268739

Wells CG, Campbell RE, DeBano LF, Lewis CE, Fredriksen RL, Franklin EC, Froelich RC, Dunn PH (1979) Effects of fire on soil: a state-of-knowledge. In ‘Gen. Tech. Rep. WO’. (United States Department of Agriculture, Forest Service)

White JD, Ryan KC, Key CC, Running SW (1996) ‘Remote sensing of forest fire severity and vegetation recovery’ *International Journal of Wildland Fire* **6**, 125–136.

Whitman E, Parisien M-AA, Thompson DK, Hall RJ, Skakun RS, Flannigan MD (2018) ‘Variability and drivers of burn severity in the northwestern Canadian boreal forest.’ *Ecosphere* **9**, e02128. doi:10.1002/ecs2.2128

Wu Z, Middleton B, Hetzler R, Vogel J, Dye D (2015) ‘Vegetation burn severity mapping using Landsat-8 and WorldView-2’ *Photogrammetric Engineering & Remote Sensing* **81**, 143–154.

Wulder MA, White JC, Alvarez F, Han T, Rogan J, Hawkes B (2009) ‘Characterizing boreal

forest wildfire with multi-temporal Landsat and LIDAR data' *Remote Sensing of Environment* **113**, 1540–1555.

Xiao X, Boles S, Liu J, Zhuang D, Liu M (2002) 'Characterization of forest types in Northeastern China, using multi-temporal SPOT-4 VEGETATION sensor data' *Remote Sensing of Environment* **82**, 335–348.

Yu X, Guo X, Wu Z (2014) 'Land surface temperature retrieval from Landsat 8 TIRS—Comparison between radiative transfer equation-based method, split window algorithm and single channel method' *Remote sensing* **6**, 9829–9852.

Zar JH (1999) 'Biostatistical analysis.' (Pearson Education India)

Zheng Z, Zeng Y, Li S, Huang W, Zhong Z, YongNian Z, SongNian L, Wei H (2016) 'A new burn severity index based on land surface temperature and enhanced vegetation index' *International Journal of Applied Earth Observation and Geoinformation* **45**, 84–94. doi:10.1016/j.jag.2015.11.002

Zhu Z, Key C, Ohlen D, Benson N (2006) 'Evaluate sensitivities of burn severity mapping algorithms for different ecosystems and fire histories in the United States. Final report JFSP 01-1-4-12' *October* **12**, 35.

2.7.2 SUPPLEMENTARY INFORMATION 2

The following table details the citations included in this study for review as well as the number of comparisons of field observations and remotely sensed data extracted for analysis. Further information regarding the data that support this study will be shared upon reasonable request to the corresponding author.

Citation	**Number of comparisons**
Allen, J. L., & Sorbel, B. (2008). Assessing the differenced Normalized Burn Ratio's ability to map burn severity in the boreal forest and tundra ecosystems of Alaska's national parks. International Journal of Wildland Fire, 17(4), 463–475.	11
Boucher, J., Beaudoin, A., Hébert, C., Guindon, L., Bauce, É., Hebert, C., Guindon, L., & Bauce, E. (2017). Assessing the potential of the differenced Normalized Burn Ratio (dNBR) for estimating burn severity in eastern Canadian boreal forests. International Journal of Wildland Fire, 26(1), 32–45. https://doi.org/10.1071/WF15122	10
Cansler, C. A., & McKenzie, D. (2012). How robust are burn severity indices when applied in a new region? Evaluation of alternate field-based and remote-sensing methods. Remote Sensing, 4(2), 456–483.	4
Chang, Y., Zhu, Z., Feng, Y., Li, Y., Bu, R., & Hu, Y. (2016). The spatial variation in forest burn severity in Heilongjiang Province, China. Natural Hazards, 81(2), 981–1001. https://doi.org/http://dx.doi.org/10.1007/s11069-015-2116-9	16
Chen, G., Metz, M. R., Rizzo, D. M., & Meentemeyer, R. K. (2015). Mapping burn severity in a disease-impacted forest landscape using Landsat and MASTER imagery. International Journal of Applied Earth Observation and Geoinformation, 40, 91–99. https://doi.org/10.1016/j.jag.2015.04.005	2

Chen, X. X., Vogelmann, J. E., Rollins, M., Ohlen, D., Key, C. H., Yang, L. M., Huang, C. Q., & Shi, H. (2011). Detecting post-fire burn severity and vegetation recovery using multitemporal remote sensing spectral indices and field-collected composite burn index data in a ponderosa pine forest. International Journal of Remote Sensing, 32(23), 7905–7927. https://doi.org/10.1080/01431161.2010.524678 5

Cocke, A. E., Fulé, P. Z., & Crouse, J. E. (2005). Comparison of burn severity assessments using Differenced Normalized Burn Ratio and ground data. International Journal of Wildland Fire, 14(2), 189–198. 2

De Santis, A., & Chuvieco, E. (2007). Burn severity estimation from remotely sensed data: Performance of simulation versus empirical models. Remote Sensing of Environment, 108(4), 422–435. 1

De Santis, A., & Chuvieco, E. (2009). GeoCBI: a modified version of the Composite Burn Index for the initial assessment of the short-term burn severity from remotely sensed data. Remote Sensing of Environment, 113(3), 554–562. https://doi.org/10.1016/j.rse.2008.10.011 3

De Santis, A., Asner, G. P., Vaughan, P. J., & Knapp, D. E. (2010). Mapping burn severity and burning efficiency in California using simulation models and Landsat imagery. Remote Sensing of Environment, 114(7), 1535–1545. https://doi.org/10.1016/j.rse.2010.02.008 1

Epting, J., Verbyla, D., & Sorbel, B. (2005). Evaluation of remotely sensed indices for assessing burn severity in interior Alaska using Landsat TM and ETM+. Remote Sensing of Environment, 96(3–4), 328–339. 4

Fang, L., & Yang, J. (2014). Atmospheric effects on the performance and threshold extrapolation of multi-temporal Landsat derived dNBR for burn severity assessment. International Journal of Applied Earth Observation and Geoinformation, 33, 10–20. https://doi.org/10.1016/j.jag.2014.04.017 1

Fernández-García, V., Quintano, C., Taboada, A., Marcos, E., Calvo, L., & Fernández-Manso, A. (2018). Remote sensing applied to the study of fire regime attributes and their influence on post-fire greenness recovery in pine ecosystems. Remote Sensing, 10(5), 733. https://doi.org/10.3390/rs10050733 4

Fernández-Manso, A., Quintano, C., Fernandez-Manso, A., & Quintano, C. (2015). Evaluating Landsat ETM+ emissivity-enhanced spectral indices for burn severity discrimination in Mediterranean forest ecosystems. Remote Sensing Letters, 6(4), 302–310. https://doi.org/10.1080/2150704X.2015.1029093 1

Fraser, R. H., Sluijs, J. Vander, & Hall, R. J. (2017). Calibrating Satellite-Based Indices of Burn Severity from UAV-Derived Metrics of a Burned Boreal Forest in NWT, Canada. Remote Sensing, 9(3), 279. https://doi.org/http://dx.doi.org/10.3390/rs9030279 2

Garcia-Llamas, P., Suarez-Seoane, S., Manuel Fernandez-Guisuraga, J., Fernandez-Garcia, V., Fernandez-Manso, A., Quintano, C., Taboada, A., Marcos, E., & Calvo, L. (2019). Evaluation and comparison of Landsat 8, Sentinel-2 and Deimos-1 remote sensing indices for assessing burn severity in Mediterranean fire-prone ecosystems. International Journal of Applied Earth Observation and Geoinformation, 80, 137–144. https://doi.org/10.1016/j.jag.2019.04.006 3

Hall, R. J., Freeburn, J. T., De Groot, W. J., Pritchard, J. M., Lynham, T. J., & Landry, R. (2008). Remote sensing of burn severity: experience from western Canada boreal fires. International Journal of Wildland Fire, 17(4), 476–489. 4

Holden, Z. A., & Evans, J. S. (2010). Using fuzzy C-means and local autocorrelation to cluster satellite-inferred burn severity classes. International Journal of Wildland Fire, 19(7), 853–860. https://doi.org/10.1071/WF08126 3

Holden, Z. A., Morgan, P., Smith, A. M. S., & Vierling, L. (2010). Beyond Landsat: a comparison of four satellite sensors for detecting burn severity in ponderosa pine forests of the Gila Wilderness, NM, USA. International Journal of Wildland Fire, 19(4), 449–458. https://doi.org/10.1071/WF07106 5

Hoy, E. E., French, N. H. F., Turetsky, M. R., Trigg, S. N., & Kasischke, E. S. (2008). Evaluating the potential of Landsat TM/ETM+ imagery for assessing fire severity in Alaskan black spruce forests. International Journal of Wildland Fire, 17(4), 500–514. 2

Hultquist, C., Chen, G., & Zhao, K. (2014). A comparison of Gaussian process regression, random forests and support vector regression for burn severity assessment in diseased forests. Remote Sensing Letters, 5(8), 723–732. 1

Karau, E. C., & Keane, R. E. (2010). Burn severity mapping using simulation modelling and satellite imagery super(A). International Journal of Wildland Fire, 19(6), 710–724. https://doi.org/10.1071/WF09018 4

Karau, E. C., Sikkink, P. G., Keane, R. E., & Dillon, G. K. (2014). Integrating Satellite Imagery with Simulation Modeling to Improve Burn Severity Mapping. Environmental Management, 54(1), 98–111. https://doi.org/http://dx.doi.org/10.1007/s00267-014-0279-x 15

Kolden, C. A., & Rogan, J. (2013). Mapping wildfire burn severity in the Arctic tundra from downsampled MODIS data. Arctic, Antarctic, and Alpine Research, 45(1), 64–76. 6

Kurbanov, E., Vorobyev, O., Leznin, S., Polevshikova, Y., & Demisheva, E. (2017). Assessment of burn severity in Middle Povozhje with Landsat multitemporal data. International Journal of Wildland Fire, 26(9), 772–782. https://doi.org/10.1071/WF16141 1

Loboda, T. V, French, N. H. F., Hight-Harf, C., Jenkins, L., & Miller, M. E. (2013). Mapping fire extent and burn severity in Alaskan tussock tundra: An analysis of the spectral response of tundra vegetation to wildland fire. Remote Sensing of Environment, 134, 194–209. 105

Mallinis, G., Mitsopoulos, I., & Chrysafi, I. (2018). Evaluating and comparing Sentinel 2A and Landsat-8 Operational Land Imager (OLI) spectral indices for estimating fire severity in a Mediterranean pine ecosystem of Greece. Giscience & Remote Sensing, 55(1), 1–18. https://doi.org/10.1080/15481603.2017.1354803 2

Meng, Q., & Meentemeyer, R. K. (2011). Modeling of multi-strata forest fire severity using Landsat TM Data. International Journal of Applied Earth Observation and Geoinformation, 13(1), 120–126. 1

Miller, J. D., & Quayle, B. (2015). Calibration and validation of immediate post-fire satellite-derived data to three severity metrics. Fire Ecology, 11(2), 12–30. http://fireecologyjournal.org/docs/Journal/pdf/Volume11/Issue02/012.pdf 8

Miller, J. D., & Thode, A. E. (2007). Quantifying burn severity in a heterogeneous landscape with a relative version of the delta Normalized Burn Ratio (dNBR). Remote Sensing of Environment, 109(1), 66–80. 13

Miller, J. D., Knapp, E. E., Key, C. H., Skinner, C. N., Isbell, C. J., Creasy, R. M., & Sherlock, J. W. (2009). Calibration and validation of the relative differenced Normalized Burn Ratio (RdNBR) to three measures of fire severity in the Sierra Nevada and Klamath Mountains, California, USA. Remote Sensing of Environment, 113(3), 645–656. 26

Murphy, K. A., Reynolds, J. H., & Koltun, J. M. (2008). Evaluating the ability of the differenced Normalized Burn Ratio (dNBR) to predict ecologically significant burn severity in Alaskan boreal forests. International Journal of Wildland Fire, 17(4), 490–499. 12

Musyimi, Z., Said, M. Y., Zida, D., Rosenstock, T. S., Udelhoven, T., Savadogo, P., Leeuw, J. de, Aynekulu, E., de Leeuw, J., & Aynekulu, E. (2017). Evaluating fire severity in Sudanian ecosystems of Burkina Faso using Landsat 8 satellite images. Journal of Arid Environments, 139, 95–109. https://doi.org/10.1016/j.jaridenv.2016.11.005 8

Parker, B. M., Lewis, T., & Srivastava, S. K. (2015). Estimation and evaluation of multi-decadal fire severity patterns using Landsat sensors. Remote Sensing of Environment, 170, 340–349. https://doi.org/http://dx.doi.org/10.1016/j.rse.2015.09.014 1

Parks, S. A., Dillon, G. K., & Miller, C. (2014). A new metric for quantifying burn severity: the Relativized Burn Ratio. Remote Sensing, 6(3), 1827–1844. 18

Parks, S. A., Holsinger, L. M., Koontz, M. J., Collins, L., Whitman, E., Parisien, M.-A., Loehman, R. A., Barnes, J. L., Bourdon, J.-F., Boucher, J., Boucher, Y., Caprio, A. C., Collingwood, A., Hall, R. J., Park, J., Saperstein, L. B., Smetanka, C., Smith, R. J., & Soverel, N. (2019). Giving Ecological Meaning to Satellite-Derived Fire Severity Metrics across North American Forests. Remote Sensing, 11(14), 1735. https://doi.org/10.3390/rs11141735 256

Parks, S. A., Holsinger, L. M., Voss, M. A., Loehman, R. A., & Robinson, N. P. (2018). Mean Composite Fire Severity Metrics Computed with Google Earth Engine Offer Improved 18

Accuracy and Expanded Mapping Potential. Remote Sensing, 10(6), 879. https://doi.org/10.3390/rs10060879

Picotte, J. J., & Robertson, K. M. (2011). Validation of remote sensing of burn severity in south-eastern US ecosystems. International Journal of Wildland Fire, 20(3), 453–464. https://doi.org/http://dx.doi.org/10.1071/WF10013 27

Quintano, C., Fernandez-Manso, A., Calvo, L., Marcos, E., Valbuena, L., Fernández-Manso, A., Calvo, L., Marcos, E., & Valbuena, L. (2015). Land surface temperature as potential indicator of burn severity in forest Mediterranean ecosystems. International Journal of Applied Earth Observation and Geoinformation, 36, 1–12. https://doi.org/10.1016/j.jag.2014.10.015 6

Schepers, L., Haest, B., Veraverbeke, S., Spanhove, T., Borre, J. Vanden, & Goossens, R. (2014). Burned Area Detection and Burn Severity Assessment of a Heathland Fire in Belgium Using Airborne Imaging Spectroscopy (APEX). Remote Sensing, 6(3), 1803–1826. https://doi.org/http://dx.doi.org/10.3390/rs6031803 1

Soverel, N. O., Perrakis, D. D. B., & Coops, N. C. (2010). Estimating burn severity from Landsat dNBR and RdNBR indices across western Canada. Remote Sensing of Environment, 114(9), 1896–1909. 6

Stambaugh, M. C., Hammer, L. D., & Godfrey, R. (2015). Performance of Burn-Severity Metrics and Classification in Oak Woodlands and Grasslands. Remote Sensing, 7(8), 10501–10522. https://doi.org/http://dx.doi.org/10.3390/rs70810501 3

Strand, E. K., Bunting, S. C., & Keefe, R. F. (2013). Influence of Wildland Fire Along a Successional Gradient in Sagebrush Steppe and Western Juniper Woodlands. Rangeland Ecology and Management, 66(6), 667–679. https://search.proquest.com/docview/1468524215?accountid=14784 3

Tanase, M. A., Kennedy, R., & Aponte, C. (2015). Fire severity estimation from space: a comparison of active and passive sensors and their synergy for different forest types. International Journal of Wildland Fire, 24(8), 1062–1075. https://doi.org/10.1071/WF15059 14

Tanase, M. A., Kennedy, R., & Aponte, C. (2015). Radar burn ratio for fire severity estimation at canopy level: an example for temperate forests. Remote Sensing of Environment, 170, 14–31. https://doi.org/10.1016/j.rse.2015.08.025 10

Tanase, M., de la Riva, J., Pérez-Cabello, F., Riva, J. de la, & Pérez-Cabello, F. (2011). Estimating burn severity at the regional level using optically based indices. Canadian Journal of Forest Research, 41(4), 863. https://doi.org/10.1139/x11-011 5

Tane, Z., Roberts, D., Veraverbeke, S., Casas, Á., Ramirez, C., & Ustin, S. (2018). Evaluating endmember and band selection techniques for Multiple Endmember Spectral Mixture Analysis using post-fire imaging spectroscopy. Remote Sensing, 10(3), 389. https://doi.org/10.3390/rs10030389 1

van Wagtendonk, J. W., Root, R. R., Key, C. H., Wagtendonk, J. W. van, Root, R. R., & Key, C. H. (2004). Comparison of AVIRIS and Landsat ETM+ detection capabilities for burn severity. Remote Sensing of Environment, 92(3), 397–408. https://doi.org/10.1016/j.rse.2003.12.015 2

Veraverbeke, S., & Hook, S. J. (2013). Evaluating spectral indices and spectral mixture analysis for assessing fire severity, combustion completeness and carbon emissions. International Journal of Wildland Fire, 22(5), 707–720. https://doi.org/http://dx.doi.org/10.1071/WF12168 1

Veraverbeke, S., Hook, S. J., & Harris, S. (2012). Synergy of VSWIR (0.4-2.5 µM) and MTIR (3.5-12.5 µM) data for post-fire assessments. Remote Sensing of Environment, 124, 771–779. https://doi.org/10.1016/j.rse.2012.06.028 1

Veraverbeke, S., Hook, S., & Hulley, G. (2012). An alternative spectral index for rapid fire severity assessments. Remote Sensing of Environment, 123, 72–80. https://doi.org/10.1016/j.rse.2012.02.025 2

Veraverbeke, S., Lhermitte, S., Verstraeten, W. W., & Goossens, R. (2010). The temporal dimension of differenced Normalized Burn Ratio (dNBR) fire/burn severity studies: The case of the large 2007 Peloponnese wildfires in Greece. Remote Sensing of Environment, 114(11), 2548–2563. https://doi.org/http://dx.doi.org/10.1016/j.rse.2010.05.029 2

Veraverbeke, S., Lhermitte, S., Verstraeten, W. W., & Goossens, R. (2011). Evaluation of pre/post-fire differenced spectral indices for assessing burn severity in a Mediterranean environment with Landsat Thematic Mapper. International Journal of Remote Sensing, 32(12), 3521–3537. 1

Veraverbeke, S., Stavros, E. N., & Hook, S. J. (2014). Assessing fire severity using imaging spectroscopy data from the Airborne Visible/Infrared Imaging Spectrometer (AVIRIS) and comparison with multispectral capabilities. Remote Sensing of Environment, 154, 153–163. https://doi.org/10.1016/j.rse.2014.08.019 2

Veraverbeke, S., Verstraeten, W. W., Lhermitte, S., & Goossens, R. (2010). Evaluating Landsat Thematic Mapper spectral indices for estimating burn severity of the 2007 Peloponnese wildfires in Greece. International Journal of Wildland Fire, 19(5), 558–569. https://doi.org/10.1071/WF09069 1

Warner, T. A., Skowronski, N. S., & Gallagher, M. R. (2017). High spatial resolution burn severity mapping of the New Jersey Pine Barrens with WorldView-3 near-infrared and shortwave infrared imagery. International Journal of Remote Sensing, 38(2), 598–616. https://doi.org/10.1080/01431161.2016.1268739 1

Whitman, E., Parisien, M.-A., Thompson, D. K., Hall, R. J., Skakun, R. S., & Flannigan, M. D. (2018). Variability and drivers of burn severity in the northwestern Canadian boreal forest. Ecosphere, 9(2), e02128. https://doi.org/10.1002/ecs2.2128 6

Wimberly, M. C., & Reilly, M. J. (2007). Assessment of fire severity and species diversity in the southern Appalachians using Landsat TM and ETM+ imagery. Remote Sensing of Environment, 108(2), 189–197. https://doi.org/10.1016/j.rse.2006.03.019 1

Wu, Z., Middleton, B., Hetzler, R., Vogel, J., & Dye, D. (2015). Vegetation burn severity mapping using Landsat-8 and WorldView-2. Photogrammetric Engineering & Remote Sensing, 81(2), 143–154. 2

Zheng, Z., Zeng, Y., Li, S., & Huang, W. (2018). Mapping Burn Severity of Forest Fires in Small Sample Size Scenarios. Forests, 9(10), 608. https://doi.org/10.3390/f9100608 4

Zheng, Z., Zeng, Y., Li, S., Huang, W., Zhong, Z., YongNian, Z., SongNian, L., & Wei, H. (2016). A new burn severity index based on land surface temperature and enhanced vegetation index. International Journal of Applied Earth Observation and Geoinformation, 45(Part A), 84–94. https://doi.org/10.1016/j.jag.2015.11.002 4

Chapter 3. Spatial alignment and temporal synchrony between field observations and remotely sensed data in empirical studies of burn severity using the Composite Burn Index

3.0 Abstract

Methods for modeling burn severity using Composite Burn Index plots and remotely sensed data are variable, with key differences among studies along several dimensions. Here, we explored spatial and temporal considerations of modeling methods, using a comprehensive set of studies comparing field-based observations of burn severity to remotely sensed data. Our aims were to: 1) explore the conceptual spatiotemporal underpinnings of remote sensing in the context of burn severity modeling (which has been less explored compared with other disciplines); 2) understand how studies deal with integrating data sources that span multiple spatial scales; and 3) investigate the importance of temporal synchrony (i.e., temporal synchrony of field and satellite measures) on model results. Addressing spatial alignment in particular is increasingly important as new sources of remotely sensed data at varying spatial resolutions become available. We reviewed studies obtained through systematic literature search to extract relevant information with regards to data characteristics defining how and when comparisons are made. Comparing results across different studies and sensors was challenging due to the lack of consistency in methods used and spectral resolutions captured, respectively. However, we provided a conceptual model useful for selecting how pixel values over plot center are defined. Additionally, the reviewed studies suggest that temporal synchrony is less important than is typically recommended. On the contrary, stronger model relationships were often found between more temporally asynchronous

datasets. We offered explicit recommendations for study design and analysis in the context of spatial alignment and temporal synchrony.

3.1 Introduction

Remotely sensed data are often calibrated with field observations to map ecosystem change due to fire, building models based on unique fire and landscape characteristics. Field samples allow burned areas to be consistently distinguished from unburned areas, separate recent from older burns, and help quantity severity of effects across a fire (Key and Benson 1999). While in some areas, remotely sensed may be the only option for assessing landscape change due to the large extents of wildfires, remoteness of areas burned, and the rugged terrain that makes fieldwork difficult and dangerous (Key and Benson 1999; Cansler and McKenzie 2012), field samples are commonly used to calibrate radiometric changes detected by satellite with actual fire effects (Montealegre *et al.* 2014). In cases that use only remotely sensed data, levels of severity (the ecological effects of fire, or fire-caused change, Lentile *et al.* 2006) and ecosystem change may be estimated using generic thresholds for spectral indices rather than field-calibrated values measured on a fire-by-fire basis. However, both remotely sensed data and field samples are necessary for a full evaluation of fire effects (French *et al.* 2008). Factors that are temporally sensitive (i.e., influenced by ecosystem dynamics after a fire) cannot rely on field sampling alone. Additionally, ecosystem characteristics that are difficult to capture with spectral information alone (e.g., variation across different vertical strata) cannot rely on remotely sensed data alone (French *et al.* 2008). Therefore, the combination of remotely sensed data with field samples provides the most comprehensive basis on which to assess post-fire ecosystem change.

The selection of appropriate remotely sensed data and collection of appropriate field observations for comparison is essential to ensure that both methods of observation capture similar ecological settings. Chapter 2 summarized key decisions in the analytical process for linking remotely sensed data to the Composite Burn Index (CBI). However, additional uncertainties may arise from mismatches in the spatial and temporal characteristics of data being compared. Identifying the ideal characteristics of field observations and remotely sensed data with regard to the size and timing of the data being assessed is an ongoing concern in remote sensing (Curran and Atkinson 1999; Reinke and Jones 2006; Woodbridge *et al.* 2014). Errors introduced as consequences of study design and analysis can make it challenging to compare outcomes across different studies Chapter 2. However, the abstraction of observations using remotely sensed data or field surveys requires defining the spatial and temporal scales of comparison. These general remote sensing concerns have yet to be addressed in detail in the context of the mapping and modeling burn severity. Here, we evaluate previous work in the context of remote sensing of burn severity and build on first principles to think about how much the spatial and temporal alignment of field samples and remotely sensed data matters.

Studies using field-based observations of burn severity and remotely sensed data to assess variability in burn severity models generally fall into one of two categories. First, studies that assume that variation exists across some gradient and parameterize models based on some stratification of their data. Second, studies may explicitly test for statistical differences between models. A number of studies reviewed in Chapter 2 used separate models by vegetation type (Wimberly and Reilly 2007; Allen and Sorbel 2008; De Santis *et al.* 2010; Chen *et al.* 2011; Veraverbeke *et al.* 2011; Picotte and Robertson 2011; Parker *et al.* 2015), pre-fire disturbance (Chen *et al.* 2015), or topography (Chang *et al.* 2016). Additionally some studies assumed

variation due to analytical decisions, including the of field plot (De Santis and Chuvieco 2009; Cansler and McKenzie 2012; Mallinis *et al.* 2018), selection of sensor(s) used (van Wagtendonk *et al.* 2004; Holden and Evans 2010; Tanase *et al.* 2015; Mallinis *et al.* 2018; Garcia-Llamas *et al.* 2019), atmospheric corrections (Fang and Yang 2014), and pixel value extraction methods (Cansler 2011; Stambaugh *et al.* 2015). However, these studies did not explicitly test whether models were statistically different from one another. On the other hand, Harvey et al. (2019) demonstrated that the models themselves may be affected by biophysical gradients including latitude, pre-fire forest structure, and pre-fire bark beetle outbreaks. That said, little work has been done to investigate the impacts of spatial alignment and temporal synchrony on model performance.

When comparing results across different burn severity studies, one of the key implied assumptions of field-observed Composite Burn Index (CBI, Key and Benson 1999) estimates to remotely sensed data is that both datasets characterize the same phenomenon. Both remotely sensed data and field observations collect 'ecosystem snapshots' at the time of acquisition via wholly different perspectives. The ecosystem attributes measured in the CBI protocol provide ecologically important information while capturing effects that collectively provide a signal detected that may be detected by aerial and space-borne sensors (Key and Benson 1999). Note that CBI was designed with the moderate spatial resolution (30 m x 30 m) of satellites in the Landsat program in mind, however multiple studies have used the method to compare observations are different scales ranging from high resolution imagery taken from unoccupied aerial systems (Fraser *et al.* 2017) to coarse resolution imagery from MODIS (Holden *et al.* 2010; Kolden and Rogan 2013). While CBI was designed to characterize the elements of a burned ecosystem that would be observable via remote sensors, it is assumed that the two

datasets capture a similar spatial footprint at a similar point in time. If this is not the case, then model results may be influenced by ecosystem changes occurring outside of the intended sample space.

Spatial mismatches between plot locations and remotely sensed pixel locations can arise from several factors in data quality (**Table 3.1**). First, there may be spatial mismatches in the size of field plots compared to the size of pixels acquired for comparison. For example, a study that uses remotely sensed data with a spatial resolution much smaller than the plots that are used to calibrate models risks misidentifying severity thresholds because of the potential that areas with vastly different severity contain individual pixels that appear similar. Second, both field observations and remotely sensed data suffer from challenges in accurately geolocating observations. For example, the positional accuracy of Landsat imagery is half a pixel (Batson *et al.* 1985; Roy *et al.* 2014; Young *et al.* 2017), while obtaining quality field sample locations is dependent on the accuracy of GPS equipment receivers, the strength of satellite configuration at the time of use, the number of recordings collected, and any potential interference from and forest canopy at a site (Piedallu and Gégout 2005). It would be almost impossible to match plot centers with pixel centers across field observations and plot centers may fall at the edge of a pixel. These factors increase the likelihood that the value of the pixel overlaying a plot center does not accurately represent the environment of the ground sample.

Table 3.1 Data quality characteristics in the content of spatial data for burn severity analysis, potential impacts on results, and mitigations for use. Table based in part on Reinke and Jones (2006) and Woodbridge et al. (2014), who assessed fitness-for-use and sources of error in relating field measurements and remotely sensed data, respectively.

Data characteristic	Description	Field data	Remotely sensed data	Result	Mitigations
Spatial alignment	Size of field plots relative to the size of remotely sensed data pixels	Field plot size may be larger or smaller than area characterized via remotely sensed data	Pixel size may be larger or smaller than area characterized via remotely sensed data	Field data and remotely sensed data characterize differently sized areas; impact on results depends on spatial variability of burn severity patterns	Design field protocol in consideration of remotely sensed data to be compared, use remotely sensed data of different spatial resolution, extract single pixel or characterize neighborhood surrounding plot using some kind of pixel smoothing or averaging of point values
Georeferencing inaccuracies (positional accuracy)	Positional accuracy of GPS data or remotely sense data (e.g. satellite image)	Site location may be poorly recorded, GPS accuracy impacted by satellite constellation, weather, topography, canopy cover	Pixel location may include uncertainty	Incorrect comparisons with remotely sensed data	Take steps to ensure high-quality GPS measurements for field data, improve georeferencing for remotely sensed data, perform smoothing or averaging of point values for pixels overlying plots
Temporal synchrony (temporal accuracy)	Timing of field plot collection relative to the remotely sensed data observation date	Field plots collected before or after remotely sensed data available	Remotely sensed data captured before or after field plots collected	Disturbances or other changes may have occurred between when field sampling and remotely sensed data acquisition took place	Time field sampling to occur when remotely sensed data is acquired

Two main methods are used to overcome the challenge of inaccuracies in field sample and remotely sensed data locations and mismatches between plots and pixels. Most studies follow the recommendation from Key and Benson (2006) to locate field plots within relatively large homogenous areas. However, results from studies that compared remote sensors that capture data at spatial scales finer than the 30 x 30 m resolution of Landsat imagery show meaningful variability in post-fire ecological effects at small spatial scales (Van Wagtendonk *et al.* 2004; Holden *et al.* 2010). The second mitigation technique is implemented during the analysis phase when methods are chosen to extract those pixel values overlaying plot center. These range from using the pixel value directly overlaying plot center to allowing nearby pixels to influence the value that is assumed to characterize the field sample. Studies such as Cansler et al. (2011) and Stambaugh et al. (2015) that compared different pixel value extraction methods found that they influenced model results. Overall, these studies suggest that model outcomes are partially dependent on both the homogeneity of the observed landscape and the number of pixels that are used to estimate change, both of which can vary at scales where spatial mismatches matter.

Two types of temporal synchrony determine what characteristics will be captured by a post-fire assessment and how well ground data and remotely sensed data will match: the timing of (1) field data collection (campaigns) relative to the timing of the fire, and (2) remotely sensed data acquisition relative to the timing of field data collection. Temporal synchrony is important because forest ecosystems are dynamic and continually experience growth as well as decay from fire, wind, insects, disease, drought, and thinning and harvesting. Thus, other ecosystem disturbance processes may contribute to change detected beyond the direct effect of the fire itself, depending on the temporal synchrony between the timing of the fire, field observations, and remotely sensed data assessments.

Based on recommendations to capture remotely sensed imagery within a few weeks of CBI plot measurements (Zhu *et al.* 2006), better model performance should be expected when field observations and remotely sensed data are more temporally synchronous (i.e. with less delay, regardless of which data type was captured first). However, the ability of studies to capture field samples and remotely sensed data at the same time may be limited by both study-design and logistical constraints. Field measurements can occur immediately after a fire, as an initial assessment (IA), or after the subsequent growing season in the case of an extended assessment (EA) (Key and Benson 2006). While such study objectives may determine the timing of field campaigns, other, more practical factors, may influence assessment timing. For example, there may be safety considerations (e.g., mudslide hazards, smoke) or logistical constraints (e.g., summer field crews, funding). Once field campaigns have been conducted and the timing of assessment set, then studies must acquire remotely sensed data that is temporally aligned as well as possible with the field observations. For remotely sensed data, it may be difficult to acquire post-fire data at specific times. Studies must select the right images for analysis, with consideration to the timing relative to the fire, minimizing differences from pre-fire data (e.g., vegetation phenology, sun angle, and weather conditions), and avoiding cloud, smoke, or snow obscuration (White et al. 1996). Alternatively, researchers may collect their own imagery, such as using unoccupied aerial systems (e.g., Fraser *et al.* 2017), which allows greater control over the timing and conditions of sampling.

The spatial alignment and temporal synchrony between field samples and remotely sensed data has not been adequately addressed in the literature, although it is a key factor that researchers and managers either must consider in their own work or in using supplied burn severity maps. The fundamental nature of pairing these two types of data is constrained on the one hand by the

cost, time, and access needed to acquire field data (van Wagtendonk *et al.* 2004; Key and Benson 2006), and on the other by the spatial, temporal, and spectral resolution of the remote sensors (Lentile *et al.* 2006). The goal of this study was to assess the potential impact of asynchronous field and satellite observations on the fidelity of burn severity measurements based on a combination of remotely sensed data and continuous CBI estimates. To determine whether spatial and temporal mismatches introduce meaningful error to severity estimates, we reviewed methods used by existing literature, developed a conceptual framework to understand synchronicity, and assessed the spatial alignment and temporal synchrony in empirical studies.

3.1.1 Research questions

1. Does the spatial alignment of plot and pixel grain drive variability in how spectral index values are extracted from imagery?
2. How temporally synchronous are (a) field data and fire ignition and (b) field data and remotely sensed data?

This study was aimed at both new entrants into the field of remote sensing of burn severity as well as experienced researchers who may gain from more intentional focus on the purpose and consequence of aligning the spatial and temporal characteristics of data for comparison. The development of the field coincides with increasingly available imagery and remotely sensed data products at various spatial, temporal, and spectral resolutions and the lack of synthesis of the impacts of integrating data and interpreting results across scales is apparent. The impact of this paper is to emphasize the importance of considering the effects of mismatched data and identify how the current body of literature deals with those issues.

3.2 METHODS

The studies used in this review were compiled in Chapter 2. They were chosen based on their use of remotely sensed data and the CBI (and similar modified protocols) as a continuous variable. In total, 62 studies published between 2004-2019 were identified during the search. Only 50 of those studies were included in this paper due to incomplete information. The information needed for this review included timing of the fire studied, field plot size, shape, and time of sampling, and remotely sensed data type, pixel size, and time of sampling. Additionally, we recorded how the pixel values overlaying field plots were extracted for modeling. Because some studies assessed model relationships using multiple pixel value extraction methods or multitemporal remotely sensed data, we considered each relationship described as a single "comparison" for this review.

Overall, the studies used remotely sensed data from 14 sensors/platforms and one simulated image (**Table 3.2**). Comparisons based on circular plots included nine remotely sensed data sources, and those for square plots included eight. Both plot types were compared mainly with imagery from the Landsat satellite program. While most comparisons were based on optical passive remotely sensed data, the Phased Array L-band Synthetic Aperture Radar (PASLAR) was included in 17 comparisons. Thus, the majority of our findings relates to the use of optical passive remotely sensed data.

We found both the size of field plots and the spatial resolution of post-fire remotely sensed in 47 studies. The majority used circular field plots (29 studies), 17 studies used square plots, and one used both circular and square field plots (range of number of comparisons per study ranged for circular plots: 1-27, for square plots: 1-26) (**Table 3.3**).

Table 3.2 Remotely sensed data used by comparisons included in this paper.

Sensor/platform	Circular	Square
APEX	1	--
AVIRIS	1	2
Deimos 1 SLIM-6-22	--	1
Landsat (TM, ETM+, OLI)	150	63
MASTER	--	1
MTBS/RAVG	8	--
PALSAR	17	--
Sentinel 2 MSI	--	1
Sentinel 2A	--	1
Landsat OLI (simulated)	--	1
SPOT 5 HRG	1	--
SPOT-4	1	--
UAV	1	--
WV-2	--	1
WV-3	1	--

Table 3.3 Number of studies and number of comparisons using circular and square field plots.

Field plot type	Studies	Comparisons
Circular	29	181
Square	17	72

To assess spatial alignment, we included all cases instances where we could identify both the size of the plot and the spatial resolution of the remotely sensed data. For temporal synchrony,

most studies did not report the fire's end date. Therefore, we used the date of fire ignition as the timing of the fire. The smallest temporal grain we could identify for all these cases was to the nearest month. These results were limited to studies that where both the timing of fires and the timing of field campaigns. This includes fires where ignition dates were not reported in the study but were available elsewhere (e.g. Monitoring Trends in Burn Severity datasets, Eidenshink *et al.* 2007).

We defined criteria for spatial alignment separately for circular and square plots. For circular plots, the size of field plots could vary for a single spatial resolution, because of the inability to perfectly match the footprint of a circular plot and a square pixel. Therefore, we considered the cases to be synchronous where the diameter of the circular plot was such that it ranged from the length of one side of a pixel (**Figure 3.1a**) to the length of the diagonal of a pixel (**Figure 3.1b**) to be synchronous. If the diameter of a plot was such that it was outside of that range, then we considered it asynchronous. These criteria fit under an assumption of perfect alignment between plot centers and pixel centers and, however unlikely, this idealized model is necessary to form a conceptual framework for assessing spatial alignment.

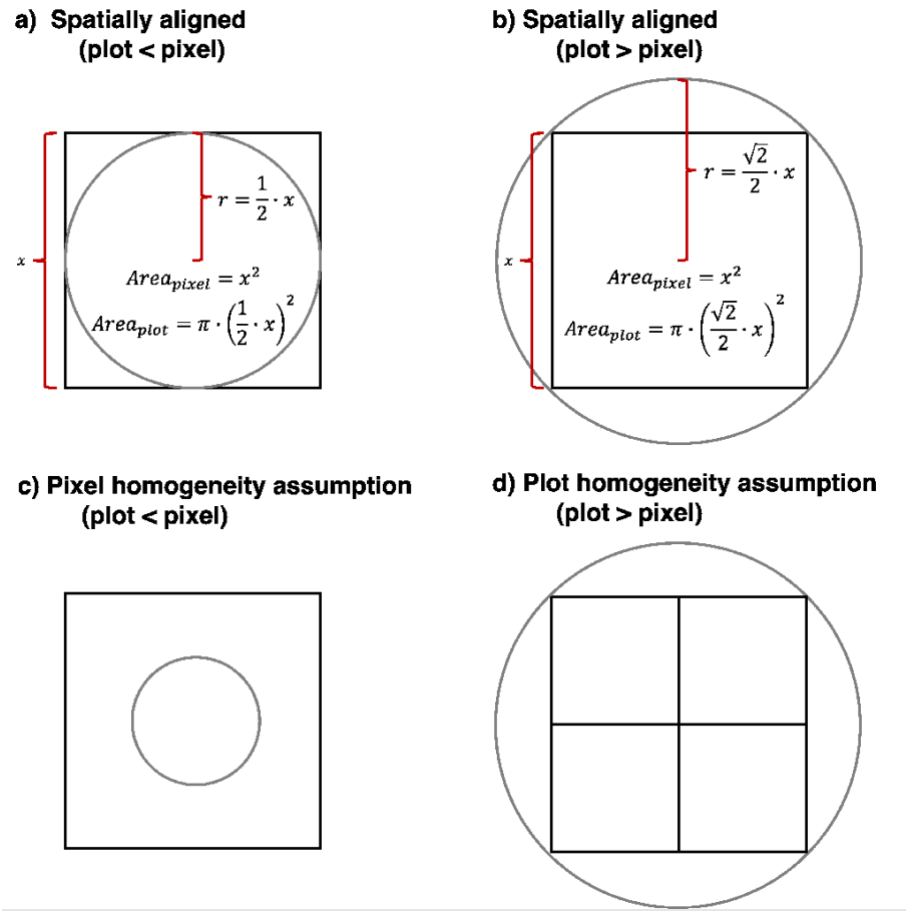

Figure 3.1 Types of spatial alignment for circular field plots. (a) Spatially aligned with field plot smaller than pixel, (b) spatially aligned with field plot larger than pixel, (c) pixel homogeneity assumption, where field plot is smaller than the minimum alignment size, and (d) plot homogeneity assumption, where field plot is larger than the maximum alignment size. Grey circle: field plots; black squares: remotely sensed data pixels. Note that rarely would pixel and plots centers overlap during sampling as shown in this diagram.

Where the resolution of remotely sensed imagery is coarser than the size of field plots, the comparison relies on the assumption that the pixel in which the plot is located is homogeneous in burn severity (i.e., a pixel homogeneity assumption) (**Figure 3.1c**). Thus, any plot placed within the spatial grain of a pixel would have the same CBI score. If the resolution of the remotely sensed imagery is finer than the size of field plots, then the comparison relies on the assumption

that the plots are spatially homogenous in burn severity (i.e., a plot homogeneity assumption) (**Figure 3.1d**). Thus, of a set of pixels that overlay a single plot, one picked at random would be equally likely to represent the fire effects on the ground.

For square field plots, we assumed spatial alignment where field plots and remotely sensed pixel size were exactly equal. When they were not equal, we assumed a spatial mismatch. Again, if the grain size of the remotely sensed data was coarser than a plot, it would rely on the pixel homogeneity assumption. In the opposite case, where the pixel size is finer than the plot size, it would rely on the plot homogeneity assumption.

Based on our definitions of spatial synchronicity, pixel homogeneity assumption, and plot homogeneity assumptions, we developed an assumption strength index (ASI) to quantify the degree to which each comparison relied on the pixel homogeneity or plot homogeneity assumptions (**Equation 3.1**). For circular plots, if the comparison fell between either size range of synchronicity, we assigned an ASI of 0. If the field plot fell outside of that range, we calculated an ASI for both diameter options (x and $\sqrt{2}x$) and used the smaller of the two resulting values. For square plots, we calculated the ASI directly as shown, where the $plot\ size_{syncrhronous}$ was equal to the pixel size.

Equation 3.1 Assessment of the magnitude of spatial mismatch using the Assumption Strength Index (ASI).

$$ASI = sign\left(plot\ size_{syncrhronous} - plot\ size_{observed}\right) * \sqrt{\left|plot\ size_{syncrhronous} - plot\ size_{observed}\right|}$$

Figure 3.2 shows the graphical interpretation of the zones of alignment and pixel or plot homogeneity assumptions for both circular and square field plots. This representation, based on **Figure 3.1**, is useful to interpret the scatterplots of pixel size against plot size. Pixel value extraction methods (e.g., bilinear, focal mean, mean of sample points within a plot) vary in the size of the neighborhood of pixels that influence the value used to represent a plot. To assess whether studies chose different pixel value extraction methods depending on the reliance on pixel versus plot homogeneity assumptions, we plotted the distribution of ASI values by pixel value extraction method. The overall number of studies and range of ASI values allowed us to determine whether there was a relationship between the type of assumption that each study relied on, and the extraction method used.

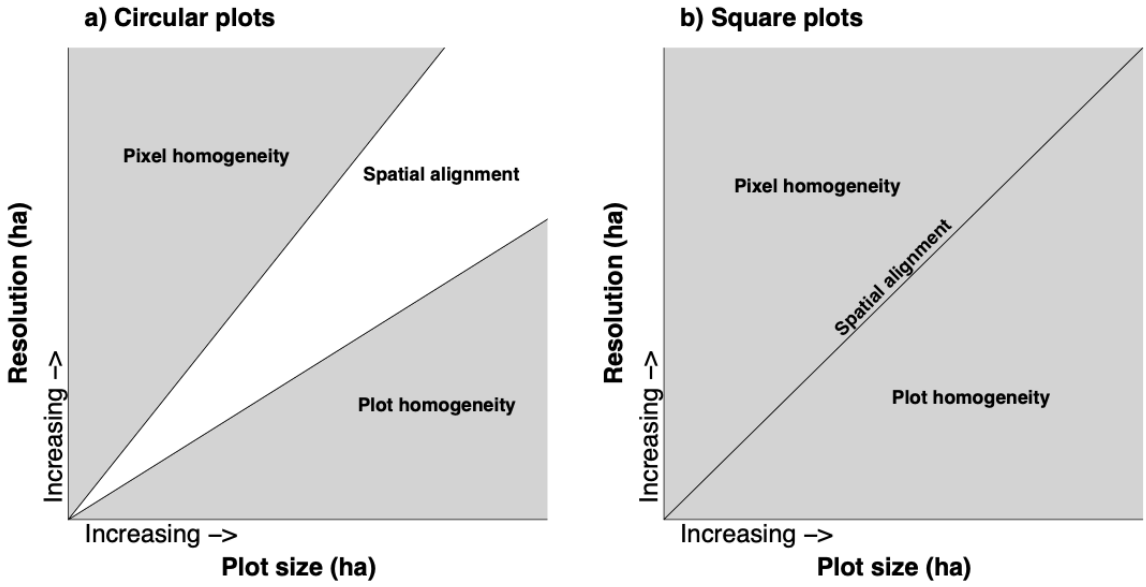

Figure 3.2 Spatial alignment and zones of pixel or plot homogeneity assumptions for (a) circular and (b) square plots. For circular plots (**a**), the zone of spatial alignment varies depending on the spatial resolution of remotely sensed data (see **Figure 3.1**). For square plots (**b**), spatial alignment follows a 1:1 line where field plots are the same size as the spatial resolution of remotely sensed data.

The assessment of temporal synchrony involved calculating the timing of the delay between fire ignition and field plot sampling and between field plot sampling and remotely sensed data acquisition. These delays were calculated in months since it was the temporal grain to which most studies reported those timings. Furthermore, because most studies and auxiliary databases used to identify fire timing reported the date of the fire relative to its ignition and not its containment, control, or extinguishment, we used this as the baseline from which to measure the timing delay in field sampling. This introduces potential bias between fires that have vastly different durations, but was a necessary step given the quality of available data.

3.3 RESULTS

3.3.1 Spatial alignment

Spatial alignment describes the size of the field plot relative to the resolution of the remotely sensed data. We identified two types of spatial mismatches: (1) where field plots had a smaller spatial grain than remotely sensed data pixels, and (2) where field plots had a larger spatial grain than remotely sensed data. For both circular and square field plots, most comparisons did not specify how spectral index values overlaying the plots were extracted from remotely sensed data (**Table 3.4**). Where the method was explicitly stated, circular plots commonly either did not use any smoothing (*i.e.*, used spectral index of value overlaying plot center), used the mean of sample points within the plot, or used a focal mean. For square plots, the most common method, where stated, was bilinear interpolation.

Table 3.4 Pixel value extraction methods used by field plot types.

Pixel value extraction method	Description	Circular	Square
Area weighted	Weighted plot averaging; weights assigned based on each pixel's	7	1
Bilinear	Mean is calculated for the values of the four nearest pixels to plot center	14	11
Focal mean	Mean is calculated for the pixels encountered in a neighborhood around a cell	32	6
Mean of sample points within plots	Mean of pixel values overlaying sample points within plot	33	3
Mean of values of pixels within distance of plot	Mean of pixel values for cells falling within specified distance of plot	10	0
None	Pixel value overlaying plot center	35	7
Not specified	N/A	50	48

Most field plots for both circular and square plot designs were slightly less than 0.1 ha. For circular plots, this corresponded to about 707 m^2, or 30 m diameter plots, which is the standard plot design suggested by the CBI protocol (Key and Benson 2006). For square plots, most comparisons were 900 m^2, or 30 x 30 m. Both sizes were designed to match remotely sensed data from the Landsat satellite program, which dominates the spatial resolution of data included in this paper (Chapter 2). Circular field plots ranged from 13 m^2 (2-m diameter, Schepers *et al.* 2014) to 6362 m^2 (Miller and Thode 2007; Miller *et al.* 2009; 45-m diameter; Miller and Quayle 2015). Square field plots ranged from 100 m^2 (10 x 10 m; Loboda *et al.* 2013) to 1600 m^2 (40 x 40 m; Fang and Yang 2014).

Because of the mismatch in geometry between circular field plots and square remotely sensed data, even studies that match the diameter of field plots to the width/height of pixels experience some level of mismatch. Therefore, we examined spatial alignment separately for comparisons made with circular or square field plots.

The magnitude of mismatch varied by index value extraction method (**Figure 3.3a-f**). For circular plots, comparisons where the method was not specified, a focal mean, or None had a larger range of grain sizes for field plots and remotely sensed data. There were also fewer comparisons falling within the spatial alignment zone. For the four other pixel value extraction methods (mean of sample points within plot, bilinear, area weighted, and mean of values of pixels within distance of plot), field plots and remotely sensed data had less variability and were finer-grained (< 0.1 ha). For square plots, comparisons showed variability in plot size and remotely sensed pixel size across all pixel value extraction methods with more than one observation (**Figure 3.4a-f**). The gain size of data, for both field plots and remotely sensed data, was finer for square plots than for circular plots.

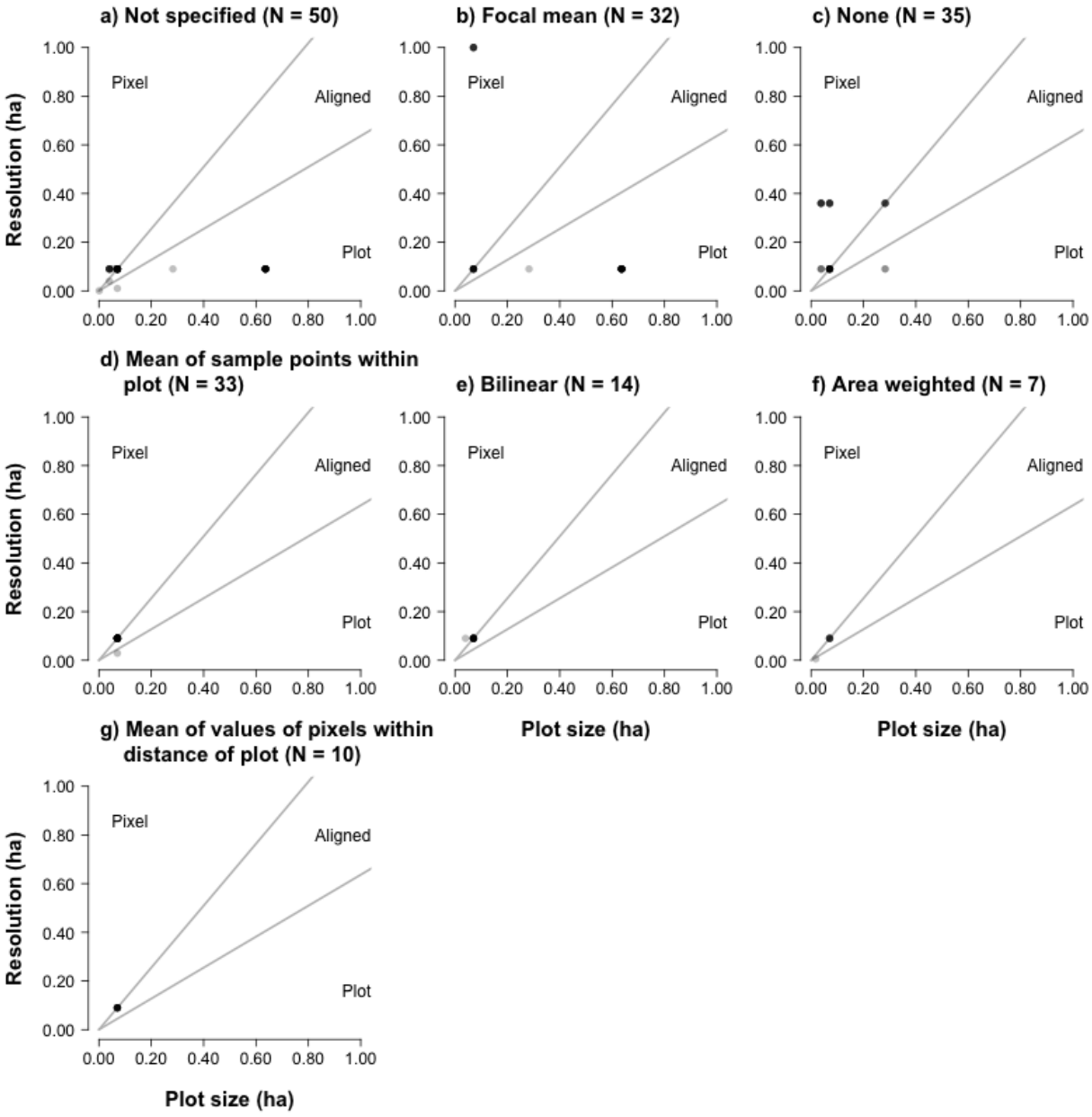
a) Not specified (N = 50)
b) Focal mean (N = 32)
c) None (N = 35)
d) Mean of sample points within plot (N = 33)
e) Bilinear (N = 14)
f) Area weighted (N = 7)
g) Mean of values of pixels within distance of plot (N = 10)
Pixel
Aligned
Plot
Resolution (ha)
Plot size (ha)
0.00
0.20
0.40
0.60
0.80
1.00

Figure 3.3 (a-g) Alignment between circular field plot size and spatial resolution of remotely sensed data for eight index value extraction methods: not specified, focal mean, none, mean of sample points within plots, bilinear, area weighted, mean of values of pixels within distance of plot, object-based. For information on index value extraction methods, see **Table 3.4**. N: number of observations for which the spatial resolution of both elements was available. The grey lines show the area that would result from alignment between plot size and remotely sensed data resolution where 'Pixel' and 'Plot' correspond to pixel homogeneity assumption and plot homogeneity assumption, respectively. 'Aligned' corresponds to the area of spatial alignment. See **Figure 3.1** and **Figure 3.2** for details on spatial alignment assumptions.

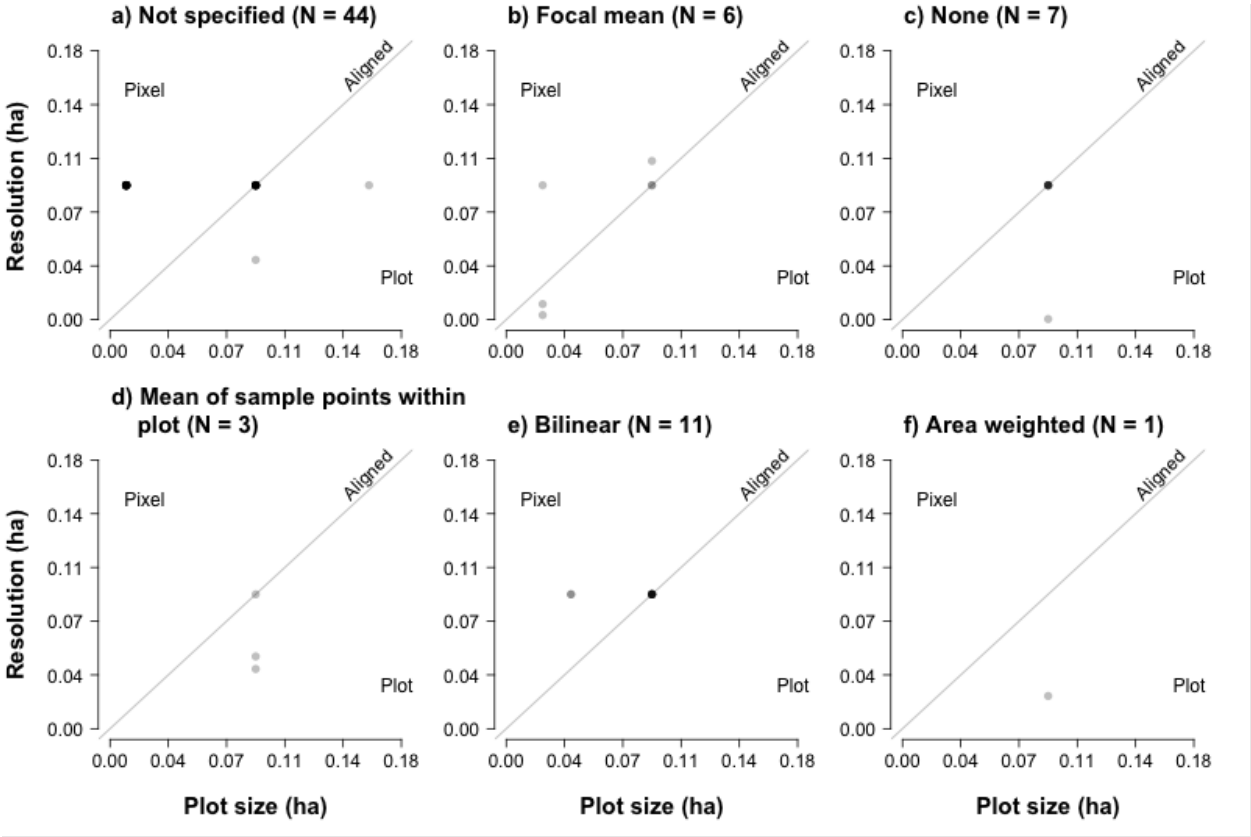

Figure 3.4 (a-f) Alignment between square field plot size and spatial resolution of remotely sensed data for eight index value extraction methods: not specified, focal mean, None, mean of sample points within plots, bilinear, and area weighted. For information on index value extraction methods, see **Table 3.4**. N: number of observations for which the spatial resolution of both elements was available. The grey line indicates a 1:1 relationship, i.e., spatial alignment, between plot size and remotely sensed data resolution, while 'Pixel' and 'Plot' correspond to pixel homogeneity assumption and plot homogeneity assumption, respectively. See **Figure 3.1** and **Figure 3.2** for details on spatial alignment assumptions.

For circular plots, comparisons that relied strongly on the pixel homogeneity assumption (ASI > 0) were more likely to use a focal mean or the value overlaying plot center (None; **Figure 3.5a**). Comparisons that relied on the plot homogeneity assumption (ASI < 0) were more likely to either not specify the value extraction method or use a focal mean. Overall, far more comparisons used data that were spatially synchronous (109 comparisons) than data that relied on either the pixel homogeneity assumption (35) or the plot homogeneity assumption (37). Comparisons that were spatially synchronous were most likely to use the mean of sample points within a plot (32), followed by not specifying a method (25) However, spatially synchronous comparisons used all pixel value extraction methods.

For square plots, comparisons that relied strongly on the pixel homogeneity assumption (ASI > 0) either did not specify a pixel extraction method or used a focal mean or bilinear interpolation (**Figure 3.5b**). Comparisons that relied on the plot homogeneity assumption (ASI < 0) were more likely to not specify a method or use a focal mean. Overall, again, more comparisons that were spatially synchronous (35 comparisons) than relied on either the pixel homogeneity assumption (27) or the plot homogeneity assumption (8). Comparisons that were spatially

synchronous were most likely to not specify a pixel value extraction method, followed by bilinear interpolation, none (value of pixel overlaying plot center), focal mean, and last the mean of sample points within the plot.

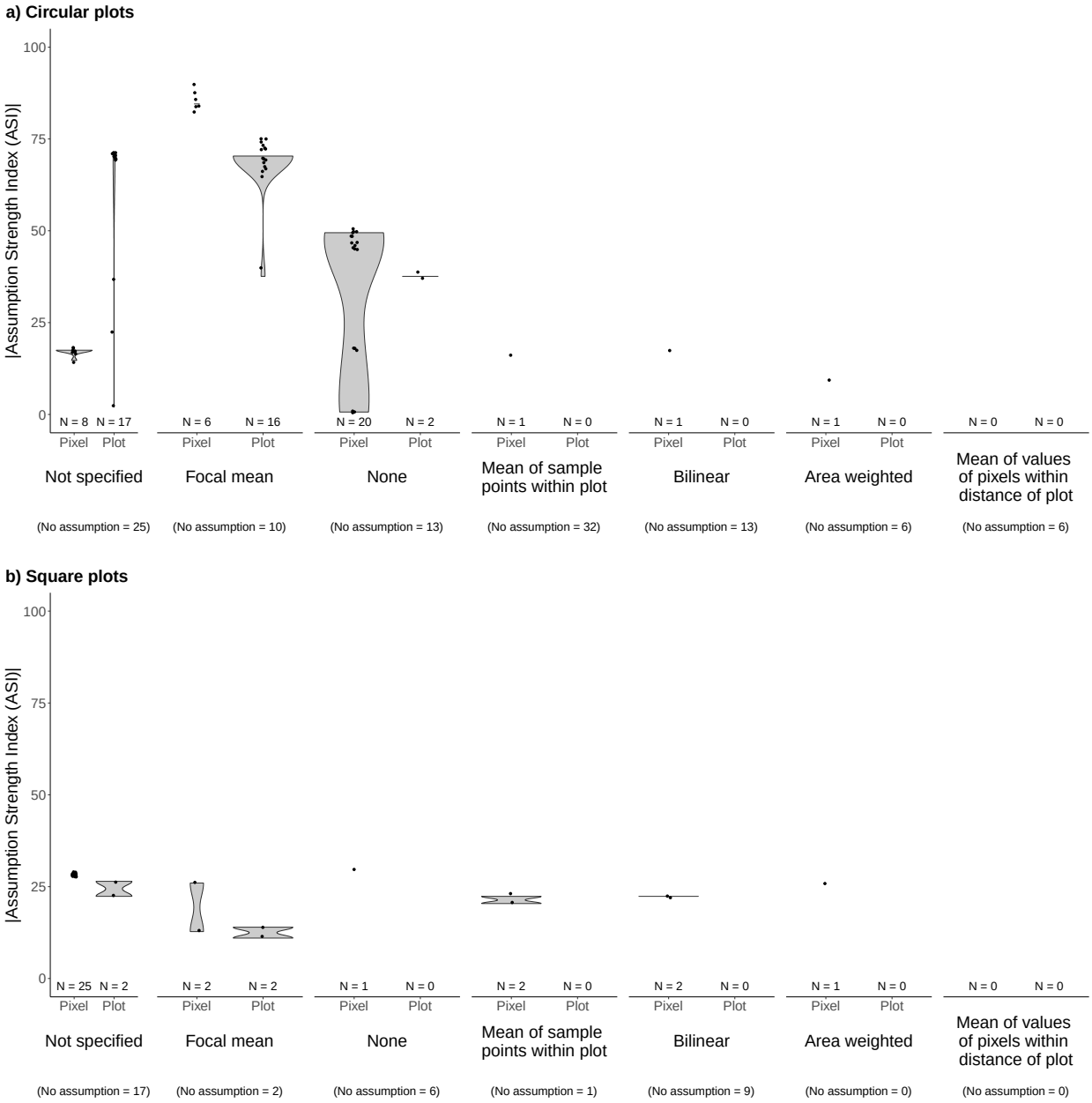

Figure 3.5 Distribution absolute value of Assumption Strength Index (ASI) comparisons, which indicates the degree to which each comparison relied on the pixel homogeneity or plot homogeneity assumptions for a) circular field plots and b) square field plots. Distributions are shown for seven index value extraction methods (not specified, focal mean, None, mean of sample points within plots, bilinear, area weighted, mean of values of pixels within distance of plot). For more information on index value extraction methods see **Table 3.4**. 'Pixel' corresponds to comparisons relying on the pixel homogeneity assumption and 'Plot' to comparisons relying on the plot homogeneity assumption. The number of observations (N) are given separately for comparisons bases on the spatial alignment assumption. See **Figure 3.1** and **Figure 3.2** for details on spatial alignment assumptions.

3.3.2 Temporal synchrony

The timing of field plots was 0-36 months after the start of the fire (average= 11.1, σ = 5.9; **Figure 3.6a-b**), indicating that most of these studies conducted extended assessments. We found a wide range of timing between post-fire remotely sensed data and field plot collection, from 18 months before to nine months after field plot collection (average 2.7 months, σ = 4.7; **Figure 3.6c-d**).

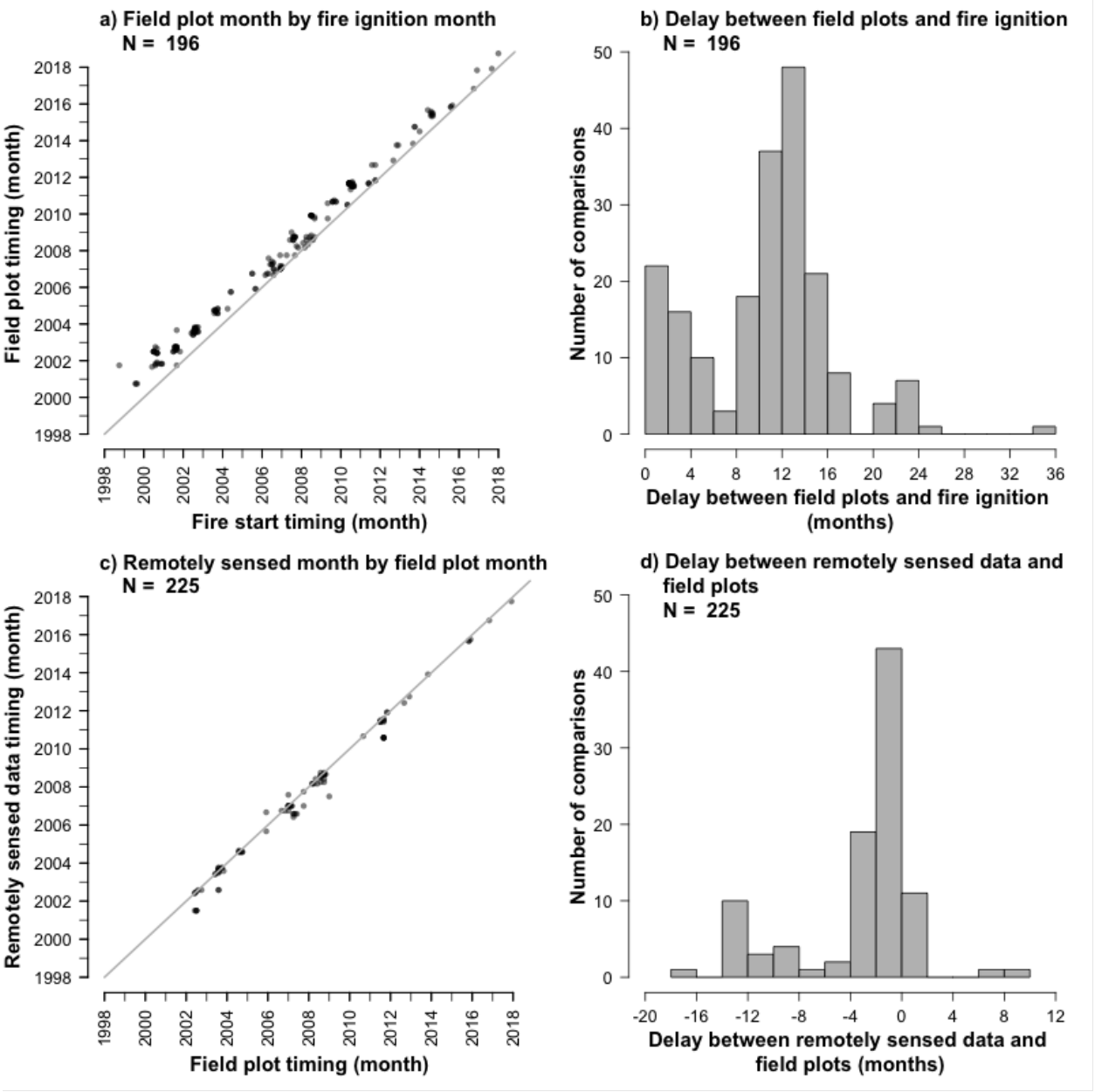

Figure 3.6 Temporal synchrony between (a) date of fire ignition and field data collection and (b) field data collection and first post-fire remotely sensed data acquisition. Delay between (c) fire ignition date and field data collection and (d) field data collection and first post-fire remotely sensed data acquisition. For (a) and (b), grey line indicates a 1:1 relationship, i.e., perfect temporal synchrony. The scatter around the line shows the variation in temporal synchrony between the respective axes. N: number of observations for which timing of both elements was available.

3.4 DISCUSSION

3.4.1 Spatial alignment

Ideally, the size of field plots would match the spatial grain of the sensor used in the analysis so that both methods capture the same field of view. True alignment would not be exactly 1:1 because field plots tend to be circular and remotely sensed data use square (**Figure 3.1**). For example, the standard CBI protocol was based on 30-m diameter plots because this matched the 30 x 30-m pixels of Landsat. Such a comparison would result in 707-m^2 field plots relative to a 900-m^2 pixel, an ASI of 13.9. This slightly imbalanced result occurs even though the field plot and pixel sizes are well aligned in their spatial footprints. However, most of the comparisons we found were more spatially mismatched than that (**Figure 3.5**).

3.4.1.1 Alignment between field plot size and post-fire remotely sensed data resolution

The tendency of comparisons to be based on circular plots field likely results because the original CBI protocol used circular plots and, potentially, the ease of establishing a single plot center instead of four corners during sampling. Circular plots may also be preferable due to having a short perimeter for given size, thereby reducing number of edge trees compared to other plot shapes of the same size (Kangas and Maltamo 2006). Additionally, the difficulty of aligning square plots with the pixel grid of remotely sensed data reduces the potential benefit of that shape.

Although circular and square plots differed in the types of pixel value extraction methods commonly used, our analysis attempted to put these methods into context based on the spatial alignment of each comparison. For most comparisons and pixel extraction methods, field plots

and remotely sensed data were outside of the defined range of spatial alignment (**Figure 3.3** and **Figure 3.4**). We found that the level of spatial alignment differed by smoothing type in both circular and square plot (**Figure 3.5**). However, no studies addressed the effect of spatial alignment on model results and the type of pixel value extraction methods that would provide the best relationships with field observations.

Because of the inherent inaccuracies in plot locations collected with GPS and geometric positioning of satellite images, it would be infeasible to establish field plots that overlap precisely with a single pixel (as in square plots) or to match plot centers with pixel centers (as in circular plots). The choice of pixel value extraction method may be based on either a quantitative framework or a conceptual framework. The quantitative framework analyzes which method results in the best performing models. The conceptual framework considers the size of field plots and resolution of remotely sensed data.

Studies based on a quantitative framework could either compare different pixel value extraction methods or cite similar work. For example, using the mean of a set of pixels is a widely accepted method to minimize the effect of potential misregistration of remotely sensed data (Ahern *et al.* 1991; Veraverbeke *et al.* 2012). We found several studies that cited Cansler and McKenzie (2012), who reported on findings by Cansler (2011) suggesting that bilinear interpolation performed better than nearest neighbor and cubic convolution methods. However, Cansler (2011) showed only small differences between models that used these three sampling methods (R^2 = 0.46-0.50). Furthermore, the study area was limited to the North Cascade Mountains, Washington, raising the question of how widely these findings might be generalized.

In contrast to a quantitative approach, a conceptual approach to selecting the type of pixel value extraction method would be linked to the level and direction of spatial alignment. A focal mean, for example, considers surrounding pixel values and thus fits the plot homogeneity assumption (**Figure 3.1d**), where the plot size is larger than a pixel. In this situation, characterizing the plot with remotely sensed data may consider a group of pixels that, together, characterize the same area covered by the plot. Such studies may use a pixel value extraction method that provides influence on a larger neighborhood of pixels. On the other hand, if a pixel is substantially larger than the plot, then using either the value of the pixel overlying the plot center (None) or a method that minimizes the area of the neighborhood quantified is preferred. Of course, such simple rules of thumb are complicated by the geometric errors in both plot and pixel locations.

The consequence of mismatched spatial alignment is difficult to assess because none of the studies in this review tested for it. The best insights may come from studies that compared multiple sensors of different spatial resolution to relate to the same field plots. We found two studies that compared similar spectral indices across sensors with differing spatial resolutions. All comparisons were made against the same sets of field plots and therefore varied in spatial alignment. van Wagtendonk et al. (2004) compared the dNBR derived from Landsat ETM+ (30 m resolution) with the AVIRIS (17 m) to predict severity responses for 30-m diameter CBI plots. Models based on Landsat data (with the more spatially synchronous pixel size; R^2= 0.894) slightly outperformed those based on AVIRIS (R^2 = 0.853). However, Mallinis et al. (2018) assessed the relationship of dNBR derived from Sentinel 2A (10- or 20-m resolution, depending on band, homogenized to 20 m) and Landsat OLI (30 m) to CBI, GeoCBI, and WCBI (using 30 x 30-m plots). dNBR from Sentinel 2A (with slightly worse spatial alignment) outperformed that of Landsat. These studies show why extrapolating from such an approach is complicated by the

confounding effects of those sensors as well as by different spectral resolution. The sensors compared by each study captured slightly different regions of the electromagnetic spectrum and, although they allowed the calculation of similar spectral indices, by necessity this calculation was based on slightly different wavelengths for each sensor.

Without a specific study designed to investigate the effect of spatial alignment on modeled severity relationships, the effect of mismatched grain size between field and remotely sensed data is difficult to assess. Future studies that compare field observations with remotely sensed data of finer or coarser spatial resolution might adjust the size of field plots or attempt to conceptually match the pixel value extraction method with the level and direction of spatial mismatch. Furthermore, studies comparing sensors of different resolutions could collect nested field plots so that each comparison used the most spatially synchronous data set.

3.4.1.2 Strength of assumptions regarding spatial alignment

Pixel value extraction methods overcome inherent error in the geolocation of remotely sensed data relative to field plot centers. This section discusses considerations in determining how to align pixel value extraction methods, depending on the spatial alignment between field plots and remotely sensed data.

Among the comparisons we evaluated that specified pixel value extraction methods, the strongest assumptions (both pixel homogeneity and plot homogeneity) were for the focal mean pixel value extraction method, followed by None. These results are surprising because conceptually, these two methods of pixel value extraction are inconsistent with their application. A focal mean, by design, lends weight to nearby pixels, so its application is preferred for

comparisons where pixel grain sizes are smaller than plot sizes. Using None is preferred where relatively strong alignment exists between pixel grain size and plot size. However, among comparisons using the pixel value directly overlaying plot center, the pixel grain size was more often larger than the plot size (**Figure 3.5**). The other methods showed relatively small assumption strength index values for both the pixel homogeneity and plot homogeneity assumptions. We excluded one object-based analysis (Hultquist *et al.* 2014) because no other studies used this approach. Although Hultquist et al. (2014) used remotely sensed data with a spatial grain of 16 m^2 and field plot size of 500 m^2, the average size of objects in which spectral indices were calculated was 8,000 m^2. Therefore, this study strongly relied on the pixel homogeneity assumption.

We identified two main conclusions from this work. First, studies used a variety of pixel value extraction methods regardless of the ASI between field plots and remotely sensed data. Second, there was little justification in the literature regarding which pixel value extraction method would conceptually make sense given the level of spatial alignment present. Future studies should explicitly explain the spatial alignment between the field plot size and remotely sensed data resolution, including discussion of whether the methodology is based on a conceptual or quantitative framework and how the resulting data alignment might affect model results. As discussed, only one study (Cansler and McKenzie 2012) based their choice of pixel value extraction method on a quantitative analysis of models using data from the same region. Although other studies cited this work, the improvement over other methods was small in Cansler (2011). Further, variation in other regions could lead to a different result. There is clearly space for a future study to assess the performance of different pixel value extraction methods across a wide geographic region. Such studies could consider the range of spatial alignment

found in this review and the potential effect of different pixel value extraction methods on model performance. This would enable a more robust framework for future studies in deciding which method to use.

One consideration for future studies is to recognize the effects of characterizing smaller areas with high resolution imagery. The reliance on Landsat-based satellites was generally explained to relate to its moderate spatial resolution and multispectral data acquisition, long historical record of near global repeat coverage, temporally and spatially consistency, and broad-area coverage (Key and Benson 2006). What is not strongly emphasized is the spatial resolution of Landsat sensors relative to the size of ecosystem characteristics being observed. The spatial resolution of Landsat pixels is generally large enough to capture multiple tree crowns. Therefore, depending on the vegetation type and environmental conditions being sampled, a single pixel is often made up of multiple trees as well as ground, the spectral reflectance of which are aggregated into a single signal being observed via satellite. With the availability of high spatial resolution imagery, such as that of Sentinal-2 (10 m), WorldView-3 (3.7), or QuickBird (2.9 m), observations have the capacity to measure a single ecosystem feature (e.g., a tree) as opposed to an aggregation of several features. Researchers using imagery from such high-resolution sources will need to consider whether the plot sizes used for comparison should match the pixel size of the sensor or capture an area the size of multiple pixels. The concept of sampling representative areas of homogenous severity classes may need to be expanded to include ensuring that field-based observations capture the multitude of ecosystem features present on a site.

3.4.2 Temporal synchrony

3.4.2.1 Timing of field campaigns relative to fire ignition

The timing of field campaigns is dictated by project goals, type of assessment to be performed (initial or extended), and logistical constraints. The decision of when to measure field plots relative to the fire event determines both whether delayed fire effects may be observed and the potential for capturing ecosystem change unrelated to the fire. In some cases, the perceived timing of field assessments can be adjusted post hoc by excluding certain measured attributes likely to be affected by extended periods between fire ignition and field data collection. For example, (Fernandez-García *et al.* 2018) omitted components of the CBI protocol related to extended assessments (percentage of living shrubs, colonizers, or change in species composition). However, this omission introduces further challenges in determining what kind of temporal synchrony exists with remotely sensed data when an exact date is not associated with field observations.

Most studies in this review collected field plots the year after fire ignition, so they were likely affected by second-order fire effects and potential impacts from weather and other disturbances. In an extended assessment, areas with faster post-fire green-up, such as those in humid climates (Soverel *et al.* 2010; Liu 2016; Rother and Veblen 2017), could exhibit apparently lower burn severity than in an initial assessment. Extended assessments may also capture ecosystem- and disturbance-dependent fire-induced mortality. Although study design would ideally consider such ecological phenomena, logistics may constrain field campaigns over study objectives. Such studies should cite logistical constraints on the timing of field campaigns that might affect severity measurements and consider them when interpreting results. Each study's results would

benefit from the context of the study site, any post-fire management, and possible impacts of weather, insects, disease, or other drivers of forest ecosystem response.

3.4.2.2 Timing of remotely sensed data acquisition relative to timing of field campaigns

Seven studies compared field observations with remotely sensed data collected at multiple time points (Cocke *et al.* 2005; Allen and Sorbel 2008; Veraverbeke *et al.* 2010; Chen *et al.* 2011; Strand *et al.* 2013; Stambaugh *et al.* 2015; Boucher *et al.* 2017). Surprisingly, most comparisons were not improved by using the index values derived from imagery with higher temporal synchrony between field observations and remotely sensed data. In general, the more temporally synchronous of the comparisons (relating to field data collection and post-fire remotely sensed data) actually had slightly worse model evaluation metrics. Only one of these seven studies (Chen *et al.* 2011) found higher model performance using imagery acquired in the same year as their field data – one month after ignition.

Overall, these studies found that imagery collected in the same year as the fire was more strongly related to field data collected one year later than when imagery was acquired in the same season as the field measurements. We suggest a potential rationale for this occurrence. Because the field observations of composite burn indices require the "recreation" of the post-fire environment, sampling done in the year following a fire can separate regeneration that has occurred post-fire from surviving pre-fire vegetation. Thus, burned plots that contain living vegetation a year later don't necessarily indicate lower severities. However, satellite imagery taken coincidentally with extended assessment field assessments cannot distinguish between post-fire regeneration and surviving pre-fire vegetation. In instances where burned plots contain living vegetation, satellite imagery would generally suggest lower severities. It is therefore possible that imagery taken

immediately after a fire may provide stronger predictions of field-based observations of severity taken at a later date if considerable regeneration has occurred in the interim.

Additionally, we found two studies that described the potential for better model performance with a smaller lag time between image capture and fieldwork even they did not conduct analyses. Parker et al. (2015) suggested that the non-significant and weak GeoCBI-dNBR relationships found within individual ecosystems may be due to environmental factors, but also, to a smaller extent, to the lag between image capture and fieldwork. Wimberly and Reilly (Wimberly and Reilly 2007) assessed field data collected several years after fire, while post-fire satellite image was obtained in the first growing season after the fire. They suggested that analyses of field-based severity measurements collected at the same time as the post-fire satellite image should result in more accurate fire severity predictions. However, these suggestions contradict the empirical results we found from those studies that did quantitative analysis. Therefore, it is clear that, at least in some instances, slight temporal asynchrony between field data and remotely sensed data does not negatively impact model performance.

Phenological and climatic changes over time may exacerbate the impacts of temporal asynchrony on model results. The timing of seasonal senescence and related changes in reflectance is known to substantially influence spectral indices used to estimate burn severity (Verbyla *et al.* 2008). If post-fire sampling coincides with phenological changes, it may be even more important to reduce any temporal asynchrony. Projected changes in climate may further exacerbate this potential source of error, as evidence suggests longer, hotter, and drier fire seasons that extend later into the year in the U.S. (McKenzie *et al.* 2004; Flannigan *et al.* 2013; Wimberly and Liu 2014) and longer fire seasons in the Mediterranean forests of Europe (Moriondo *et al.* 2006). Furthermore,

evidence suggests a delaying trend in the wind down of fire season in autumn (Piao *et al.* 2019). These factors introduce considerable uncertainty in how changes in the timing of fire season and seasonal senescence will influence the outcomes we reviewed. We suggest the potential for future studies that integrate these factors into assessments of the influence of temporal synchrony on model results.

3.5 Recommendations

The main results of this study provided 1) an assessment of methods used to extract the value of spectral reflectance over sampled field plots, which affects the implied spatial alignment between field observations and remotely sensed data; and 2) a summary of the temporal synchrony between field observations and remotely sensed data and its effect on model performance. We suggest several recommendations to future studies based on this work. First, regarding spatial alignment, we propose that study design and analysis consider the spatial scales of data being compared and:

- attempt to match the size of field plots sampled with the spatial resolution of remotely sensed data to be used in analysis,
- collect nested field plots in the case of comparing remotely sensed data at varying spatial resolutions,
- select appropriate pixel value extraction methods that either produce better model results based on comparative analysis or align with implied assumptions outlined in this paper about pixel versus plot homogeneity.

Second, regarding temporal synchrony, we found it difficult to strictly endorse recommendations to capture remotely sensed imagery within a few weeks of CBI plot measurements (Zhu *et al.*

2006). While remote sensing theory supports an expectation of better model performance when field observations and remotely sensed data are more temporally synchronous, this was not supported by the studies we reviewed. More research is likely needed to understand the mechanisms driving stronger relationships found between less temporally synchronous data, likely taking into account the presence of post-fire regeneration versus surviving pre-fire vegetation.

3.6 Conclusion

We reviewed spatial alignment and temporal synchrony between field observations and remotely sensed data in studies investigating the Composite Burn Index (CBI). This review introduced a framework of pixel and plot homogeneity assumptions that is useful for conceptualizing how study design and inherent geometric inaccuracies in data may influence model results. We also emphasized the importance of the size of field plots and the spatial grain of remotely sensed data when selecting a pixel value extraction method and the timing of field campaigns relative to fire ignition and remotely sensed data availability.

Our analyses did not quantitatively assess the effects of spatial alignment and temporal synchrony on model results. However, they 1) emphasized the value of experimental design to determine how to extract pixel values overlaying field plots; 2) highlighted how few studies have collected field data more than two years after a fire, and the subsequent lack of information on longer-term (3-10 years) relationships between field observations and remotely sensed data; and 3) showed that strong synchrony between the timing of field observations and remotely sensed data acquisition, while conceptually important, does not, in most cases, reduce model performance.

Overall, our review suggested that more work could be done to quantify the effects spatial alignment on model results. While several studies have demonstrated that remote sensors with differing spatial resolutions can impact model results, it remained unclear how much coincidently varying spectral resolutions influence those outcomes. Additionally, few studies have assessed the impacts of different pixel value extraction methods, and their geographic range is considerably small relative to the extent at which the results have been applied. Sampling within large areas of relatively homogenous conditions and utilizing best practices for geolocating observations may reduce the impact of spatial mismatches between field data and remotely sensed data. However, the variability in post-fire ecological effects can occur at very small spatial scales in meaningful ways. With regards to temporal synchrony, our review demonstrated that severity assessments conducted with remotely sensed data collected later in time than field samples should not be a major concern.

This review contributes the conceptual understanding of spatial and temporal considerations of integrating field-based observations with remotely sensed data. These fundamental concerns in the field of remote sensing have, to date, have received little attention in the field of burn severity modeling. Researchers working to make robust conclusions with regards to the effects of different ecosystem characteristics (*e.g.*, vegetation type, pre-fire disturbance, topography) or analytical decisions (*e.g.*, plot type, sensor(s) used, atmospheric corrections) on the model variability generally seek to minimize any additional sources of uncertainty. Understanding the methods and consequences matching spatial and temporal characteristics of field-observations and remotely sensed data can improve study design, field data collection protocols, analysis, and potentially lead to changes in funding mechanisms to ensure adequate timing of field campaigns.

3.7 References

Ahern FJ, Erdle T, Maclean DA, Kneppeck ID (1991) 'A quantitative relationship between forest growth rates and Thematic Mapper reflectance measurements' *International Journal of Remote Sensing* **12**, 387–400.

Allen JL, Sorbel B (2008) 'Assessing the differenced Normalized Burn Ratio's ability to map burn severity in the boreal forest and tundra ecosystems of Alaska's national parks' *International Journal of Wildland Fire* **17**, 463–475.

Batson RM, Kieffer HH, Borgeson WT (1985) 'Geometric accuracy of Landsat-4 and Landsat-5 thematic mapper images'

Boucher J, Beaudoin A, Hébert C, Guindon L, Bauce É, Hebert C, Guindon L, Bauce E (2017) 'Assessing the potential of the differenced Normalized Burn Ratio (dNBR) for estimating burn severity in eastern Canadian boreal forests.' *International Journal of Wildland Fire* **26**, 32–45. doi:10.1071/WF15122

Cansler CA (2011) 'Drivers of burn severity in the northern Cascade Range, Washington, USA. University of Washington. Seattle, WA: 128 p'

Cansler CA, McKenzie D (2012) 'How robust are burn severity indices when applied in a new region? Evaluation of alternate field-based and remote-sensing methods' *Remote sensing* **4**, 456–483.

Chang Y, Zhu Z, Feng Y, Li Y, Bu R, Hu Y (2016) 'The spatial variation in forest burn severity in Heilongjiang Province, China' *Natural Hazards* **81**, 981–1001.

doi:http://dx.doi.org/10.1007/s11069-015-2116-9

Chen G, Metz MR, Rizzo DM, Meentemeyer RK (2015) 'Mapping burn severity in a disease-impacted forest landscape using Landsat and MASTER imagery' *International Journal of Applied Earth Observation and Geoinformation* **40**, 91–99. doi:10.1016/j.jag.2015.04.005

Chen XX, Vogelmann JE, Rollins M, Ohlen D, Key CH, Yang LM, Huang CQ, Shi H (2011) 'Detecting post-fire burn severity and vegetation recovery using multitemporal remote sensing spectral indices and field-collected composite burn index data in a ponderosa pine forest.' *International Journal of Remote Sensing* **32**, 7905–7927. doi:10.1080/01431161.2010.524678

Cocke AE, Fulé PZ, Crouse JE (2005) 'Comparison of burn severity assessments using Differenced Normalized Burn Ratio and ground data' *International Journal of Wildland Fire* **14**, 189–198.

Curran PJ, Atkinson PM (1999) Issues of scale and optimal pixel size. In 'Spat. Stat. Remote Sens.' pp. 115–133. (Springer)

Eidenshink J, Schwind B, Brewer K, Zhu ZL, Quayle B, Howard S (2007) 'A project for monitoring trends in burn severity' *Fire Ecology Special Issue* **3**, 2–21.

Fang L, Yang J (2014) 'Atmospheric effects on the performance and threshold extrapolation of multi-temporal Landsat derived dNBR for burn severity assessment.' *International Journal of Applied Earth Observation and Geoinformation* **33**, 10–20. doi:10.1016/j.jag.2014.04.017

Fernandez-García V, Quintano C, Taboada A, Marcos E, Calvo L, Fernandez-Manso A (2018) 'Remote Sensing Applied to the Study of Fire Regime Attributes and Their Influence on Post-Fire Greenness Recovery in Pine Ecosystems' *Remote Sensing* **10**, 733. doi:http://dx.doi.org/10.3390/rs10050733

Flannigan M, Cantin AS, De Groot WJ, Wotton M, Newbery A, Gowman LM (2013) 'Global wildland fire season severity in the 21st century' *Forest Ecology and Management* **294**, 54–61. doi:10.1016/j.foreco.2012.10.022

Fraser RH, Sluijs J Vander, Hall RJ (2017) 'Calibrating Satellite-Based Indices of Burn Severity from UAV-Derived Metrics of a Burned Boreal Forest in NWT, Canada' *Remote Sensing* **9**, 279. doi:http://dx.doi.org/10.3390/rs9030279

French NHF, Kasischke ES, Hall RJ, Murphy KA, Verbyla DL, Hoy EE, Allen JL (2008) 'Using Landsat data to assess fire and burn severity in the North American boreal forest region: an overview and summary of results' *International Journal of Wildland Fire* **17**, 443–462.

Garcia-Llamas P, Suarez-Seoane S, Manuel Fernandez-Guisuraga J, Fernandez-Garcia V, Fernandez-Manso A, Quintano C, Taboada A, Marcos E, Calvo L (2019) 'Evaluation and comparison of Landsat 8, Sentinel-2 and Deimos-1 remote sensing indices for assessing burn severity in Mediterranean fire-prone ecosystems' *International Journal of Applied Earth Observation and Geoinformation* **80**, 137–144. doi:10.1016/j.jag.2019.04.006

Harvey BJ, Andrus RA, Anderson SC (2019) 'Incorporating biophysical gradients and uncertainty into burn severity maps in a temperate fire-prone forested region' *Ecosphere*. doi:10.1002/ecs2.2600

Holden ZA, Evans JS (2010) ‘Using fuzzy C-means and local autocorrelation to cluster satellite-inferred burn severity classes.’ *International Journal of Wildland Fire* **19**, 853–860. doi:10.1071/WF08126

Holden ZA, Morgan P, Smith AMS, Vierling L (2010) ‘Beyond Landsat: a comparison of four satellite sensors for detecting burn severity in ponderosa pine forests of the Gila Wilderness, NM, USA.’ *International Journal of Wildland Fire* **19**, 449–458. doi:10.1071/WF07106

Hultquist C, Chen G, Zhao K (2014) ‘A comparison of Gaussian process regression, random forests and support vector regression for burn severity assessment in diseased forests’ *Remote sensing letters* **5**, 723–732.

Kangas A, Maltamo M (2006) ‘Forest inventory: methodology and applications.’ (Springer Science & Business Media)

Key CH, Benson NC (1999) Measuring and remote sensing of burn severity. In ‘Proc. Jt. fire Sci. Conf. Work.’, 284. (University of Idaho and International Association of Wildland Fire Moscow, ID)

Key CH, Benson NC (2006) ‘Landscape assessment (LA)’ *FIREMON: Fire effects monitoring and inventory system Gen Tech Rep RMRS-GTR-164-CD, Fort Collins, CO: US Department of Agriculture, Forest Service, Rocky Mountain Research Station*.

Kolden CA, Rogan J (2013) ‘Mapping wildfire burn severity in the Arctic tundra from downsampled MODIS data’ *Arctic, Antarctic, and Alpine Research* **45**, 64–76.

Lentile LB, Holden ZA, Smith AMSS, Falkowski MJ, Hudak AT, Morgan P, Lewis SA, Gessler

PE, Benson NC (2006) ‘Remote sensing techniques to assess active fire characteristics and post-fire effects’ *International Journal of Wildland Fire* **15**, 319–345. doi:10.1071/WF05097

Liu Z (2016) ‘Effects of climate and fire on short-term vegetation recovery in the boreal larch forests of Northeastern China’ *Scientific reports* **6**, 37572.

Loboda T V, French NHF, Hight-Harf C, Jenkins L, Miller ME (2013) ‘Mapping fire extent and burn severity in Alaskan tussock tundra: An analysis of the spectral response of tundra vegetation to wildland fire’ *Remote Sensing of Environment* **134**, 194–209.

Mallinis G, Mitsopoulos I, Chrysafi I (2018) ‘Evaluating and comparing Sentinel 2A and Landsat-8 Operational Land Imager (OLI) spectral indices for estimating fire severity in a Mediterranean pine ecosystem of Greece’ *Giscience & Remote Sensing* **55**, 1–18. doi:10.1080/15481603.2017.1354803

McKenzie DMC, Gedalof Z, Peterson DL, Mote P (2004) ‘Climatic Change, Wildfire, and Conservation’ *Conservation Biology* **18**, 890–902.

Miller CW, Harvey BJ, Kane VR, Moskal LM, Alvarado EC ‘Inconsistent methods make comparing studies of burn severity challenging: A review of methods used to link remotely sensed data with the Composite Burn Index’ *[Manuscript submitted for publication]*.

Miller JD, Knapp EE, Key CH, Skinner CN, Isbell CJ, Creasy RM, Sherlock JW (2009) ‘Calibration and validation of the relative differenced Normalized Burn Ratio (RdNBR) to three measures of fire severity in the Sierra Nevada and Klamath Mountains, California,

USA' *Remote Sensing of Environment* **113**, 645–656.

Miller JD, Quayle B (2015) 'Calibration and validation of immediate post-fire satellite-derived data to three severity metrics.' *Fire Ecology* **11**, 12–30. Available at http://fireecologyjournal.org/docs/Journal/pdf/Volume11/Issue02/012.pdf

Miller JD, Thode AE (2007) 'Quantifying burn severity in a heterogeneous landscape with a relative version of the delta Normalized Burn Ratio (dNBR)' *Remote Sensing of Environment* **109**, 66–80.

Montealegre AL, Lamelas MT, Tanase MA, De la Riva J (2014) 'Forest fire severity assessment using ALS data in a mediterranean environment' *Remote Sensing* **6**, 4240–4265. doi:10.3390/rs6054240

Moriondo M, Good P, Durao R, Bindi M, Giannakopoulos C, Corte-Real J (2006) 'Potential impact of climate change on fire risk in the Mediterranean area' *Climate research* **31**, 85–95.

Parker BM, Lewis T, Srivastava SK (2015) 'Estimation and evaluation of multi-decadal fire severity patterns using Landsat sensors' *Remote Sensing of Environment* **170**, 340–349. doi:http://dx.doi.org/10.1016/j.rse.2015.09.014

Piao S, Liu Q, Chen A, Janssens IA, Fu Y, Dai J, Liu L, Lian XU, Shen M, Zhu X (2019) 'Plant phenology and global climate change: Current progresses and challenges' *Global change biology* **25**, 1922–1940.

Picotte JJ, Robertson KM (2011) 'Validation of remote sensing of burn severity in south-eastern

US ecosystems' *International Journal of Wildland Fire* **20**, 453–464. doi:http://dx.doi.org/10.1071/WF10013

Piedallu C, Gégout J-C (2005) 'Effects of forest environment and survey protocol on GPS accuracy' *Photogrammetric Engineering & Remote Sensing* **71**, 1071–1078.

Reinke K, Jones S (2006) 'Integrating vegetation field surveys with remotely sensed data' *Ecological Management & Restoration* **7**, S18–S23.

Rother MT, Veblen TT (2017) 'Climate drives episodic conifer establishment after fire in dry ponderosa pine forests of the Colorado Front Range, USA' *Forests* **8**, 159.

Roy DP, Wulder MA, Loveland TR, Woodcock CE, Allen RG, Anderson MC, Helder D, Irons JR, Johnson DM, Kennedy R (2014) 'Landsat-8: Science and product vision for terrestrial global change research' *Remote sensing of Environment* **145**, 154–172.

De Santis A, Asner GP, Vaughan PJ, Knapp DE (2010) 'Mapping burn severity and burning efficiency in California using simulation models and Landsat imagery' *Remote Sensing of Environment* **114**, 1535–1545. doi:10.1016/j.rse.2010.02.008

De Santis A, Chuvieco E (2009) 'GeoCBI: a modified version of the Composite Burn Index for the initial assessment of the short-term burn severity from remotely sensed data.' *Remote Sensing of Environment* **113**, 554–562. doi:10.1016/j.rse.2008.10.011

Schepers L, Haest B, Veraverbeke S, Spanhove T, Borre J Vanden, Goossens R (2014) 'Burned Area Detection and Burn Severity Assessment of a Heathland Fire in Belgium Using Airborne Imaging Spectroscopy (APEX)' *Remote Sensing* **6**, 1803–1826.

doi:http://dx.doi.org/10.3390/rs6031803

Soverel NO, Perrakis DDB, Coops NC (2010) 'Estimating burn severity from Landsat dNBR and RdNBR indices across western Canada' *Remote Sensing of Environment* **114**, 1896–1909.

Stambaugh MC, Hammer LD, Godfrey R (2015) 'Performance of Burn-Severity Metrics and Classification in Oak Woodlands and Grasslands' *Remote Sensing* **7**, 10501–10522. doi:http://dx.doi.org/10.3390/rs70810501

Strand EK, Bunting SC, Keefe RF (2013) 'Influence of Wildland Fire Along a Successional Gradient in Sagebrush Steppe and Western Juniper Woodlands' *Rangeland Ecology and Management* **66**, 667–679. Available at https://search.proquest.com/docview/1468524215?accountid=14784

Tanase MA, Kennedy R, Aponte C (2015) 'Fire severity estimation from space: a comparison of active and passive sensors and their synergy for different forest types' *International Journal of Wildland Fire* **24**, 1062–1075. doi:10.1071/WF15059

Veraverbeke S, Lhermitte S, Verstraeten WW, Goossens R (2010) 'The temporal dimension of differenced Normalized Burn Ratio (dNBR) fire/burn severity studies: The case of the large 2007 Peloponnese wildfires in Greece' *Remote Sensing of Environment* **114**, 2548–2563. doi:http://dx.doi.org/10.1016/j.rse.2010.05.029

Veraverbeke S, Lhermitte S, Verstraeten WW, Goossens R (2011) 'Evaluation of pre/post-fire differenced spectral indices for assessing burn severity in a Mediterranean environment

with Landsat Thematic Mapper' *International Journal of Remote Sensing* **32**, 3521–3537.

Veraverbeke S, Somers B, Gitas I, Katagis T, Polychronaki A, Goossens R (2012) 'Spectral mixture analysis to assess post-fire vegetation regeneration using Landsat Thematic Mapper imagery: Accounting for soil brightness variation' *International Journal of Applied Earth Observation and Geoinformation* **14**, 1–11.

Verbyla DL, Kasischke ES, Hoy EE (2008) 'Seasonal and topographic effects on estimating fire severity from Landsat TM/ETM+ data' *International Journal of Wildland Fire* **17**, 527–534.

Van Wagtendonk JW, Root RR, Key CH (2004) 'Comparison of AVIRIS and Landsat ETM+ detection capabilities for burn severity' *Remote Sensing of Environment* **92**, 397–408.

van Wagtendonk JW, Root RR, Key CH, Wagtendonk JW van, Root RR, Key CH (2004) 'Comparison of AVIRIS and Landsat ETM+ detection capabilities for burn severity' *Remote Sensing of Environment* **92**, 397–408. doi:10.1016/j.rse.2003.12.015

Wimberly MC, Liu Z (2014) 'Interactions of climate, fire, and management in future forests of the Pacific Northwest' *Forest Ecology and Management* **327**, 270–279.

Wimberly MC, Reilly MJ (2007) 'Assessment of fire severity and species diversity in the southern Appalachians using Landsat TM and ETM+ imagery' *Remote Sensing of Environment* **108**, 189–197. doi:10.1016/j.rse.2006.03.019

Woodbridge J, Fyfe RM, Roberts N (2014) 'A comparison of remotely sensed and pollen-based approaches to mapping Europe's land cover' *Journal of Biogeography* **41**, 2080–2092.

Young NE, Anderson RS, Chignell SM, Vorster AG, Lawrence R, Evangelista PH (2017) ‘A survival guide to Landsat preprocessing’ *Ecology* **98**, 920–932.

Zhu Z, Key C, Ohlen D, Benson N (2006) ‘Evaluate sensitivities of burn severity mapping algorithms for different ecosystems and fire histories in the United States. Final report JFSP 01-1-4-12’ *October* **12**, 35.

CHAPTER 4. BALANCING ACCURACY AND PRECISION: HOW ANALYTICAL DECISIONS IMPACT FIDELITY OF SATELLITE-BASED BURN SEVERITY MODELING

4.0 ABSTRACT

Many analytical pathways exist for modeling burn severity using remotely sensed data and continuous measures of severity based on the Composite Burn Index. Yet, uncertainty remains how these decisions affect model accuracy and precision. This study undertook a thorough sensitivity analysis of several key decisions in the modeling framework in order to investigate how much difference it makes which methods are used, the sensitivity of decisions to the overall workflow, differences on model accuracy, and the potential influence on the interpretation of the burn severity disturbing for the King Fire. Our results indicated that, while model accuracy and precision differ by pathway, there was no evidence that existing methods could be employed in such as combination as to substantially improve model fit. We did, however, call attention to several potential concerns that could arise during the model selection phase depending on the research objectives of a study or application of resulting models. Overall, this study suggests that much of the information available in Landsat optical imagery that is useful for modeling burn severity has been sufficiently extracted. Future studies may consider placing stronger emphasis on aligning methods with the ecological phenomena of interest and ensuring models enable robust interpretations of burn severity patterns.

4.1 INTRODUCTION

The Composite Burn Index (CBI, Key and Benson 1999) provides a rapid, convenient way to evaluate burn severity – define as the ecological effects of fire, or fire-caused change (Lentile *et*

al. 2006). The relationships between CBI plots and remotely sensed spectral fire indices are generally robust (Parks *et al.* 2019), providing a framework for mapping wall-to-wall burn severity using a combination of ground-based measurements and aerial- or space-borne observations. However even as more and more studies collect and model CBI observations with remotely sensed data, inconsistencies remain in how field-observsations are linked with remotely sensed data. As a result, there is considerable uncertainty with regards to the impact of methodological decisions on model results, and it remains unclear how comparable studies that use different methods are. This complicates the interpretation of results by requiring researchers to weight whether observed differences result from analytical choices or are reflective of true ecological phenomena of interest.

Field observations using CBI are often used in combination with spectral indices in order to calibrate radiometric changes detected by satellite with actual fire effects (Montealegre *et al.* 2014). Ideally, methods for linking field observations to remotely sensed data would result in accurate models that are not sensitive to specific choices in the analytical process and provide ecolgocially meaningful predictions across the full spectrum of potential severity values. However, prior studies highlight the lack of consensus on the best approach for linking CBI estimates with remotely sensed data (Chapter 2). Additionally, relatively few studies have compared the uncertainty introduced by these decisions in the analytical workflow. Of those that have, the focus has been on only a handful of important options, and we lack a comprehensive analysis of the relative importance of those decisions in terms of 1) their result on model accuracy and 2) their sensitivity to other decisions in the analysis framework. One of the consequences of this lack of consistency across studies is that it is unclear how the interpretation

of a single fire may change because of using a different methodological approach to model field-based composite burn severity measurements.

The CBI protocol itself has been scrutinized for a number of reasons. First, it's construction as a composite measure means that it is removed from the direct ecological phenomena that may be of interest (Morgan *et al.* 2014). Second, the lack of pre-fire observations for comparison – especially in large patches of intensly burned landscapes – creates challenges for observers to estimate the post-fire change caused by fire (Van Wagtendonk *et al.* 2004; Key 2006). Lastly, those visual estimates are calcualted in a subjective manner and may themselves be prone to observer bias (Lentile *et al.* 2009).

That said, CBI data have emerged as a standard for measuring the general effects of fire on forested landscapes. For general assessments of burn severity, the CBI may actually be more complete than other classification systems based on single indicators of burn severity (Sikkink 2015) since it integrates multiple metrics across vegetation strata and soil which can be used together (as site burn severity), providing an overall idea of damage caused by fire. Such a comprehensive measure of burn severity is desirable if only to generate maps that facilitate broad-scale rehabilitation prioritization (Karau *et al.* 2014). Additionally, individual components may be considered separately, depending on what is considered key for post-fire management (Key and Benson 2006; Zhu *et al.* 2006; Keeley 2009).

The original CBI protocol has been adapted to a wide range of environments (Quintano *et al.* 2015), as well as modified in attempts to improve its relationship with remotely sensed data (see Chapter 2 for details). One major modification was the development of the geometrically structured composite burn index (GeoCBI) (De Santis and Chuvieco 2009), which attempts to

resolve key issues with the way CBI is constructed. With moderate resolution passive remote sensing, as is most commonly used in mapping modeled burn severity (Chapter 2), individual components of a site (*e.g.*, trees, shrubs, downed woody debris) are not detectable and are reduced to a single, synoptic value for the whole pixel (Key 2006). Therefore, the spectral response of an overall plot is strongly related to the vegetation coverage per stratum (De Santis and Chuvieco 2009).

Ranges of CBI values do not have unique spectral signatures. For example, because the fraction of cover for each strata is not commonly used to compute the CBI, the same CBI score could come from different vegetation cover fractions, which would have different reflectance. Therefore, estimations based on remotely sensed data will inevitably produce errors, regardless the specific spectral technique applied (De Santis and Chuvieco 2009). The GeoCBI incorporates additional measurements to account for differences in fractional cover of each stratum or changes in leaf area index for the intermediate and tall tree strata (**Figure 4.1**). These additions describe the influence of vegetation cover on reflectance of different strata within a given plot (De Santis and Chuvieco 2009), and prior research has found that GeoCBI performs better in some circumstances (Chapter 2).

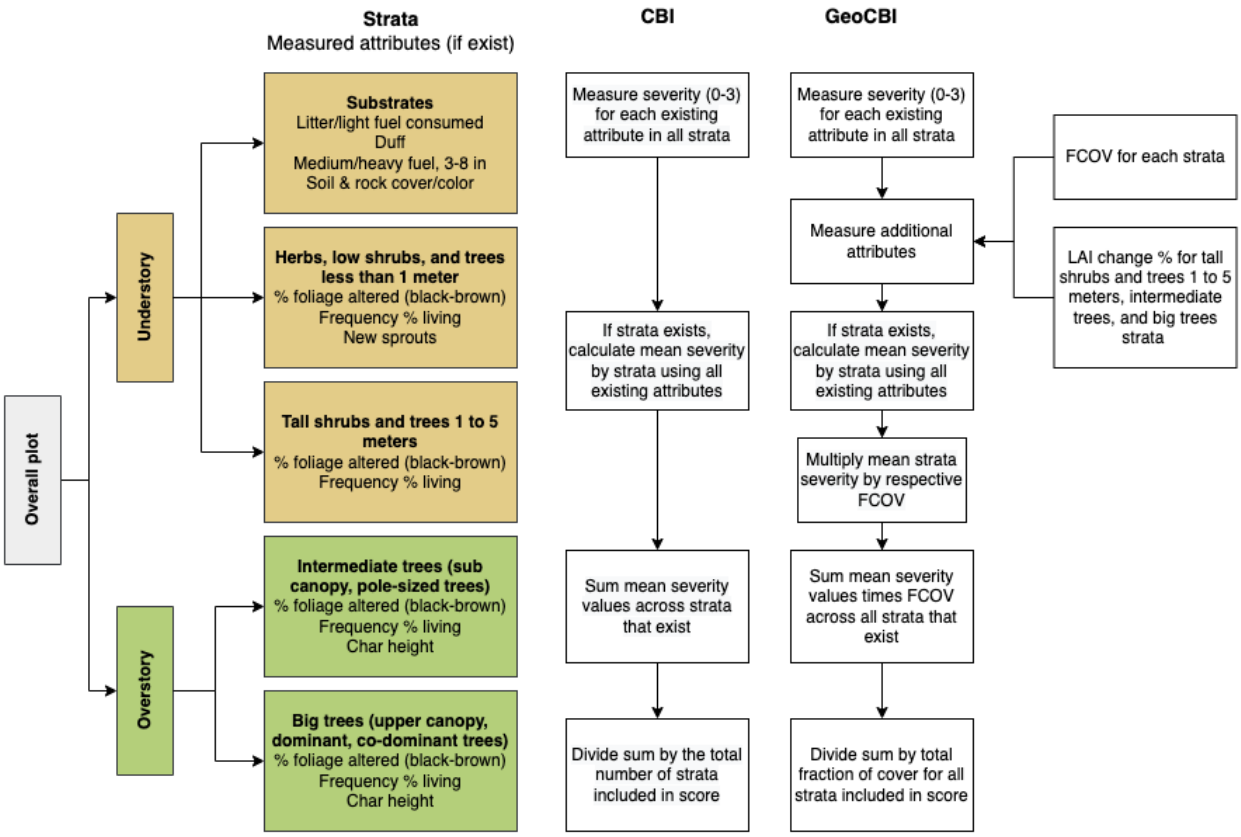

Figure 4.1 Strata and respective ecosystem attributes measured by the Composite Burn Index (CBI) and geometrically structured composite burn index (GeoCBI) protocol on the King Fire. Columns to the right show how the calculation of severity scores differ for CBI versus GeoCBI. 'FCOV' denotes fraction of cover and 'LAI' denotes leaf area index.

The increasing reliance on composite burn severity metrics, such as CBI and GeoCBI, results from a large number of studies showing strong relationships with specrtral data – particularly imagery captured by the Landsat satellite program (Chapter 2). Landsat provides a long record of earth observations (dating back to 1984) at consistent spatial and spectral resolutions, and was recently made available freely for public use. The Monitoring Trends in Burn Severity program (MTBS), a multi-agency program that aims to consistently map the burn severity and extent of large fires across all lands of the United States, relies on data from the Landsat mission to

consistently map burn severity on fires across all lands of the U.S. from 1984 to present (Eidenshink *et al.* 2007).

4.1.1 Research questions

The objective of this study was to take a practical look at the importance of different decisions in the analytical workflow linking field-based composite burn severity to remotely sensed data. We conducted what we believe is the most comprehensive sensitivity analysis to date, using the King Fire (2014 in the Sierra Nevada, California) as a case study to assess the accuracy and sensitivity resulting from decisions in the analysis workflow and develop a synthesis providing best known practices. Our specific research questions were:

1. How much difference does it make which method you use to model CBI using *NBR*-based spectral indices (post-fire *NBR*, *dNBR*, *RdNBR*, and *RBR*)?
2. Which options at one decision point are generally result in higher model accuracy? Which options are less sensitive to the other decisions made in the analytical framework?
3. As a demonstration of the effects of these decisions, how does the interpretation of burn severity distribution for the King Fire change depending on model selection?

4.2 METHODS

4.2.1 Analytical framework

Prior review work on the conceptual framework for linking field observations of burn severity to remotely sensed data revealed the potential range of options for each analytical decision (Chapter 2). This sensitivity analysis focused on a key set of options that have each been previously shown to impact model outcomes (**Figure 4.2**). Our analysis combines:

- 12 different ways of collecting or stratifying field observations;
- 14 different combinations of remotely sensed imagery and spectral index calculations;
- 8 methods for extracting the value of a spectral index that overlies each plot; and
- 11 different regression models.

In total, this resulted in 1,344 different sets of response and predictor variables that were assessed with 11 models each.

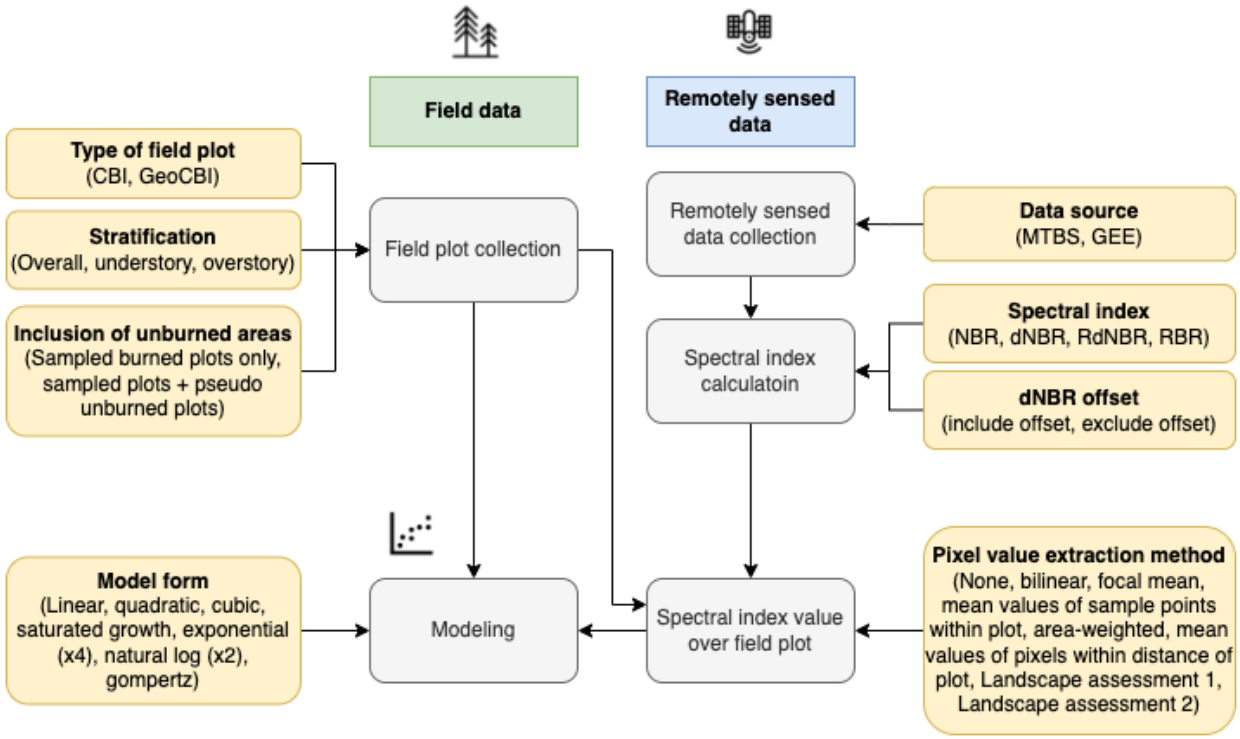

Figure 4.2 Diagram of overall analytical framework and key decision points included in this sensitivity analysis. To see a full set of potential decisions, review **Figure 2.11, Figure 2.12**, and **Figure 2.13** in Chapter 2.

4.2.2 Study area

The King Fire was a human-caused fire that was started on September 13, 2014, near Pollock Pines, approximately 80 km east of Sacramento, California (**Figure 4.3**). It burned 39,544 ha

including lands on the Eldorado National Forest in El Dorado and Placer Counties, a small portion of the American River District on the Tahoe National Forest, and on private lands. The topography of the area is quite variable and ranges from 800 to 1700 m, is very steep, and has a river valley running through the middle of the Rubicon Canyon (Stavros *et al.* 2016). The fire's rapid growth (including an approximately 16,200 ha afternoon run) and size were driven by fire-induced winds and submesoscale winds within the Rubicon Canyon (Coen *et al.* 2018), Much of the Rubicon Canyon area burned at high severity, with much more mixed severity along the canyon margins and at both the lower and higher elevations.

The dominant overstory vegetation at lower elevations and canyon bottoms consists of oak woodlands, grey pine (*Pinus sambiniana*), and ponderosa pine (*Pinus ponderosa*) with a moderate to heavy shrub and grasslands understory component (2014 King Fire Fuel Treatment Effectiveness Summary). Additionally, knobcone pine (*Pinus attenuata*) occurs along lower elevation ridgetops. At higher elevations, the dominant vegetation consists of mixed conifer stands of ponderosa pine, white fir (*Abies concolor*), incense cedar (*Calacedrus decurrens*), and black oak (*Quercus kelloggii*). In the northernmost portion of the fire, high elevation firs such as red fir (*Abies magnifica*) are common (Estes *et al.* 2016).

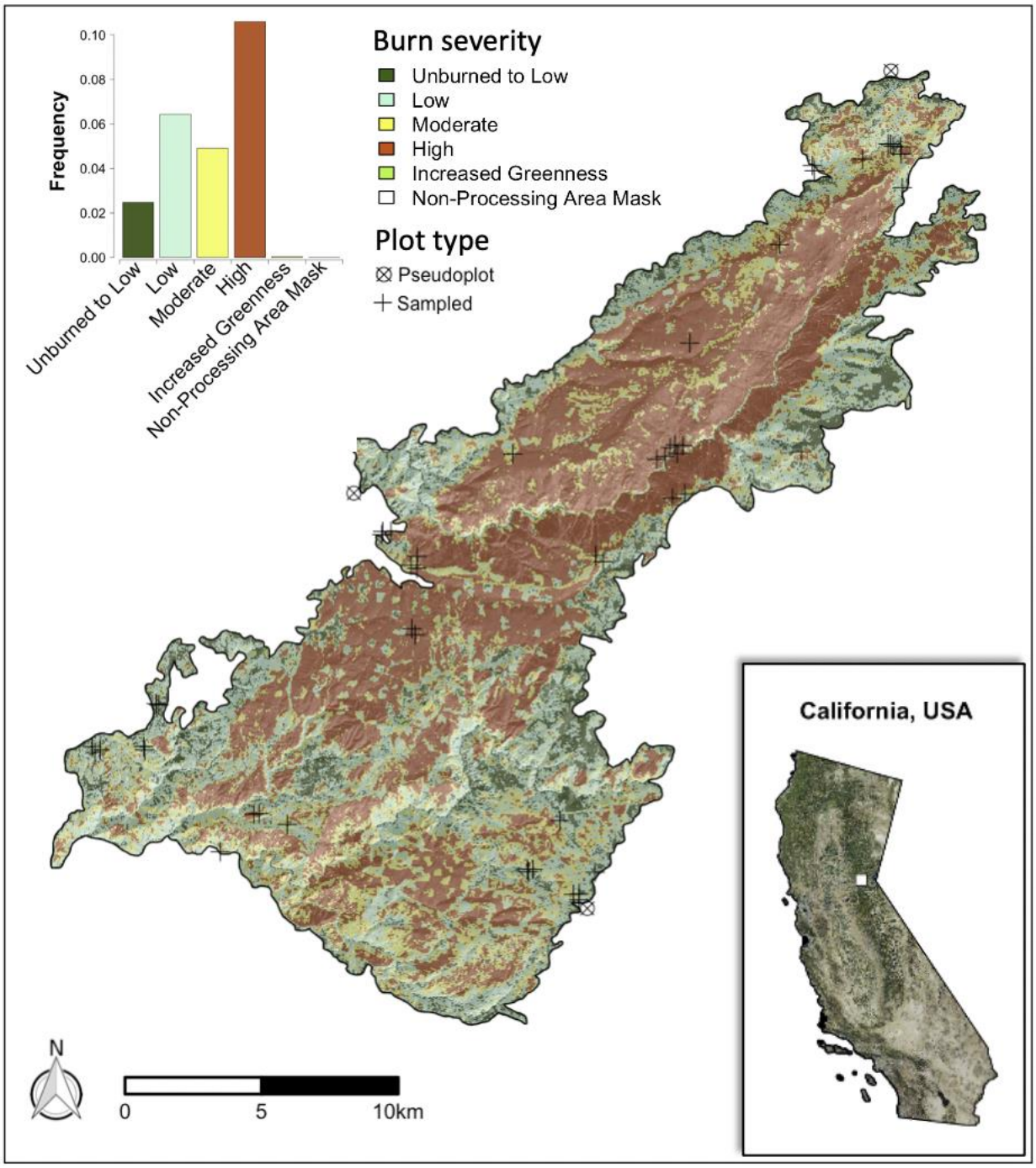

Figure 4.3 MTBS mapped severity classes of the King Fire, 2014. Ground-sampled CBI plots and "pseudoplots" (randomly placed points outside the burned area and assigned an unburned severity score) are identified.

The climate in the region is classified as warm temperate with summer dry precipitation and warm to hot summer temperatures according to the Köppen-Geiger climate classification (Kottek *et al.* 2006). The nearest comparable climate data provided by the National Weather Service characterizes Blue Canyon, located approximately 58 km north of Pollock Pines. The mean annual precipitation in the area is 143 cm, and the wet season is generally October through May. The mean annual temperature is 11.2 degrees C, with monthly mean temperatures ranging from a low of 3.8 degrees C in December and February to a high of 20.9 degrees C in July.

4.2.3 Spectral data

Two sets of spectral imagery were collected for analysis: 1) from the Monitoring Trends in Burn Severity (MTBS) project (Eidenshink *et al.* 2007) which uses a single set of paired pre- and post-fire images and 2) from the Google Earth Engine (GEE) script presented by Parks et al. (2018) with uses sets of composite pre- and post-fire images (**Table 4.1**). The MTBS download for the King Fire includes pre- and post-fire USGS Level 1 terrain-corrected (Level T1) Landsat Operational Land Imager (OLI) scenes. The selection of the imagery is typically based on 'peak of green' condition or as close in time as cloud-free data are obtainable. Imagery is provided in an Albers Equal Area projection and contains top-of-atmosphere (TOA) reflectance values. The GEE script produces a composite raster based on all scenes from the Landsat 5, 7, and 8 surface reflectance tier 1 collections between June 1 and September 30 one year prior to the fire (pre-fire) and one year after the fire (post-fire), where mages were mased for clear pixels and composited. The spatial extent of the output for the GEE script was defined by the MTBS polygon-based fire perimeter.

Table 4.1 Image details for Monitoring Tends in Burn Severity (MTBS) and Google Earth Engine (GEE) data sources. GEE imagery was created using the mean composite approach described in Parks et al. (2018). 'TOA' indicates top-of-atmosphere reflectance and 'SR' indicates surface reflectance.

Image source	Timing	Date	Sensor	Atmospheric corrections	Land cloud cover	Geographic coordinate system
MBTS	Pre-fire	July 30, 2013	Landsat 8 OLI/TIRS[a]	TOA	0.06	USA Contiguous Albers Equal Area Conic USGS version
	Post-fire	August 5, 2015			0.08	
GEE	Pre-fire	June 1 – Sept. 30, 2013	Landsat 5, 7, 8	SR	N/A	WGS 84
	Post-fire	June 1 – Sept. 30, 2015			N/A	

[a] USGS Landsat Collection 1 Level-1 path and row: 43/33

Four spectral indices were chosen for modeling (**Table 4.2**), each based on the normalized burn ratio (NBR). Equations for the spectral indices varied slightly between the MTBS and GEE datasets, except in the case of RBR. For NBR and dNBR, the difference is only a matter of scaling, where MTBS multiplies NBR by 1000 before differencing pre- minus post-fire values in the dNBR equation while the GEE script maintains the original scale of spectral values in the NBR equation and then scales dNBR by 100 after differencing pre- and post-fire values. Thus, this slight discrepancy would not affect the relationships between spectral values and plot observations. The RdNBR index, on the other hand, varies more considerably. The MTBS version follows the index equation as it was presented in (Miller and Thode 2007) which can be problematic as the denominator can be zero when $\mathrm{NBR}_{\mathrm{prefire}}$ is zero and allow the equation to reach infinity and fail. The modified formula provided in Parks et al. (2018) corrects this with an $\mathrm{NBR}_{\mathrm{prefire}}$ qualifier that substitutes 0.001 in instances where $\mathrm{NBR}_{\mathrm{prefire}} < 0$.

For bitemporal and relativized indices, versions with and without a *dNBR* offset value were calculated. The MTBS program includes a *dNBR* offset value in their metadata, however it is not included in the correction in *dNBR* as distributed. MTBS analysts look for a homogenous area of unburned vegetation that closely matches the composition of the vegetation that burned. They use a minimum area of 1000 pixels and aim for a mean offset between -100 and 100 with a standard deviation less than 50. These being outer bounds, they try to get a larger area with values as close to 0 as possible. The GEE script uses a 180-m ring outside the supplied fire perimeter.

Table 4.2 Satellite-derived spectral indices used in analysis. 'Pre' and 'post' indicate pre-fire and post-fire timing of index calculation. 'NIR' stands for the near infrared band and 'SWIR' for the shortwave infrared band. For Landsat 5, the NIR band is band 4 (0.76 – 0.90 μm); Landsat 7 is band 4 (0.76 – 0.90 μm); and Landsat 8 is band 5 (0.85-0.88 μm). The SWIR band is band 7 for Landsat 5 (2.08-2.35 μm); band 7 for Landsat 7 (2.09-2.35 μm) and band 7 for Landsat 8 (2.11-2.29 μm). 'MTBS' denotes calculations used for imagery acquired from the Monitoring Trends in Burn Severity program (Eidenshink *et al.* 2007), and 'GEE' denotes calculations used for imagery produced from the Google Earth Engine script (Parks *et al.* 2018). Where included, dNBR offsets were retrieved from MTBS metadata or calculated on the fly in the GEE script using a 180 m ring outside the fire perimeter as provided by MTBS.

Index	Description	Offset	Formula	Key citation(s)
NBR	Normalized burn ratio	N/A	MTBS: $\left(\frac{NIR-SWIR}{NIR+SWIR}\right) \times 1000$ GEE: $\left(\frac{NIR-SWIR}{NIR+SWIR}\right)$	García and Caselles (1991); Key and Benson (1999)
dNBR		No	MTBS: $NBR_{pre} - NBR_{post}$	Key and Benson (2006)

	Differenced normalized burn ratio	Yes	GEE: $\left(NBR_{pre} - NBR_{post}\right) \times 1000$ MTBS: $NBR_{pre} - NBR_{post} - dNBR_{offset}$	
			GEE: $\left(NBR_{pre} - NBR_{post} - dNBR_{offset}\right) \times 1000$ MTBS: $\frac{dNBR}{\left\lvert\frac{NBR_{pre}}{1000}\right\rvert^{0.5}}$	
		No		
RdNBR	Relativized differenced normalized burn ratio		GEE: $\begin{cases} \frac{dNBR}{\lvert NBR_{pre}\rvert^{0.5}}, \lvert NBR_{pre}\rvert \geq 0.001 \\ \frac{dNBR}{\lvert 0.001\rvert^{0.5}}, \lvert NBR_{pre}\rvert < 0.001 \end{cases}$ MTBS: $\frac{dNBR - dNBR_{offset}}{\left\lvert\frac{NBR_{pre}}{1000}\right\rvert^{0.5}}$	Miller and Thode (2007) Parks et al. (2018)
		Yes		
			GEE: $\begin{cases} \frac{dNBR - dNBR_{offset}}{\lvert NBR_{pre}\rvert^{0.5}}, \lvert NBR_{pre}\rvert \geq 0.001 \\ \frac{dNBR - dNBR_{offset}}{\lvert 0.001\rvert^{0.5}}, \lvert NBR_{pre}\rvert < 0.001 \end{cases}$	
RBR	Relativized burn ratio	No	MTBS & GEE: $\frac{dNBR}{NBR_{pre}+1.001}$	Parks et al. (2018)
		Yes	MTBS & GEE: $\frac{dNBR - dNBR_{offset}}{NBR_{pre}+1.001}$	

4.2.2 Field data

Field-based burn severity data were collected between November 2014 and January 2015 following the burn (Stavros *et al.* 2016). These consist of 52 plots following the protocol of Key and Benson (Key and Benson 1999) and De Santis and Chuvieco (De Santis and Chuvieco 2009). However, two plots were dropped from this analysis because they fell outside the delineated fire boundary from MTBS. This boundary was used in the GEE script to provide the extent of the fire footprint, thus requiring either additional mapping to account for the unmapped burned area or dropping those plots from both the MTBS and GEE analysis. The 30 m diameter plots were placed at least 90 m apart (the closest plots were 94 m apart) and chosen in areas of at least 60 x 60 m with relatively homogenous fuel type and fire effects (Key and Benson 2006).

The evaluation encompasses five vegetation strata (substrates; herbs, low shrubs and trees less than 1 m; tall shrubs and trees 1 to 5 m; intermediate trees of 5 to 20 m; and big trees >20 m and incorporates factors such as the condition and color of the soil, amount of vegetation or fuel consumed, resprouting from burned plants, establishment of new colonizing species, and blackening or scorching of trees (**Figure 4.1**). Up to 23 different ecosystem attributes are rated on a continuous scale between 0 and 3 where 0 is unburned and 3 is severely burned (**Table 4.3**). Observations were measured by ocular estimation and aggregated to a single unitless score that provides a continuous measure of burn severity. Plot centers were GPS with a survey grade GPS unit (Javad GNSS). Digital photographs were taken from the plot center to the four cardinal directions as well as upwards and downwards to provide qualitative information about vegetation structure and soil conditions (**Figure 4.4**). When assessing understory and overstory plot severity, strata were combined according to **Figure 4.1**.

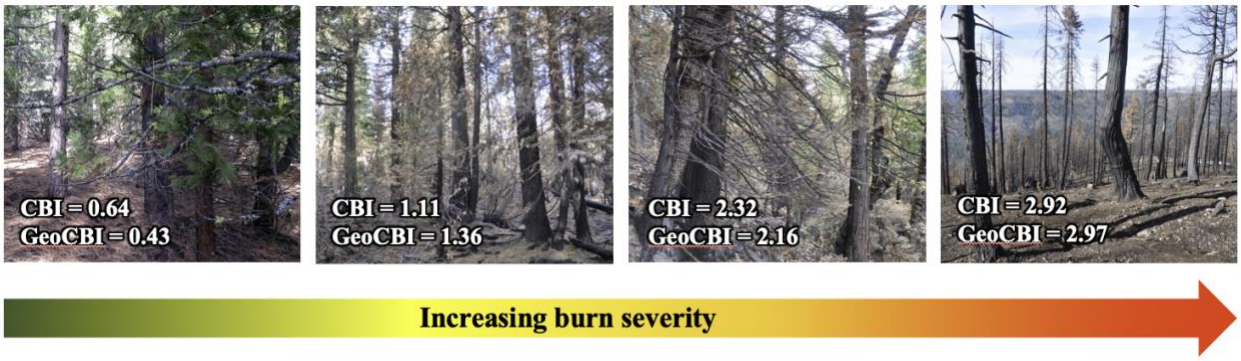

Figure 4.4 Sample images of plots with overall CBI and GeoCBI scores.

Table 4.3 Ecosystem attributes measured following GeoCBI protocol in De Santis and Chuvieco (2009). 'FCOV' denotes fraction of cover and 'LAI' denotes leaf area index.

	Burn severity scale						
	No effect		**Low**		**Moderate**	**High**	
Strata	**0**	**0.5**	**1**	**1.5**	**2**	**2.5**	**3**
Substrates				Soil depth (cm)			
Litter (L)/light fuel (LF) Consumed (%)	0	-	50% L	-	100% L	>80% LF	98% LF
Duff (%)	0	-	Light char	-	50	-	Consumed
Medium/heavy fuel (%)	0	-	20	-	40	-	>60
Soil & rock cover/color (%)	0	-	10	-	40	-	>80
Herbs, low shrubs, and trees <1 m				FCOV			
Foliage altered (%)	0	-	30	-	80	95	100
Frequency living (%)	100	-	90	-	50	<20	0
New sprouts	Abundant	-	Moderate-high	-	Moderate	-	Low-none
Tall shrubs and trees 1-5 m				FCOV			
Foliage altered (%)	0	-	20	-	60-90	>95	Branch loss
Frequency living (%)	100	-	90	-	30	<15	<1
LAI change	0	-	15	-	70	90	100
Intermediate trees 5-20 m				FCOV			
Green (unaltered) (%)	100	-	80	-	40	<10	None
Black/brown (%)	0	-	20	-	40-60	>95	Branch loss
Frequency living (%)	100	-	90	-	30	<15	<1
LAI change (%)	0	-	15	-	70	90	100
Char height (m)	None	-	1.5	-	2.8	-	>5
Big trees >20 m				FCOV			
Green (unaltered) (%)	100	-	80	-	50	<10	None
Black/brown (%)	0	-	20	-	60-90	>95	Branch loss
Frequency living (%)	100	-	90	-	30	<15	<1
LAI change (%)	0	-	15	-	70	90	100
Char height (m)	None	-	1.8	-	4	-	>7

The field crew that sampled the King Fire did not locate any plots in unburned areas, so for the sensitivity analysis we identified three unburned pseudoplots outside the fire perimeter following approaches detailed in other studies (De Santis and Chuvieco 2007; Picotte and Robertson 2011; Zheng *et al.* 2016; Zhong *et al.* 2018; Parks *et al.* 2019). Following the suggestion by Parks et al. (2019) that at least 5% of the plots be represented by CBI ≤ 0.25, the three unburned pseudoplots were randomly located outside the fire perimeter at a distance of 200 meters. A refined dataset of forest management records aggregated from the USFS′ Forest Activity Tracking System (FACTS) and the California Department of Forestry and Fire Protection (CAL FIRE) provided by Knight et al. (2022) was used to ensure the pseudoplots fell outside of areas harvested between 2013 and 2015 (the years of spectral image collection). Randomly placed plot locations were manually adjusted to ensure did not fall on roads and the absence of treatments or other disturbances between image dates was visually verified using 2013 and 2015 National Agriculture Imagery Program (NAIP) aerial imagery.

The distribution of field plot severities scores generally reflects the overall fire effects, where more of the landscape was affected by high severity fire than low severity fire (**Figure 4.5**). For models using just the 50 field-sampled burned plots, in general CBI severity scores were higher than GeoCBI scores for the overall plot, as well as the understory and overstory strata (**Table 4.4**). The effect was especially pronounced in the overstory strata. While understory plots tended to burn at higher severities than overstory plots, the overstory plots did experience a full range of severities, leading to higher coefficients of variation. When unburned pseudoplots were included, the distributions were slightly less skewed towards the low range of severities (**Table 4.5**). However, the overall distribution was still highly disproportionate in reflecting high severity fire effects.

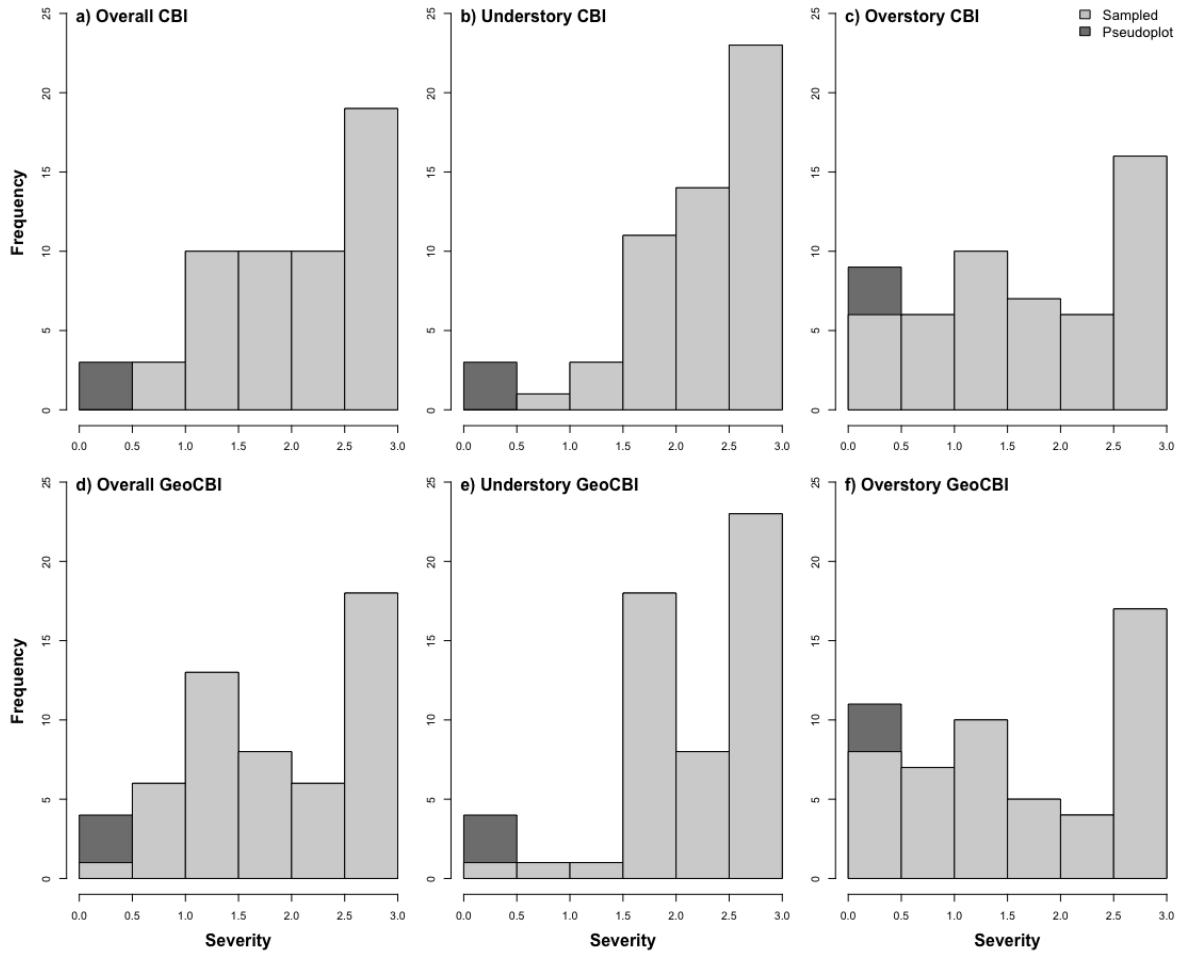

Figure 4.5 Response variables including CBI and GeoCBI for overall plot severity, understory, and overstory severity. Field-sampled plots are shown in light grey, while unburned pseudoplots from outside the fire perimeter added during analysis are shown in dark grey.

Table 4.4 Summary statistics for CBI and GeoCBI by strata for field-sampled plots (within the burned areas). Overall, there were 50 burned plots.

Strata	Type	Min	Median	Mean	Max	SD	CV
Overall	CBI	0.64	2.12	2.11	2.94	0.67	31.86
	GeoCBI	0.43	1.88	1.96	2.99	0.8	40.58

Understory	CBI	1.00	2.37	2.33	3.00	0.54	23.26
	GeoCBI	0.50	2.24	2.25	3.00	0.65	28.76
Overstory	CBI	0.10	1.65	1.75	3.00	0.96	54.86
	GeoCBI	0.17	1.54	1.68	3.00	1.00	59.21

Table 4.5 Summary statistics for CBI and GeoCBI by strata for all plots (including those field-sampled within the burned areas and unburned pseudoplots added outside the fire perimeter). This includes the 50 burned plots as well as an additional three unburned pseudoplots.

Strata	**Type**	**Min**	**Median**	**Mean**	**Max**	**SD**	**CV**
Overall	CBI	0.00	2.06	1.99	2.94	0.82	41.07
	GeoCBI	0.00	1.74	1.85	2.99	0.9	48.52
Understory	CBI	0.00	2.18	2.13	3.00	0.82	38.57
	GeoCBI	0.00	2.29	2.19	3.00	0.76	34.42
Overstory	CBI	0.00	1.62	1.65	3.00	1.02	61.76
	GeoCBI	0.00	1.46	1.59	3.00	1.05	65.88

4.2.3 Analysis

Preprocessing of field observations and remotely sensed imagery included converting plot coordinate systems to match spectral imagery, calculating the spectral indices, and extracting the spectral index values overlaying plot centers (**Figure 4.6**). Plot locations were reprojected to match the coordinate system of each of the spectral data sources, MTBS and GEE to avoid any potential errors introduced by reprojecting the raster data. Reprojecting the rasters would require selecting a resampling method when creating a new raster object, potentially with a different number of columns and rows than the original.

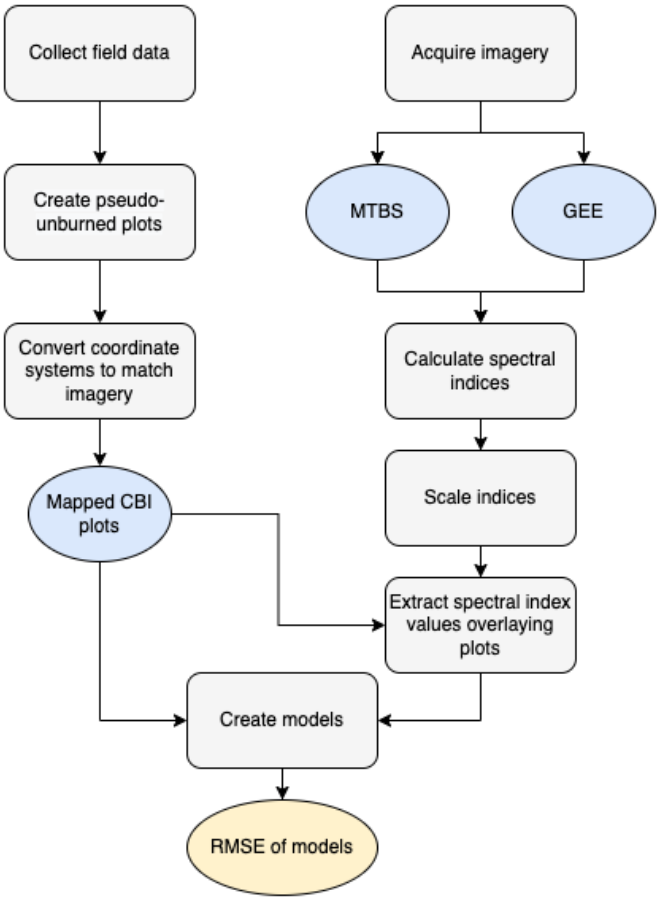

Figure 4.6 Preprocessing and modeling workflow.

After the spectral indices were calculated, the rasters were masked by fire boundary which had been buffered by 300 m to account for unburned pseudoplots. Following that, the values outside of the 1st and 99th percentile were reclassified to the 1st and 99th percentile values, respectively, to exclude outliers. The bands were then rescaled to 0 to 3 to match the potential range of CBI scores. This step is not generally done in prior research using spectral indices to predict CBI-based severity, however provided flexibility for running nonlinear models sensitive to starting parameters across a set of predictor variables with varying scales. The 0 to 3 range was chosen to match the potential range of CBI scores. Spectral index values overlaying each plot location

were extracted according to eight methods that had been used in previous studies (Chapter 2) or described in the Landscape Assessment General Technical Report by Key and Benson (2006).

When using $NBR_{postfire}$ as a predictor variable, the index was multiplied by negative one. This did not affect the relationship with plot values; however, it produced a relationship that matched the other spectral indices included in this analysis (a monotonically increasing trend). Flipping the sign on NBR supported easier modeling by allowing the same starting parameters and interpretation for non-linear functions as were used on the other indices.

To calculate the spectral index value to associate with each field plot, we used eight different methods of pixel value extraction (**Table 4.6**). Each of these methods appeared in prior literature assessing composite burn severity metrics with remotely sensed data (Chapter 2) or were presented in the Landscape Assessment report by Key and Benson (2006).

Table 4.6 Pixel value extraction methods for calculating the spectral index value overlaying field plots. See spatial depictions of each method in **Figure 4.7**.

Pixel value extraction method	Abbreviation	Description
None	None	Pixel value overlaying plot center
Focal mean	Focal mean	Mean is calculated for the pixels encountered in a neighborhood (3x3 window) around a cell
Bilinear	Bilinear	Mean is calculated for the values of the four nearest pixels to plot center weighted by their distance to the point
Mean values of sample points within plot	Sample points	Mean of pixel values overlaying sample points within plot

Area-weighted average	Area-weighted	Weighted plot averaging: weights assigned based on each pixel's percentage of area within a plot
Mean values of pixels within distance of plot	Closest 4 pixels	Mean of pixel values for cells falling within specified distance of plot (4 pixels closest to plot center)
Landscape Assessment method 1	LA1	Weight the center pixel by two or three times, and throw out one pixel that has the most different value from the center pixel
Landscape Assessment method 2	LA2	A five-point pixel average, where the points for sampling are the plot center, and theoretically plus or minus 15 m from plot center

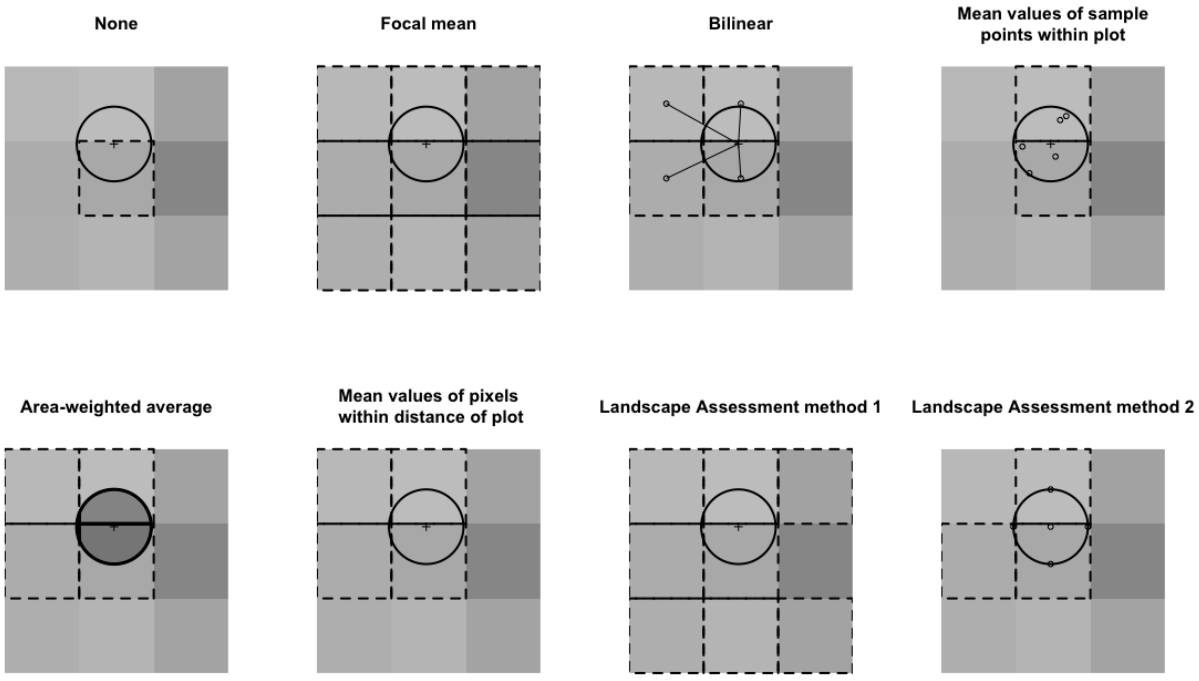

Figure 4.7 Spatial depiction of spectral index value extraction methods. Shaded pixels represent variation in spectral index raster, the cross and circle represent the plot center and plot perimeter, respectively, and the dashed lines indicate the pixel contributes to the calculation of the spectral index value that is associated with the plot for analysis.

For each unique predictor/response combination (1344 different sets), a set of 11 regression models were constructed (**Table 4.7**d). All modeling was done in R (Team 2021) using the *optim*

function with the "SANN" method (Simulated-annealing) to minimize cost function (RMSE) for each model form. Due to the sensitivity of the model outputs to the starting parameters, 10 runs were conducted using random starting parameters between -5 and 5. The model with the lowest RMSE from those runs was kept.

Table 4.7 Model forms used to predict CBI/GeoCBI based on spectral indices.

Model form	Model abbreviation	Equation
Linear	Linear	$y = a + bx$
Quadratic	Quadratic	$y = ax^2 + bx + c$
Cubic	Cubic	$y = ax^3 + bx^2 + cx + d$
Natural logarithm	Natural log 1	$y = \ln(ax + b)$
	Natural log 2	$y = a * \ln\left(\frac{bx+c}{d}\right)$
Exponential	Exponential 1	$y = a + bx^c$
	Exponential 2	$y = a + b * exp(bx)$
	Exponential 3	$y = ax^b$
	Exponential 4	$y = ae^{bx}$
Saturated growth	Saturated growth	$y = x(ax + b)^{-1}$
Gompertz	Gompertz	$y = a * e^{-e^b - cx}$

We compared the influence of model selection on burn severity interpretation by assessing the best performing model (empirically fit the data the best based on RMSE) for each response variable (overall, understory, and overstory CBI and GeoCBI). Next, we compared the best performing models for GeoCBI against ones that contained all plots (both field-sampled burned plots and unburned pseudoplots) using linear and Gompertz model forms. Including unburned pseudoplots in the model anchors the regression at the low end of the range of severity, often forcing the resultant model to predict some areas within the modeling extent as unburned. To

better understand the implications of model selection on post-fire management, each of these selected models was mapped back onto the landscape based on its model parameters and associated decision criteria. The resulting distribution was then categorized according to seven classes (unburned to very low, low, low to moderate, moderate, moderate to high, high, and extremely high). While infrequent to use so many classifications to map burn severity, the King Fire exhibited many areas of extremely high severity and splitting out more categories allowed an in-depth look at how pixels straddling the margins of two classes might change depending on model selection. Severity classes were split according to the following distribution: [0], (0, 0.5], (0.5, 1], (1, 1.5], (1.5, 2], (2, 2.5], (2.5, 3].

4.3 Results

4.3.1 Impact of methods on model fit

The marginal distributions of each option in the modeling framework indicate that no single decision has an outsized influence on the overall model results, in terms of RMSE (**Figure 4.8**). These marginal distributions display the RMSE for each of the 14,784 models generated (1,344 pathways to generate predictor and response variables times 11 model forms) over the distributions of all discarded variables (different options not contained in the decision of focus). For example, the "Overall CBI" violin plot in panel (a) contains models based on both field-sampled burned plots only as well as field-sampled burned plots plus unburned pseudoplots outside the fire perimeter. Long tails in the distributions of certain decision options show the potential for poor model fit. For example, the understory CBI and understory GeoCBI selections result in numerous outliers. The spectral indices $NBR_{postfire}$, dNBR, RdNBR, and RBR similarly exhibit long tails relative to the other criteria in that decision point. For model forms, the

saturated growth selection stands out has having particularly large outliers when compared with alternative model forms.

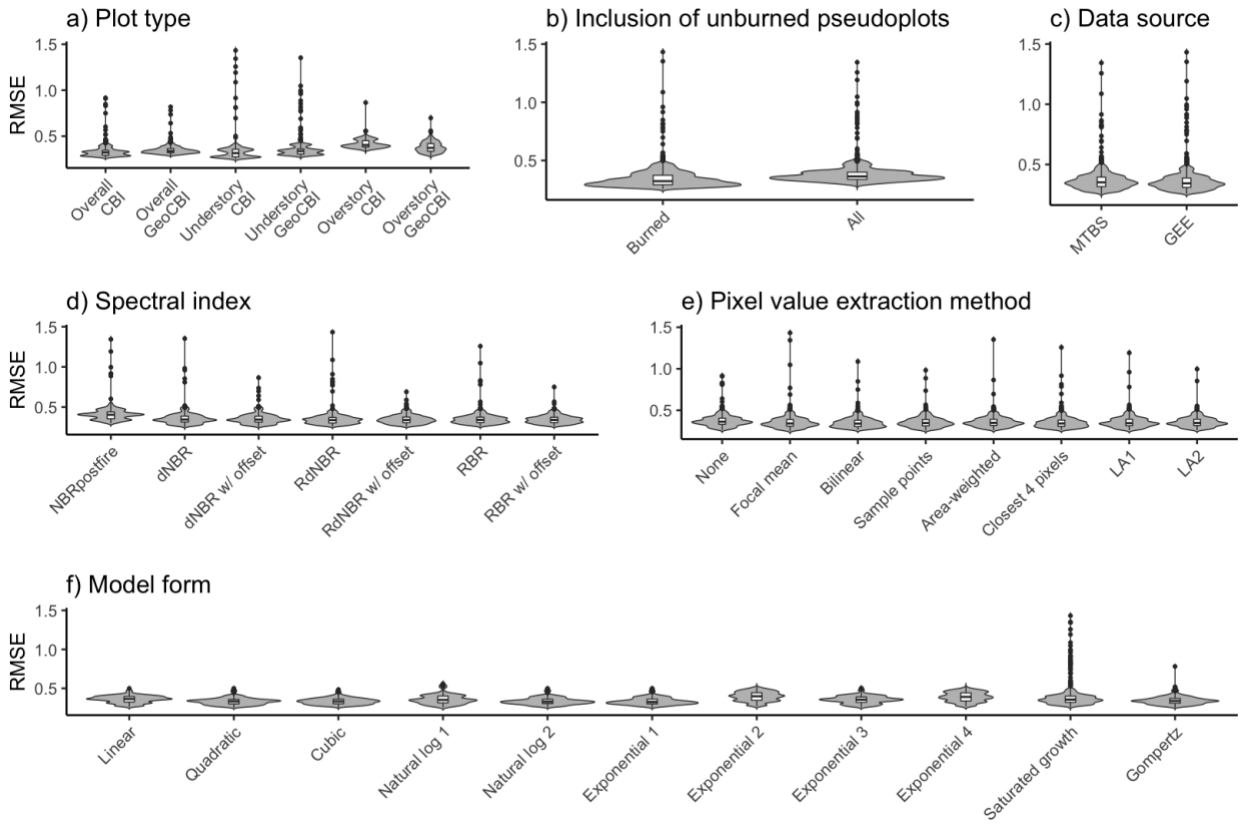

Figure 4.8 Marginal distributions of RMSE for each decision option in the analysis framework. Each plot represents the distribution of RMSE for all models based on that single approach.

4.3.2 Accuracy and precision of methodological decisions

We assessed overall model behavior using RMSE based on the marginal distributions of each option in the decision framework (**Table 4.8**). In general, where a specific selection results in a low mean RMSE, it indicates that that option, agnostic of the decisions in other categories, results in models that fit the data well (high accuracy). Low minimum RMSE values indicate that the that selection may resulting the best fit model, while low maximum RMSE values indicate

any model fit with that option will fit the data at least that well (*i.e.*, never worse than that RMSE). The standard deviations and coefficients of variation are indicators of how sensitive that selection is to other choices in the modeling framework (*i.e.*, model precision).

Table 4.8 Root mean square error (RMSE) statistics for key decisions in the analysis framework. The mean, minimum, and maximum RMSE are indications of model accuracy, while standard deviation and coefficient of variation are indications of mode precision (*i.e.*, how sensitive is this option to other selections in the analytical workflow). The lowest values for each decision are shown in bold and the highest values in italics. See **Table 4.2** for information on spectral indices, **Table 4.6** for information on pixel value extraction methods, and **Table 4.7** for information on model forms.

Decision	Options	Accuracy			Precision		Count
		Mean RMSE	Min RMSE	Max RMSE	SD RMSE	CV RMSE	
Plot type	Overall CBI	0.327	0.264	0.917	0.047	14.483	2464
	Overall GeoCBI	0.346	0.286	0.818	**0.037**	10.764	2464
	Understory CBI	**0.322**	**0.251**	*1.433*	*0.066*	*20.523*	2464
	Understory GeoCBI	0.343	0.271	1.353	0.058	16.898	2464
	Overstory CBI	*0.416*	*0.335*	0.865	0.044	**10.704**	2464
	Overstory GeoCBI	0.380	0.281	**0.698**	0.055	14.355	2464
Inclusion of unburned pseudoplots	Burned	**0.337**	**0.251**	*1.433*	*0.062*	*18.38*	7392
	All	*0.374*	*0.268*	**1.344**	**0.055**	**14.849**	7392
Data source	MTBS	*0.359*	**0.251**	**1.344**	**0.060**	**16.847**	7392
	GEE	**0.352**	*0.255*	*1.433*	*0.062*	*17.725*	7392
	$NBR_{postfire}$	*0.405*	*0.298*	1.344	*0.066*	16.289	2112

	dNBR	0.353	0.252	1.353	0.063	17.892	2112
	dNBR w/ offset	0.352	**0.251**	0.865	0.057	16.187	2112
Spetcral	RdNBR	**0.343**	0.258	*1.433*	0.061	*17.914*	2112
index	RdNBR w/ offset	0.345	0.257	**0.690**	0.051	14.706	2112
	RBR	0.346	0.258	1.257	0.057	16.441	2112
	RBR w/ offset	0.344	0.259	0.750	**0.049**	**14.283**	2112
	None	*0.369*	0.263	**0.915**	0.062	16.926	1848
	Focal mean	0.353	**0.251**	*1.433*	*0.069*	*19.569*	1848
	Bilinear	**0.349**	*0.264*	1.087	0.059	16.834	1848
Pixel value	Sample points	0.354	0.255	0.982	0.059	16.694	1848
extraction	Area-weighted	0.358	0.262	1.353	0.060	16.769	1848
method	Closest 4 pixels	0.350	0.263	1.257	0.061	17.565	1848
	LA1	0.356	0.260	1.192	0.061	17.245	1848
	LA2	0.356	0.262	0.996	**0.057**	**16.085**	1848
	Linear	0.360	0.262	0.499	0.046	12.818	1344
	Quadratic	**0.333**	0.252	0.500	0.044	13.344	1344
	Cubic	0.334	0.252	**0.484**	**0.042**	**12.482**	1344
	Natural log 1	0.359	0.258	0.557	0.061	17.023	1344
	Natural log 2	0.335	0.254	0.499	0.044	13.219	1344
Model form	Exponential 1	0.334	**0.251**	0.499	0.045	13.544	1344
	Exponential 2	*0.396*	*0.270*	0.525	0.060	15.210	1344
	Exponential 3	0.354	0.256	0.503	0.048	13.680	1344
	Exponential 4	0.389	0.268	0.526	0.061	15.711	1344
	Saturated growth	0.374	0.256	*1.433*	*0.104*	*27.914*	1344
	Gompertz	0.343	0.252	0.781	0.049	14.287	1344

Our results showed that using the understory CBI plots as the response variable produce the overall best fit model, both in terms of minimum RMSE and mean RMSE. Therefore, this

selection resulted in the single best fit model amongst all the modeling pathways as well as the generally best fit when other selections were manipulated. The low maximum RMSE of overstory GeoCBI models indicated that they minimized the worst-case scenarios relative to the modeling pathways that could be used to compare other plot types. In terms of model precision, both Overall GeoCBI (lowest standard deviation) and overstory CBI (lowest coefficient of variation) performed better than the other plot types in terms of absolute and relative error, respectively. Models predicting overstory CBI often produced less accurate results (higher RMSE) but gave similar model fits given different selections at other steps in the analysis. In other words, care could be taken to assess the impact of each decision, but the result would not generally produce an accurate model relative to the other potential plot types. On the other hand, models based on this response tended to perform similarly regardless of what other decisions were made.

The inclusion of unburned pseudoplots tended to resulted in less accurate (higher RMSE) but more precise (lower standard deviation and coefficient of variation) models. The most accurate model was fit using only burned plots, and other models using only burned plots tended to produce more accurate results than models that included unburned pseudoplots.

Using GEE data as the source of spectral imagery generally resulted in more accurate models than MTBS imagery. However, MTBS imagery resulted in more precise models in general, albeit only slightly so.

For spectral indices, RdNBR produced the most accurate models on average, followed closely by the other relativized indices (RBR w/ offset, RdNBR w/ offset, RBR) (See **Table 4.2** for information on spectral indices). The most precise models were based on RBR with an offset

value, while the least precise models were based either on $NBR_{postfire}$ or RdNBR, depending on whether absolute or relative precision was considered. Additionally, $NBR_{postfire}$ resulted in lower accuracy models in general.

Bilinear interpolation resulted in the most accurate models on average. However, both the mean of the closest 4 pixels and a focal mean also resulted in similar accuracy (see **Table 4.6** for information on pixel value extraction methods). In general, the most precise models were based on a focal mean, while the least precise were based on the landscape assessment 2 method.

Regarding model forms, in general the most accurate models resulted from a second-order polynomial (quadratic model) and the least accurate models were based on the exponential 2 model (see **Table 4.7** for information on model forms). Saturated growth models were on average had the least precision, however, looking at the minimum RMSE indicates that they did in some cases result in a relatively accurate fit with the data.

Each option amongst the decisions in the modeling framework was assessed using it's mean RMSE and mean CV relative to the other options in that category (**Figure 4.9**). Here, we define generally good choices as those that generally result in relatively high model accuracy (low RMSE) and were less sensitive to the selections at other steps in the analysis (low CV). The results indicate that composite burn severity metrics based on the overall plot (both CBI and GeoCBI) were good choices, generally result in higher model accuracy (lower RMSE) less sensitivity. Understory burn severity generally resulted in more accurate models than overstory severity, however it was more sensitive to the other selections in the analysis. The inclusion of unburned pseudoplots resulted in relatively less accurate models, but those models were less sensitive. Similarly, MTBS imagery resulted in relatively less accurate models, but was less

sensitive than GEE-derived imagery. For spectral indices, RdNBR with an offset value and RBR with an offset value were generally good choices compared with the other spectral indices assessed. All bitemporal spectral indices incorporating a dNBR offset value resulted in more precise models than those that did not. Both bilinear and sampling of random points within the plot center were generally good choices for pixel value extraction methods. However, using the mean of the closest four pixels, either landscape assessment method, or an area-weighted approach – while somewhat less accurate or more sensitive – did not fall far bilinear or sample points in either accuracy or sensitivity. Good choices for model form based on this analysis were quadratic, cubic, natural log 2, or exponential 1 (see **Table 4.7** for full model equations).

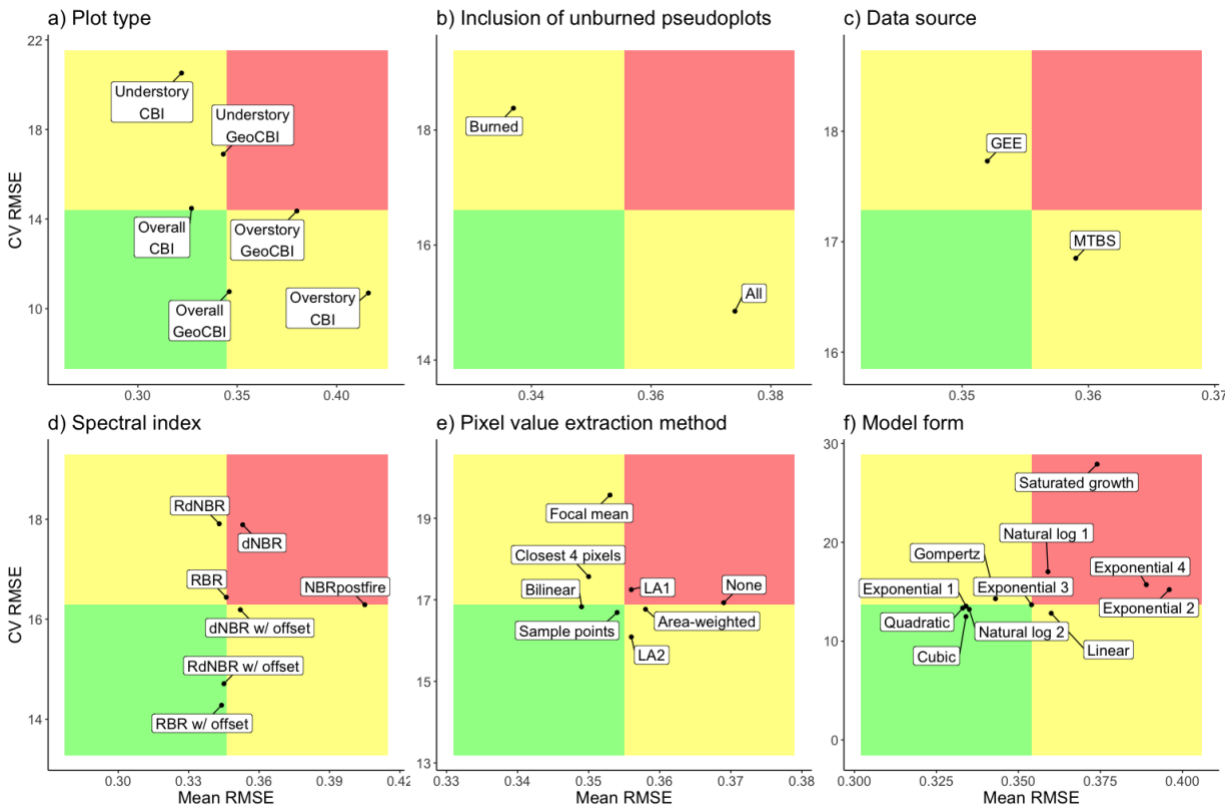

Figure 4.9 Average root mean square error (RMSE) versus coefficient of variation (CV) for each decision option in the analysis framework. The quadrants of each plot are divided using the median RMSE and median CV for each decision, where the green quadrant represents selections that produce relatively low RMSE and CV (in other words, these selections generally result in more accurate models and are less sensitive to the choices in other decision points). The yellow quadrants represent selections that either result in more accurate models or are less sensitive to the choices in other decisions points, but not both. The red quadrant represents selections that result in both relatively low model accuracy and are more sensitive to the choices in other decision points. See **Table 4.2** for information on spectral indices, **Table 4.6** for information on pixel value extraction methods, and **Table 4.7** for information on model forms.

4.3.3 Influence of model selection on interpretation of burn severity

Models were evaluated according to the following criteria and rational:

- Model fit (RMSE): lower RMSE values indicate the model better fits the data.
- Absence of a reduction in severity predictions at very high spectral index values: models that predict lower severity scores at very high spectral index values fail to separate areas of high severity from areas of extremely high severity.
- Models have a y-intercept near zero: models that don't have a y-intercept near zero fail to predict unburned or very-low severity areas within the modeling extent.

The best fit models based on RMSE showed several potential pathologies (**Figure 4.10**). First, for the overstory CBI model based on a third-order polynomial (cubic model), the model predicted a reduction in severity at very high values of the spectral index (in this case, RdNBR). This behavior doesn't match the expected behavior of the system and means that areas of extremely high severity would not be distinguishable from slightly lower areas. Second, models for overstory CBI and understory GeoCBI intercept the y-axis above zero, indicating they would never predict unburned areas within the modeling extent. Because we buffered the MTBS fire perimeters by 300 m prior to scaling the spectral indices, it is highly probable that the landscape includes some portions of unburned areas at least on the periphery of the fire. Furthermore, the model would fail to distinguish unburned "islands" from low severity areas where they are interspersed within the burned area. Third, models for the understory CBI and overstory CBI predict negative severity values, which is not possible given the 0-3 scale of the field protocols.

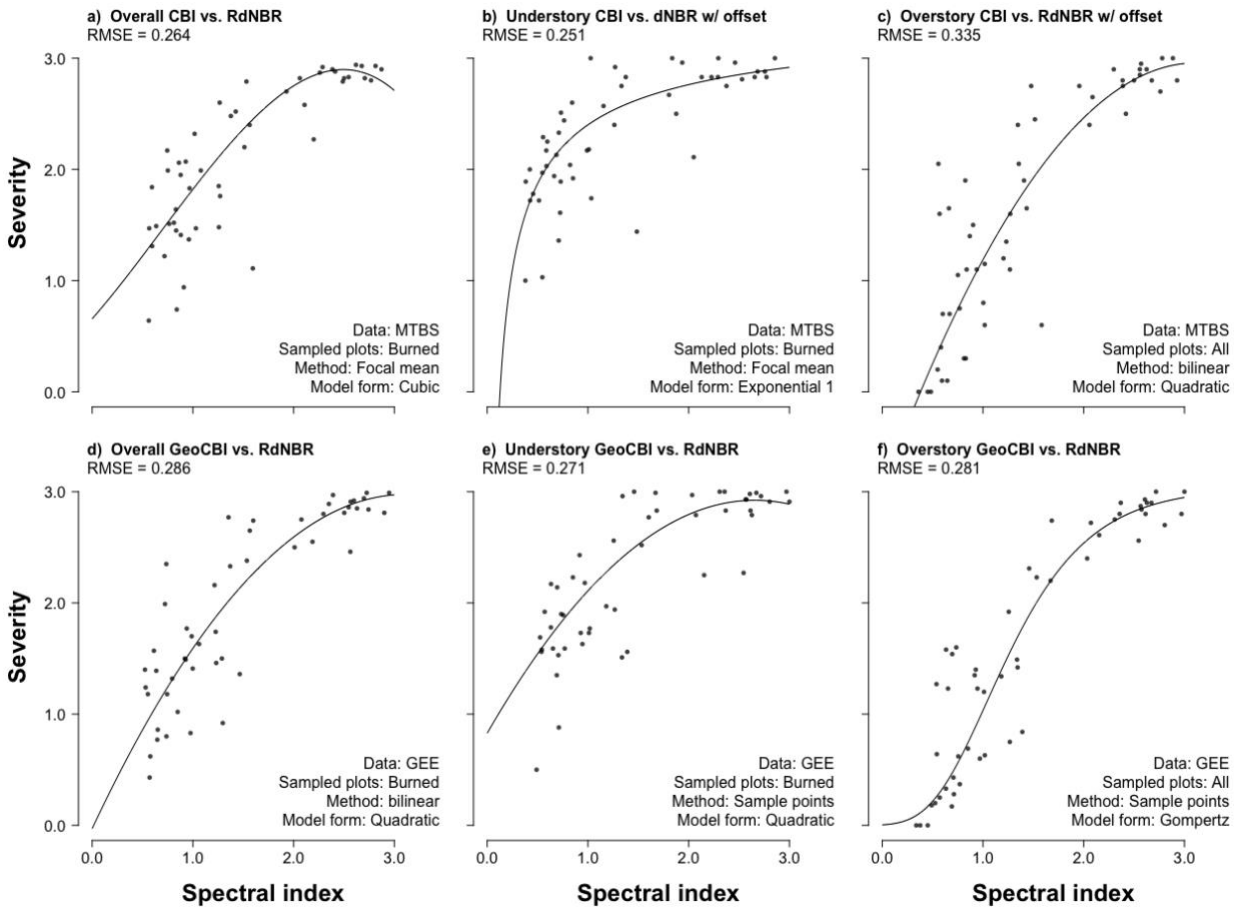

Figure 4.10 Overall best fit models (based on RMSE) for a) Overall CBI, b) understory CBI, c) overstory CBI, d) Overall GeoCBI, e) understory GeoCBI, and f) overstory GeoCBI. Details on data source, sample plots used, pixel value extraction method (see **Table 4.6** for details), and model form (see **Table 4.7** for details) are shown in the lower right. Data source refers to imagery acquired from either Monitoring Trends in Burn Severity ('MTBS') or Google Earth Engine ('GEE'). Sampled plots refers to either only field-sampled burned plots ('Burned') or both field-sampled burned plots and unburned pseudoplots ('All'). Each model may be based on one of seven spectral indices (see **Table 4.2** for details) as indicated in the plot title.

To compare the impact of model selection on the potential interpretation of the fire, we assessed a best fit (based on lowest RMSE) model with a linear and Gompertz model forms (**Figure 4.11**, **Table 4.9**). Linear and Gompertz models were chosen as comparisons for two key reasons: 1)

the linear model form represents the simplest model that has been used in prior studies, and 2) the Gompertz tends to better conform to certain expected ecological behaviors (*e.g.*, does not predict reductions in severity at high values of the spectral index and reaches zero within the range of severities). Both linear and Gompertz models used for comparison also included unburned pseudoplots in the data. Our results indicate that the Gompertz models outperform linear models in terms of accuracy and have the effect that predictions at the lower range of severities match real-world expectations in two ways: 1) the model reaches an asymptote at the upper end of the spectral index values, and it never results in predictions of lower severity at the extreme high range of index values, and 2) the model predicts zero or near-zero values of severity at the low range of spectral indices.

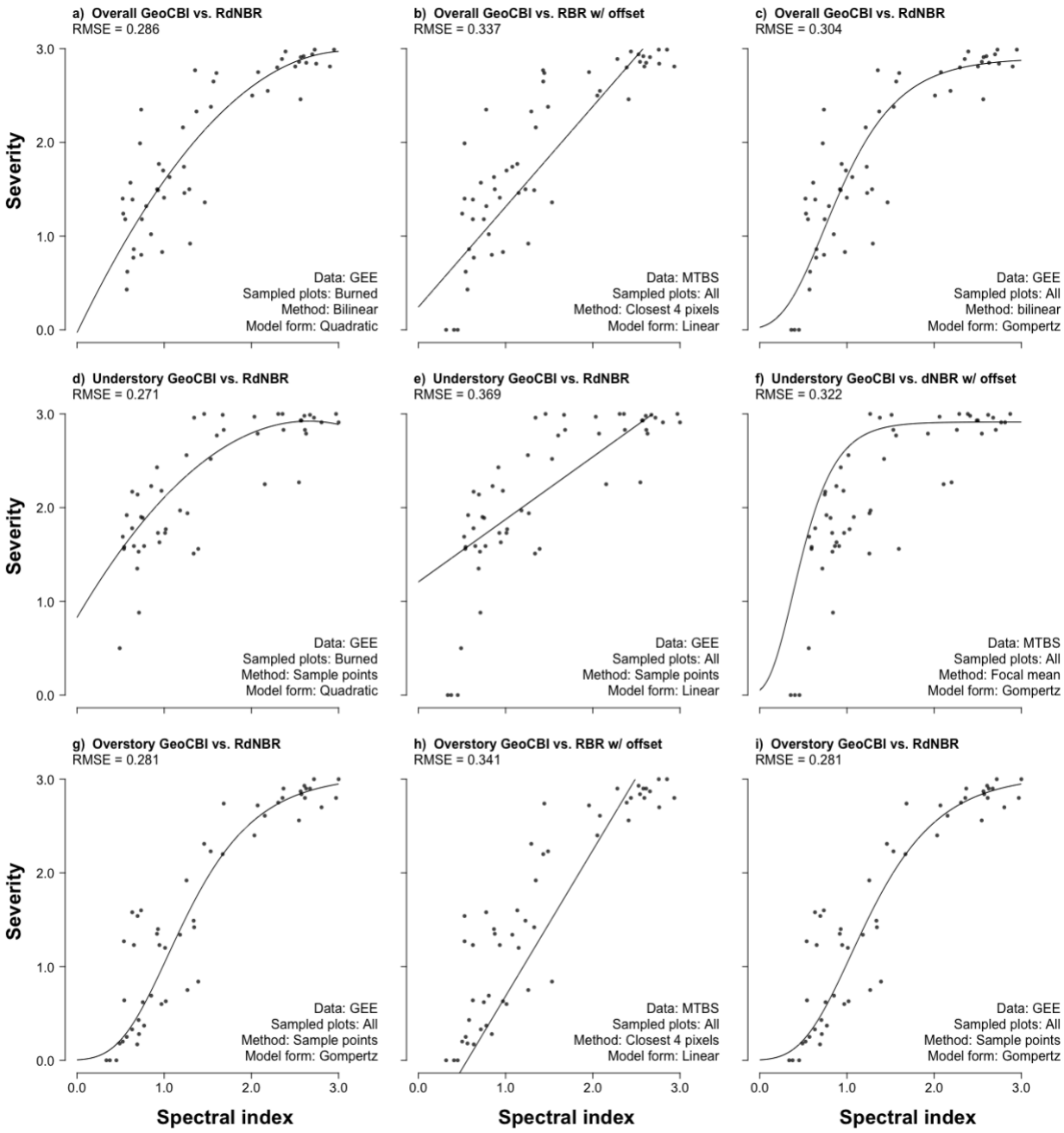
a) Overall GeoCBI vs. RdNBR
RMSE = 0.286
Data: GEE
Sampled plots: Burned
Method: Bilinear
Model form: Quadratic
b) Overall GeoCBI vs. RBR w/ offset
RMSE = 0.337
Data: MTBS
Sampled plots: All
Method: Closest 4 pixels
Model form: Linear
c) Overall GeoCBI vs. RdNBR
RMSE = 0.304
Data: GEE
Sampled plots: All
Method: bilinear
Model form: Gompertz
d) Understory GeoCBI vs. RdNBR
RMSE = 0.271
Data: GEE
Sampled plots: Burned
Method: Sample points
Model form: Quadratic
e) Understory GeoCBI vs. RdNBR
RMSE = 0.369
Data: GEE
Sampled plots: All
Method: Sample points
Model form: Linear
f) Understory GeoCBI vs. dNBR w/ offset
RMSE = 0.322
Data: MTBS
Sampled plots: All
Method: Focal mean
Model form: Gompertz
g) Overstory GeoCBI vs. RdNBR
RMSE = 0.281
Data: GEE
Sampled plots: All
Method: Sample points
Model form: Gompertz
h) Overstory GeoCBI vs. RBR w/ offset
RMSE = 0.341
Data: MTBS
Sampled plots: All
Method: Closest 4 pixels
Model form: Linear
i) Overstory GeoCBI vs. RdNBR
RMSE = 0.281
Data: GEE
Sampled plots: All
Method: Sample points
Model form: Gompertz
Severity
Spectral index
0.0
1.0
2.0
3.0

Figure 4.11 Comparison of overall best fit model (based on RMSE) versus linear and Gompertz models for overall (a, b, c), understory (d, e, f), and overstory (g, h, i) GeoCBI. While the overall best fit model was allowed to use either only field-sampled burned plots or field-sampled burned plots and unburned pseudoplots, the linear and Gompertz models were selected as the lowest RMSE models from the subset that included unburned pseudoplots. Details on data source, sample plots used, pixel value extraction method (see **Table 4.6** for details), and model form (see **Table 4.7** for details) are shown in the lower right. Data source refers to imagery acquired from either Monitoring Trends in Burn Severity ('MTBS') or Google Earth Engine ('GEE'). Sampled plots refers to either only field-sampled burned plots ('Burned') or both field-sampled burned plots and unburned pseudoplots ('All'). Each model may be based on one of seven spectral indices (see **Table 4.2** for details) as indicated in the plot title.

Table 4.9 Models based on lowest RMSE versus linear and Gompertz, where linear and Gompertz models were forced to include all plots (both field-sampled burned plots and unburned pseudoplots). Key decision criteria include plots: inclusion of just field-sampled burned plots ('Burned') or field-sampled burned plots and unburned pseudoplots ('All'); data source: imagery from the Monitoring Trends in Burn Severity program (MTBS) or Google Earth Engine (GEE) (see **Table 4.1** for details); index: spectral index used as predictor variable (see **Table 4.2** for details); and method: pixel value extraction method (see **Table 4.6** for details). The model with the lowest RMSE for each plot type is shown in bold, and the model with the highest RMSE is in italics.

Plot type	Model form	Key decision criteria	Model equation	RMSE
Overall GeoCBI	Linear	Plots: All Data: MTBS Index: RBR w/ offset Method: Closest 4 pixels	$\text{Overall GeoCBI} = 1.070 \times RBR\ w/offset + 0.242$	*0.337*
	Cubic	Plots: Burned	$\text{Overall GeoCBI} = -0.123 \times RdNBR^3 + 0.252 \times RdNBR^2 + 1.036 \times RdNBR + 0.656$	**0.264**

		Data: MTBS RdNBR Method: Focal mean		
	Gompertz	Plots: All Data: GEE Index: RdNBR Method: Bilinear	$\text{Overall GeoCBI} = 2.900 \times e^{-e^{1.552}-2.108\times RdNBR}$	0.304
Understory GeoCBI	Linear	Plots: All Data: GEE Index: RdNBR Method: Sample points	$\text{Understory GeoCBI} = 0.667 \times RdNBR + 1.208$	*0.369*
	Quadratic	Plots: Burned Data: GEE Index: RdNBR Method: Sample points	$\text{Understory GeoCBI} = -0.297 \times RdNBR^2 + 1.577 \times RdNBR + 0.828$	**0.271**
	Gompertz	Plots: All Index: MTBS dNBR w/ offset Method: Focal mean	$\text{Understory GeoCBI} = 2.914 \times e^{-e^{2.914}-1.394\times dNBR\ w/offset}$	0.281
	Linear	Plots: All	$\text{Overstory GeoCBI} = 1.557 \times RdNBR - 9.872$	*0.341*

		Data: MTBS RBR w/ offset Method: Closest 4 pixels		
Overall GeoCBI	Gompertz (Also lowest RMSE)	Plots: All Data: GEE Index: RdNBR Method: Sample points	$\text{Overstory GeoCBI} = 3.038 \times e^{-e^{1.867}-1.791\times RdNBR}$	**0.281**

We found that the decision criteria and model selection altered the resulting distribution of severity classes observed on the post-fire landscape (**Figure 4.12**). For overall GeoCBI, the best fit model (lowest RMSE) resulted in severity distributions in between the linear and Gompertz models for most all classes. The Gompertz model resulted in considerably higher proportion of the landscape being classified as 'extremely high' severity as well as higher proportions of low and low to moderate severity than the cubic model, which showed the lowest RMSE. It also showed lower proportions in the moderate, moderate to high, and high severity classes. Therefore, using a Gompertz model pushed the distribution to the edges of the range of possible severities. The simplest model, based on a first-order polynomial, showed a lower proportion of the fire being classified as extremely high severity and higher proportions at the moderate, moderate to high, and high severity classes. It therefore tended to push the distribution into the less severe categories.

For understory GeoCBI, the resulting pattern was similar to overall GeoCBI. While the model with the lowest RMSE was different (quadratic versus cubic), the resulting distribution was also generally between the linear and Gompertz model forms. Additionally, Gompertz and linear

model forms behaved similarly as they did for overall GeoCBI, albeit with a slightly more pronounced effect. In the overstory GeoCBI models, the best fit model happened to have the same decision criteria and form as the Gompertz-based model (**Table 4.9**). Compared to the linear form, the Gompertz model resulted a substantially lower proportion of the landscape classified as extremely high severity. Most of the lower severity classifications were higher than the linear model form.

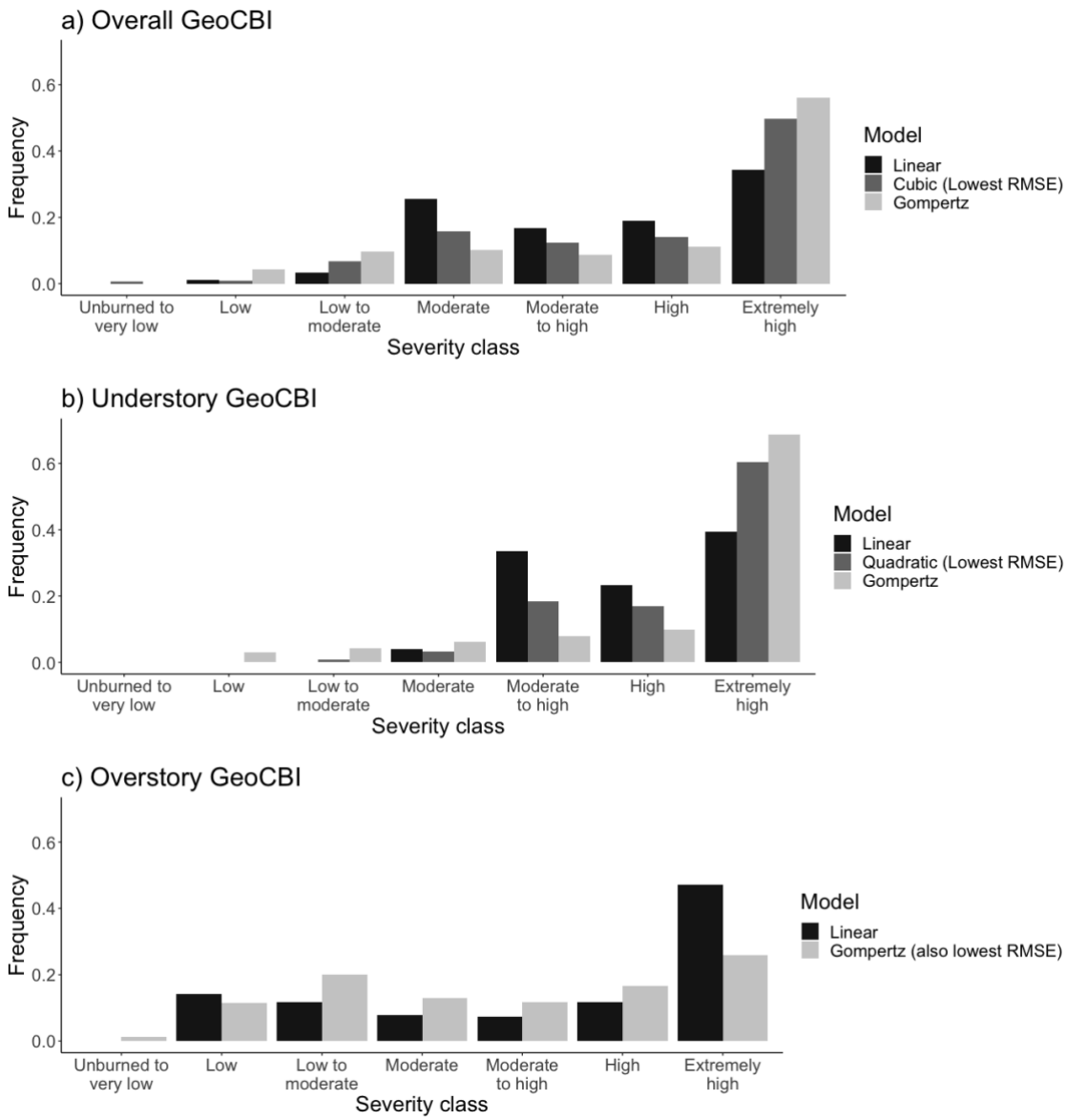

Figure 4.12 Distribution of severity classes for a) overall GeoCBI, b) understory GeoCBI, and c) overstory GeoCBI. Models shown were based on the best fit (lowest RMSE), a linear model, and a Gompertz model. The linear and Gompertz model forms included unburned pseudoplots in the data. Model parameters and decision criteria for the analysis are shown in **Table 4.9**.

4.4 DISCUSSION

Overall, our results indicated that no single option within the key decisions assessed had an overwhelming impact on model results. However, the selection of model form influenced the

interpretation of the overall fire severity distribution. Several major themes arose from the analysis completed here. Firstly, many potential pathways and models that can be undertaken to link continuous measures of field-based composite burn severity metrics with remotely sensed data, and there was no single "best" model. In fact, many models behaved similarly, as evidenced by the groupings of RMSE error in (**Figure 4.8**). Second, we identified accuracy and precision as two key factors that should be considered when selecting specific choices in the analytical framework. Third, selecting a model uncritically based on a performance metric alone can potentially introduce undesirable outcomes in the model's behavior.

Prior review of analytical pathways for linking composite burn severity metrics to remotely sensed data revealed inconsistent methodologies across studies (Chapter 2). One dilemma posed by those different approaches was whether substantial uncertainty was introduced that confounded the interpretation of ecological phenomena of interest. Researchers and managers making comparisons across studies where inconsistent methodologies were used could end up questioning whether observed differences were a result of those analytical approaches or were truly reflective of the ecological phenomena being considered. Our results generally suggested that many potential modeling pathways exist that produce strong performance (either in terms of accuracy, sensitivity, or matching the expected behavior of the ecological phenomenon of interest). We therefore propose that future studies may focus on the ecological applications of their work and that results are generally comparable across different approaches. Model form, however, did present several key pathologies that may be of interest for studies seeking to understand specific phenomena on the landscape.

There is ongoing debate in the literature concerning the merits of model selection (Chapter 2). On the one hand, models may seek to achieve high accuracy through optimizing a specific performance metric, such as R^2, RMSE, etc. On the other hand, models may be selected to reflect the expectations of the sensor and system behavior. For example, Hall et al. (2008) highlights the potential reduction in severity at very high values of spectral indices that can occur with second-order polynomials. Many prior studies have found that second order polynomials result in better performance metrics than linear models (Chen *et al.* 2011; Veraverbeke *et al.* 2011; Fernández-Manso *et al.* 2015). However, differences are often slight and would not result in considerably different interpretations of fire effects. When more complex models were considered (*e.g.*, cubic, natural logarithm, saturated growth), they did not always result in better performance (Hall *et al.* 2008; Tanase *et al.* 2011; Kurbanov *et al.* 2017). However, the saturated growth model has the advantage reaching an asymptote at high severities and not predicting reductions when spectral index values are very large.

Our results showed similar pathologies with second- and third-order polynomials that don't reflect expected ecosystem-sensor behavior. In some cases, models selected based on the lowest RMSE value resulted in lower predicted values of composite burn severity metrics for very high spectral index values. This behavior is potentially problematic given the intended application; for example, if such a model was used in an attempt distinguish high from extremely high burn severity areas, it would likely produce considerable errors of commission since multiple points on the range of the spectral index would result in the same severity level. In addition, we found two other pathologies with model behavior that may be potentially undesirable depending on the application: 1) failure to predict very low severity to unburned areas within the analysis area and 2) predictions of negative severity values. Because the MTBS fire perimeters were buffered by

300 m prior to scaling the spectral indices, the presence of unburned areas should at least be expected at the edge of our modeling extent. Any model that does not reach zero (unburned) on the composite burn severity range would fail to identify these unburned areas around the fire perimeter as well as the presence of unburned "islands" scattered within the burned area. If these models were intended to be used for identifying potential seed sources within a burned landscape, the inability to map unburned and very low severity area may result in missing areas with valuable biological legacies.

We caution against uncritical model selection based on performance metrics (*e.g.*, R^2, RMSE) alone. For most of the models tested here, the accuracy and precision were not substantially different. The quadratic model resulted in the lowest mean RMSE, however only slightly less than the Gompertz model form. We identified the Gompertz model as a good candidate for general burn severity applications due to the presence of an asymptote at high severities (eliminating potential for predictions of reduction of severity at high value of the spectral index), reaching zero or close to zero at low values of the spectral index (allowing predictions of unburned and very low severity areas) and avoidance of negative predictions of severity. One of the benefits of the CBI is that it may be considered more complete than other classification systems based on single indicators of burn severity (Sikkink 2015) and may be used generate maps that facilitate broad-scale rehabilitation prioritization (Karau *et al.* 2014). When used in a general way, CBI may be best paired with a model form such as Gompertz that behaved well at both the low and high range of severities. However, certain models may be well suited to specific tasks, even if pathologies exist outside the scope of interpretation.

Debate continues in the literature regarding the best spectral index to use to predict composite burn severity metrics. There are two main threads to this debate: 1) which NBR-based spectral index results in the best model fit for a single fire or set multiple fires compared together; and 2) which NBR-based spectral index results in the most comparable metric across multiple fires. To date, among the studies that have compared the relative performance of models based on two or more NBR-based spectral indices (**Table 4.10**), no consensus has emerged on which derivation of spectral index ($NBR_{postfire}$, dNBR, RdNBR, or RBR) performs best.

Surprisingly, several studies have found that using NBR based on a single post-fire image actually generates better model fits compared with either the bitemporally differenced dNBR or relativized versions RdNBR or RBR. For examples of this result, we point the reader to Chang et al. (2016), Epting et al. (2016), Fraser et al. (2017), or Hoy et al. (2017). That said, our results indicated that $NBR_{postfire}$ generally resulted in the lowest model fit based on RMSE. RdNBR generally resulted in the best model fits but was closely followed by all other NBR-based derivations. However, if seeking to minimize the 'worst case' scenario, several indices stood out as producing the lowest minimum RMSE values: RdNBR w/ offset, RBR w/ offset, and dNBR w/ offset. These three indices also showed relatively high precision and low sensitivity compared to the other options.

Table 4.10 Studies that have compared two or more NBR-based spectral indices when modeling a field-based composite burn severity metric.

Spectral indices compared	References
$NBR_{postfire}$, dNBR	Cansler and McKenzie (2012); De Santis and Chuvieco (2007); De Santis et al. (2010); Epting et al. (2005); Fraser et al. (2017); Hoy et al. (2008); Meng and Meentemeyer (2011); Picotte et al. (2011); Strand et al. (2013)
dNBR, RdNBR	Chang et al. (2016); Fernández-García et al. (2018); García-Llamas et al. (2019); Veraverbeke et al. (2013)
$NBR_{postfire}$, NBR, RdNBR	Kolden and Rogan (2013); Loboda et al. (2013); Miller and Thode (2007); Musyimi et al. (2017); Soverel et al. (2010); Stambaugh et al. (2015); Veraverbeke et al. (2011)
dNBR, RdNBR, RBR	Mallinis et al. (2018); Parks et al. (2014, 2018); Whitman et al. (2018); Zheng et al. (2016)

Beyond the capacity of these spectral indices to serve as predictor models in a single-fire analysis, discussion in prior literature also points to some conceptual reasons to select one over another. RdNBR has been suggested to improve comparisons across fires by producing similar classification thresholds (Zhu *et al.* 2006; Miller and Thode 2007; Miller, Knapp, *et al.* 2009; Cansler and McKenzie 2012). Therefore, if the intention of the analysis is to assess patterns in severity across multiple fires, researchers may accept some reduction in model accuracy to achieve more comparable values. A new qualifier in the RdNBR equation introduced by Parks et al. (2018) prevents equation failure when $NBR_{prefire}$ equals zero (see equation in **Table 4.2**).

Spectral indices that included a dNBR offset value were more precise than their counterparts that excluded it, albeit with little impact on accuracy. Possibly the most compelling reason to include an offset value when calculating spectral indices is the theoretical reasoning. Both Parks (2014)

and Miller and Thode (2007) support the assertion that the inclusion of the dNBR offset should be considered when making comparisons among fires, regardless of which burn severity metric is used. Additionally, omitting a correction for change due not to fire, but to natural phenological differences or atmospheric effects between acquisitions, can result in false positives for fire effects near or within burn perimeters (Key 2006).

Three prior studies have compared whether including a dNBR offset value improve relationships with CBI (Allen and Sorbel 2008; Picotte and Robertson 2011; Parks *et al.* 2018). Two of those studies and that the inclusion of a dNBR offset decreased the agreement between CBI and dNBR (Allen and Sorbel 2008; Picotte and Robertson 2011). Picotte et al. (2011) suggests that continued growth and disturbance of forests outside the burned area does not provide a static reference point between pre- and post-fire imagery. Parks et al. (2018), on the other hand, found that including a dNBR offset generally improved model accuracy. However, it did not have a substantial impact.

The inclusion of only field-sampled burned plots or the addition of unburned pseudoplots also presented a tradeoff in model accuracy and precision. Our results indicated that models fit using only the burned field-sampled plots better fit the data than when the unburned pseudoplots were included. Model precision was slightly reduced though, indicating that studies seeking models that most accurately represent the data, outside of any intended ecological application, may wish to omit sampling of unburned areas. However, depending on the intent of the analysis, including unburned field plots may be a valid approach even if it results in lower model accuracy. No prior studies were found to present quantitative results regarding the inclusion or exclusion of unburned field plots from analysis. However, Murphy et al. (2008) did state that including

unburned sites resulted in non-linear residual structure and therefore they refit linear models using just burned sites. For model comparison, including field observations both at severely burned sites and unburned sites to capture the full range of fire effects is needed to adequately assess the suitability of linear or non-linear model forms (French *et al.* 2008).

Unburned field plots provide an anchor at the low range of CBI for assessing relationships with remotely sensed data. A primary reason to measure unburned and low severity plots is to identify potential fire refugia in the post-fire landscape. The importance of these areas is recognized for providing habitat to individuals and populations to survive and persist in the post-fire environment (Robinson *et al.* 2013). While there is no clear consensus on whether fire refugia should refer only to unburned areas or also include low-severity patches, these areas may result in different compositional and structural attributes being present (Meddens *et al.* 2018). Therefore, distinguishing between unburned and low-severity areas is important to understand the impacts of a fire and the potential functionality of the landscape as a fire refugia. If mapping fire refugia is one of the objectives of analysis, then sampling in unburned areas to capture the range of spectral values that could be associated with them is important.

Some of the decision points in our analysis produced little influence on model outcomes. The choice of an image source showed particularly small differences when comparing MTBS and GEE-derived spectral indices. Our results agree with Parks et al. (2018) who found that GEE based imagery on average outperformed MTBS imagery in terms of model fit. However, we did find that the best single model fit (predicting understory CBI) did use MTBS imagery. As a result, we conclude that the GEE composite image product performs well which suggests the

potential for more immediate analysis that avoids potential delay from MTBS due to the individual scene selection and dNBR offset analysis by specialists.

Additionally, the selection of a pixel value extraction method showed relatively small differences between the majority of approaches tested. Overall, we found little difference in the average RMSE across the eight tested methods. However, the maximum RMSE showed more variation which indicates that several of the methods may lead to relatively poor model fits in conjunction with selections made at other steps in the analysis. For example, using the mean of a 3x3 window (focal mean) or an area-weighted approach resulted in considerably higher maximum RMSE as compared to the value of the pixel overlying plot center (none), the average of pixel values overlying sample points placed randomly within a plot (sample points), or the landscape assessment 2 (LA2) method. In general, the narrow range of both the mean and coefficient of variation of RMSE for different methods suggests that it may not be overly impactful on model results. However, to be safe, methods that produced low maximum RMSE values could be suggested to reduce the 'worst case' scenario.

Several studies have mentioned comparisons of different pixel value extraction methods on model fit (Cansler and McKenzie 2012; Stambaugh *et al.* 2015; Harvey *et al.* 2019). Stambaugh et al. (2015) quantified the effect of bilinear smoothing versus no smoothing and found that the effect of bilinear interpolation varied by strata, by spectral index (dNBR vs. RdNBR), and by assessment type (initial vs. extended). Two other studies (Cansler and McKenzie 2012; Harvey *et al.* 2019) reported performing exploratory analysis and finding that the bilinear method resulted in the better model fit. However, our results here demonstrate the most comprehensive assessment of methods to date. The relatively low impact of this decision is likely due to most

studies deliberately placing plot locations in homogenous areas (Chapter 2), thereby reducing the effect of different calculations. More work could be done to understand the influence of the spatial heterogeneity of spectral index values on this decision.

Finally, our analysis of the composite burn severity metrics by strata revealed better model accuracy (and lower precision) in the understory than the overstory strata. This result is counterintuitive to suggestions that the signal measured by passive optical imagery is saturated by overstory strata (Patterson and Yool 1998; Hudak *et al.* 2004; Cansler and McKenzie 2012), a similar result was found by Hoy et al. (2008). Here, we suggest that our results are due in part to the decoupled nature of the King Fire. The field-plot distribution of burn severity values (**Figure 4.5**) indicate that the understory experienced disproportionately higher burn effects than the overstory. This resulted in a more limited set of values for the models to predict, potentially contributing to increased accuracy within that range. Low representations of certain burn severity levels can make it difficult to estimate the relationship between composite burn severity metrics and spectral indices across the full range of potential severity (Allen and Sorbel 2008; Picotte and Robertson 2011). While those studies suggest poor fits due to a limited range of burn severity observations, the saturation of relationships at high values of the spectral index and near total absence of low severity plots in the understory could result in a good fit with the data for that narrower range. This finding suggests that passive optical imagery can in some cases serve as relatively good source of information for ecosystem change in the lower canopy.

4.5 Conclusion

The sensitivity analysis presented here reflected a robust analysis of key decision points in the modeling of continuous CBI measurements using remotely sensed data. We highlighted two key

elements that may inform future studies: 1) tradeoffs in accuracy versus precision for different options, and 2) potential impacts of model behavior on interpretations of burn severity patterns.

Weighing model accuracy and precision may be important when objectives require mapping a single fire (where accuracy may be most important) or comparing results across multiple fires (where precision may be more important). Furthermore, studies seeking to avoid extensive exploratory analysis may be well suited to select options that are less sensitive to the modeling pathway. However, we do not identify a single "best" model, and it was clear that many good performing models depending on how "good" performance is defined (e.g., accuracy, sensitivity).

We suggested that future studies consider the goals of an analysis and generate criteria for assessing model quality in terms of the specific ecological objectives rather than uncritically picking a model based on performance metrics alone. Specifically, we identified considerations around the ability to discriminate between unburned/very low severity areas from moderately burned areas and high severity from extremely high severity areas. In general, our results suggested that more studies focus on the ecological consequences rather than methodological ways of modeling.

4.6 References

Allen JL, Sorbel B (2008) 'Assessing the differenced Normalized Burn Ratio's ability to map burn severity in the boreal forest and tundra ecosystems of Alaska's national parks' *International Journal of Wildland Fire* **17**, 463–475.

Avery TE, Berlin GL (1992) 'Fundamentals of Remote Sensing and Airphoto Interpretation. 5th'

Prentice Hall, London.

Bastarrika A, Chuvieco E, Martín MP (2011) 'Mapping burned areas from Landsat TM/ETM+ data with a two-phase algorithm: Balancing omission and commission errors' *Remote Sensing of Environment* **115**, 1003–1012.

Cansler CA, McKenzie D (2012) 'How robust are burn severity indices when applied in a new region? Evaluation of alternate field-based and remote-sensing methods' *Remote sensing* **4**, 456–483.

Chang Y, Zhu Z, Feng Y, Li Y, Bu R, Hu Y (2016) 'The spatial variation in forest burn severity in Heilongjiang Province, China' *Natural Hazards* **81**, 981–1001. doi:http://dx.doi.org/10.1007/s11069-015-2116-9

Chen XX, Vogelmann JE, Rollins M, Ohlen D, Key CH, Yang LM, Huang CQ, Shi H (2011) 'Detecting post-fire burn severity and vegetation recovery using multitemporal remote sensing spectral indices and field-collected composite burn index data in a ponderosa pine forest.' *International Journal of Remote Sensing* **32**, 7905–7927. doi:10.1080/01431161.2010.524678

Coen JL, Stavros EN, Fites-Kaufman JA (2018) 'Deconstructing the King megafire' *Ecological applications* **28**, 1565–1580.

Coppin P, Jonckheere I, Nackaerts K, Muys B, Lambin E (2004) 'Review ArticleDigital change detection methods in ecosystem monitoring: a review' *International journal of remote sensing* **25**, 1565–1596.

Eidenshink J, Schwind B, Brewer K, Zhu ZL, Quayle B, Howard S (2007) ‘A project for monitoring trends in burn severity’ *Fire Ecology Special Issue* **3**, 2–21.

Epting J, Verbyla D, Sorbel B (2005) ‘Evaluation of remotely sensed indices for assessing burn severity in interior Alaska using Landsat TM and ETM+’ *Remote Sensing of Environment* **96**, 328–339.

Escuin S, Navarro R, Fernandez P (2008) ‘Fire severity assessment by using NBR (Normalized Burn Ratio) and NDVI (Normalized Difference Vegetation Index) derived from LANDSAT TM/ETM images’ *International Journal of Remote Sensing* **29**, 1053–1073.

Estes BL, Jacobson KW, Jirka AL, Ebert BC, Scott RS (2016) ‘2014 King Fire fuel treatment effectiveness summary’ 49.

Fang L, Yang J (2014) ‘Atmospheric effects on the performance and threshold extrapolation of multi-temporal Landsat derived dNBR for burn severity assessment.’ *International Journal of Applied Earth Observation and Geoinformation* **33**, 10–20. doi:10.1016/j.jag.2014.04.017

Fernández-García V, Quintano C, Taboada A, Marcos E, Calvo L, Fernández-Manso A (2018) ‘Remote sensing applied to the study of fire regime attributes and their influence on post-fire greenness recovery in pine ecosystems.’ *Remote Sensing* **10**, 733. doi:10.3390/rs10050733

Fernández-Manso A, Quintano C, Fernandez-Manso A, Quintano C (2015) ‘Evaluating Landsat ETM+ emissivity-enhanced spectral indices for burn severity discrimination in

Mediterranean forest ecosystems.' *Remote Sensing Letters* **6**, 302–310. doi:10.1080/2150704X.2015.1029093

Fraser RH, Sluijs J Vander, Hall RJ (2017) 'Calibrating Satellite-Based Indices of Burn Severity from UAV-Derived Metrics of a Burned Boreal Forest in NWT, Canada' *Remote Sensing* **9**, 279. doi:http://dx.doi.org/10.3390/rs9030279

French NHF, Kasischke ES, Hall RJ, Murphy KA, Verbyla DL, Hoy EE, Allen JL (2008) 'Using Landsat data to assess fire and burn severity in the North American boreal forest region: an overview and summary of results' *International Journal of Wildland Fire* **17**, 443–462.

Garcia-Llamas P, Suarez-Seoane S, Manuel Fernandez-Guisuraga J, Fernandez-Garcia V, Fernandez-Manso A, Quintano C, Taboada A, Marcos E, Calvo L (2019) 'Evaluation and comparison of Landsat 8, Sentinel-2 and Deimos-1 remote sensing indices for assessing burn severity in Mediterranean fire-prone ecosystems' *International Journal of Applied Earth Observation and Geoinformation* **80**, 137–144. doi:10.1016/j.jag.2019.04.006

García MJL, Caselles V (1991) 'Mapping burns and natural reforestation using Thematic Mapper data' *Geocarto International* **6**, 31–37.

Gorelick N, Hancher M, Dixon M, Ilyushchenko S, Thau D, Moore R (2017) 'Google Earth Engine: Planetary-scale geospatial analysis for everyone' *Remote Sensing of Environment* **202**, 18–27.

Hall RJ, Freeburn JT, De Groot WJ, Pritchard JM, Lynham TJ, Landry R (2008) 'Remote sensing of burn severity: experience from western Canada boreal fires' *International*

Journal of Wildland Fire **17**, 476–489.

Harvey BJ, Andrus RA, Anderson SC (2019) 'Incorporating biophysical gradients and uncertainty into burn severity maps in a temperate fire-prone forested region' *Ecosphere*. doi:10.1002/ecs2.2600

Holden ZA, Morgan P, Smith AMS, Vierling L (2010) 'Beyond Landsat: a comparison of four satellite sensors for detecting burn severity in ponderosa pine forests of the Gila Wilderness, NM, USA.' *International Journal of Wildland Fire* **19**, 449–458. doi:10.1071/WF07106

Hoy EE, French NHF, Turetsky MR, Trigg SN, Kasischke ES (2008) 'Evaluating the potential of Landsat TM/ETM+ imagery for assessing fire severity in Alaskan black spruce forests' *International Journal of Wildland Fire* **17**, 500–514.

Hudak AT, Robichaud P, Evans JS, Clark J, Lannom K, Morgan P, Stone C (2004) 'Field validation of Burned Area Reflectance Classification (BARC) products for post fire assessment'

Ju J, Roy DP (2008) 'The availability of cloud-free Landsat ETM+ data over the conterminous United States and globally' *Remote Sensing of Environment* **112**, 1196–1211.

Karau EC, Sikkink PG, Keane RE, Dillon GK (2014) 'Integrating Satellite Imagery with Simulation Modeling to Improve Burn Severity Mapping' *Environmental Management* **54**, 98–111. doi:http://dx.doi.org/10.1007/s00267-014-0279-x

Keeley JE (2009) 'Fire intensity, fire severity and burn severity: a brief review and suggested usage' *International Journal of Wildland Fire* **18**, 116–126. doi:10.1071/WF07049

Key CH (2006) ‘Ecological and sampling constraints on defining landscape fire severity’ *Fire Ecology* **2**, 34–59.

Key CH, Benson NC (1999) Measuring and remote sensing of burn severity. In ‘Proc. Jt. fire Sci. Conf. Work.’, 284. (University of Idaho and International Association of Wildland Fire Moscow, ID)

Key CH, Benson NC (2006) ‘Landscape assessment (LA)’ *FIREMON: Fire effects monitoring and inventory system Gen Tech Rep RMRS-GTR-164-CD, Fort Collins, CO: US Department of Agriculture, Forest Service, Rocky Mountain Research Station*.

Knight CA, Tompkins RE, Wang JA, York R, Goulden ML, Battles JJ (2022) ‘Accurate tracking of forest activity key to multi-jurisdictional management goals: A case study in California’ *Journal of environmental management* **302**, 114083.

Kolden CA, Rogan J (2009) ‘Spectral unmixing of MODIS pixels to derive burn severity: an alternative approach to Landsat-derived dNBR.’ (Association of American Geographers, 1710 16th St, NW Washington, DC 20009 USA) Available at https://search.proquest.com/docview/745927669?accountid=14784

Kolden CA, Rogan J (2013) ‘Mapping wildfire burn severity in the Arctic tundra from downsampled MODIS data’ *Arctic, Antarctic, and Alpine Research* **45**, 64–76.

Kottek M, Grieser J, Beck C, Rudolf B, Rubel F (2006) ‘World map of the Köppen-Geiger climate classification updated’ *Meteorologische Zeitschrift* **15**, 259–263.

Kurbanov E, Vorobyev O, Leznin S, Polevshikova Y, Demisheva E (2017) ‘Assessment of burn

severity in Middle Povozhje with Landsat multitemporal data' *International Journal of Wildland Fire* **26**, 772–782. doi:10.1071/WF16141

Lentile LB, Holden ZA, Smith AMSS, Falkowski MJ, Hudak AT, Morgan P, Lewis SA, Gessler PE, Benson NC (2006) 'Remote sensing techniques to assess active fire characteristics and post-fire effects' *International Journal of Wildland Fire* **15**, 319–345. doi:10.1071/WF05097

Lentile LB, Smith AMS, Hudak AT, Morgan P, Bobbitt MJ, Lewis SA, Robichaud PR (2009) 'Remote sensing for prediction of 1-year post-fire ecosystem condition' *International Journal of Wildland Fire* **18**, 594–608.

Loboda T V, French NHF, Hight-Harf C, Jenkins L, Miller ME (2013) 'Mapping fire extent and burn severity in Alaskan tussock tundra: An analysis of the spectral response of tundra vegetation to wildland fire' *Remote Sensing of Environment* **134**, 194–209.

Mallinis G, Mitsopoulos I, Chrysafi I (2018) 'Evaluating and comparing Sentinel 2A and Landsat-8 Operational Land Imager (OLI) spectral indices for estimating fire severity in a Mediterranean pine ecosystem of Greece' *Giscience & Remote Sensing* **55**, 1–18. doi:10.1080/15481603.2017.1354803

McCarley TR, Kolden CA, Vaillant NM, Hudak AT, Smith AMSS, Wing BM, Kellogg BS, Kreitler J (2017) 'Multi-temporal LiDAR and Landsat quantification of fire-induced changes to forest structure' *Remote sensing of environment* **191**, 419–432. doi:10.1016/j.rse.2016.12.022

McCarley TR, Kolden CA, Valliant NM, Hudak AT, Smith AMS, Kreitler J (2017) 'Landscape-scale quantification of fire-induced change in canopy cover following mountain pine beetle outbreak and timber harvest' *Forest Ecology and Management* **391**, 164–175. doi:10.1016/j.foreco.2017.02.015

Meddens AJH, Kolden CA, Lutz JA, Smith AMS, Cansler CA, Abatzoglou JT, Meigs GW, Downing WM, Krawchuk MA (2018) 'Fire refugia: what are they, and why do they matter for global change?' *BioScience* **68**, 944–954.

Meng Q, Meentemeyer RK (2011) 'Modeling of multi-strata forest fire severity using Landsat TM Data' *International Journal of Applied Earth Observation and Geoinformation* **13**, 120–126.

Miller JD, Knapp EE, Key CH, Skinner CN, Isbell CJ, Creasy RM, Sherlock JW (2009) 'Calibration and validation of the relative differenced Normalized Burn Ratio (RdNBR) to three measures of fire severity in the Sierra Nevada and Klamath Mountains, California, USA' *Remote Sensing of Environment* **113**, 645–656.

Miller JD, Safford HD, Crimmins M, Thode AE (2009) 'Quantitative evidence for increasing forest fire severity in the Sierra Nevada and southern Cascade Mountains, California and Nevada, USA' *Ecosystems* **12**, 16–32.

Miller JD, Thode AE (2007) 'Quantifying burn severity in a heterogeneous landscape with a relative version of the delta Normalized Burn Ratio (dNBR)' *Remote Sensing of Environment* **109**, 66–80.

Montealegre AL, Lamelas MT, Tanase MA, De la Riva J (2014) ‘Forest fire severity assessment using ALS data in a mediterranean environment’ *Remote Sensing* **6**, 4240–4265. doi:10.3390/rs6054240

Morgan P, Keane RE, Dillon GK, Jain TB, Hudak AT, Karau EC, Sikkink PG, Holden ZA, Strand EK (2014) ‘Challenges of assessing fire and burn severity using field measures, remote sensing and modelling’ *International Journal of Wildland Fire* **23**, 1045–1060. doi:10.1071/WF13058

Murphy KA, Reynolds JH, Koltun JM (2008) ‘Evaluating the ability of the differenced Normalized Burn Ratio (dNBR) to predict ecologically significant burn severity in Alaskan boreal forests’ *International Journal of Wildland Fire* **17**, 490–499.

Musyimi Z, Said MY, Zida D, Rosenstock TS, Udelhoven T, Savadogo P, Leeuw J de, Aynekulu E, de Leeuw J, Aynekulu E (2017) ‘Evaluating fire severity in Sudanian ecosystems of Burkina Faso using Landsat 8 satellite images’ *Journal of Arid Environments* **139**, 95–109. doi:10.1016/j.jaridenv.2016.11.005

Parks SA, Dillon GK, Miller C (2014) ‘A new metric for quantifying burn severity: the Relativized Burn Ratio’ *Remote Sensing* **6**, 1827–1844.

Parks SA, Holsinger LM, Koontz MJ, Collins L, Whitman E, Parisien M-A, Loehman RA, Barnes JL, Bourdon J-F, Boucher J, Boucher Y, Caprio AC, Collingwood A, Hall RJ, Park J, Saperstein LB, Smetanka C, Smith RJ, Soverel N (2019) ‘Giving Ecological Meaning to Satellite-Derived Fire Severity Metrics across North American Forests’ *Remote Sensing* **11**, 1735. doi:10.3390/rs11141735

Parks SA, Holsinger LM, Voss MA, Loehman RA, Robinson NP (2018) 'Mean Composite Fire Severity Metrics Computed with Google Earth Engine Offer Improved Accuracy and Expanded Mapping Potential' *Remote Sensing* **10**, 879. doi:10.3390/rs10060879

Patterson MW, Yool SR (1998) 'Mapping fire-induced vegetation mortality using Landsat Thematic Mapper data: A comparison of linear transformation techniques' *Remote Sensing of Environment* **65**, 132–142.

Pereira JMC (1999) 'A comparative evaluation of NOAA/AVHRR vegetation indexes for burned surface detection and mapping' *IEEE transactions on geoscience and remote sensing* **37**, 217–226.

Pereira MC, Setzer AW (1993) 'Spectral characteristics of fire scars in Landsat-5 TM images of Amazonia' *Remote Sensing* **14**, 2061–2078.

Picotte JJ, Robertson KM (2011) 'Validation of remote sensing of burn severity in south-eastern US ecosystems' *International Journal of Wildland Fire* **20**, 453–464. doi:http://dx.doi.org/10.1071/WF10013

Quintano C, Fernandez-Manso A, Calvo L, Marcos E, Valbuena L (2015) 'Land surface temperature as potential indicator of burn severity in forest Mediterranean ecosystems' *International Journal of Applied Earth Observation and Geoinformation* **36**, 1–12. doi:10.1016/j.jag.2014.10.015

Robinson NM, Leonard SWJ, Ritchie EG, Bassett M, Chia EK, Buckingham S, Gibb H, Bennett AF, Clarke MF (2013) 'Refuges for fauna in fire-prone landscapes: their ecological function

and importance' *Journal of Applied Ecology* **50**, 1321–1329.

De Santis A, Asner GP, Vaughan PJ, Knapp DE (2010) 'Mapping burn severity and burning efficiency in California using simulation models and Landsat imagery' *Remote Sensing of Environment* **114**, 1535–1545. doi:10.1016/j.rse.2010.02.008

De Santis A, Chuvieco E (2007) 'Burn severity estimation from remotely sensed data: Performance of simulation versus empirical models' *Remote Sensing of Environment* **108**, 422–435.

De Santis A, Chuvieco E (2009) 'GeoCBI: a modified version of the Composite Burn Index for the initial assessment of the short-term burn severity from remotely sensed data.' *Remote Sensing of Environment* **113**, 554–562. doi:10.1016/j.rse.2008.10.011

Sikkink PG (2015) Comparison of six fire severity classification methods using Montana and Washington wildland fires. In 'Keane, Robert E.; Jolly, Matt; Parsons, Russell; Riley, Karin. Proc. large Wildl. fires Conf. May 19-23, 2014; Missoula, MT. Proc. RMRS-P-73. Fort Collins, CO US Dep. Agric. For. Serv. Rocky Mt. Res. ', 213–226

Soverel NO, Perrakis DDB, Coops NC (2010) 'Estimating burn severity from Landsat dNBR and RdNBR indices across western Canada' *Remote Sensing of Environment* **114**, 1896–1909.

Stambaugh MC, Hammer LD, Godfrey R (2015) 'Performance of Burn-Severity Metrics and Classification in Oak Woodlands and Grasslands' *Remote Sensing* **7**, 10501–10522. doi:http://dx.doi.org/10.3390/rs70810501

Stavros EN, Tane Z, Kane VR, Veraverbeke S, McGaughey R, A LJ, Ramirez C, Schimel DS (2016) ‘Remote Sensing Data Before and After California Rim and King Forest Fires, 2010-2015’ doi:10.3334/ornldaac/1288

Strand EK, Bunting SC, Keefe RF (2013) ‘Influence of Wildland Fire Along a Successional Gradient in Sagebrush Steppe and Western Juniper Woodlands’ *Rangeland Ecology and Management* **66**, 667–679. Available at https://search.proquest.com/docview/1468524215?accountid=14784

Tanase M, de la Riva J, Pérez-Cabello F, Riva J de la, Pérez-Cabello F (2011) ‘Estimating burn severity at the regional level using optically based indices.’ *Canadian Journal of Forest Research* **41**, 863. doi:10.1139/x11-011

Team RC (2021) ‘R: A language and environment for statistical computing’ Available at https://www.r-project.org/

Veraverbeke S, Hook SJ (2013) ‘Evaluating spectral indices and spectral mixture analysis for assessing fire severity, combustion completeness and carbon emissions’ *International Journal of Wildland Fire* **22**, 707–720. doi:http://dx.doi.org/10.1071/WF12168

Veraverbeke S, Lhermitte S, Verstraeten WW, Goossens R (2010) ‘The temporal dimension of differenced Normalized Burn Ratio (dNBR) fire/burn severity studies: The case of the large 2007 Peloponnese wildfires in Greece’ *Remote Sensing of Environment* **114**, 2548–2563. doi:http://dx.doi.org/10.1016/j.rse.2010.05.029

Veraverbeke S, Lhermitte S, Verstraeten WW, Goossens R (2011) ‘Evaluation of pre/post-fire

differenced spectral indices for assessing burn severity in a Mediterranean environment with Landsat Thematic Mapper' *International Journal of Remote Sensing* **32**, 3521–3537.

Verbyla DL, Boles SH (2000) 'Bias in land cover change estimates due to misregistration' *International Journal of Remote Sensing* **21**, 3553–3560.

Verbyla DL, Kasischke ES, Hoy EE (2008) 'Seasonal and topographic effects on estimating fire severity from Landsat TM/ETM+ data' *International Journal of Wildland Fire* **17**, 527–534.

Wagtendonk JW van, Root RR, Key CH (2004) 'Comparison of AVIRIS and Landsat ETM+ detection capabilities for burn severity.' *Remote Sensing of Environment* **92**, 397–408. doi:10.1016/j.rse.2003.12.015

Van Wagtendonk JW, Root RR, Key CH (2004) 'Comparison of AVIRIS and Landsat ETM+ detection capabilities for burn severity' *Remote Sensing of Environment* **92**, 397–408.

White JD, Ryan KC, Key CC, Running SW (1996) 'Remote sensing of forest fire severity and vegetation recovery' *International Journal of Wildland Fire* **6**, 125–136.

Whitman E, Parisien M-AA, Thompson DK, Hall RJ, Skakun RS, Flannigan MD (2018) 'Variability and drivers of burn severity in the northwestern Canadian boreal forest.' *Ecosphere* **9**, e02128. doi:10.1002/ecs2.2128

Zheng Z, Zeng Y, Li S, Huang W, Zhong Z, YongNian Z, SongNian L, Wei H (2016) 'A new burn severity index based on land surface temperature and enhanced vegetation index' *International Journal of Applied Earth Observation and Geoinformation* **45**, 84–94.

doi:10.1016/j.jag.2015.11.002

Zhong Z, YongNian Z, SongNian L, Wei H (2018) ‘Mapping burn severity of forest fires in small sample size scenarios.’ *Forests* **9**, 608. doi:10.3390/f9100608

Zhu Z, Key C, Ohlen D, Benson N (2006) ‘Evaluate sensitivities of burn severity mapping algorithms for different ecosystems and fire histories in the United States. Final report JFSP 01-1-4-12’ *October* **12**, 35.

CHAPTER 5. CONCLUSIONS

The overall objectives of this dissertation were to: 1) summarize methodological pathways used to model continuous estimates of burn severity (based on the composite burn index) using remotely sensed data, 2) dive into the fundamental theory regarding spatial alignment and temporal synchrony of field observations and remotely sensed data, and 3) perform an in-depth case study of key methodological decisions using the King Fire to assess tradeoffs in accuracy and sensitivity of the resulting outcomes. Broadly, the research presented here suggested that the information available to correlate with composite burn indices within optical bands from Landsat imagery has largely been exhausted. There appeared little room for additional improvements in terms of model accuracy regardless of what analytical pathways are used. Rather than try to continue fine tuning methods to wring out what might be slightly better performance metrics in individual cases, these results suggest that the research community instead use the suite of possible decisions presented here and focus on the ecological interpretation. By critically assessing (either qualitatively or quantitatively) what has been done to date, this work implied some guidelines for best practices for future burn severity modeling (**Box 1**). The outcomes of this research contribute to broad knowledge about the variety of methods used to link field observations to remotely sensed data, their conceptual underpinnings, and the tradeoffs associated with using different analytical pathways.

Box 1. Suggested best practices for future burn severity modeling using remotely sensed data and continuous estimates of burn severity based on the composite burn index or related field protocols.

Field plot collection	• Collect field data in a way that multiple composite indices (*e.g.*, CBI, GeoCBI, WCBI) may be calculated • Attempt to balance field plot distribution across range of severities • Sample unburned areas or include pseudo-unburned plots to anchor regressions at the low range of severity values • Share field data in public repositories so that it is available for further analysis and potential meta-analysis across multiple fires/ecoregions
Remotely sensed data	• Standard products derived from MTBS or GEE derived imagery produce similar results, but GEE may be preferable in many cases due to the faster availability of the data • Inclusion of dNBR offset values can produce more accurate and precise results, as well as being conceptually more comparable across fires • Both absolute differenced and relativized NBR based indices (dNBR and RdNBR) are comparable in terms of model accuracy or precision; however, they do differ in their ecological interpretation so, if all else is equal, select one based on the application of the model
Linking models	• Select a pixel value index extraction method using justification based on either a conceptual understanding of the spatial alignment or a quantitative comparison done during analysis or by an appropriate (comparable geographic scope) prior study • Add precision to the analysis of models (in addition to assessing model accuracy) • Show that models behave well across range of inference (*e.g.*, at separating unburned and low severity areas, high to extremely high severity areas, or across the full range of severities)
Overall	• To allow comparability, report the full suite of key steps and decisions in the process of field data collection, remotely sensed data acquisition, pre-processing, and modeling • Provide rationale to defend key decisions in analytical framework including relation to study objectives and/or conceptual underpinnings of remote sensing and fire ecology

The first two objectives were accomplished using an in-depth literature search of studies published through 2019. One of the key results was a blueprint of the overall investigative framework and specific methods used at key points in the analysis. This outcome should be useful to new practitioners in the field seeking to understand the general tools and techniques of the trade as well as seasoned professionals looking for new research directions. The results showed numerous pathways are used to model composite burn severity indices using remotely sensed data and, with mixed results common among the few comparative studies that have been conducted, considerable uncertainty remains when comparing data from studies that used different methods. This forces scientists and managers looking to synthesis multiple studies to weight whether outcomes were truly due to the ecological phenomena of interest or overly biased by the approaches taken to process and model the data.

Beside calling attention to the lack of consensus in methodologies and potential errors introduced by different pathways, the literature review also uncovered several key research gaps related to the distribution in the types and locations of fires studied, limited range in the size and timing of field plot collection, and modeling of composite burn indices across strata. The vast majority of research in this area has been done in western North America, and specifically in temperate conifer and boreal ecosystems. While other forest systems have been studied in less detail (*e.g.*, oak woodlands, mixed chaparral, eucalyptus, sagebrush steppe), the heavy bias towards conifer forests is likely because the field protocol and expected behavior of the spectral reflectance signatures are heavily tailored towards the forest dynamics of these systems. Fire effects are generally visible in aerial imagery soon after a fire and remain so for several years due to relatively slow recovery rates. That said, the limited size and timing of field plot collection

shows there is still many unknowns regarding the spatial and temporal scales of heterogeneity in fire effects and variability in the strength of observations using remotely sensed data.

The in-depth assessment of spatial alignment and temporal synchrony laid out a conceptual framework for helping determine which methods may be appropriate for extracting spectral index values to associate with each field plot and demonstrated that strict synchrony in timing of field plot collection and remotely sensed data acquisition did not generally improve model results. Few studies have shown quantitative comparisons using different spectral index extraction methods, and those that have were in some cases cited outside the geographic scope of their study. Presenting a conceptual framework for thinking through the potential mismatch between field plot size and remotely sensed image grain hopefully encourages future researchers to think more critically about the consequences of this decision. One suggested approach for further investigation would be to collect nested field data and compare different approaches across multiple scales. The analysis of temporal synchrony showed that, in some instances, when field plots were measured in the year following a fire, remotely sensed imagery collected in the previous year produced better model fits than imagery collected more synchronous to the field plots. While this outcome generally runs counter to suggestions that field data and remotely sensed data be collected within a few weeks of one another, a potential explanation is that living vegetation present in field plots can be characterized as either surviving vegetation or regeneration by field crews whereas remotely sensed data does not make this distinction. Finally, the study showed a lack of information on longer-term relationships between field observations and remotely sensed data.

Tradeoffs in accuracy and precision for key decision criteria in the modeling workflow were assessed in the sensitivity analysis on the King Fire. Another key element of this study was to highlight the potential deficiencies that emerge during model selection. Specifically, some models exhibit undesirable pathologies that don't reflect expected behavior, which could be problematic depending on their application. The results showed that, while no single decision in the analysis framework had an overwhelming impact on model fit, there were differences in accuracy and precision that might be considered depending on whether objectives include comparing results across multiple fires or focusing the investigation on a single fire. Because overall results were generally comparable across the different modeling pathways, strong evidence was not found that any single approach will result in big gains. This suggested that researchers can stop worrying so much about how these analyses are being processed and focus more on their ecological applications. Finally, the study showed that modeling selection in particular can affect the interpretation of fire and should be undertaken with consideration of the study objectives. In other words, the findings should deter future researchers from picking model form uncritically based on performance metric and instead focus on which ranges of severity are of interest. For example, different model forms (and their respective pathologies) may be preferential for mapping unburned to very low severity areas, separating high and extremely high severity areas, or capturing general trends across the full range of severities.

Overall, this body of work demonstrated the long and varied use of remotely sensed data to model and map burn severity in forest ecosystems. The vast majority of work that has been done to date is based on the Landsat satellite program. However, studies are increasingly making use of imagery with high spatial and spectral resolution, expanding to thermal wavelengths, using radar and even lidar data. The sensitivity analysis presented here begs for repetition in new

landscapes and using new datasets. It also demonstrated the strength of Landsat data and ability to tailor a methodology to specific ecological phenomena of interest. While new sensors may provide more accuracy or precision, none can yet compete with the convenience of tried-and-true methodologies combined with a near 40-year record that provides an unrivaled ability to investigate fire effects over time.

VITA

Colton Miller graduated with a degree in Geography/Environmental Studies from University of California, Los Angeles, where he engaged in undergraduate research working with Dr. Greg Okin studying soil carbon and nitrogen analysis using samples collected in the Kalahari Desert of Botswana. After receiving a Bachelor of Arts, he went on to work in a plant microbiology and genetics laboratory in Seattle and then at a forest research station in northern Minnesota investigating the impacts of a changing climate on tree species distributions. Colton then returned to academia, receiving a Master of Science degree in Forest Soils from the University of Washington under Drs. Darlene Zabowski, Rob Harrison, Eric Turnblom, and Dan Vogt. For his thesis, Colton researched the impacts of different forestry reclamation techniques at a surface coalmine in Centralia, Washington. During his coursework, he gained a deep appreciation for the diversity of Washington's forest ecosystems, including the old growth forests west of the Cascades and the frequent-fire dry forests east of the Cascades. Seeking experience in the technical aspects of forest management, Colton went on to work as a pre-sale forester for the Quinault Indian Nation where he got his boots dirty performing forest reconnaissance, timber cruising, and appraisal/contract work. While working in Taholah, Washington, and living on the Olympic Peninsula, Colton immersed himself as much as possible in the culture and traditions of the Quinault Indian Nation. Some brief experiences working in wildland fire and using remotely sensed data put him on the path towards this degree and dissertation. It is Colton's sincere wish that his work and experience contribute in some small way to encouraging the diverse landowners in the western United States collaborate towards creative solutions for preserving biological legacies (big, awesome trees) and reducing the impacts of wildfire and smoke on underprivileged communities.